Technische Universität München

Fakultät Chemie

Professur für Industrielle Biokatalyse

Screening and Characterization of Oleaginous Yeasts and Modeling of Flocculation-based Algae Harvest

Felix R. Bracharz

Vollständiger Abdruck der von der Fakultät für Chemie der Technischen Universität München zur Erlangung des akademischen Grades eines Doktors der Naturwissenschaften genehmigten Dissertation.

Vorsitzender:	Prof. Dr. rer. nat. Tom Nilges
Prüfer der Dissertation:	1. Prof. Dr. rer. nat. Thomas Brück
	2. Prof. Dr. rer. nat. Wolfgang Liebl

Die Dissertation wurde am 23.3.2017 bei der Technischen Universität München eingereicht und durch die Fakultät für Chemie am 6.7.2017 angenommen.

Eidesstattliche Erklärung

Hiermit versichere ich, dass ich die vorliegende Dissertation selbstständig verfasst, sowie die Ausführungen und Gedanken, welche anderen Schriften sinngemäß oder wörtlich entnommen wurden, sowie weitere Quellen und Hilfsmittel kenntlich gemacht habe. Die vorliegende Arbeit wurde bisher weder in gleicher noch ähnlicher Form einer anderen Prüfungsbehörde vorgelegt oder anderweitig veröffentlicht.

München, den …….

Acknowledgments

Prof. Thomas Brück has given me tremendous support throughout my work in this group. He was never too busy to aid me by critically reviewing my work or discuss strategies on how to approach scientific questions. It was an enriching experience to witness the group develop and flourish in this challenging scientific and academic environment. Further, I am deeply grateful to my students, some of which truly excelled at their work. I have grown personally and professionally by working with Isabel Aschenbrenner, Kathrin Bach, Daniel Helmdach, Dominik Schum, Valeria Guidolin and all others.

I thank Veronika Redai for her patience, encouragement and the great deal of work she has put into our oil yeast projects. Even in the most dire of times, I could always count on the constructive scientific and culinary feedback of my office neighbor Johannes Schmidt. Further, I thank Martina Haack and Tom Schuffenhauer for the technical support and the unique office atmosphere. Norbert Mehlmer and Christian Görner were incessant sources of ideas and provided me with great scientific feedback. Finally, I want to thank Farah Qoura for passing on the things he learned at Clariant.

Special appreciation goes to my colleagues and friends: Markus Reinbold, Wojtech Jurkowski, Gülnaz Celik, Samer Younes, Dania Awad, Elias Kassab, Matthias Glemser, Wolfgang Mischko, Monika Fuchs and Mahmoud Masri.

Summary

This thesis comprises the characterization and genetic engineering of the non-conventional oleaginous yeast *Cutaneotrichosporon oleaginosus* as well as optimization of flocculation of the microalgae *Scenedesmus obtusiusculus.*

Part 1: Screening and Characterization of Oleaginous Yeast

Oleaginous organisms are a promising, renewable source of single cell oil (SCO), which in turn holds great potential for replacing plant based lipids. In contrast to the latter, production of SCO yields much higher lipid contents (up to 80% g/g biomass) and does not directly compete with food supply.

In this work, oleaginous yeasts were isolated from environmental samples and together with commercial strains screened for lipid productivity. Out of a total of 102 strains, *Cutaneotrichosporon oleaginosus* ATCC 20509 emerged as the most suitable strain for lipid production in semisynthetic as well as natural substrate. Lipid productivity of the respective strain was not improved by random in vivo mutagenesis and directed evolution.

Lipid accumulation in microorganisms is mainly induced by limitation of nutrients such as nitrogen, phosphorus or sulfur. By testing different methods of nutrient limitations in *C. oleaginosus*, depletion of nitrogen was confirmed as the most suitable way of inducing lipid accumulation. Sulfur and phosphate limitation had much more pronounced effects on growth kinetics, whereas sulfur limitation did not result in significantly increased triglyceride yields.

An essential step in understanding the process of lipid accumulation is the elucidation of the underlying signaling network. The two target-of-rapamycin-complexes (TORCs) are central integrators of metabolic signals including carbon and nitrogen availability. TORC1 is specifically inhibited by rapamycin, leading to a cell state of simulated nutrient limitation. Supplementation with rapamycin increased intracellular lipid content of *C. oleaginosus* and affected growth kinetics, but not cell granularity or microscopic features except for Nile red fluorescence. Further, the spectrum of intracellular fatty acids was shifted towards a pattern characteristic for lipid accumulation. This indicated the inhibition of the target of rapamycin complex 1 (TORC 1), but not TORC 2. A homology based signaling network around TORC was assembled, showing similarity to *Schizosaccharomyces pombe* in some cases (e.g. signaling of carbon availability) whereas other regulatory paths (e.g. autophagy) were highly dissimilar to any described species.

Another important way of improving lipid productivity in oleaginous organisms is genetic engineering. Classic bottlenecks of triglyceride synthesis (diacylglycerol acyltransferase or lysophosphatidic acid acyltransferase) were overexpressed in *C.oleaginosus*, but did not yield

the expected increase in lipid content or productivity. This indicated, that both enzymatic steps are not rate-limiting for lipid synthesis in *C. oleaginosus* cultivated in full medium. Generation of knockout strains using CRISPR-Cas9 presumably failed due to unfavorable codon usage and weak promoter strength of the respective nuclease and respective insufficient expression levels.

Part 2: Energy-efficient Harvest of the Microalgae *S. obtusiusculus* by Flocculation

Another potential source of SCO are microalgae, which have the added benefit of being phototrophic and hence use a zero-value substrate. A main disadvantage however is the low achievable biomass concentration in the culture arising from limited RuBisCO efficiency and shading of cells. Consequently, the process step of harvesting and dewatering of microalgae makes up 20% of the cost of algae biomass. Whereas many other methods of harvest, such as filtration or centrifugation are energy- and labor-intensive, flocculation-sedimentation is a simple and efficient alternative, which is explored in this work.

Experiments are conducted using the microalgae *Scenedesmus obtusiusculus* A189, a newly isolated strain of Chlorophyta with high growth rates in fresh and brackish water as well as high lipid and carbohydrate content. Cultivation is done in artificial salt water, which is especially challenging for flocculation-sedimentation procedures due to its high ionic strength and somewhat higher density. The focus of this work is on non-sterile cultivation to mimic open pond cultivation.

The effects and relationships of different factors on flocculation efficiency (FE) and the complexity of interaction between those factors are explored. In summary, modified tannin was comparable in performance to chitosan. However, its much lower price, independence of culture pH and very high effectiveness in the absence of algae organic matter make it an interesting alternative. Further, a synergy between those two agents was observed despite their mechanistic similarity.

Entirely independent of added polymeric substances, autoflocculation was induced by pH shift, whereas a >96% FE was achieved using $Ca(OH)_2$ at a cost of $40 / ton algae biomass. This is comparable to previously published values achieved in fresh water. However, raising the pH to the required range (~ pH 10.5 - 11) exacerbates the reuse of the respective medium, which likely relates to buffering effects.

Zusammenfassung

Die Arbeit umfasst im ersten Teil die Charakterisierung und genetische Modifikation der nicht-konventionellen, ölbildenden Hefe *Cutaneotrichosporon oleaginosus* sowie im zweiten Teil die Optimierung der Ernte der Mikroalge *Scenedesmus obtusiusculus* über Flokkulation.

Teil 1: Screening und Charakterisierung ölbildender Hefen

Öl-akkumulierende Organismen sind eine vielversprechende, nachhaltige Quelle von Einzelleröl, mit dem Potential, bestehende Pflanzen-basierte Lipide zu ersetzen. Im Gegensatz zu Pflanzenlipiden konkurriert die Produktion von Einzelleröl nicht mit der Nahrungsmittelproduktion und weist weitaus höhere Lipidausbeuten (bis zu 80% g/g Biomasse) auf.

In dieser Arbeit wurden Öl-bildende Hefen aus Umweltproben isoliert und zusammen mit aus Stammsammlungen beschafften Stämmen auf Lipidproduktivität selektiert. Aus insgesamt 102 Stämmen wurde *Cutaneotrichosporon oleaginosus* ATCC 20509 als der am besten geeignete Stamm zur Produktion von Lipiden sowohl auf semisynthetischem als auch natürlichem Substrat identifiziert. Das Ziel einer Steigerung der Lipidproduktivität konnte durch zufällige in vivo Mutagenese und gerichtete Evolution nicht erreicht werden.

Lipidakkumulation in Mikroorganismen wird vor allem durch die Limitierung bestimmter Nährstoffe wie Schwefel, Stickstoff oder Phosphor induziert. Verschiedene Limitierungen wurden in *C. oleaginosus* getestet und Stickstofflimitierung als geeignetste Methode zur Induktion von Lipidakkumulation bestätigt. Schwefel- und Phosphorlimitierung hatten ausgeprägte, negative Effekte auf die Wachstumskinetik und Schwefellimitierung resultierte nicht in einem signifikant erhöhten Lipidgehalt.

Ein essentieller Schritt für ein besseres Verständnis der Lipidakkumulierung ist die Aufklärung des betreffenden Signalnetzwerkes. Zwei *target of rapamycin* Komplexe (TORC1, TORC2) sind zentrale Komplexe für die Integration metabolischer Signale wie die Verfügbarkeit von Kohlenstoff- oder Stickstoffquellen. TORC1 wird spezifisch von Rapamycin inhibiert, was in der Zelle zu einem simulierten Zustand der Nährstofflimitierung führt. Zugabe von Rapamycin führte zur Erhöhung des intrazellulären Lipidanteils in *C. oleaginosus* und beeinflusste die Wachstumskinetik, nicht jedoch Zellgranularität oder mikroskopisch erkennbare Zellstrukturen abgesehen von einer erhöhten Nilrotfluoreszenz. Dies weist auf eine Hemmung des TORC1, nicht jedoch des TORC2 hin. Ein Homologie-basiertes Signalnetzwerk um die TORCs zeigte gewisse Ähnlichkeiten zu *S. pombe* im Hinblick auf Detektion von Kohlenstoffverfügbarkeit auf,

wobei andere regulatorische Pfade, wie Induktion von Autophagie, sich stark von anderen, beschriebenen Organismen unterschieden.

Eine weitere Möglichkeit zur Erhöhung des Lipidgehaltes in Mikroorganismen besteht in der genetischen Modifikation. In anderen Organismen als limitierende, enzymatische Schritte der Triglyceridsynthese identifizierte Enzyme (Diacylglycerolacyltransferase und Lysophosphatidatacyltransferase) führten jedoch in Überexpressionsexperimenten in *C. oleaginosus* nicht zu einer erhöhten Lipidausbeute oder –produktivität. Dies ist ein Hinweis darauf, dass beide enzymatischen Schritte möglicherweise in *C. oleaginosus* nicht limitierend für die Produktion von Triglyceriden sind. Herstellung von Knockout-Stämmen über CRISPR-Cas9 scheiterte wahrscheinlich an ungünstiger Codonnutzung des betreffenden Genes, zu schwacher Promotorstärke und der daraus resultierenden unzureichenden Expressionsraten der Nuklease.

Teil 2: Energieeffiziente Ernte der Mikroalge *S. obtusiusculus* über Flokkulation

Eine weitere potentielle Quelle für Einzelleröl sind Mikroalgen. Diese haben den zusätzlichen Vorteil, Licht als Energiequelle zu nutzen. Einer der Hauptnachteile ist die niedrige Biomassekonzentration im Medium, welche sich einerseits durch die niedrige RuBisCO-effizienz sowie Zellverschattung während der Kultivierung begründet. Daraus folgt, dass die Algenernte und die damit einhergehende Entwässerung etwa 20% der Gesamtkosten für die Produktion von Algenbiomasse ausmachen. Während viele andere Erntemethoden, wie Filtration oder Zentrifugation energie- und arbeitsintensiv sind, stellt die Flokkulation-Sedimentation eine einfache und effiziente Alternative dar.

Die betreffenden Experimente wurden mit der Mikroalge *Scenedesmus obtusiusculus* A189 durchgeführt, welche erst kürzlich isoliert wurde und sowohl hohe Wachstumsraten als auch hohe Lipid und Kohlenhydratanteile aufweist. Die Kultivierungen wurden in künstlichem Brackwasser durchgeführt, welches aufgrund der hohen Ionenstärke und höheren Dichte eine besondere Herausforderung für die Flokkulation-Sedimentation darstellt. Der Fokus der Arbeit liegt auf nicht-steriler Kultivierung, wie sie während der *open pond* Kultivierung vorkommt.

Auf die Effekte und Beziehungen verschiedener Faktoren auf die Flokkulationseffizienz (FE) und die aus der Interaktion der betreffenden Faktoren entspringende Komplexität wurde experimentell eingegangen. Zusammengefasst ist modifiziertes Tannin, welches bisher als Flokkulationsmittel kaum beschrieben wurde, vergleichbar zum weitaus etablierteren Chitosan. Die pH-Unabhängigkeit und der geringere Preis qualifizieren modifizierte Tannine als besonders vielversprechende Alternative. Des Weiteren wurden trotz gleichem

mechanistischem Ansatz zwischen den beiden beschriebenen Flokkulationsmitteln synergistische Effekte gefunden.

Vollständig unabhängig von zugefügten Polymeren kann Autoflokkulation über einen *pH-shift* ins Basische induziert werden. FEs von mehr als 96% wurden mit $Ca(OH)_2$ erreicht, was in Kosten von etwa $40 pro Tonne Algenbiomasse resultierte. Dies ist vergleichbar mit früheren Studien, in denen jedoch weniger produktive Algenstämme in Frischwasser kultiviert wurden. Die Änderung des pH-Wertes auf die benötigten, basischen Werte impliziert jedoch Herausforderungen bei der Rezyklierung des Mediums, die bei der Nutzung biologischer Polymere weitaus weniger prägnant sind.

List of related articles

The following related articles were generated during the thesis:

[1] Bracharz, F., Beukhout, T., Mehlmer, N., & Brück, T. (2017). Opportunities and challenges in the development of *Cutaneotrichosporon oleaginosus* ATCC 20509 as a new cell factory for custom tailored microbial oils. Microbial cell factories, 16(1), 178.

[2] Bracharz, F., Redai, V. Bach, K. Qoura, F. & Brück, T. (2017) The effects of TORC signal interference on lipogenesis in the oleaginous yeast *Trichosporon oleaginosus*. *BMC Biotechnology* in print

[3] Görner, C., Redai, V., **Bracharz, F**., Schrepfer, P., Garbe, D., & Brück, T. (2016). Genetic engineering and production of modified fatty acids by the non-conventional oleaginous yeast *Trichosporon oleaginosus* ATCC 20509. *Green Chemistry*. 18, 2037-2046

[4] Kourist, R., **Bracharz, F**., Lorenzen, J., Kracht, O. N., Chovatia, M., Daum, C., ... & Grigoriev, I. V. (2015). Genomics and Transcriptomics Analyses of the Oil-Accumulating Basidiomycete Yeast *Trichosporon oleaginosus*: Insights into Substrate Utilization and Alternative Evolutionary Trajectories of Fungal Mating Systems. *mBio*, *6*(4), e00918-15.

[5] Brück, W., **Bracharz, F**., Brück, D. W., & Brück, T. B. (2015). Von der Krebsschale in die Creme. *Biologie in unserer Zeit*,*45*(3), 160-167.

Sections containing previously published data

Sections of paper [2] (The effects of TORC signal interference on lipogenesis in the oleaginous yeast *Trichosporon oleaginosus*, BMC Biotechnology) were introduced into sections 2.3.5.4, 2.3.7.2 and 2.4.6 as well as Supplemental 26-29 of this thesis.

Contributions of the respective paper were as follows:

FB, VR and TB conceived the study and participated in its design and coordination. FB, VR, KB carried out the experimental work relating to the effects of rapamycin on Trichsporon oleaginosus growth. FQ supervised the experimental work and prepared scientific reports. FB carried out detailed bioinformatic studies to reconstruct the cell signaling pathways involved in rapamycin addition to the cultivation medium. The manuscript was drafted by FB and finalized by TB. The final manuscript version was approved by all authors.

Sections of paper [1] (Opportunities and challenges in the development of Cutaneotrichosporon oleaginosus ATCC 20509 as a new cell factory for custom tailored microbial oils) were introduced into in section 2.1.3- 2.1.6 in this thesis.

Contributions of the respective paper were as follows:

FB conceived the review in its design. TB contributed information about phylogeny microbial and biochemical properties associated with the genus. The manuscript was drafted and finalized by all authors. All authors read and approved the final manuscript.

Raw data from sections 2.4.1, 2.4.4, 2.4.5, 2.4.8 and 3.4 were at least in part obtained by students in the course of internships or during Bachelors' or Masters' Theses. Details are given in the respective sections.

Table of Contents

List of Symbols and Abbreviations

(v/v)	Volume per volume	LPA	Lysophosphatidic acid
(*w*/*w*)	Weight per weight	MetOH	Methanol
µg	Microgram	mg	Milligram
µL	Microliter	min	Minutes
µM	Micromolar	ml	Milliliter
ACAT	Acyl-CoA:cholesterol acyltransferase	mM	Millimolar
ACL	ATP-citrate lyase	MNM C	Minimal nitrogen medium fermentation
ACS	Acyl-CoA synthase	MNM S	Minimal nitrogen medium standard
ADT	Acyl-DHAP reductase	NAD	Nicotinamide adenine dinucleotide
AGAT	Acyl-G-3-P acyltransferase	NADP	NAD phosphate
AMP	Adenosine monophosphate	NCBI	National Center for Biotechnology Information
AMP	Adenosine monophosphate	ng	Nanogram
Ara	Arabinose	NHEJ	Non-homologous end joining
ATCC	American Type Culture Collection	OD_{600}	Optical density
ATMT	*Agrobacterium tumefaciens* mediated transformation	OriV	Origin of replication V
ATP	Adenosine triphosphate	PA	Phosphatic acid
bp	Basepair	PAGE	Polyacrylamide gel electrophoresis
Cas	CRISPR -associated	PAM	Protospacer adjacent motif
cDNA	Coding DNA	PAP	Phosphatidate phosphatase
CFU	Colony forming units	PCR	Polymerase chain reaction
CoA	Coenzyme A	PEG	Polyethylene glycol
CRISPR	Clustered regularly interspaced short palindromic repeats	PUFA	Poly unsaturated fatty acid
crRNA	CRISPR RNA	RGR	Ribozyme-gRNA-Ribozyme complex
DAG	Diacylglycerol	rpm	Revolutions per minutes
DF	dilution factor	s	Seconds
Dga	Diacylglycerol acyltransferase	SBB	Sudan black B
DHAP	Dihydroxyacetone phosphate	SCO	Single cell oil
DHAPAT	DHAP acyltransferase	SDS	Sodium dodecyl sulfate
DMP	Dimetoxypropane	S-IMAS	Solid induction medium with acetosyringon
DMSO	Dimethyl sulfoxide	TAE	TRIS-Acetat-EDTA
DNA	Deoxyribonucleic acid	TAG	Triacylyglycerol
dNTP	Desoxynukleosidtriphosphate	TCA	Trichloro acetic acid
DSMZ	Deutsche Sammlung von Mikroorganismen und Zellkulturen	T-DNA	Transfer DNA
DTT	Dithiothreitol	TFA	Total cellular fatty acid content
EDTA	Ethylenediaminetetraacetic acid	TOR	Target of rapamycin
EMS	Ethyl methanesulfonate	TORC	TOR complex
ER	Endoplasmic reticulum	tracrRNA	Transactivating CRISPR RNA
EtOH	Ethanol	Tris	Tris(hydroxymethyl)aminomethane
FAME	Fatty acid methyl ester	tRNA	Transfer RNA
FI	Arbitrary fluorescence units	VLC	Very long chain

FID	Flame ionisation detector
G3P	Glycerol-3-phosphate
Gal	Galactose
GAT	Glycerol-3-phosphate acyltransferase
GC	Gas chromatography
GDH	Glycerol-aldehyde-3-phosphate dehydrogenase
Glc	Glucose
GPD	Glyceraldehyde-3-phosphate dehydrogenase
gRNA	Guide RNA
h	Hour
hph	Hygromycin B resistance gene
IDH	Isocitrate dehydrogenase
kB	Kilobasepairs
L	Liter
Lac	Lactose
LB	Lysogeny broth
VLCPUFA	Very long chain poly unsaturated fatty acids
Xyl	Xylose
YFP	Yellow fluorescent protein
YPD	Yeast extract peptone dextrose
HR	Homologous recombination
FDBM	Final dry biomass concentration
FA	Fatty acid
CCD	Central composite design
YM	Yeast and mold medium
FACS	Flourescent activated flow cytometry
PTFE	Polytetrafluorethylene
FE	Flocculation efficiency
DLS	Dynamic light scattering
AOM	Algae organic matter
RSD	Response surface design

1 General Introduction

1.1 Context

The second law of thermodynamics states, that the total entropy of a closed system always increases over time. Thus it appears to be the nature of the universe to follow a stream of increasing entropy towards a state in which all energy is equally distributed, a scenario termed “heat death of the universe”. Seeing life from this perspective entails, that living organisms are local, spatially restricted entities, which maintain a low-entropy zone in respect to their environment. This is achieved either by the dissipation of heat (enthalpy-driven growth) or generation of products with lower entropy than their substrate (entropy-driven growth)[1].

Inside this low entropy zone created by organisms, conditions for chemical reactions are emerging, which would be impossible or at least infinitely improbable to occur by chance in an environment without life. It appears obvious to harness these mechanisms for the benefit of humankind. Owed to the high complexity and small component size of living systems, for most of human history they were considered as black boxes, often “inspirited” by a supreme, non-material force. However, this did not stop knowingly or unknowingly applying biotechnology, such as the principles of mutation and selection in agriculture or fermentation processes[2].

Nowadays, one of the most demanding technological and social tasks is the transition from a society with wasteful and linear production streams to one with cyclic streams and sustainable resource management. This includes issues of energy supply and replacing fossil oil-derived products. In the long term, decreasing supply of these products will cause raising prices for oil, gas and associated commodities. However, with rising prices, more and more invasive technologies (fracking or oil sand mining) are employed. So far, the devastating ecological effects of these methods are not factored into the price of the resulting commodities and limits to exploitation of natural resources are only given by political or social intervention.

Accordingly, technological innovations for facilitating a more sustainable way of living are required. This thesis focuses on questions in regards to the production of low value products from microbial organisms by addressing lipid accumulation in *Cutaneotrichosporon oleaginosus* and energy efficient harvest of the algae *Scenedesmus obtusiusculus*.

1.2 ABV Consortial research project

The work described in this thesis was conducted as part of the work on the “Advanced Biomass Value” (ABV) research project. The goal of the project was the development of an integrated biorefinery, which operates ecologically, economically and without the generation of waste streams. The process can be broken down into two main process streams: The production of high value lubricant additives as well as a low value alkane mix suitable for usage as aircraft fuel (Figure 1).

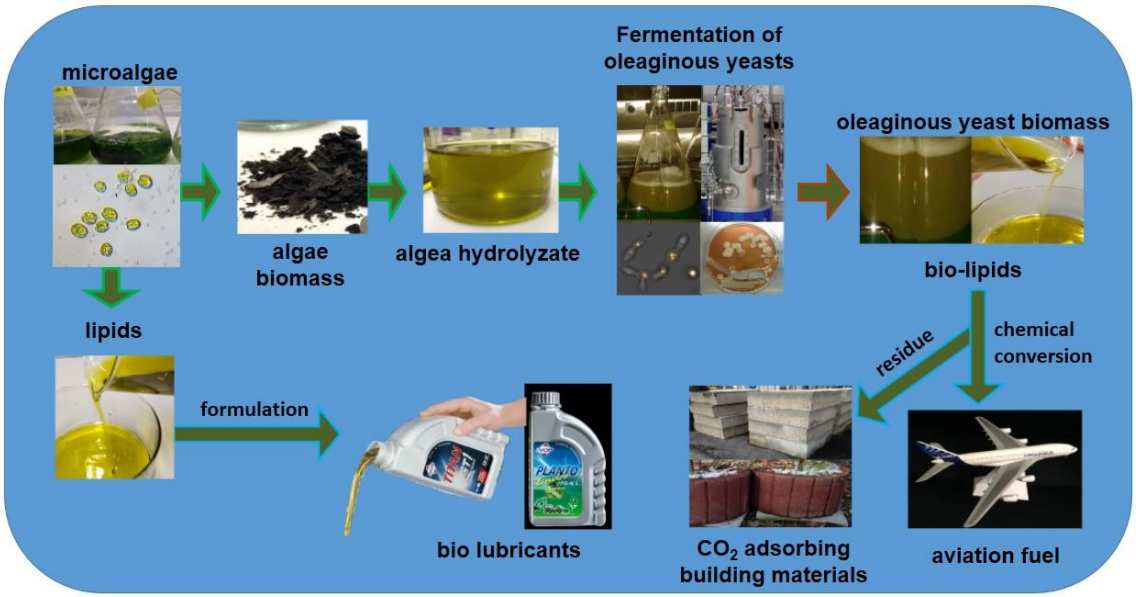

Figure 1: Structure of the ABV Process

The basis of the project is the generation of algal biomass by growth in closed circuit reactors. The extraction of lipids via supercritical CO_2 avoids the use of toxic solvents. Enzymatic functionalization of the generated lipids facilitates the usage of tailor-made lipid profiles, which can be adapted for different application fields.

The remaining algal biomass is enzymatically hydrolyzed and used as substrate for oleaginous yeast. The very high lipid content of these yeast enables the direct transformation of generated biomass to alkanes using thermocatalytic means. Residues of these processes are used as CO_2 adsorbent building materials.

2 Screening and Characterization of Oleaginous Yeast

2.1 Introduction

2.1.1 Oleaginous Organisms

First descriptions of lipid accumulating microorganisms date back more than 100 years[3]. Making use of a somewhat arbitrary threshold, which dates back to a paper by Ratledge[4], organisms exceeding a triacylglycerol (TGA) content of 20% w/w dry biomass are referred to as oleaginous. Single celled oleaginous species are found in fungi (both yeasts and molds), bacteria and both pro- and eukaryotic algae[5], [6], and can exhibit lipid contents of more than 80% w/w lipids[7]. The first more in-depth research was done in Germany with the goal of commercial, large scale production of microbial oil as fuel replacement, especially during world war I and II[8]. During that time, it was found that lipid accumulation was not a constitutive feature, but an adaptive reaction to certain environmental conditions. For oleaginous organisms, an environment which is abundant in a carbon source, usually carbohydrates, but lacks nutrients such as phosphorus, nitrogen, iron or sulfur, making proliferation impossible, the organism reacts by converting the excess carbon into fatty acids and incorporating them into triglycerides. Those triglycerides are stored in specialized organelles, lipid bodies (also known as lipid droplets, oil bodies or adiposomes). However, they are not to be confused with liposomes, which are confined by a phospholipid double layer, whereas lipid bodies display micelle-like monolayers)[9].

As nitrogen is commonly the easiest nutrient to deplete for heterotrophic organisms and yields the most prominent effects[5], [6], [10], [11], nitrogen deficient media are used in most cases to induce lipid accumulation. To quantify and evaluate this effect, the Carbon to Nitrogen ratio (C:N ratio) of the medium was consulted, leading to the insight, that with increasing C:N ratios, the lipid share is increasing. In contrast, under very strong nitrogen limitation, lipid yield suffers from the small amount of biomass[12].

Consulting the C:N ratios, under defined conditions, process modeling can be done with decent accuracy, however this approach does not do justice to the complexity of factors involved in the process of lipid accumulation. Oxygen supply, carbon source, the form in which the nitrogen is supplied to the cell (protein, amino acid, ammonium or urea), or the absolute concentration of available carbon source strongly impacts on lipid productivity as well[13].

Compared to plant oils, lipids from microorganisms (or single cell oil, SCO) have a number of favorable properties: They can be produced in much shorter production cycles independent of

seasons or weather[6] and exhibit higher lipid yields, thus generating smaller waste streams. They also do not compete with food crop for land, avoiding the “food vs. fuel” dilemma of first generation biofuel[14]. Hence, SCOs are considered a second generation biofuel, as they are using inexpensive and sustainable bio-based feedstock or possibly waste streams[15].

In recent years, there has been an increasing interest in oleaginous organisms (Figure 2), however there is so far no process, which allows for economic SCO production.

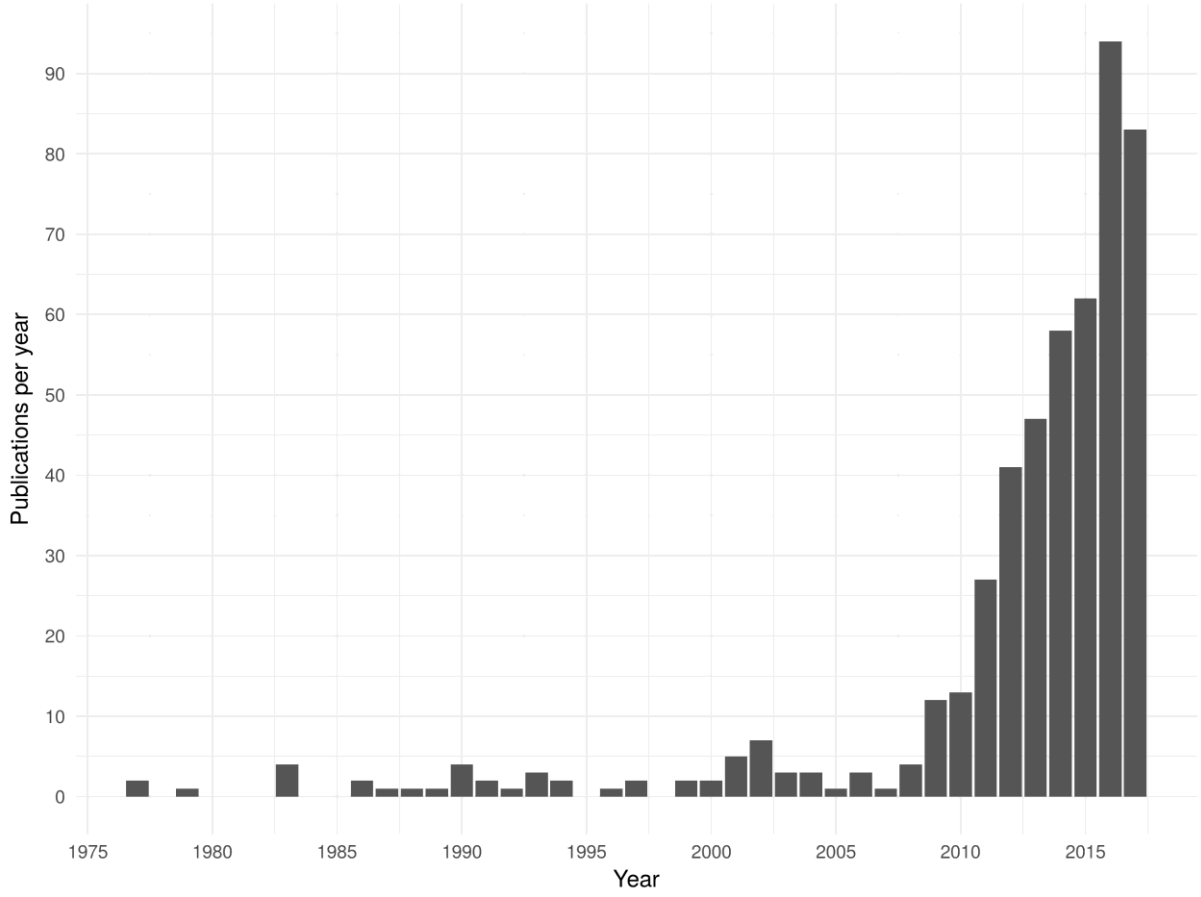

Figure 2: Number of publications with term “oleaginous yeast” as found on Pubmed[16] *per year.*

Even when employing very low cost substrates, competing with fossil resources for the generation of a dedicated energy-use product will not be possible for SCO derived processes in the near future. However high-value fats and specialty products, especially considering increases in genetic accessibility of uncommon yeasts, could be viable in the intermediate term[17].

2.1.2 Mechanism of Lipid Accumulation

The main pathway of lipid production is universally found in all lipid accumulating cells, from bacteria to human adipocytes[18] (Figure 3). However, triglyceride synthesis itself is not essential in *Saccharomyces cerevisiae*. A clinical trial for Pradigastat, a Diacylglycerol-acyltransferase (DAGAT) inhibitor has recently ended successfully[19]. An application for the treatment of obesity is made unlikely by side effects involving the digestive tract[20].

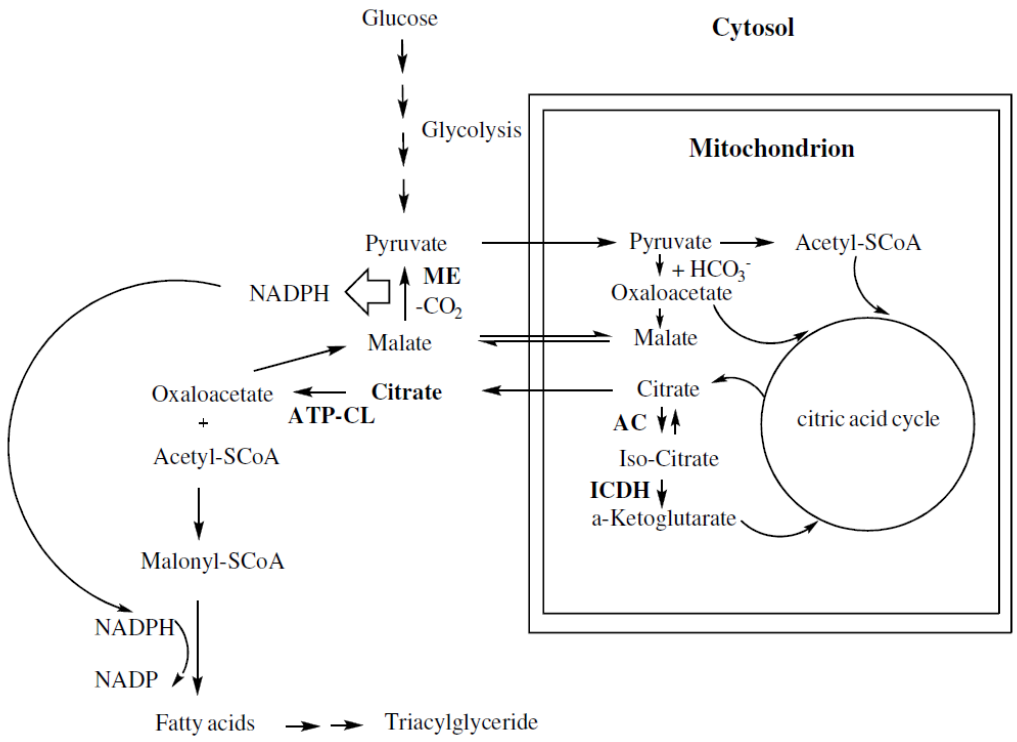

Figure 3: Overview of central metabolic pathways relevant for lipid production in oleaginous yeast. Enzyme abbreviations: ACL, ATP-citrate lyase; ICDH, iso-citrate dehydrogenase; ME, malic enzyme. Figure adapted from Goerner[21] *and Aggelis*[22].

The main pathway for lipid catabolism leads over glycolysis, where glycerol for the triglyceride backbone is generated, as well as the citric acid cycle. It is postulated, that nitrogen starvation leads to an increase in AMP deaminase activity, which brings the citric acid cycle to a halt, leading to an accumulation of citrate within the mitochondrion, which is then transported out of the cell with a citrate/malate antiporter. Cytosolic citrate is converted to Acetyl-CoA by the enzyme ATP-citrate lyase. This enzyme has been found in all lipid accumulating organisms and appears to be essential for this phenotype. Acetyl-CoA is then fed into the fatty acid synthase complex, after which the resulting fatty acids are sometimes elongated and desaturated. The modified fatty acids are added to the glycerol backbone in 4 distinct steps

occurring at the endoplasmatic reticulum (ER). SNARE-like proteins then facilitate the budding of the lipid droplets from the ER[22].

As oleaginous yeasts are poorly characterized in comparison to e.g. *Saccharomyces cerevisiae*, little is known about the regulatory framework behind lipid accumulation, and no evidence on the protein level has so far been obtained. However, much can be inferred from *S. cerevisiae* research and TORC (target of rapamycin complex) related pathways play a key role in lipid accumulation. TORC components, some of which are strongly conserved from yeast to mammals, have been found in *Yarrowia lipolytica*[23] and *Cutaneotrichosporon oleaginosus*[24].The TOR complex is a central controlling complex of cell proliferation and homeostasis. It processes information about the current status of the cell, possible energy or nutrient deficiencies. It is active in favorable growth conditions, but is inhibited when for example nitrogen supply is depleting[25]. TORC1 can therefore be assumed to be the crucial element for lipid accumulation regarding cell signaling. TORC2 on the other hand functions as a controller of cell polarization the cytoskeleton and is also closely tied into control of proliferation. However, it is not sensitive to rapamycin and its signaling inputs are so far poorly characterized.

2.1.3 Cutaneotrichosporon oleaginosus

2.1.3.1 Origin and Phylogeny

C. oleaginosus was isolated by Moon *et al*. in 1987 from samples taken from factory drains of the Iowa State University Dairy Farm[26]. It was deposited under the name *Candida curvata* D at the American type culture collection, and since then was reclassified to *Apiotrichum curvatum*[12], *Cryotoccus curvatus*[27], *Trichosporon cutaneum*[28] and since 2011 as *Trichosporon oleaginosus*[29]. Liu *et al*. published a comprehensive phylogenetic study of the Tremellomycetes[30], placing *T. oleaginosus* in the genus of *Cutaneotrichosporon* while keeping its epithet. *C. oleaginosus* forms basidiocarps, sexual reproduction and ethanol fermentation are, like for any other species of this genus, not observed[31]. It also grows in filamentous form, presumably in nature preferred as filamentous fungus in soil and on leaf litter[32]. The GC content of the genome is high with 61%[24] and the organism is strongly adapted to changing nutrient supply, as oleaginous properties and very low maintenance energy show [12], [33], [34].

2.1.3.2 Substrate Spectrum

C. oleaginosus does not grow on cellulosic material and in general on untreated, polysaccharide-based substrates[35]. Predicted cellulases[24], are presumed to only be of intracellular relevance. However, it readily utilizes glucose, galactose, cellobiose, xylose,

sucrose, lactose as carbon source[36]–[38]. Liang *et al*.[36] reported depletion of arabinose in *C. oleaginosus* cultivation medium, but Meo[39] showed that arabinose titers decrease very slowly and the sugar is not used for generation of biomass. The results suggest that *C. oleaginosus* is suffering from arabinose transporter deficiency[40] and/or cofactor imbalance of arabinose oxidoreductase pathway[41]. The strain is able to metabolize ammonium, nitrate[42] and urea[24], [43] up to a concentration of 1 g/l without sacrificing for growth[44].

Furthermore, the yeast is able to metabolize glycerol[45] even from industrial origin[44], N-acetylglucosamine[46], volatile fatty acids[42] and ethanol and able to metabolize 4-hydroxymethylfurfural[36]. The related *Candida sp.* can also use n-alkanes as carbon source, but this has not yet been shown for *C. oleaginosus*[47]. Regarding the biochemistry of substrate utilization only two lactose hydrolases were studied more in depth, yielding that *C. oleaginosus* contains a high activity, highly specific beta-galactosidase requiring metal ions as cofactors as well as a cofactor-independent lower activity and lower specificity beta glycosidase[48].

2.1.3.3 Substrate Preferences

In batch experiments, Meo[39] found the highest biomass yield with mannose as substrate, followed by galactose and glucose. Xylose and arabinose showed significantly lower biomass and lipid yield. No diauxic effect between hexose sugars has been observed so far[39], [49]. Indeed, a mixture of sugars leads to higher substrate assimilation- and maximum growth rates than individual sugars[39]. However in the presence of mannose and glucose, metabolization of galactose was somewhat delayed[39] and in the presence of glucose, xylose consumption was greatly decreased[50]. In flask experiments glucose, mannose and xylose resulted in comparable lipid content, however the lipid yield was highest with glucose followed by mannose and xylose. Again, xylose and galactose resulted in lower biomass and lipid yield. In chemostat experiments with single carbon sources, xylose was the most suitable sugar to achieve high lipid yield followed by lactose and sucrose[38]. However, Görner *et al*. found lipid productivity with xylose to be significantly better than with glucose or N-acetyl glucosamine, both of which were comparable[51]. This hints at possible metabolization by phosphoketolases, which would yield 1.3 mol AcCoa / 100 g xylose as opposed to 1 mol AcCoa / 100 g xylose over the pentose phosphate way. Over glycolysis, 1.1 mol AcCoa can be generated from 100 g glucose[52]. In general, metabolic flux from lactose or xylose as carbon source to lipid appears to be less favorable[53], but this likely depends on the presence of further carbon sources and possibly cultivation conditions. Preferred carbon source for lipid accumulation were asparagine and urea, which yielded higher lipid than yeast extract[44].

In *R. toruloides*, lipid accumulation can be induced by nitrogen, phosphate or sulfur starvation[54]–[56]. Meo[39] evaluated these limitations by employing different C:N, C:P and

C:S ratios in fed batch cultivations in two phases. In the first phase, limitation ratios of batch media were varied, whereas in the second phase, limitation ratios of feed were changed. C:N ratios of batch media between 5 and 20 g/g showed no strong variation. Maximum lipid content was observed at C:N of 15 g/g. For subsequent feeding of this culture, C:N ratios showed to have a significant impact. Whereas lipid content decreased moderately with decreasing C:N ratio, there was a strong decrease between C:N 75 g/g (48% g/g lipids per biomass) and C/N 50 g/g (21% g/g lipid content). This is supported by results from Park *et al*.[57], whereas Ykema *et al*. found the critical C:N ratio at 11 g/g. Variation of C/S or C/P ratios of batch media also had little impact on lipid content and no lipid accumulation was induced by sulfate limitation (max 15% g/g lipid content after feeding). A C:P ratio of 702 g/g was sufficient for the accumulation of 40% g/g lipids, but subsequent feeding required absence of phosphate for cells to remain at this level.

Described pH optima for lipid yield differ vastly between 4.8[58] and 7[42], owing to the wide spectrum of substrates (natural, semi-defined and synthetic) and fermentation modes. In synthetic media, small differences in pH between 5 and 6, values which are most commonly used for cultivation, have no significant effect on lipid production[39].

There is no comprehensive model capable of predicting biomass yield and lipid content for *C. oleaginosus* grown in arbitrary complex media. Solely relying on carbon source concentration and C:N:S:P ratio for predictions is insufficient for this task as interaction effects with other fermentation parameters and concentrations of media constituents are likely (see linear modeling).

2.1.3.4 Growth Inhibition

Acidic saccharification of natural, polymeric substrates is accompanied by the generation of inhibitory byproducts[59]. These comprise weak organic acids, furan derivatives and phenolic compounds[60]. *C. oleaginosus* has been shown to be resistant against some of these compounds and proliferated comparatively well growth in non-detoxified hydrolysates[61].

Growth is significantly inhibited by 1 g/l furfural[61] to 20% w/w final dry biomass (FDBM) compared to the control, however at higher concentrations, FDBM remains constant[53]. Inhibition by HMF, polyhydroxybutyrate (PHB) and syringaldehyde is low at 1 g/l (<5% w/w FDBM), whereas vanillin at the same concentration reduces FDBM by 20% w/w at 1 g/l and 40% w/w at 1.5 g/l. Volatile fatty, despite their general suitability as substrate, impair growth at moderate concentrations (43% w/w FDBM reduction at 5 g/l for acetic acid[62]). Up to 40 g/l potassium acetate (KAc), only growth rate and lag phase, but not final biomass are impaired[63]. Glycerin concentrations beyond 20 g/l[64] and 100 g/l glucose (Data not published) are inhibitory, maximum growth rate decreases by 20% at concentrations of 100 g/l

glycerin and 80% at 150 g/l[44]. High initial pH appears to lead to an increase in lag phase duration[63].

Lipid content (LC) is impacted in a similar way as FDBM. Furfural reduces LC to 40% w/w compared to the control, reduction of LC by PHB and syringaldehyde are below 5% w/w. Inhibition of both growth and lipid content can depend on substrate utilization: Grown on glucose, 1 g/l vanillin reductions of 22% w/w FDBM and 10% w/w LC were observed. With xylose as main carbon sources, the reduction was 30% w/w FDBM and 22% w/w LC[53]. In the presence of inhibitors, an inoculum of 10% v/v of overnight culture is recommended.

2.1.3.5 Cell Wall and Sugars

The cell wall of *C. oleaginosus* consists mostly of neutral carbohydrate (63% w/w), the remainder is comprised of protein (11% w/w), glucosamine (9% w/w) and glucuronic acid (13% w/w)[32]. The comparatively low amount of neutral carbohydrates compared to other yeasts (*S. cerevisiae*: 80-90% w/w[65], *C. albicans*: 80% w/w[66]) combined with the high amount of chitin are characteristics, which are more typical for cell walls of filamentous fungi. Mannose content is significantly lower than for *S. cerevisiae* and content of uronic acids is unusually high for fungi in general. The cell wall is susceptible to digestion by Novozyme 234[67].

It is known that yeasts can accumulate large amounts of disaccharides, trehalose or polysaccharides such as glycogen or pullulan[68]. With increasing limitation, lipid content as well as carbohydrate content in *C. oleaginosus* increase[12]. However, lipid accumulation continues even in the stationary phase and is accompanied by decrease in intracellular carbohydrates[69]. The main notion is that, not as previously hypothesized[12], glucose (or any corresponding carbon source) uptake is the rate limiting step for lipid production, but that the subsequent conversion to fatty acids is the main bottleneck. This leads to accumulation of sugars in the cell, which act as a “short term” storage product[70]. No studies have further qualitatively characterized these sugars. However, amongst the highly upregulated genes under nitrogen limiting conditions is an Endoglucanase[24] (Triol1|310356), possibly associated with the decomposition of intracellular polysaccharides.

2.1.3.6 Fatty Acid Content

Temperature had no significant effect on the fatty acid (FA) spectrum of *C. oleaginosus* between 27 and 33°C in liquid medium[71]. However grown at 15°C on solid medium, FA content shifts towards longer chain and higher unsaturated fatty acid content[72]. No differences were found between cells grown at pH 6 and 7, whereas at pH 8 the concentration of C18:0 and at pH 9 concentrations of C16:0 and C18:2 were increased[63]. In comparison to glucose as carbon source, FA content was strongly shifted in favor of C18:2 when galactose or arabinose were used. FA spectra of cells grown on cellobiose, mannose and xylose were not significantly different from those grown on glucose[53]. In different carbon sources,

presence of inhibitory hydrolysis byproducts (furfural, PHB, syringaldehyde and vanillin) shifted the FA spectrum on average away from C16:0, C18:0 and C18:1 towards C18:2[53]. A similar effect was observed for ammonia as nitrogen source as compared to nitrate[42]. Using volatile fatty acids (VFAs) as substrate on average decreased the amount of C18:2 and using propionate as substrate made the generation of odd-numbered fatty acids such as C17:0 or C17:1 possible[42], which are usually not found in yeast. FA desaturase inhibitors were used to modify the FA spectrum in a related strain[73], but not yet in *C. oleaginosus*. The same applies to oxygen starvation during lipid production phase, which is reported to modify fatty acid content in different oleaginous yeasts[74]. Effects of different genetic modifications on FA distribution in *C. oleaginosus* are shown in Supplemental 2.

2.1.3.7 Mechanism and Regulation of Lipid Accumulation

Relevance of citrate has described early as part of the “standard model” of lipid accumulation by Ratledge[68]. Fatty acid synthesis requires Acetyl-CoA (AcCoA) and Malonyl-CoA. AMP-dependent isocitrate dehydrogenase (IDH) shows activity at very low AMP concentrations, as they are present during nitrogen limitation[75]. Citrate accumulates in the mitochondrion and is exported into the cytosol via a citrate/malate antiporter. ATP-citrate-lyase cleaves citrate to acetyl-CoA and oxaloacetate, which is reintroduced into the citric acid cycle[68]. Presence of ACL is considered a defining feature of oleaginous yeasts[76], but non-oleaginous strains with ACL have been described[4]. Supply of NADH has not been fully elucidated, but both introduction of glucose-6-phosphate (by glucose-6-phosphate dehydrogenase, G6PDH) into the pentose phosphate way and shunting of pyruvate to oxaloacetate by malic enzyme are likely sources of reducing equivalents.

Kourist *et al*.[24] described a transcriptomic analysis of in *C. oleaginosus*, comparing nitrogen limited medium containing glucose as carbon source with full complex medium. Amongst the most strongly upregulated genes were amino acid and ammonium transporters, many proteases were upregulated to facilitate the recycling of nitrogen in nonessential peptides and proteins. Within central nitrogen metabolism, equilibrium shifted away from ammonium and glutamine towards glutamate, which in turn is responsible for nitrogen supply to non-essential amino acids over transamination. The mitochondrial isocitrate exporter (Triol1|270035) was not upregulated and hence the export of citrate to cytosol is most likely not a rate limiting step.

Supply of Acetyl-CoA (AcCoA) and Malonyl-CoA (MaCoA) for lipid synthesis was ensured by upregulation of ATP-citrate lyase (ACL) and AcCoA-Carboxylase (ACC). The two constituents needed for the production of fatty acids are processed by fatty acid synthases (FAS1, FAS2): Both genes were upregulated. NADPH supply required for FA synthesis was most likely served over G6PDH, as glucose-6-phosphate dehydrogenase was upregulated, but malic enzyme (Triol1|326761) was not.

The detection of lipid stress and relevant cell signaling pathways were addressed in detail by Bracharz *et al*. Target of rapamycin complexes (TORCs) were identified as central, conserved integrators of stress signals. Involvement of TORC1 in response to nutrient stress was confirmed by inhibition with rapamycin, leading to a raise in lipid content and a shift in fatty acid spectrum towards a pattern typical for nitrogen limitation. A homology based TORC signaling network assembled by the authors indicates, that cell signaling response to carbon depletion is conserved, whereas response to nitrogen limitation and autophagy are not.

2.1.4 Fermentations of *Cutaneotrichosporon oleaginosus*

2.1.4.1 Chemostat, Batch and Fed-Batch

As *C. oleaginosus* was isolated from a dairy farm, many earlier publications focused on whey or whey permeate as substrate, achieving between 0.13 g/l culture/hour for batch experiment and 0.38 g/l/h for chemostat cultivation. Highest lipid productivities were commonly between 0.4 and 0.6 g/l/h, 1 g/l/h for chemostat with partial recycling appears to be an outlier. Fermentation pH was mostly set between 5 and 6 (see substrate and growth preferences) whereas temperature was almost kept at 30°C. Lipid yield was around 16 ± 8.4 g/ 100 g substrate on average while stoichiometric maximum of lipid yield is 33 g lipids / 100 g sugar[77]. Average lipid content was at 39.3 ± 14.4 with a maximum of 74% w/w and lipid production was at 14.3 ± 11.8 g/l with a maximum of 49 g/l. Average lipid production was higher at samples quantified by GC/FID (17.1 g/l) in comparison to gravimetric measurements (11.4 g/l), which was however not significant at α=0.05. Single-stage continuous fermentation requires shorter average residence time than batch fermentation for sugar utilization[78] and showed on average higher lipid productivity. An overview of *C. oleaginosus* fermentations reported in literature can be found in Supplemental 1, Supplemental 2 and Supplemental 3.

If applied properly, statistical design of experiments and linear models can be suitable tools for finding interacting independent variables or making predictions about yield. Using a Plackett-Burman design, Zheng *et al*.[79] tested the influence of different media supplements and cultivation parameters on *C. oleaginosus* FDBM with H_2 producing sludge as substrate. Acetate concentration had the strongest positive impact on FDBM, followed by pH, EDTA content (Metal limitation) and pH. Increasing concentrations of ammonium chloride, magnesium sulfate and peptone had a negative effect. Significant dependent variables were picked for a central composite design (CCD), but as effects of single dependent variables are confounded with higher order effects in the screening, not all significant factors might have been included. From the CCD, almost only found linear effects and two way interactions: Effects of ammonium chloride and acetate concentration were interacting with pH, ammonium chloride effect further interacted with acetate and EDTA with magnesium sulfate. Model quality is questionable, as experimental confirmation fit poorly with the predicted FDBMs.

Vega *et al*. optimized FDBM of *C. oleaginosus* on banana juice[80] containing 25% w/w sugars. A second order CCD was employed to find optimal pH, concentration of substrate as well as asparagine and yeast extract supplementation. The factors initial pH (4.8-6.2) and asparagine concentration (15-255 mg/l) were not significant. Factor yeast extract was only significant at juice concentrations under 19% v/v, indicating a lack of nutrients in the juice. Optimum growth was achieved at 21% v/v juice (5% w/w sugars), beyond which growth was impaired. In a 2-level full factorial design, method of sterilization, aeration plug and all previous variables were

used as factors. Significantly higher yields were obtained with filter sterilization over autoclaving and milk filters over dispo plugs. With a 2 factor second order CCD, interaction effect between cultivation temperature and substrate concentrations were found: As juice concentration is increased, the optimal temperatures decreased.

Cui *et al*. used a Box-Behnken design to estimate effects of substrate (glycerol) concentration, pH and temperature on lipid productivity[64]. Both glycerol concentration (10-30 g/l) and temperature (27-33°C) had more significant effects on biomass yield than pH (5-6). At pH 6, temperature optimum was 30°C and optimal glycerol concentration was 20 g/l. For biomass, the significant factors were glycerol (negative), glycerol quadratic (negative), temperature (negative) and the interaction effect between temperature and pH (positive). For the lipid content pH (positive), glycerol (negative) and glycerol quadratic (negative) were significant factors. The optimum was positioned at pH 6, 20 g/l glycerol and 30°C. Experimental confirmation fit well with predicted cell dry weight and lipid content.

2.1.4.2 Other Modeling

Ykema *et al*.[12] used a kinetic model to predict lipid production in a chemostat using semi-defined medium and glucose as substrate in dependence of dilution rate and C:N ratio. The model predicted lipid production in dependence of C:N ratio well, but did not capture the dynamics of carbohydrate content. Due to its scope, dependence of productivity was modeled only in dependence of few parameters and is therefore applicable only in these defined conditions. The same applies to Browns' approach [78], [81] of separating growth into three phases and modeling nitrogen, non-lipid biomass, lactose and lipids using a set of differential equations.

2.1.5 Genetic Modification of *Cutaneotrichosporon oleaginosus*

2.1.5.1 Random Mutagenesis

N-methyl-N'-nitro-N'-nitrosoguanidine (MNNG) and ICR-170 were suitable mutagens for generating amino acid auxotrophic mutants of *C. oleaginosus*, whereas mutagenesis with ethyl methanesulfonate (EMS) and UV irradiation were less successful[82]. Fatty acid and unsaturated fatty acid auxotrophs were generated by Ykema *et al*.[82], mutants were created with a modified fatty acid distributions by intraspecific spheroblast fusion with methionine auxotrophs[83]. Also, revertants were characterized for their modified FA spectrum[84] and growth on whey permeate[85]. Fatty acid mutants were also generated by mutagenesis with EMS[86] and characterized (Supplemental 2). As opposed to the description of Ochsner *et al*[67] for strain *T. dermatis* (DSM70698), plasmid transformation into *C. oleaginosus* did not yield stable transformants (data not published).

2.1.5.2 Agrobacterium mediated transformation

Görner *et al*. established a method for the stable integration of expression cassettes into the *C. oleaginosus* genome using agrobacterium mediated transformation (ATMT)[51]. Codon optimized yellow fluorescent protein was expressed using glyceraldehyde-3-phosphate dehydrogenase (GDH) promoter and the respective GDH terminator from *C. oleaginosus*. Selection was done by also expressing hygromycin b phosphotransferase (*hph* gene) from *E. coli* using a truncated GDH promoter. Following this proof of concept, different bacterial enzymes for fatty acid modification were expressed to change the fatty acid spectrum of neutral and phospholipids. The approach suffers from the fact, that the GDH appears to be downregulated in limiting conditions[24], limiting productivity of tailor made lipids in *C. oleaginosus*. So far, no other promoters for functional heterologous expression are described.

2.1.6 Model Organism *Yarrowia lipolytica*

A process of *C. oleaginosus* fermentation with whey permeate as substrate for production of triglycerides was already patented in 1980[87]. However, since then, no further attempts at commercialization have been conducted. The majority of oleaginous yeast research has been focused on the organism *Yarrowia lipolytica*, which resulted in a sizeable body of literature with over 2'400 articles. As the main metabolic paths leading to synthesis of triglycerides are highly conserved, many of the findings could be transferable to other oleaginous yeasts. However, it is becoming apparent, that the bottlenecks in these pathways are not the same: Overexpression of endogenous diacylglycerol acyltransferases or lysophosphatidic acid acyltransferase did not yield significantly higher lipid contents in *C. oleaginosus*. The lipid content of Y. lipolytica wild type is typically around 20[88]-35% w/w[89], [90].

However, this metric can be raised to 45% w/w[89] or even up to 90% w/w with sophisticated genetic engineering[91]. This also yielded in excess of 25 g l-1 lipids, a value which was achieved by cultivation of wild type *C. oleaginosus*. Further, *Y. lipolytica* requires engineering for utilization of xylose and sucrose or to overcome strong diauxic effects[92].

2.2 Materials

2.2.1 Instruments

Model	Supplier	Description
Multidrop	Labsystems	96-well Liquid Dispenser 200 µL
Multidrop	Labsystems	96-well Liquid Dispenser 2 ml
Pioneer	ohaus	Analysis Scale
	Bio-Rad	Gel Electrophoresis System
VX/VE	Systec	Autoclave
Research Plus	Eppendorf	Pipettes
KF85	Migel	Ice machine
Le1z	indecipherable	Desiccator
B180	Nabertherm	Incinerator
EmulsiFlex-B15	Avestin	High pressure homogenizer
RCT	IKA	Magnet Stirrer
GelDoc XR System	BioRad	Gel Documentation System
EKT Hei-Con	Heidolph	pH-Meter
Inova44	New Brunswick	Shaker
LaminAir HB2448	Heraeus	Sterile Bench
Comfort	Eppendorf	Thermo Mixer
Vortex Genie 2	Scientific Industries	Vortexer
Laboport	KNF Lab	Vacuum Pump
5810R	Eppendorf	Centrifuge
5424R	Eppendorf	Centrifuge
2300 EnSpire	Perkin Elmer	Fluorescence - Plate Reader
8453	hp	Photometer
Labfors 5 lux	Infors	Fermenter 5 l
dasgip ga4	Eppendorf	Fermenter 1 l
S3	BioRad	FACS
Axiolab A1	Zeiss	Fluorescence Microscope
GC-2025	Shimadzu	GC/FID System
1100 HPLC Spectrum	Agilent	HPLC System

2.2.2 Consumables

Consumable	Supplier
Syringe Filter 13 mm w 0.2 µm Nylon	Pall Life
Eppendorf tubes	Eppendorf
Erlenmeyer flasks	VWR
Falcon tubes 15ml, 50ml	VWR
Glas tubes with screw caps	Ochs
HPLC/GC Vials with screw caps	VWR
Syringes	Sarstedt
96-well Plates black and transparent	Sarstedt
Protein Ladder	PageRuler Protein Ladder
DNA Ladder	PageRuler 1kb, 100bp
Lytic Enzyme L1412	Sigma
Driselase D8037	Sigma
Herring Sperm ssDNA	Sigma
PVDF Blotting Membranes	GE Healthcare
Anti-Cas9 mAb, mouse	Thermo Fisher
Anti-mouse mAb, goat	Thermo Fisher
Cas9 Nuclease	Thermo Fisher
Clear 6 well plate	Corning
GeneJET Gel Extraction Kit	Thermo Fisher
Agarose Gel Extraction	Thermo Fisher

2.2.3 Chemicals

Chemical	Supplier
Acetone	Roth
Acetosyringone	TCI America
Agar-Agar	Roth
Agarose	Roth
Ammonium nitrate	Roth
(Di-)Ammonium sulfate $(NH_4)_2SO_4$	VWR
Ampicillin	AppliChem
Bactotryptone	Roth
Caffeine	Applichem
Calcium Chloride dihydrate	Roth
Chloramphenicol	Roth
Chloridric acid	Merck
Chloroform	Sigma
Copper sulfate pentahydrate	Roth
Dithiothreitol (DTT)	Sigma
Dimethyl sulfoxide (DMSO)	VWR
Dimethoxypropane	Roth
Driselase	Sigma
EDTA	Sigma
ERT4 resuspension buffer	Sigma
Ethanol	Roth
Ethylmethane sulfonate (EMS)	Merck
Gentamicin	Thermo Fisher
Glucose	VWR
Glycerol	Roth
Glyceryl tridodecanoate	Roth
Hexane	Roth
Lithium Acetate	VWR
Lytic Enzyme	Sigma
Magnesium sulfate heptahydate	Alfa Aesar
Malt extract	Roth
Manganese chloride tetrahydrate	Roth
Marine Oil FAME Mix	Restek
Methyl decanoate	Fluka
Nile red	Sigma
Potassium phosphate (KH_2PO_4)	Roth
PEG6000	Sigma
Sodium chlorate	Sigma
Sodium dodecylsulfate (SDS)	Roth
Sodium methoxide	Sigma
Sodium thiosulfate	Merck
Sorbitol	Sigma
Sudan Black B	Sigma
Tetracycline	Roth
Toluol	Roth
Tris HCl	Sigma

Chemical	Supplier
Yeast extract	Roth
Yeast nitrogen base	Amresco
Zinc sulphate heptahydrate	Roth

2.2.4 Strains

Organism Name	Internal Identifier	Official Identifier	Supplier
Yeast			
Saccharomyces cerevisiae	IBY001		MPI Tübingen,
Saccharomyces cerevisiae	IBY002		-
Pichia pastoris	IBY003	CBS 7435	CBS
Candida shehatae	IBY004	ATCC 22984	ATCC
Candida shehatae UV-Mutant	IBY005	ATCC 22985	ATCC
Saccharomyces cerevisiae	IBY006	Ethanol Red	-
Saccharomyces cerevisiae	IBY007	Thermosacc	Lallemand
Saccharomyces cerevisiae	IBY008	Ferm Prot	Fermsolutions
Cryptococcus curvatus	IBY009	CBS 5324	CBS
Cryptococcus aerius	IBY010	CBS 4192	CBS
Geotrichum fermentans	IBY011	CBS 439.83	CBS
Rhodosporidium sphaerocarpum	IBY012	CBS 6985	CBS
Rhodosporidium toruloides	IBY013	CBS 5745	CBS
Rhodosporidium toruloides	IBY014	CBS 5490	CBS
Rhodotorula minuta	IBY015	CBS 2177	CBS
Cryptococcus terricola	IBY016	CBS 4517	CBS
Lipomyces starkeyi	IBY017	CBS 8728	CBS
Trichosporon asahii	IBY018	CBS 2497	CBS
Candida khmerensis	IBY019	CBS 9784	CBS
Cutaneotrichosporon oleaginosus	IBY020	DSM 11815	DSMZ
Rhodosporidium toruloides	IBY021	DSM 4444	DSMZ
Lipomyces starkeyi	IBY022	DSM 70295	DSMZ
Cryptococcus curvatus	IBY023	DSM 70022	DSMZ
Xanthophyllomyces dendrorhous	IBY024/2	CBS6938	Univ. Frankfurt
Yarrowia Lipolytica Po1g	IBY025		ATCC
Yarrowia Lipolytica Po1f	IBY026		ATCC
Yarrowia Lipolytica Po1h	IBY027		ATCC
Yarrowia Lipolytica Po1t	IBY028		ATCC
Rhodosporidium Toruloides	IBY029	CBS 349	CBS
X. dendrorhous	IBY030	CBS6938	CBS
R. toruloides	IBY036	CBS14	CBS
R. toruloides	IBY037	NP11	Zhao *et al*.[93]
R. toruloides	IBY038	NP52	Zhao *et al*.[93]

Organism Name	Internal Identifier	Official Identifier	Supplier
Bacteria			
Streptomyces rapamycinicus	IBB018	DSM 41530	DSMZ
Escherichia coli		DH5a	
Escherichia coli		NEB10	NEB
Escherichia coli		XL10Gold	Agilent
Agrobacterium tumefaciens		AGL1 BAA101	DSMZ
Algae			
Scenedesmus obtusiusculus		A189	EMAU

Environmental isolates NZ and WO were obtained from Christian Görner[21]:

NZ	-Ireland, Letterkenny	-Crab Shells	-nA
WO	-Germany,Ebersberg	-Soil Sample	-48°7'52.85"N 11°58'32.29"E

2.2.5 Primers

oCas9_cas_fw	GTTACAGGTACCCCTCCTCCGGCACCATTAC
oCas9_cas_rv	GTTACAGCGGCCGCGTTACAACTAGTTGCCTCAGCACTATTCGGG
oHyg_cas_fw	GTTACAGCTAGCCCTCCTCCGGCACCATTAC
oHyg_cas_rv	GTTACAGCGGCCGCGTTACAACTAGTTGCCTCAGCACTATTCGGG
pRF_Hyg_BB_KpnI	GTTGACGGTACCTGGTGGTAATGGTGCCGGAGGAGG
pRF_Hyg_BB_LguI	GTTGACGCTCTTCCGCTTCAGAATGCACAGGTACACTTGTTTAGAGGTAATCCT
oDga2_OLpyfp_fw	TCCTCTTCTCAAAACTATTCCCCTCCTCCCAAAAATCAACTTGATCAACAATGCGGAGTACGGAGCTG
oDga2_OLpyfp_rv	TCCTCTGGTACTGCTACTGCTACGCGGAAACCATGCTACAACCTAGAAAGTCACTGACGGACACGATGGGG
nhe_spe.not_Cass_fw	GTTACAGCTAGCGGGGATTGGCGTCATCAAGT
nhe_spe.not_Cass_rv	GTTACAGCGGCCGCGTTACAACTAGTATCCGCTGACATTGGACCTTT
SLC_OL_fw	TCCTCTTCTCAAAACTATTCCCCTCCTCCCAAAAATCAACTTGATCAACAATGCCCATATCTTGGGTCCTCAAGCC
SLC_OL_rv	TCCTCTGGTACTGCTACTGCTACGCGGAAACCATGCTACAACCTAGAAAGTCACTCGGCCTTTGGTCTCTTGAGGAC
Hyg_OL_full_fw	TCCTCTTCTCAAAACTATTCCCCTCCTCCCAAAAATCAACTTGATCAACAATGAAAAAGCCTGAACTCACCGCG
Hyg_OL_full_rv	TCCTCTGGTACTGCTACTGCTACGCGGAAACCATGCTACAACCTAGAAAGTCCCGGTCGGCATCTACTCTATTCC
KanMX_fw	ATGGGTAAGGAGAAGACCCACGTTT
KanMX_rv	TCAGAAAAACTCGTCGAGCATGAGGT
ARB1	GGCCACGCGTCGACTAGTACNNNNNNNNNNGATAT
ARB2	GGCCACGCGTCGACTAGTAC
ARB6	GGCCACGCGTCGACTAGTACNNNNNNNNNNACGCC

2.2.6 RNA Synthesis

Synthesis of gRNA sequences directly as RNA was done by Microsynth. Synthesized molecules were stabilized by not further defined modification, presumably functionalization using a sugar[94].

2.2.7 Software

Software	Application
EnSpire 3.0	Plate reader
Chromeleon 2.40	HPLC
GCSolution	GC/FID
ImageLab	Gel Documentation
8453 UV-Vis	Photometer
R 3.3	Statistical Analysis and Plotting
Origin	Plotting

2.3 Methods

2.3.1 Media and Buffer

It is not uncommon to prepare and autoclave YPD in a single vessel, especially when required only as substrate for proliferation of recombinant microorganisms. For physiological studies however, this should be avoided due to formation of toxic and unpredictable compounds by Maillard reaction and caramelization[95], a form of pyrolysis. All media were prepared using bidestilled water ($_{dd}H_2O$).

2.3.1.1 Yeast Peptone Dextrose (YPD)

A 40% Glucose stock was sterilized by autoclaving. A base medium was prepared containing peptone 20 yeast extract 10 (g/l). Glucose was subsequently added to the base medium to a final concentration of 2%.

2.3.1.2 Yeast and Mold Medium (YM)

YM was prepared in the same way as YPD, however the base medium contained peptone 5 yeast extract 3 and malt extract 3 (g/l) and glucose was added to a final concentration of 1%.

2.3.1.3 Minimal Nitrogen Medium S (MNM-S)

A 40% w/v Glucose stock was sterilized by autoclaving. A base medium was prepared containing yeast extract 0.75 KH_2PO_4 0.4 and $MgSO_4x7H_2O$ 1.5 (g/l). Approximately 80% of the total required amount of water was added and the solution was autoclaved. A 10x NPS Stock (Nitrogen, Phosphate, Sulfur) was prepared containing $CaCl_2x2H_2O$ 2.2 $(NH_4)_2SO_4$ 0.012 Na2HPO4 9.1 (g/l) and autoclaved. A 1000x stock of a trace element solution based on Meesters *et al.*[45] was prepared containing $ZnSO_4x7H_2O$ 0.55 $MnCl_2x4H_2O$ 24.2 $CuSO_4x5H_2O$ 25 FeSO4 25 (g/l) and sterile filtered.

After sterilization, the base medium was supplemented with the NPS stock, the trace elements as well as glucose to a final concentration of 2%.

2.3.1.4 Minimal Nitrogen Medium S (MNM-S)

An adapted MNM-S medium for fed batch fermentations containing higher concentrations of phosphate and ammonium was prepared in the same way as MNM-S and consists of the same components, but the NPS-solution contains $(NH_4)_2SO_4$ 0.3 and Na_2HPO_4 0.91 (g/l).

2.3.1.5 LB-Miller

Base media components, tryptone 10 yeast extract 5 and NaCl 5 (g/l) were weighed, water was added and the media were autoclaved.

2.3.1.6 Agar Plates

All plates were created by adding 20 g/l agar to the base medium before autoclaving.

2.3.1.7 Agrobacterium tumefaciens medium

While routinely cultivated in LB, *Agrobacterium tumefaciens* mediated transformation was achieved in liquid induction medium containing acetosyringone, K_2HPO_4 2.05, KH_2PO_4 1.45 g/l, NaCl 0.15, $MgSO_4 \cdot 7H_2O$ 0.5 (g/l) 2-4-Morpholineethanesulfonic acid monohydrate (MES), 7.8 g/l; glucose, 1.8 g/l; as well as $CaCl_2 \cdot 2H_2O$ 67.0. $FeSO_4 \cdot 7H_2O$ 2.5, $(NH_4)_2SO_4$ 0.5 and acetosyringone 39.24 (mg/l) and glycerol 5% (v/v). A trace elements solution with Na_2MoO_4, $MnSO_4 \cdot H_2O$, $ZnSO_4 \cdot 7H_2O$, $CuSO_4 \cdot 5H_2O$ (100 mg each) H_3BO_3 in 1L ddH20, 5% (v/v), pH 5.6) and solid induction medium with acetosyringone were used.

2.3.1.8 Spheroplasting Buffers

Buffer II contained sorbitol 2 M, EDTA 0.1, DTT 0.1 and TrisHCl 10 mM at pH 7.5. Buffer III consisted of sorbitol 1.5 M, EDTA 0.1, DTT 0.1, TrisHCl 10 mM at pH 7.5. Recovery Buffer SY comprised sorbitol 1 M and 67% v/v YPD. SYTC contained PEG6000 20% v/v, TrisHCl 10 mM and CaCl 10 mM.

2.3.1.9 Yeast Selection Plates

5-FOA Medium contained YNB 1.7, NH4SO4 5, Uracil 0.035 and 5-FOA 1 g/l as needed. Final glucose and agar concentrations were 2 and 20 g/l respectively.

Adenine (Ade) selection plates contained YNB 1.7, NH_4SO_4 5, KCl 7.6 and amino acid mix 1.4 g. Amino acid mix did not contain histidine, leucine, tryptophane and adenine. Leucine 60, histidine 20, tryptophan 20 as well as adenine 10 mg/l as needed were added. Final glucose and agar concentrations were 2 and 20 g/l respectively. Uracil (Ura) selection plates contained YNB 1.7, NH4SO4 5, KCl 7.6 and Aminoacid mix 1.4 g. Aminoacid mix was. Leucine 60, histidine 20, tryptophan 20 as well as uracil 20 mg/l as needed were added. Final glucose and agar concentrations were 2 and 20 g/l respectively.

2.3.1.10 Algae Hydrolysate

Algae Hydrolysate was prepared by hydrolyzing *Scenedesmus obtusiusculus* A189 at 50 g/l in 50 mM sodium acetate buffer at 50°C and 120 rpm using 0.5% Cellulase (CelliCtec 2 from Novozymes). Buffer and enzyme were sterile filtered and algae biomass were autoclaved dry before the hydrolysis was performed for 72 hours.

2.3.2 Isolation of Oleaginous Yeast Strains

2.3.2.1 Environmental Samples

Seven environmental samples were obtained in Romania, Mexico, France and Kenya. Sample sites were chosen according to the following criteria: High abundance of carbohydrates, high temperature in the summer, possibly high variability of nutrient availability, which would

encourage storage of carbon and high general biodiversity. Samples were taken by collecting approximately 10 g of material in a 50 ml falcon tube and stored at 5°C until strain isolation.

Table 1: Environmental samples used for the isolation of new yeast strains

Number	Sample	Description	Sample Origin	Location
1	BC40 CS	Sand	France	50°02′08″N 2°01′51″E
2	P Beach	Sand	Mexico	21°16′48″N 89°40′12″W
3	PF EG	Leaves	Romania	46°43'56.8"N 23°32'08.1"E
4	PF NTC	Soil sample	Romania	46°43'50.3"N 23°32'01.4"E
5	PF H1W	Soil sample	Romania	46°44'32.3"N 23°32'12.3"E
6	ND1	Soil sample	Kenya	1°19'10.5"S 36°47'43.5"E
7	PF RB	Sand	Romania	46°43'50.3"N 23°32'01.4"E
8	4U1	Brown algae	Kenya	4°15'57.4"S 39°35'56.8"E
9	4U2	Green algae	Kenya	4°15'57.4"S 39°35'56.8"E

2.3.2.2 Isolation Procedure

50 ml of YPD or YM containing chloramphenicol and ampicillin (1 mg/l) were inoculated using 10 mg of environmental sample and cultivated at 28°C and 120 rpm. After 24 hours, 10 µl of the culture was taken and diluted 1:1000. 100 µL of this dilution were subsequently plated out on YPD plates. Colonies were distinguished visually and cells evaluated using brightfield microscopy at 100-fold magnification. Subsequently, only yeasts were further cultivated, stained with Sudan Black B, Nile red and genetically identified (Section 2.3.3).

2.3.2.3 High-Throughput Determination of Growth

Determination of growth was achieved using a modified protocol of the Centraalbureau voor Schimmelcultures of the Royal Netherlands Academy of Arts and Sciences (CBS KNAWL). The organization manages a strain collection containing over 51’000 strains (01.05.2016).

Microplate wells (Nunc clear, 96-wells, flat bottom) were filled with 100 µl media using a Labsystems multidrop dispenser in a sterile bench. Inoculation was done from agar plates

using inoculation loops. The plates were then sealed using cellulose sealing film, loosely wrapped but not sealed airtight with cellophane and incubated at 28°C. The seal was removed after 3 and 5 days, replaced with a clear 96-well lid and optical density at 600 nm was measured in a plate reader after agitation at 600 rpm (linear, 2 mm) for 30 seconds. The basis for the screening was the IBK strain collection as well as isolates obtained from Christian Görner from Ireland and Munich (Section 2.2.4).

2.3.2.4 High-Throughput Lipid Estimation

For cultivation in 96 deep well plates, a Labsystems multidrop dispenser was used to fill the plates with 1 ml medium under a sterile bench. The plates were sealed using cellulose sealing film and cultivated at 28°C and 300 rpm.

Measurements were done daily for 5 days by transferring 50 µl culture from the deep well plates to a 96-well microtiter plate (Nunc black, 96-wells, flat bottom) containing 150 µL bidest in each well using a multichannel pipette. The plate was placed in the microplate reader and the HT-LE protocol executed (Table 2)

Table 2: High throughput lipid estimation protocol for plate reader with dispenser unit

Step	Action	Repetition
1	Agitation at 600 rpm, 2 mm, linear	Repeat 3x
2	Measurement of OD at 600 nm (OD)	
3	Agitation at 600 rpm, 2 mm, linear	Repeat 3x
4	Measurement of Nile red background at 590 nm (FI)	
5	Dispensing 25 µl of DMSO into each well	
6	Dispensing 25 µl of Nile red in DMSO (50µg/ml) into each well	
7	Agitation at 600 rpm, 2 mm, linear	Repeat 15x
8	Measurement of Nile red Background at 590 nm (FI)	

The automated dispensing and staining was validated by measuring 96-wells with the same amount of yeast (*Cutaneotrichosporon oleaginosus ATCC 20509*, 200 µl at OD_{600}=1, Supplemental 4).

2.3.3 Lipid Analytics

2.3.3.1 Sudan Black B Staining

Sudan Black B (Figure 4) is a non-fluorescent, thermostable fat-soluble diazo dye and used for staining of neutral triglycerides, lipids on frozen sections and lipoproteins on paraffin sections. The use of Sudan as fat stain dates back to 1896[96], Sudan Black B was then later

introduced in 1934 and has since been one of the standard methods of lipid staining. It is, however, not strictly specific to lipids and not suitable for quantification. For staining of sections, Sudan Black has mostly been superseded by the use of Oil Red O. It is still suitable to make qualitative statements as to whether yeast cells grown on a plate are possibly oleaginous.

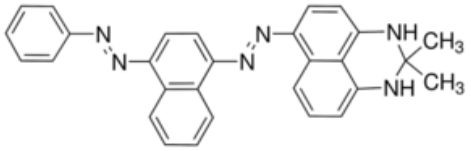

Figure 4: Structure of Sudan Black B. (2,2-dimethyl-1,3-dihydroperimidin-6-yl)-(4-phenylazo-1-naphthyl) diazene

A modified Sudan Black B staining protocol by Evans *et al*.[97] was used in this work. Whatman filter papers were placed on agar plates with streaked out yeasts, which were grown for 5 – 7 days. The filter paper was subsequently placed on an evaporating dish, dried in an oven at 50°C and frozen at 2 hours before being placed in Sudan Black B Solution (0.08% in 95% Ethanol) for 30 minutes. After washing the filter paper twice with 95% ethanol, it was left to dry at room temperature.

2.3.3.2 Nile Red Staining

Nile red 9-diethylamino-5-benzo[α]phenoxazinone (Figure 5), is a lipophilic dye used for detection and semi-quantitative analysis of neutral lipids, which was first described by Greenspan *et al*[98].

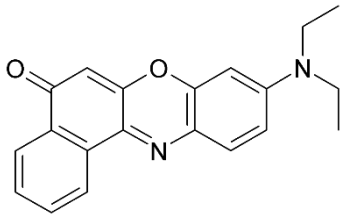

Figure 5: Structure of Nile red (9-diethylamino-5-benzo[α]phenoxazinone)

Originally, it was employed to observe lipid droplets in mouse macrophages and muscle cells[99], but was then quickly adapted for the use in algae[100] and yeast[101], [102] and even ciliates[103].

It is a near-ideal lysochrome, being fluorescent only in a hydrophobic environment and displaying strong solubility in lipids. It has a high quantum yield of 0.7 and does not interact with cell constituents, especially neutral lipids. The reaction is temperature independent

between 20 and 50°C. However, the reaction is sensitive to a number of parameters: cell density and dye concentration, structure and composition of the cells or solvent concentration[98].

Cooksey, who first popularized the application of Nile red for staining of lipid droplets, described it as a “semi-quantitative method”, as there is no possibility to generate a stable standard lipid and stain it[104], which could then be used to create a standard curve. Hence, the Nile red fluorescence remains an estimator, not a quantifier for the lipid content. Nevertheless, due to its easy, fast and cost efficient application, Nile red staining remains one of the standard methods in lipid research.

Samples were analyzed according to a modified protocol from Sitepu *et al*.[105] Cell density was adjusted to OD_{600}=1.0 using $_{dd}H_2O$ and 200 µL of the dilution was transferred to a black 96-well Nunc plate. 25 µL of DMSO were added to each well and initial absorbance reading was taken at 600 nm and fluorescence was measured at 590 nm with an excitation at 530 nm to obtain the background. 25 µL Nile red solution in DMSO (50 µg/ml), were added to each well and the plate was shaken for 30 seconds at 600 rpm (linear). The fluorescence was then measured again for 15 minutes in 60 s interval to obtain the staining kinetics.

2.3.3.3 Fluorescence Microscopy

Microscopy was done using an AxioLab A1 equipped with an Axio Cam ICm1 from Zeiss. The Zeiss E-PI 10x/20 oculars offered a 10x magnification whereas the Zeiss A-plan objectives with 10x, 40x and 100x magnification were used. For staining of lipid bodies, cells were washed with $_{dd}H_2O$ and resuspended in 25 µg/ml Nile red in DMSO. The suspension was vortexed and incubated for 10 minutes in darkness. Subsequently, cells were again washed with ddH_20 twice and 8 µl of the suspension was placed on a Roth microscope slide and analyzed.

2.3.3.4 Fluorescence Activated Cell Sorting

Cells were washed with $_{dd}H_2O$ and set to a concentration of OD_{600}=1. 200 µl of the dilution were filtered through a 100 µm filter and 25 µl of 50 µg/ml Nile red in DMSO were added, yielding a final concentration of 20% v/v DMSO and 5 µg/ml Nile red. The suspension was incubated for 10 minutes in darkness before analysis in an S3 cell sorter.

2.3.3.5 Fatty Acid Determination

Fatty acid profiles were determined by simultaneous extraction and transesterification of yeast lipids to generate fatty acid methyl esters (FAMEs) which was quantified using GC-FID.

Transesterification was done in DURAN screw top reagent tubes and tops with PTFE septa. A modified protocol from Griffiths *et al* was used[106]. Lyophilized samples were weighed (10-20 mg) and added to 450 µl Toluol and 50 µl C-19 TAG-Stock in hexane to determine transesterification efficiency. 100 µl 2,2-dimethoxypropane (DMP) and 1 ml sodium methoxide

(25% w/v) in methanol are added. After shaking at 800 rpm (orbital, horizontal) and 80°C for 20 minutes, the tubes were cooled down on ice for 5 minutes and 1 ml of HCl in methanol are added. The incubation step was repeated and 400 µl $_{dd}H_2O$ and 360 µl hexane with 40 µl C10 methyl ester stock were added. The tubes were vortexed for 30 seconds, centrifuged for 1 minute at 1200 rcf and 200 µl of the upper phase was transferred to GC Vials.

Fatty Acid analysis using GC-FID was performed on a GC-2010 by Shimadzu with a PEG column (polyethylene glycol, length 30 m, ID 0.32 mm, film 0.25 µm)

1 µL of sample was injected with the injector being at 240°C using a split ratio of 1:10. The column was heated to 150°C for 1 min and the temperature was subsequently increased by 5°C per minute until a temperature of 240°C was achieved. This temperature was held for 6 minutes. Column flow was set to 3 mL/min with H_2 as carrier gas. Signals were obtained by FID at 245°C.

2.3.3.6 Gravimetric Lipid Quantification

Total cell lipids were determined by using a modified Method by Folch *et al*[107]. For this, 12 ml of $_{dd}H_2O$ washed culture were homogenized using an Avestin Emulsiflex at 1200 bar pressure at the sample port (8 bar chamber pressure). 3 falcons were filled with 4 ml of homogenizate and 6 ml of Folch solution were added. Extraction was done overnight at room temperature and 120 rpm. Subsequently, 1.2 ml of 0.9% NaCl were added to aid phase separation. The lower phase was then taken out using a syringe, added to pre-weighed glass vessels and the chloroform was fully evaporated under a stream of nitrogen. The weight of the triplicate samples was averaged to yield the total amount of lipids for yeast cells in 4 ml of culture.

2.3.3.7 Biomass Determination

Preweighed 2 ml Eppendorf tubes were filled with 2 ml of culture, centrifuged at 14.4k g, washed with $_{dd}H_2O$ and dried at 60°C overnight. The dry biomass from 2 ml culture was determined by weighing the Eppendorf tubes again and subtracting the weight of the empty tubes.

2.3.4 Molecular Biology Methods

2.3.4.1 Isolation of Yeast Genomic DNA

Genomic DNA of yeast from the culture collection as well as of own isolates was extracted using the Yeast DNA Extraction Reagent Kit from Thermo Scientific according to the manufacturer's recommendations.

2.3.4.2 Isolation of Genomic DNA

1.5 ml of liquid culture in the exponential growth phase were pelleted at max rpm and resuspended in Harju buffer containing Triton X-100 2%, SDS 1%, NaCl 100mM, TrisHCl pH8 10 mM and EDTA 1 mM. Tubes were subjected twice to a liquid nitrogen bath for 2 minutes and transferred to a 95°C water bath. After adding 200 µl of chloroform, samples were vortexed for 2 minutes and pelleted. The upper, aqueous phase was transferred to a tube containing 400 µl ice-cold ethanol. After mixing by inversion or gentle vortexing, samples were frozen at -20°C. After centrifugation, supernatant was discarded and the pellet was washed with 0.5 ml of 70% ethanol. Cells were pelleted again and the supernatant was discarded. After air drying the pellets at room temperature under a nitrogen stream, they were resuspended in water.

2.3.4.3 Determination of DNA Concentration

DNA was determined according to recommendations from Promega[108]. Absorption at 230 nm (chaotropic salts), 260 nm (DNA), 280 nm (protein) and 320 nm (turbidity) was measured in a HP Photometer Workstation Ag using a Hellma Traycell 5.800 Quarz Microcuvette.

1 $$DNA\ Concentration\ [mg/\mu l] = DF \times 50 \times A_{260nm} - A_{320nm}$$

2 $$DNA\ Yield\ [mg] = [DNA] \times V$$

3 $$\text{DNA Purity (Protein)} = \frac{A_{260nm} - A_{320nm}}{A_{280nm} - A_{320nm}}$$

4 $$\text{DNA Purity (Salt)} = \frac{A_{260nm}}{A_{230nm}}$$

Concentration of DNA was determined by measuring the absorption of DNA at 260 nm and correcting for general turbidity as well as the dilution factor (DF). The yield was calculated by the concentration in relation to the total volume of the elution (V). The purity of the DNA was calculated by again correcting DNA concentration for turbidity and relating it to protein concentration corrected for turbidity. A typical value for $A_{260nm/280nm}$ is 1.7 – 2.0. Lower values indicate significant contaminations. The A_{320nm} should be as low as possible. It is usually close to 0. The salt purity should be greater than 1.5. Lower values can indicate the presence of chaotropic salts such as thiocyanate salt, which may interfere with any subsequent DNA modification or transformation.

2.3.4.4 Strain Determination (18S rRNA)

Ribosomal RNA (rRNA) serves as a widely used genomic marker for phylogenetic research, as it is present in all cells containing gDNA and consists of strongly conserved as well highly variable regions[109]. In this work, a forward primer binding to the internal transcribed spacer 1 (ITS1) between the 18S and 5.8S rRNA Region was used. The reverse primer binds in the D1D2 Region within the 26S rRNA (Figure 6).

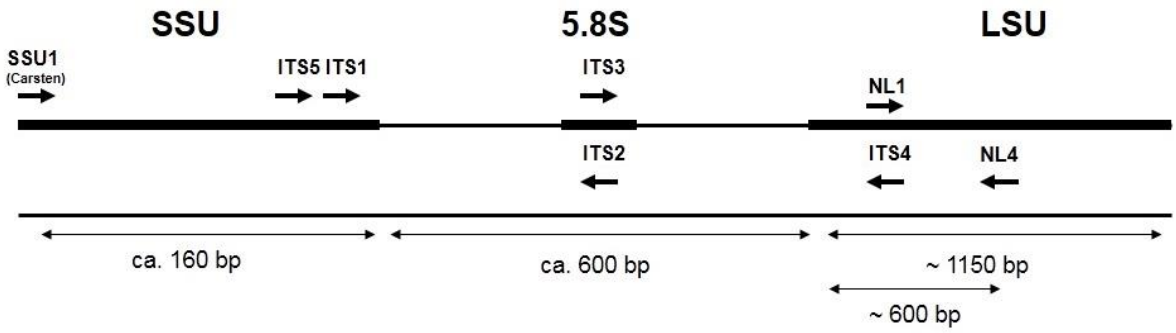

Figure 6: General Structure of Yeast rRNA Genes with used ITS1 and NL4 Primers. Other common primers are displayed as well. Image adapted from Buscot et al., University Leipzig[110].

For amplification by PCR, the following program was used: Initial denaturation was done at 94°C for 4 minutes, followed up with 30 cycles of denaturation (94°C, 30 seconds), annealing (55°C, 30 seconds) and extension (72°C, 60 seconds). After a final extension step at the same temperature, for 10 minutes, the samples were cooled to 16°C until analysis by gel electrophoresis.

Relevant bands were extracted into 30 µL of $_{dd}H_2O$ and 15 µL of DNA was then mixed with 2 µL of primer (50 µM) and sent for sequencing at Eurofins Genomics. The sequencing results were searched using the basic localized alignment search tool (BLAST) and highest hits were assumed to be the strain at hand.

2.3.4.5 Agarose Gel Electrophoresis

Biorad Gel Chambers were used to pour agarose gels, commonly at a concentration of 1% and supplemented with 3 µl ServaStain per gel (35 ml). 5 µL of 1 kb Gene Ruler was used as standard. The gel was run usually for approximately 45 minutes at 100 volts, for large fragments, electrophoresis time was extended; for preparative gels, the current was reduced to 90 Volts. The gel was observed under UV light and documented using a Molecular Imager® Gel Doc™ XR System. In the case of DNA preparation, the illuminated bands were cut and collected in eppendorf tubes for extraction, which was done with a DNA extraction from agarose gel kit from Analytik Jena.

2.3.4.6 Agrobacterium tumefaciens mediated transformation

Plasmids for *Agrobacterium tumefaciens* mediated transformation (ATMT) were first introduced into *A. tumefaciens* by heat shock transformation: Thermocompetent *A. tumefaciens* were thawed on ice with 2 µg plasmid. After 10 min at 37°C, 500 µl LB were added immediately and cells were regenerated at 28°C and 250 rpm for 2 hours. After centrifugation, cells were resuspended in 100 µl LB and plated out on plates containing 50 µg/ml kanamycin.

For transformation into *C. oleaginosus*, an overnight culture of *A. tumefaciens* carrying the plasmid in LB with 30 µg/ml kanamycin at 28°C was used to inoculate a 10 ml shake flask culture containing L-Imas medium and cultivated at the same temperature for 6 hours. Meanwhile, an overnight culture of *C. oleaginosus* was centrifuged and resuspended in L-IMAS medium to achieve an OD_{600} of 0.5. Of each culture, 500 µl were taken and mixed. 100 µl of this mixture were plated on a blotting membrane, which in turn was placed on S-IMAS agar plates. After 48 hours of incubation at 24°C, membranes were transferred to YPD agar plates containing varying amounts of hygromycin B or gentamicin (G418) and 300 µg cefotaxime. *C. oleaginosus* transformants were cultivated in YPD and insertions of expression cassettes were checked via PCR.

2.3.4.7 Spheroplast transformation

All procedure steps were done in 6-well plates. The original spheroplasting transformation by Glumoff *et al*. [111] required the Novozyme 234 mix, which is not available anymore. An alternative combination of enzymes for cell wall degradation based on the same paper was chosen. For each 10^8 cells, 7 mg lytic enzyme and 0.94 mg driselase were solved in 1 ml of Buffer II. An overnight culture of *C. oleaginosus* was washed and resuspended in Buffer II / enzyme mix. After incubation for 2 h at 28°C without shaking, osmosensitivity was checked by adding 50 µl 10% SDS to a sample of 500 µl cell suspension. Spheroplasts were washed twice in Buffer III and subsequently recovered in Buffer SY. After 1 hour at 28° without shaking, cells were washed and resuspended in 100 µl SYTC. 1-5 µg template DNA and 20-30 µg carrier DNA were added and after 45 minutes of incubation, 600 µl of SYTC were added for regeneration overnight at 28°C. Cells were plated out the next day on YPD or selection plates.

2.3.4.8 E. coli Heat Shock Transformation

$CaCl_2$ competent cells were thawed on ice for 10 minutes with 1-5 µl of ligation or Gibson assembly sample or 1 µl of plasmid at 50 µg/ml for retransformation. The tube was carefully flicked to mix DNA with the cells and placed on ice for 30 minutes. Heat shock at 42°C was applied for 30 minutes without mixing and again placed on ice for 5 minutes. 1 ml of LB Medium was added and shaken at 250 rpm for 60 minutes. Cells were centrifuged for 3 minutes at 3000 rcf, resuspended in LB and plated on prewarmed selection plates (37°C). Plates were cultivated overnight at 37°C

2.3.4.9 Gibson Assembly

Gibson Assembly was done according to NEB recommendations[112].

2.3.4.10 Dga2 and Slc1 Overexpression Plasmids

For convenience, all cloning strategies are based on a Biobrick-like system, in which multiple cassettes containing the same restriction sites can subsequently be cloned into a vector backbone.

The Dga2 overexpression cassette was generated by amplifying Dga2 from genomic DNA using Primers oDga2_OLpyfp_fw and oDga2_OLpyfp_rv inserting it between promoter and terminator of the YFP expression cassette[21] using Gibson assembly. Amplification using primers nhe_spe.not_Cass_fw and nhe_spe.not_Cass_rv containing NheI and XbaI restriction sites yielded the expression cassettes ready for cloning into the backbone.

In the same way, the codon optimized KanMX gene[113] (primers KanMX_fw and KanMX_rv), the *C. oleaginosus* Slc1 gene coding for lysophosphatidic acid-acyltransferase (primers SLC_OL_fw and SLC_OL_rv) and the hygromycin resistance gene[114] (primers Hyg_OL_full_fw and Hyg_OL_full_rv) were inserted between promoter and terminator of the YFP expression cassette. Amplification using primers nhe_spe.not_Cass_fw and nhe_spe.not_Cass_rv containing NheI and XbaI restriction site yielded the expression cassettes ready for cloning into the backbone. All gene sequences are shown in Supplemental 5.

The backbone of the *A. tumefaciens* shuttle plasmid pRF_HU2[51], [111] was amplified with SpeI and XbaI restriction sites and respective cassettes were inserted by cloning the backbone with SpeI and XbaI and the cassette to be inserted with NheI and XbaI. As NheI and SpeI are compatible, both restriction sites disappear and the assembled plasmid only contains the two restriction sites present in the reverse primer of the insertion cassette: SpeI and XbaI.

All primer names can be found in the figures, all primer sequences are in the materials and methods. Cloning strategies in detail are shown in Supplemental 6, Supplemental 7 and Supplemental 8.

2.3.4.11 Cas9 Gene Editing

As the gRNA has to be exactly the correct size for formation of an active nuclease complex, a RNA-polymerase 3 promoter has to be used for transcription. Most commonly the U6 snRNA promoter is used. However, no information about *C. oleaginosus* polymerase 3 promoters was available and despite conservation, no U6 snRNA – match was found in the genome.

If a polymerase I promoter is used, such as the one employed by Görner *et al*.[51] the resulting transcript has to cleave itself after transcription. This can be achieved by employing ribozymes, as described by Zhao *et al*.[115]. Ribozyme-gRNA-ribozyme (RGR) cassettes were constructed by placing hammerhead (HH) respectively HDV ribozymes at both the 5’ and 3’ end of the ribozymes (Figure 7)

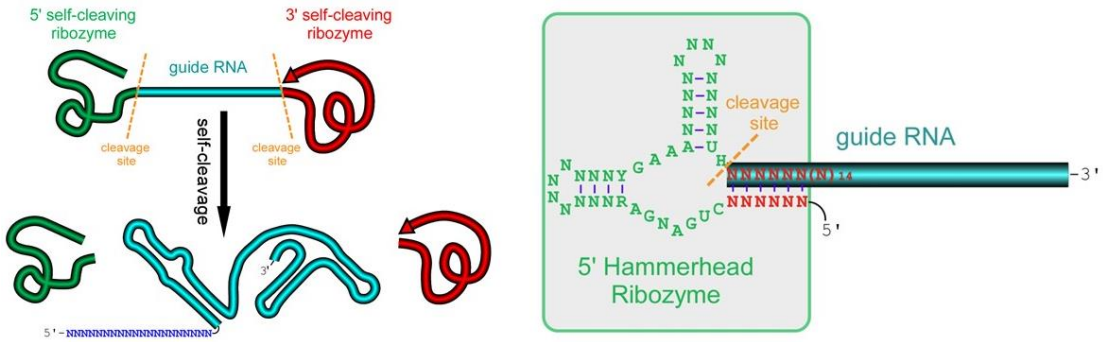

Figure 7: Left: Structure and self-cleavage of Ribozyme:gRNA:Ribozyme assembly. Right: Structure of Hammerhead Ribozyme at 5' end of crRNA sequence of gRNA. Both images by Gao et al. [115]

As microbiologically easily selectable targets, Ade2 and Ura3 homologues were chosen, resulting in the sequences in Supplemental 9. For cloning, Cas9 with human optimized codon usage was amplified with overlaps to promoter and terminator of hygromycin B cassette from Görner *et al*. The cassette was amplified using primers oCas9_cas_fw and oCas9_cas_rv and subcloned into pBluescript with restriction sites KpnI and NotI. The plasmid pRF_Hyg was also template for the hygromycin cassette, which was amplified using primers oHyg_cas_fw and oHyg_cas_rv. The hygromycin b resistance cassette was then cloned into pSK_Cas by cutting the backbone with SpeI and NotI and the cassette with compatible SpeI compatible NheI and NotI. This yielded the Cas9 expression cassette set in the pBluescript backbone pSK_Cas_Hyg. The gRNA sequence was synthesized and inserted as expression cassette into pSK_Cas_Hyg the same way as the cas9 cassette into pBluescript.

For both pSK_Cas_Hyg and pSK_Cas_Hyg_grna1 and pSK_Cas_Hyg_grna2 the cassette sets were extracted by using restriction sites KpnI and LguI to be cloned into the pRF_HYG backbone, which was amplified using primers pRF_Hyg_BB_KpnI and pRF_Hyg_BB_LguI. gRNAs were designed to target Ura3 in *C. oleaginosus*, to allow for easy screening using 5-FOA (Ura-Blaster methodology[116]).

2.3.4.12 Localization of ATMT Insertion Sites

Localization of ATMT insertion sites was done by using random hexamers for an arbitrarily primed PCR, a special case of TAIL PCR[117]. The method is based on two subsequent PCRs which in the end yields a fragment flanking the insertion cassette (Figure 8). For the first PCR, one primer binding to the expression cassette (inner primer) and a second primer with a random sequence on the 5' end and a specific sequence at the 3' end are used. For the second PCR, a second primer pair is used with the first primer binding to the expression cassette at a sequence, which had previously been amplified (outer primer) and the second primer being identical to the tag of the first arbitrary primer.

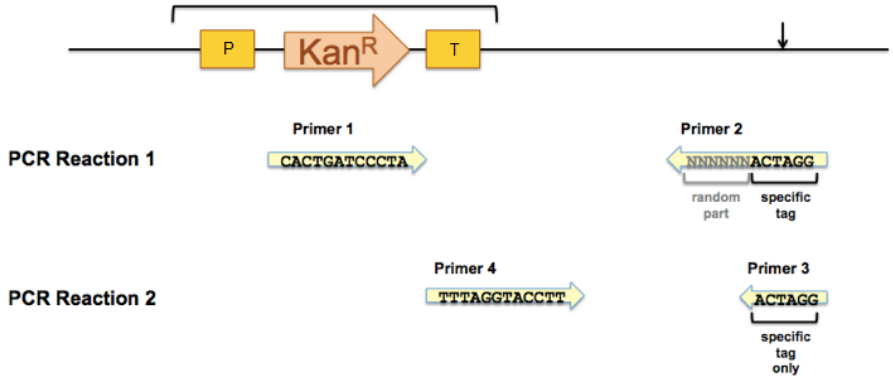

Figure 8: Schematics of arbitrary PCR using random hexamers. The upper line shows genomic integration with an integration cassette containing a promoter (P) Terminator (T) and a kanamycin resistance (KanR). The arrow marks the binding of Primer 2 of PCR Reaction 1 of the arbitrary two. The resulting product is used as template for PCR Reaction 2. Figure adapted by Minikel[118].

Primer sequences can be found in section 2.2.5. For PCR reaction 1, thermocycler was run for 5 minutes at 95°C for initial strain separation. The first 5 repeats included 94°C for 30 seconds, 30°C for 30 seconds and 72°C for 1 minute. The second 30 repeats included 94°C for 30 seconds, 45°C for 30 seconds and 72°C for 1 minute. After another 5 minutes at 72°C, the PCR was ended. PCR reaction 2 was run, by using 30 repeats including 94°C for 30 seconds, 45°C for 30 seconds and 72°C for 1 minute with another 5 minutes at 72°C. PCR products were purified by agarose gel extraction and subsequently sequenced at eurofins genomics GmbH.

2.3.5 Microbiological and Biochemical Methods

2.3.5.1 Flask Cultivation

If not stated differently, yeasts were routinely cultivated at 28°C and 120 rpm for flasks with a volume larger than 30 ml and 15 ml as well as 50 ml Falcons. If not stated otherwise, flasks with baffles were used to allow for sufficient aeration.

2.3.5.2 Culture Stocks

5 ml of overnight culture were centrifuged at 3000 rpm for 5 minutes. The pellet was resuspended in 0.5 ml YPD and 0.5 ml 50% Glycerol. Tubes were placed on ice for 30 minutes before being stored at -80°C.

2.3.5.3 Ura and Ade Selection Media

Ura3 clones were selected by plating 20% v/v on 5-FOA plates. 80% v/v of cells were plated on Ura+ plates and then replicated on Ura- plates to find auxotroph strains. Ade2 clones were selected by plating cells out on Ade+ plates and replicating them on Ade- plates as soon as colonies were visible.

2.3.5.4 Rapamycin and Caffeine Supplementation

C. oleaginosus was cultivated as triplicate in YPD with different concentrations of rapamycin solution for 7 days at 28°C in 500 mL baffled shake flasks. Cultivation was carried out in 100 ml YPD and nitrogen limitation medium (MNM) with glucose. Cells from an overnight culture grown YPD medium under the same cultivation conditions were washed in $_{dd}H_2O$ and used to inoculate all cultivations at OD_{600}=0.5. Where applicable, rapamycin was added 8 hours after inoculation and adjusted to varying concentrations. 6 ml samples were taken daily for analysis of cell-dry weight, lipid content and fatty acid distribution.

Online OD measurements were conducted by measuring real-time backscatter at 525 nm with a Cell Growth Quantifier (Aquila biolabs - Baesweiler) using 100 mL YPD in 250 mL shake flask without baffles for 72 hours. Rapamycin concentration was adjusted to 5 µM 8 hours after inoculation. The backscatter signal was calibrated with a manual 2 point OD_{600} measurement by an HP 8453 photometer.

2.3.5.5 Western Blotting

C. oleaginosus protein was extracted by taking growing in YPD for 5 days at 120 rpm and 28°C in baffled flasks. 50 ml of culture were washed twice with $_{dd}H_2O$ and resuspended in 10 ml ERT4 resuspension buffer in a 50 ml falcon. After high pressure homogenizing at 8 bars (2400 bar at outlet) for 4 times, cell fragments were spun down for 1 hour at maximum speed and 4°C. 30 ml of ice cold 13.3% TCA in acetone with 0.2% DTT and frozen overnight at -20°C. The next day, falcons were centrifuged at 14.4 k rcf and 4°C for 10 minutes. After washing with MeOH (0.2% DTT) to discard the TCA, cells were again washed with acetone (0.2% DTT) and

after centrifugation, pellets were air dried for 5 minutes and resuspended in 8 M urea. Sonification was used to aid resuspension and different concentrations of the sample were loaded on a PAGE.

Western blotting for detection of Cas9 was done by introducing 30 µl of *C. oleaginosus* protein extract as well as 10 µl of Cas9 protein (20 µg/ml) as positive control were loaded on a 12% SDS-gel for 2 hours at 100 Volts. It was then blotted semidry on a PDVF membrane overnight at 4°C and 30 Volts. The membrane was blocked with TBST and 5% milk powder overnight again at 4°C. After washing with TBS, a monoclonal mouse anti-Cas9 antibody was used, followed by an anti-mouse antibody coupled to horseradish peroxidase. Ecl Reagent was used for detection.

2.3.5.6 Ethylmethanesulfonate mutagenesis (EMS)

EMS induces random mutations in DNA. The ethyl group of EMS typically reacts with guanine or cytosine (Fig. 7), making the formation of the third hydrogen bond impossible. During DNA replication, a thymine or adenine base are then placed instead of the target base of EMS. The mutations, which therefore occur mostly are C/G to A/T transitions, but double strand breaks, which are repaired by homologous recombination (HR) or non-homologous end joining (NHEJ) have been described[119], [120]. Considering results of extremely poor homologous recombination in *Cutaneotrichosporon oleaginosus* (Data not shown), NHEJ appears to be much more likely in this organism. This was also previously described for *Y. lipolytica*[121].

2.3.5.7 Directed Evolution

Directed evolution was done by cultivation of *C. oleaginosus* in 50 ml YPD and MNM-S for 96 hours at 120 rpm at 30°C. After staining cells with Nile red as described in section 2.3.3.2, 150’000 cells of subpopulations of cells with the lowest and highest 5% fluorescence were sorted into eppendorf tubes. Recultivation and sorting procedure were repeated 3 times.

2.3.5.8 Sugar Analytics

Sugar concentration of hydrolysate was determined by HPLC-RI. Samples were prepared by filtration over a 10 kD centrifugation filter (14.4 rcf for 10 minutes). Subsequently, 5 µl sample were injected on a HPX-87P column (8% cross-linked resin, lead ionic, Bio-Rad) and separated at 70°C with bidest as mobile phase. Run time was 30 minutes at 0.4 ml/minute and detection was done at 50°C and RI signal of samples was aligned with that of internal standard curves.

2.3.6 Bioprocessing Methods

2.3.6.1 48x 10 ml Fermentation

16 different base media with different C:N, C:P and C:S ratios (Supplemental 10) were supplemented with modified Meesters *et al*.[45] trace elements solution (Section 2.3.1.3). The pH was set at 6.5 with acetic acid and the temperature was adjusted to 28°C. 100 µl samples for OD_{600} measurement were taken every 4 hours. At the end of the cultivation (34 hours) culture samples were taken for gravimetric lipid determination (5 ml), fatty acid determination (2 ml) and dry biomass determination (2 ml). All cultivations were done as triplicate. *C. oleaginosus* grown overnight in YPD was washed with 20 mM NaP_i buffer and used to inoculate to an OD_{600} of 1.

Using R, growth curve parameters were extracted (lag phase, maximum growth rate, maximum achieved OD). All growth curves and corresponding fitted growth curves predictions can be found in Supplemental 11 and Supplemental 12. As suggested by the grofit package[122], Gompertz, logistic and Richards functions were used to approximate growth curves (Supplemental 13).

2.3.6.2 1 l Fermentation

A DASGIP ga4 4x parallel fermenter by Eppendorf (Hamburg, Germany) was used for evaluation of Dga2 overexpressing *C. oleaginosus* clones. Inoculation was done with 50 ml preculture of *C. oleaginosus* wild type and Dga2 clones 1, 5 and 6 grown in YPD overnight. Initially, X ml YPD were used as base medium with 500 g/l glucose being fed at 0-50 ml/h. pH was set at 6.5 using 12% v/v H_3PO_4 and 3 M NaOH. pO_2 was kept over 30% of total oxygen solubility by stirring between 200 and 500 rpm and aeration between 0 and 1 v/v/h. Analysis of dry biomass, lipids and Nile red was done as described in section 2.3.3.2.

2.3.7 Bioinformatics

2.3.7.1 Codon Tables and Codon Adaption Indices

Transcripts were obtained from JGI, however, these sequences also included non-coding regions[123]. In the case of the TOP20 and the GDH Codon Usage, coding regions within these transcripts were extracted by hand by following the annotation given by the JGI database. For the full dataset, Transdecoder[124] was used to extract the ORFs. Notepad++ v 6.7.7 [125] was used to check the resulting, large number of sequences of sequences[126]. CodonW and Kazusa's Codon Usage Analyser[127] were used to generate the codon tables. Codon distributions of different groups were averaged and compared. The Codon Adaption Index (CAI), a measure of how strongly the codon usage of a gene of interest represents the

codon usage of a specific organism, was determined using CAICalculator2[128] and CAIcal[129].

2.3.7.2 Assembly of TORC Network

Previously published genomic and transcriptomic data of C*. oleaginosus*[24] were searched for TORC homologues using sequences from *Schizosaccharomyces pombe, Saccharomyces cerevisiae, Candida curvata* and *Cryptococcus neoformans*.

2.4 Results and Discussion

2.4.1 Isolation of Oleaginous Yeast Strains

The isolation studies presented here were executed under my guidance as part of the Bachelor's thesis "Isolation, characterization and mutagenesis of oleaginous yeast" by Valeria Guidolin (2014). The data were reevaluated and discussed for this chapter.

2.4.1.1 Isolation from Environmental Samples

A total of 26 visually distinct colonies were obtained by the isolation procedure described in section 2.3.2.2. Each isolate was given a unique isolate number (Table 3). Using bright field microscopy, isolate 18, 21, 23, 25 and 26 were identified as mycelia forming. As the primary interest was the isolation of unicellular yeasts, isolates with hyphae-like phenotype were excluded from further analysis. In Table 3, they were categorized as molds, however it could not be excluded for the regarding colonies to be hyphae-forming actinomycetes. In general, it is possible for some yeast to form pseudohyphae, which usually occurs under stress conditions, which were not present during the isolation procedure[130]. A number of isolates were visually identified as bacteria, as they were small in size (< 2 µm) and often displayed flagella.

Sudan Black B (SBB) Stain was used to determine which strains were to be further characterized (Table 4). Strains that showed positive staining with SBB were subsequently cultivated in full medium (YPD), genomic DNA was extracted and strain determination with rRNA sequencing was done as described in the methods section.

Extraction of gDNA and amplification of rRNA sequences was successful for all strains. Hence, the identity of all strains was determined, yet no oleaginous strain displayed sufficient deviation from known rRNA sequences to justify further phylogenetic characterization.

Table 3: List of obtained isolates with isolate number and source (number and identifier of environmental sample). Colony description and result of Sudan Black B Stain (SBB) are shown on the right, whereas SBB stain was only applied to yeast.

Sample Number	Isolate Number	Environmental Sample	Categorized as	SBB Stain
4	1	PF NTC	Bacterium	
7	2	PF RB	Bacterium	
7	3	PF RB	Bacterium	
6	4	ND1	Bacterium	
6	5	ND1	Bacterium	
7	6	PF RB	Bacterium	
3	7	PF EG	Bacterium	
3	8	PF EG	Yeast	-
3	9	PF EG	Yeast	-
8	10	4U1	Yeast	+
8	11	4U1	Yeast	+
9	12	4U2	Yeast	+

9	13	4U2	Yeast	+
1	14	BC40 CS	Yeast	-
2	15	PB	Yeast	+
2	16	PB	Yeast	+
3	17	PF EG	Bacterium	
3	18	PF EG	Mold	
4	19	PF NTC	Yeast	+
5	20	PF H1W	Bacterium	
7	21	PF RB	Mold	
8	22	4U1	Yeast	+
8	23	4U1	Mold	
8	24	4U1	Yeast	+
9	25	4U2	Mold	
9	26	4U2	Mold	

Table 4: Result of 18S-rRNA amplification and sequencing of yeast isolates.

Isolate	**Strain**	**Query covery (%)**	**Max Identity (%)**	**Lipid Accumulation (Literature)**	**Nile Red**	**Sudan Black B**
8	*Bulleromyces albus*	83	99	No	No	No
10	*Rhodotorula mucilaginosa*	90	100	No	No	Yes
12	*Rhodotorula glutinis*	100	100	Yes	No	Yes
14	*Candida railenensis*	100	99	No	No	No
15	*Rhodotorula mucilaginosa*	99	99	No	No	Yes
16	*Cutaneotrichosporon oleaginosus*	100	99	Yes	Yes	Yes
19	*Rhodotorula mucilaginosa*	99	99	No	No	Yes
24	*Lecanicillium saksenae*	99	98	No	No	No

For further characterization, isolates were cultivated in MNM-S Medium and their growth and lipid accumulation were estimated using Nile red fluorescence and OD_{600}. All yeasts were able to grow sufficiently fast to consider larger scale cultivation (Supplemental 14), except for

Candida railenensis, which showed an especially long lag phase. Nile red measurements were conducted after 96 hours, a time point at which lipid accumulation was expected to peak.

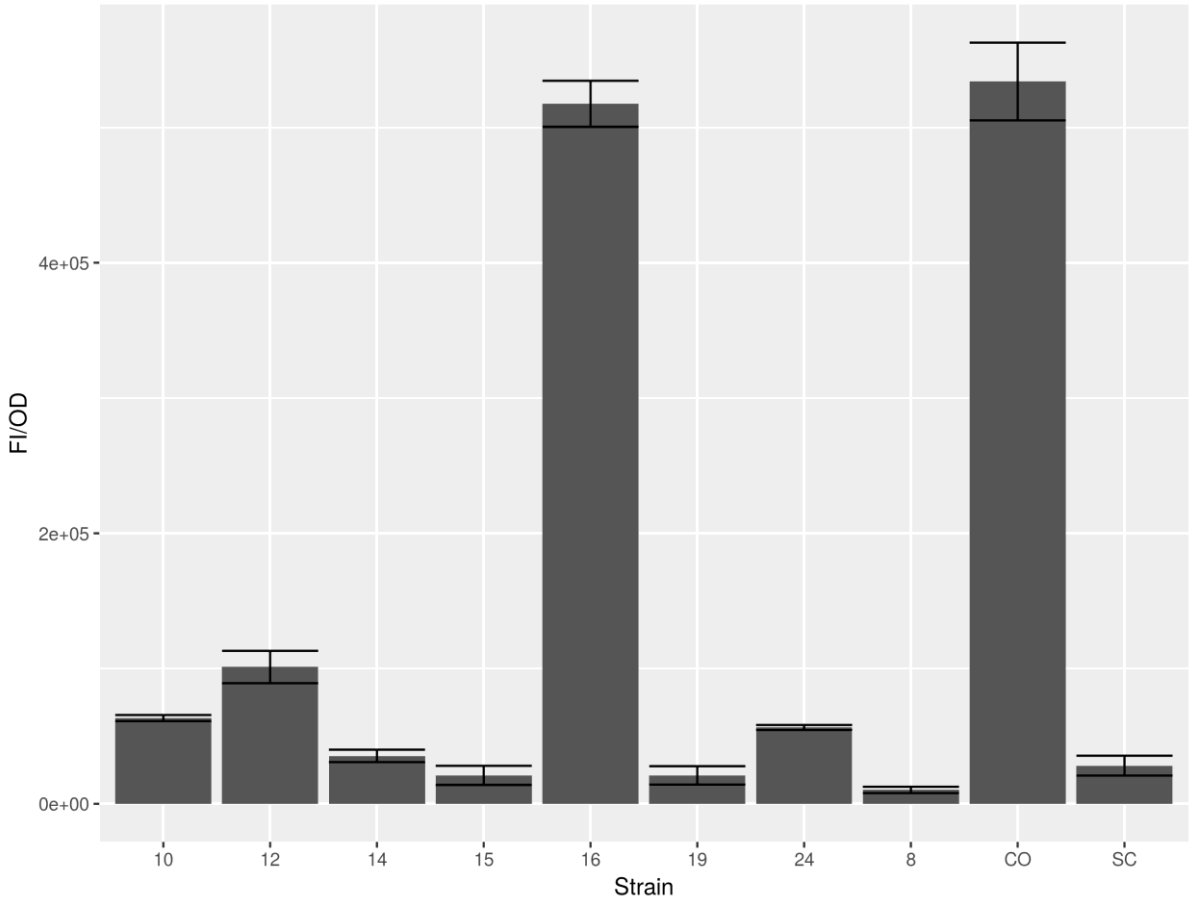

Figure 9: Nile red assay of yeast isolates. C. oleaginosus ATCC 20509 (CO) served as positive and Saccharomyces cerevisiae BY4741 (SC) as negative control. The unit of measurement is arbitrary fluorescent units (FI) corrected for the optical density at 600 nm (OD_{600}). Error bars show standard deviations of triplicates.

Fluorescence of isolate 16, a *Cutaneotrichosporon oleaginosus* isolate, was comparable and in fact not significantly different to the signal from *C. oleaginosus* ATCC 20509 obtained from the DSMZ strain collection (Figure 9: “CO”). Signals obtained from all other strains were small in comparison. However, as the staining kinetics for each strain is different, this should be interpreted as a trend and not as a reliable quantifier for the amount of intracellular lipids in the isolates grown under the specific conditions. For quantification, total lipids extraction is necessary.

2.4.1.2 Lipid Content of Isolates

Isolates displaying highest Nile red fluorescence, isolate 10 (*Rhodotorula mucilaginosa*), isolate 12 (*Rhodotorula glutinis)* and isolate 16 (*C. oleaginosus),* were selected for further characterization by gravimetric lipid analysis. Significant deviation between the extracted single cell lipid to the Nile red data was found. This is not surprising, as the staining behavior

of each strain is different and the OD was not adjusted before measurement, leading to further differences as the lipid – fluorescence/OD_{600} correlation is only linear in a certain range of cell density and different staining kinetics are observed outside of the specified parameters[105]. However, the predicted tendency of *R. mucolaginosa* (I10) having a lower lipid content than *R. glutinis* (I12), which in turn had a lower lipid content than *C. oleaginosus*, was confirmed.

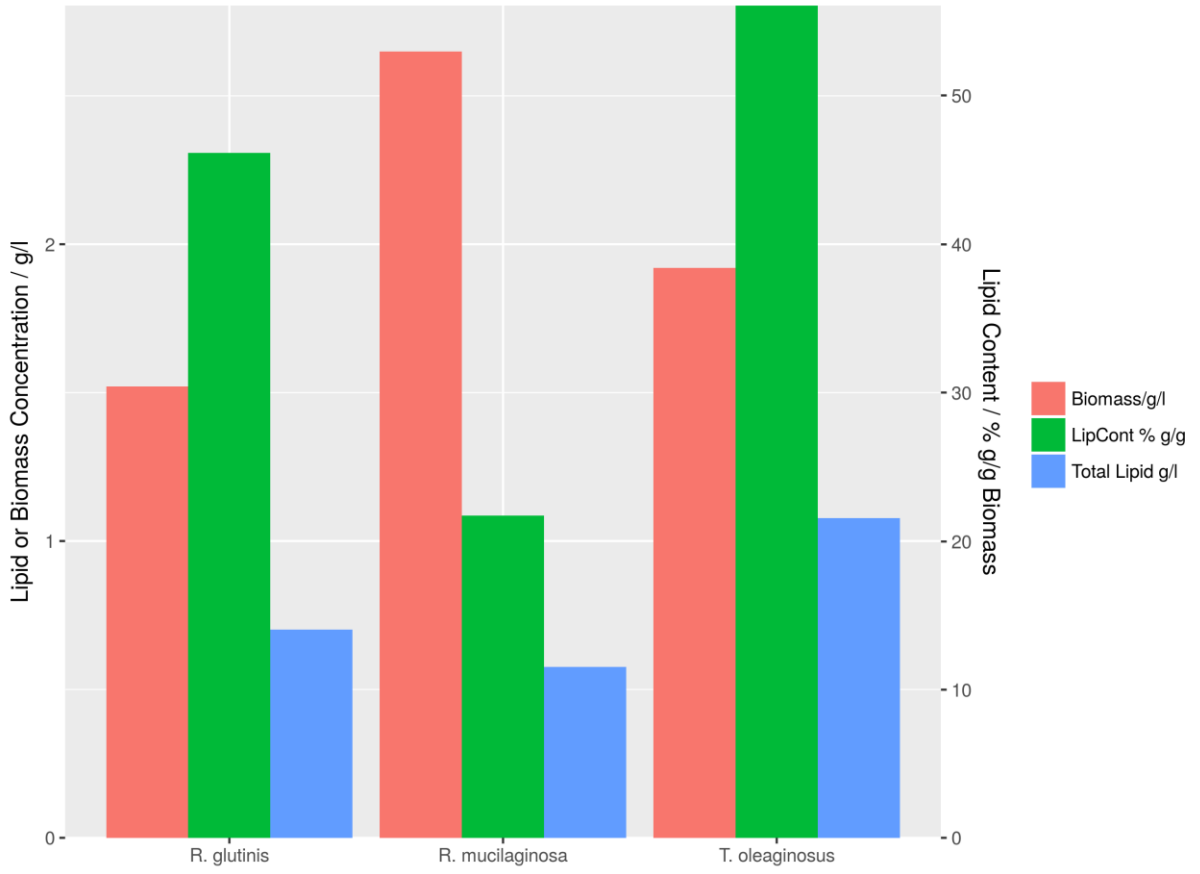

Figure 10: Biomass and lipid concentration as well as lipid content of newly isolated and identified yeast strains that previously showed the highest fluorescence in Figure 9. Error bars show standard deviations of triplicates.

With lipid yields between 0.5-2.5 g/l in non-optimized conditions, all three characterized isolates are in principle worth investigation as potential lipid accumulating organisms (Figure 10). However, *R. mucilaginosa* barely exceeded a lipid content of 20% w/w, beyond which a yeast are commonly termed oleaginous[4]. *C. oleaginosus* was confirmed as the most productive strain in terms of lipid productivity and lipid content. These results were reiterated by the findings of screening the strain collections, which focused on the growth on natural substrates (Section 2.3.2.3 and 2.3.2.4).

2.4.1.3 Fatty Acid Spectrum of Isolates

Three Isolates, *Rhodoturula mucilaginosa* (I10), *Rhodotorula glutinis* (I12), *C. oleaginosus* (I16) were compared with *C. oleaginosus* ATCC 20509 from the strain collection (SC).

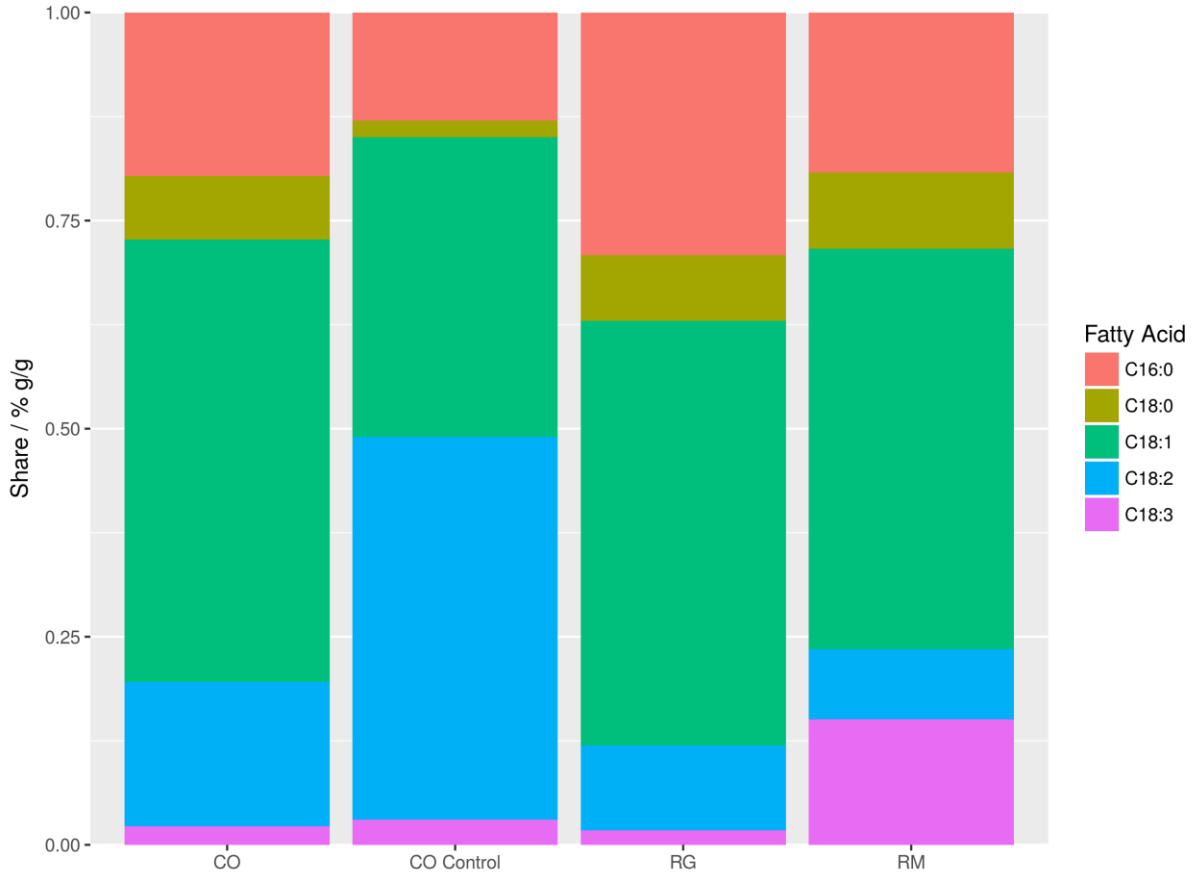

Figure 11: Distribution of detected C16 and C18 fatty acids of three isolates Rhodoturula mucilaginosa (RM), Rhodotorula glutinis (RG), Cutaneotrichosporon oleaginosus (CO) comparison to reference strain C. oleaginosus ATCC 20509. Error bars show standard deviations of triplicates.

In all isolated yeasts, oleic acid (C18:1) was the major constituent of yeast lipid (Figure 11). Herein they differ from the reference strain, *C. oleaginosus* ATCC 20509, which displays a higher amount of unsaturated linoleic acid (C18:2). Stearic acid (C18:0) was low in all tested strains. *Rhodoturula mucilaginosa* showed an increased amount of linolenic acid (18:3) and can be considered a potential candidate for a Δ6-desaturase. Fatty acid profile is inherently tied to living conditions of the specific organism: increasingly desaturated fatty acids correlate with more fluid cell membranes and appear to be favorable in colder environments, as they maintain fluidity in lower temperatures[131]. In a more proximate way, FA spectrum depends on presence and activity of FA modifying enzymes[132], their expression rates and preference of acyltransferases[133]. Screening for oleaginous organisms is a valid tool for finding producers of lipids with desired fatty acid spectra[134]. However, recombinant methods are increasingly successful employed in generating tailor-made lipid profiles[51], [135].

2.4.2 Cultivation on Natural Substrate

2.4.2.1 Optimization of Hydrolysis

For the saccharification of algal biomass, a number of different enzyme mixes were tested including a cellulase mix (Celli-Ctec2, Novozymes), a hemicellulose-mix (Celli-Htec2, Novozymes), a pectinase mix (Pectinex, Novozymes), an amylase mix (Fungamyl, Novozymes) and a proprietary cellulase/hemicellulase mix (Liquibeet, Clariant).

To evaluate the success of sugar monomerization, the cellulase mix was tested in different concentrations (Figure 12), which showed a saturation between 10 and 12 g/l. Hence, 1% v/v of cellulase mix was combined with different concentrations of other enzyme mixes, none of which yielded significantly higher concentrations.

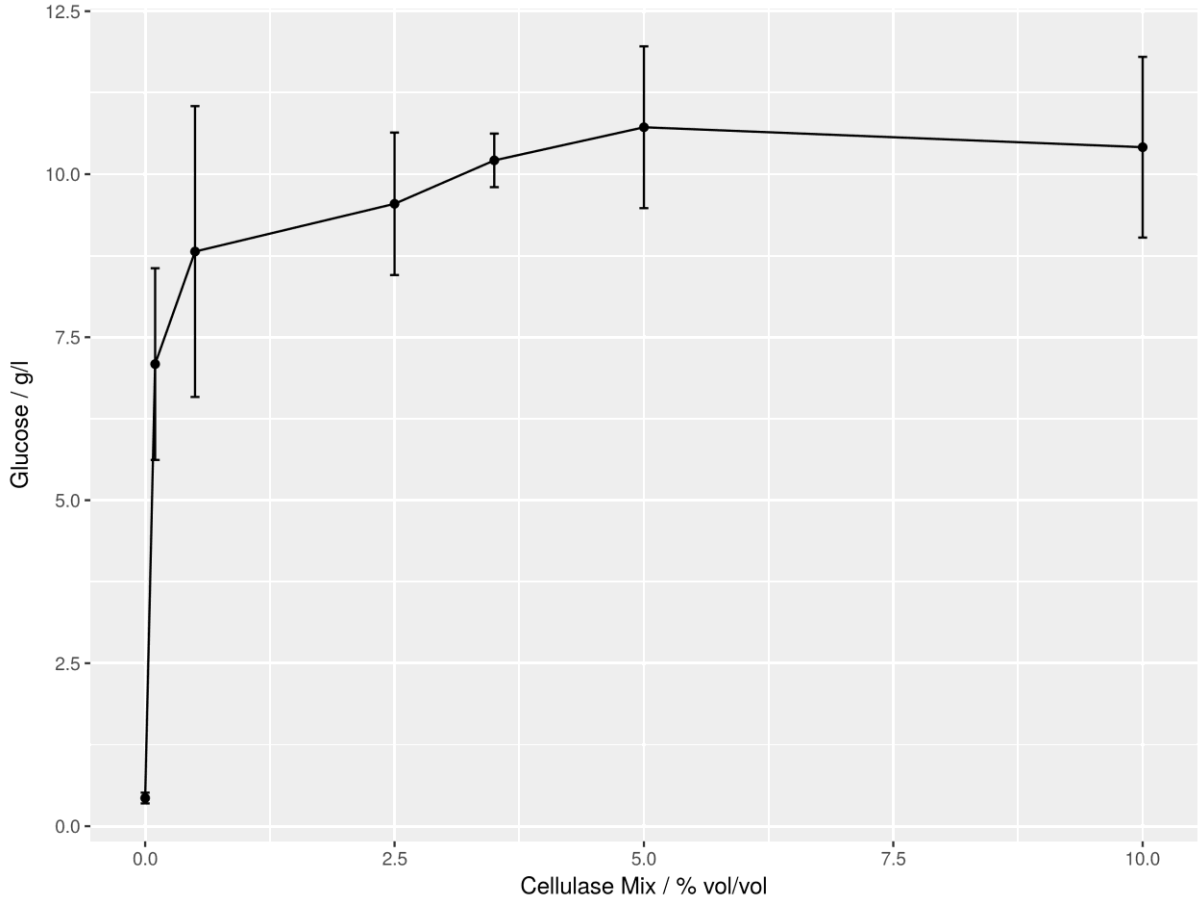

Figure 12: Glucose concentration of Scenedesmus obtusiusculus hydrolysate in dependence of cellulase concentration. As the cellulase mix combines a number of different enzymatic activities (exo- and endo glucanase activity, some proteinase activity etc.), concentration of the enzyme mix is simply given in% v/v. In the left, formula of the shown logarithmic regression and its R^2 value are given. Error bars show standard deviation of n=3.

To confirm that cellulase mix was indeed sufficient for liberation of all glucose in algal biomass, results were compared with an acidic hydrolysis of the biomass (Figure 12) Indeed, for glucose

conversion efficiencies between 90 and 100% were achieved with glucose making up two thirds of total carbohydrates. Conversion of Mannose and Galactose, which could not be distinguished by HPLC (Section 2.3.5.8), was between 20 and 25%. The reason for this lies in the diverse, heteropolymeric structure of algal cell wall[136]. Commonly available mixes were not able to liberate monosaccharides from these structures.

Table 5: Comparison of monosaccharides after acidic hydrolysis and after enzymatic hydrolysis. For enzymatic hydrolysis a) monosaccharide content in hydrolysate was measured directly by HPLC ($^{+}$) and b) hydrolysis residue was hydrolyzed again by TFA and resulting sugars were measured by LCMS (*).

Sugar	**Acidic Hydrolysis** [% g/g $dw_{Biomass}$]	**Enzymatic** [% g/g $dw_{Biomass}$]	**Conversion** Efficiency
Glucose	22	20^{*}-22^{+}	90^{*}-100^{+}%
Mannose + Galactose	10	2^{*}-2.5^{+}	20^{*}-25^{+}%
Rhamnose	<1.5	0	0%
Fucose	<1.5	0	0%
Ribose	<1.5	0	0%

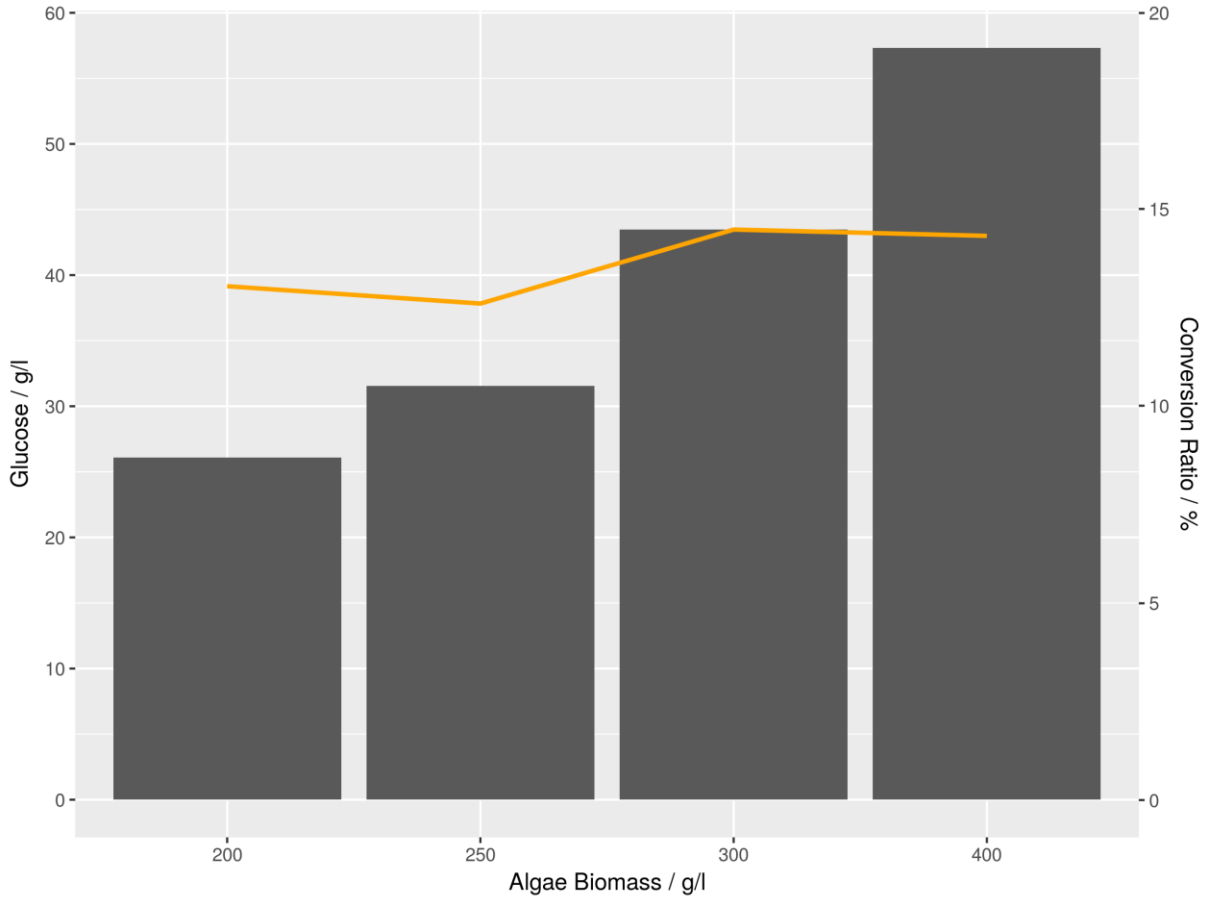

Figure 13: Different concentrations of algae biomass were used for enzymatic hydrolysis using 1 v/v cellulase mix. Glucose yield (bar chart) increases linear, while conversion efficiency (line) remains constant with increasing substrate concentration.

Total sugar concentration in hydrolysate (10 – 11 g/l glucose) was still relatively low, derived from the total carbohydrate content of the algae of 33% w/w (Supplemental 15) and the biomass concentration in the hydrolysate (50 g/l). Hence, the hydrolysis was repeated with higher concentrations of biomass (Figure 13). As a result, glucose concentration of the hydrolysate was raised to 60 g/l while keeping conversion efficiency constant.

In summary, quantitative conversion of microalgal biomass by enzymatic hydrolysis using a cellulase mix was possible, even when raising algae biomass concentration up to 400 g/l. Beyond this point, viscosity was too high for effective hydrolysis.

2.4.3 Oleaginous Yeast Screening

2.4.3.1 High-throughput Determination of Growth

High throughput determination of yeast growth (Section 2.3.2.3) was conducted using 32 isolates from Ireland (NZ), 32 isolates from Ebersberg (WO) and 32 strains from the IBK strain collection (IBY). A total of 96 strains were grown simultaneously in one 96-well plate in hydrolysate. Hydrolysates were prepared as described in sections 2.3.1.10. The maximum growth rate within the first 5 days was calculated and taken as a measure of growth ability on hydrolysates. Details of the results are shown Supplemental 16, Supplemental 17 and Supplemental 18. Strain names can be found in section 2.2.4. Proprietary isolates were not suitable for growth on algae hydrolysate. No isolate was able to surpass a growth rate of 0.05 OD_{600}/day. Therefore, only IBY-strains were selected for more in-depth characterization.

2.4.3.2 High-throughput Lipid Estimation

As accumulation of intracellular lipids in oleaginous yeast is induced by a lack of nutrients required for cell proliferation, MNM-S Medium was used for high throughput lipid screening with Nile red. To evaluate the lipid productivity, the increase in fluorescence over time was observed and the growth rate was calculated. For this, only the timeframe was considered in which exponential growth was observed. Strains were plotted according to their growth rate and the 3 strains displaying fastest increase in Nile red fluorescence were chosen for characterization (Supplemental 19). Those strains were IBY9 (*Cryptococcus curvatus CBS5324*), IBY38 (*Rhodosporidium toruloides NP11*) and IBY20 (*C. oleaginosus* ATCC20509)

2.4.3.3 Strain Characterization

C. oleaginosus (ATCC20509), *Rhodosporidium toruloides* (NP11) as well as *Cryptococcus curvatus (CBS5324)* were selected for further characterization. The selected strains were cultivated for 7 days on different media and lipid productivity was calculated. Hydrolysates were prepared as described in section 2.3.1.10.

In all cases, nitrogen limiting medium MNM-S yielded the highest productivities and model hydrolysate with a C:N 7 mol/mol (adjusted to Redfield ratio[137]) yielded the lowest lipid productivity values. In all cases, full medium YPD yielded higher productivities than hydrolysates. Interestingly, hydrolysates yielded negative productivities for all strains except *C. oleaginosus*. This effect cannot only be explained by the fact that the hydrolysate itself contains lipids and other hydrophobic, extractable components.

A more likely possibility is that inhibition of triglyceride accumulation due to metabolically active agents in hydrolysates caused negative productivities. Under the given conditions, a lipid content between 20-30% g/g was achieved in full medium. However this is not the minimum lipid content of cells, as can be seen in Figure 14. Hence, *C. oleaginosus* was identified as the only strain able to generate more lipids from algae hydrolysate than were assimilated from the hydrolysate itself.

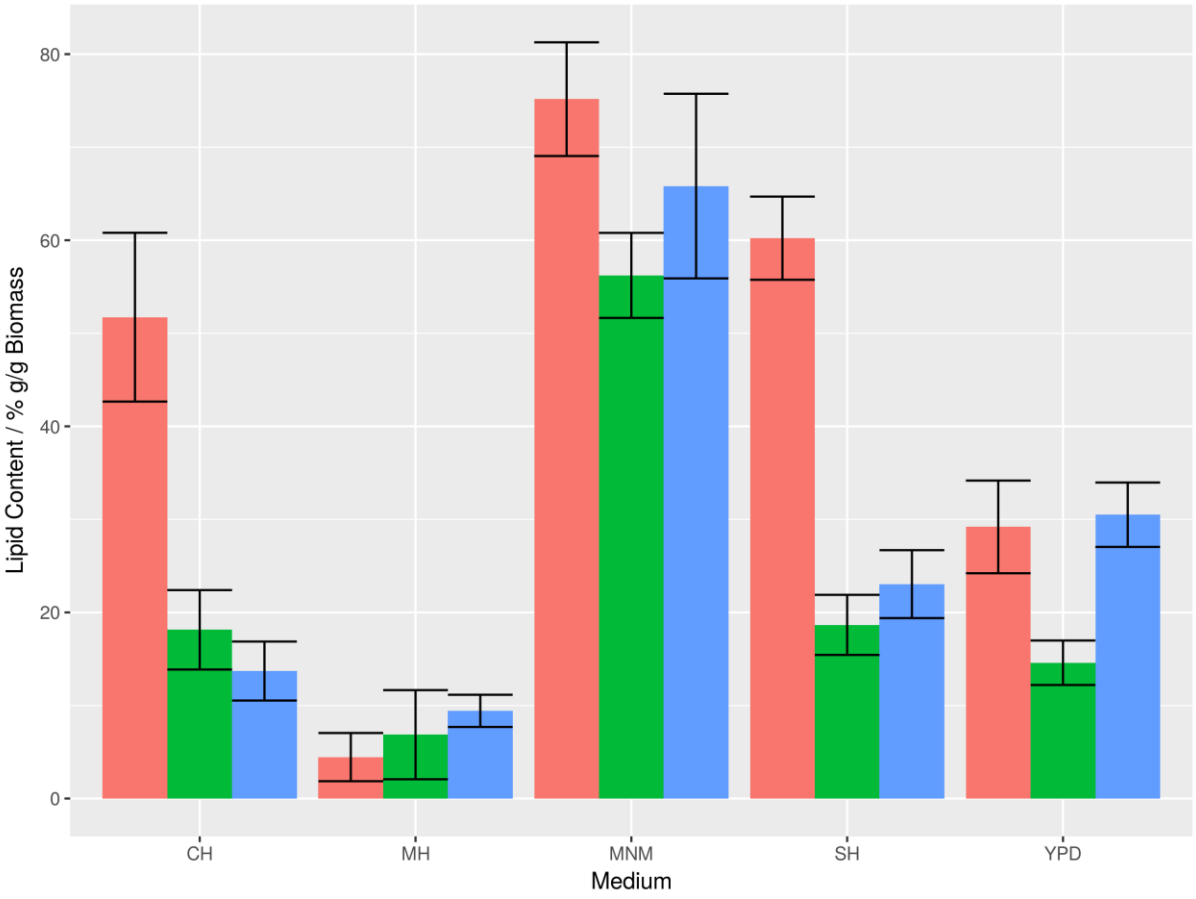

Figure 14: Lipid content of oleaginous yeast with highest lipid productivity, C. oleaginosus ATCC 20509, in different media after 7 days cultivation at 28°C and 120 rpm in baffled flasks (30ml). Error bars show standard deviations of triplicates.

C. oleaginosus ATCC20509 was chosen as the basis for any further work, including modification and fermentation approaches. As a first step, the lipid content in different media was determined and compared. Whereas model hydrolysate served as a negative - and MNM-S as positive control, lipid content on algae hydrolysates was lower than in MNM-S medium. However, both lipid content and productivity were higher than in full medium (YPD). This confirms, that *C. oleaginosus* can not only grow on algal hydrolysate, but also displays significant lipid accumulation (Figure 14).

2.4.4 Mutagenesis and Repeated Selection

Preliminary testing of EMS mutagenesis (2.4.4.1) presented here was executed under my guidance as part of the Bachelor's thesis "Isolation, characterization and mutagenesis of oleaginous yeast" 2014. The data were reevaluated and discussed for this chapter.

2.4.4.1 EMS Mutagenesis

Colony forming units (CFU) declined with an increased exposure time to ethylmethane sulfonate (EMS) in an inverse fashion. Samples with cell survival rates under 30% were pooled and used for subsequent directed evolution. *R. toruloides* showed higher resistance to EMS than *C. oleaginosus*, which could potentially be attributed to higher ploidy levels[138] or cell wall constitution[139].

2.4.4.2 FACS Nile-Red Staining

To establish a FACS staining protocol with Nile red, the quality of the stain was estimated by the capacity to distinguish cells with high intracellular lipid content (grow in lipid induction medium, MNM-S) from low intracellular lipid content (grown in full medium, YPD). Hence, the goal was to maximize the quotient in measured fluorescence between the two samples. Total concentration of cells, Nile red concentration and DMSO concentration were varied. However, changes in the staining procedure yielded no significantly improved result (Figure 15).

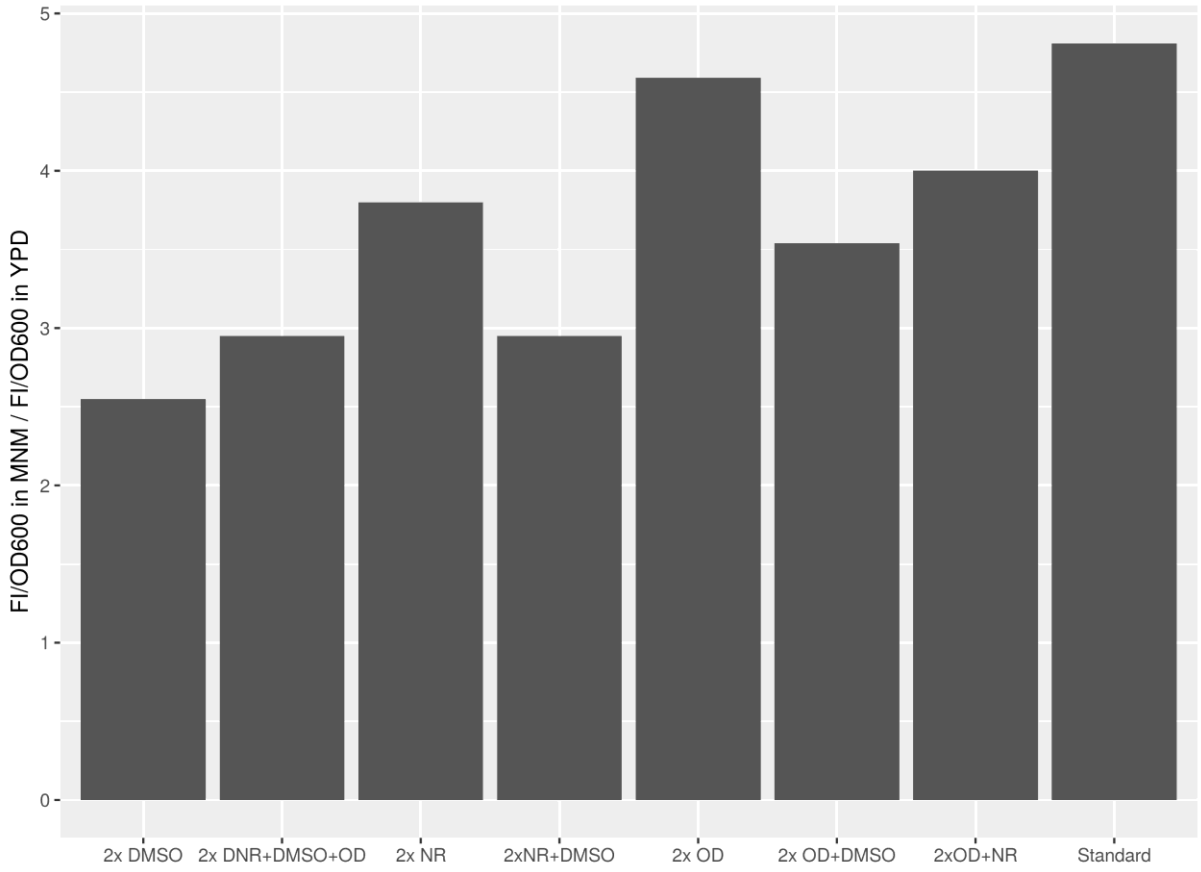

Figure 15: Optimization of FACS - Nile red staining by changing of dependent variables associated with the staining quality. Total cell concentration (OD), Nile red concentration and DMSO concentration were varied in different combinations by doubling the specific factor. Fold change in fluorescence intensity between lipid rich (MNM-S) and low lipid (YPD) C. oleaginosus cells was calculated to quantify quality of the stain.

Due to its volatile nature, which results in a large pipetting error, and suboptimal permeating characteristics in comparison to DMSO[105], acetone was not considered as alternative solvent for staining.

Subsequently, fluorescence signal of cells stained with Nile red in the sorter was compared with the staining in a plate reader. Cells from cultures grown in full medium (YPD) with low lipid content and nitrogen limitation medium (MNM-S) stained by using the protocol described in section 2.3.3.2 were also measured in a plate reader. Supplemental 20 shows the result of the staining procedures. As the factor between high and low lipid populations was similar for cells obtained from the plate reader (Factor 3.18) and flow cytometry (Factor 3.19), the quality of the staining and measurement method were deemed comparable (Supplemental 21).

2.4.4.3 Mutagenesis and Repeated Selection

The directed evolution approach was achieved by combining EMS mutagenesis with repeated selection using FACS and recultivation in YPD as well as MNM-S. A comparatively long cultivation time was employed to encourage a knockout or downregulation of triglyceride-

lipases, which facilitate breakdown of lipid after long cultivation times. However, with increasing number of selection cycles, a decrease not only in lipid, but also in cell density was observed (Figure 16).

The reason for this decrease in fitness could lie in a mechanism, which is well described for asexually proliferating organisms and is based on genetic drift: A combination of high mutation rate and low population size can cause a decrease in fitness, commonly “mullers ratchet”[140]. With a certain probability (depending on the mutation rate and population size), “optimal” alleles of the genotype of the wild type may be lost. Through this, the total population fitness is decreased, since the most “fit” individuals within the population are missing. The probability of a spontaneous back mutation is very low, which means that the wild type allele is lost and the fitness of the population as a whole is permanently decreased.

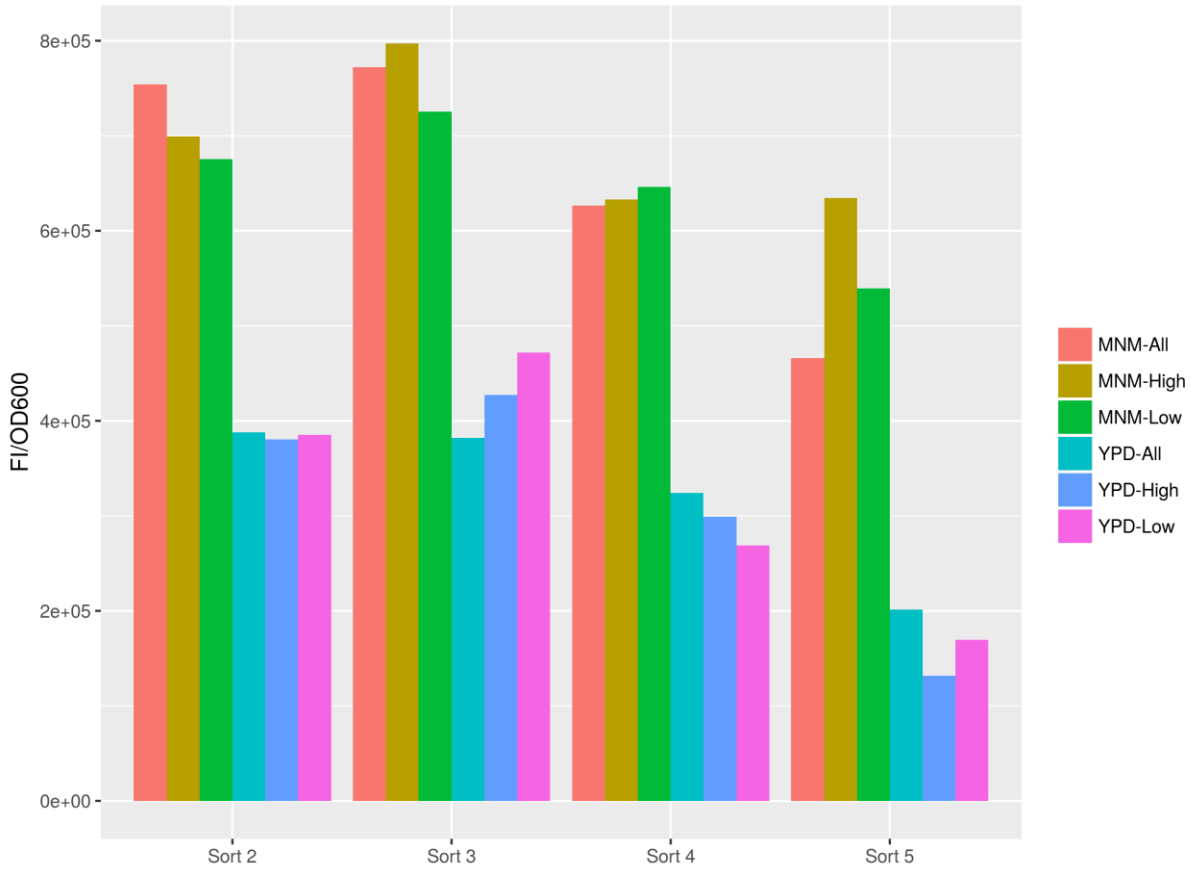

Figure 16: Fluorescence of subsequent generations of C. oleaginosus after mutagenesis and selection for High (top 5%), Low (bottom 5%) and ALL (all cells) on the Nile-Red fluorescence channel (FL2). Selection was always done after 7 days of cultivation on either minimal nitrogen medium (MNM-S) or full medium (YPD).

For the present approach, a population based orientation was chosen. Many current studies adopt a single cell approach[141]–[144]. Another issue for the lack of success with random

mutagenesis methods might be effective DNA repair mechanisms or high ploidy level. Further, a high rate of genetically destructive mutations might cause a narrow “mutagenic index” between an insufficient amount of mutations and lethal “overmutation” of cells. Indeed, for ATCC 20509, EMS might not be an ideal mutagen[82], as m-nitro-nitrosoguanidine yielded higher numbers of auxotrophic mutant in a replication screening approach[82]. As EMS also induces double strand breaks and *C. oleaginosus* does not favor homologous recombination as repair mechanism, mutagenized cells might resort to the much more error prone non-homologous end joining, which in turn could yield a higher number of non-viable cells in relation to every mutation. In relation to *Y. lipolytica*, mostly recombinant methods have been employed so far[88], but using lower density of high lipid subpopulations in combination with EMS mutagenesis, lipid productivity was raised by 55%[145]. The described approach has the advantage of not selecting a few hundred thousand cells, but billions of cells. The genetic variation is much higher, Mullers ratchet is avoided and the selection system in itself is more easily controllable.

2.4.5 Media Optimization

Fermentations in 48x format were planned together with- and conducted by Andrea Meo[39]*. The resulting data were not previously analyzed or published in any work and are evaluated and discussed for this chapter.*

For media optimization, cultivation was done in a 48x parallel fermenter. C:N, C:P and C:S ratios were varied individually to estimate the impact of the respective limitations in a full synthetic medium.

2.4.5.1 Dry Biomass and Lipid Content

At the end of the cultivation time after 72 hours, fatty acid spectrum and dry biomass were determined (Figure 17). With increasing nitrogen stress, an increase in lipid content with a peak at a C:N ratio of 145 g/g was observed. Raising the C:N ratio even higher lead to a decrease in lipid share, which can be explained by recruitment of lipid reserves of the cells for survival even in the presence of ample glucose. Biomass continuously decreased with increasing C:N ratio, owing to a lack of nitrogen in the medium required for cell proliferation.

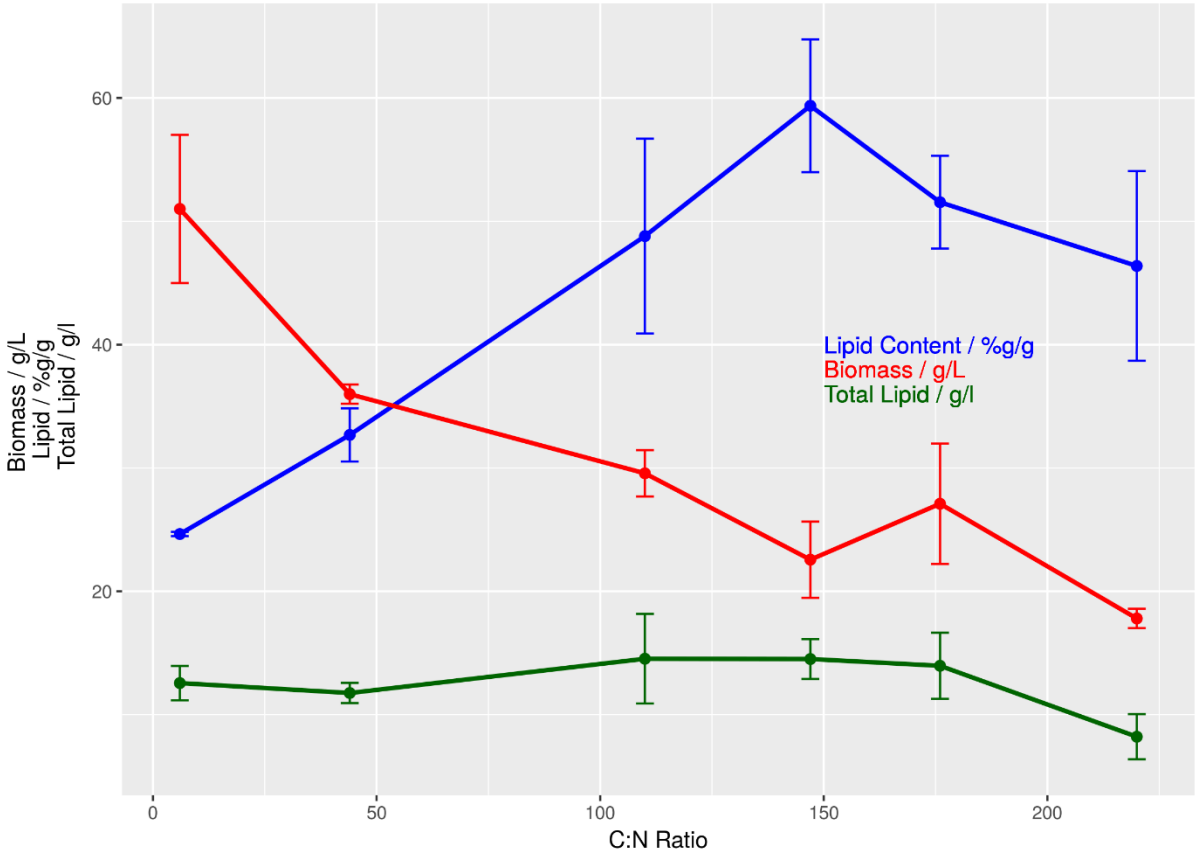

Figure 17: C:N ratio effect on lipid content (% w/w), biomass (g/l) and total lipid (g/l). Error bars show standard deviation of n=3.

This is in contradiction with previous findings, which predict an optimum for total lipid production at a C:N between 30-60 g/g[57], [146]. This, in combination with the fact that already at extremely low C:N ratios, a comparatively high lipid content was found, hints at a secondary limitation acting independently from nitrogen, sulfur or phosphorus stress. Considering the media components (Supplemental 10), it is possible that an iron limitation was induced. In turn, iron limitation was previously described to induce lipid accumulation, especially in conjunction with nitrogen limitation[147]. The resulting limitation in growth would lead to a decrease in total lipid yield and could also lower the lipid content.

Raising C:P ratios (Supplemental 22) had little effect on the lipid content until extremely low concentrations of phosphorus were reached. It was speculated, that with such small concentrations of this critical nutrient, which is essential for cell signaling processes, the cell cannot readjust its metabolism to degrade triglycerides. As with rising C:N ratios, lowering phosphorus content of the medium continuously decreased biomass formation by limiting proliferation. Total lipid yield remained nearly constant.

For sulfate limitation (Supplemental 23), an optimum of lipid content at a C:S ratio of 8’000 was observed followed by a 30% decrease at a C:S ratio of 16’000. Sulfur is a component of two

amino acids and is required for generation of disulfide bonds in and between proteins as well as part of iron-sulfur clusters as cofactors. However, sulfate limitation does not appear to inhibit recruitment of carbon from triglycerides. Biomass decreases continuously, but is almost constant between C:S ratios between 4'000 and 8'000.

2.4.5.2 Analysis of Growth Curve Parameters

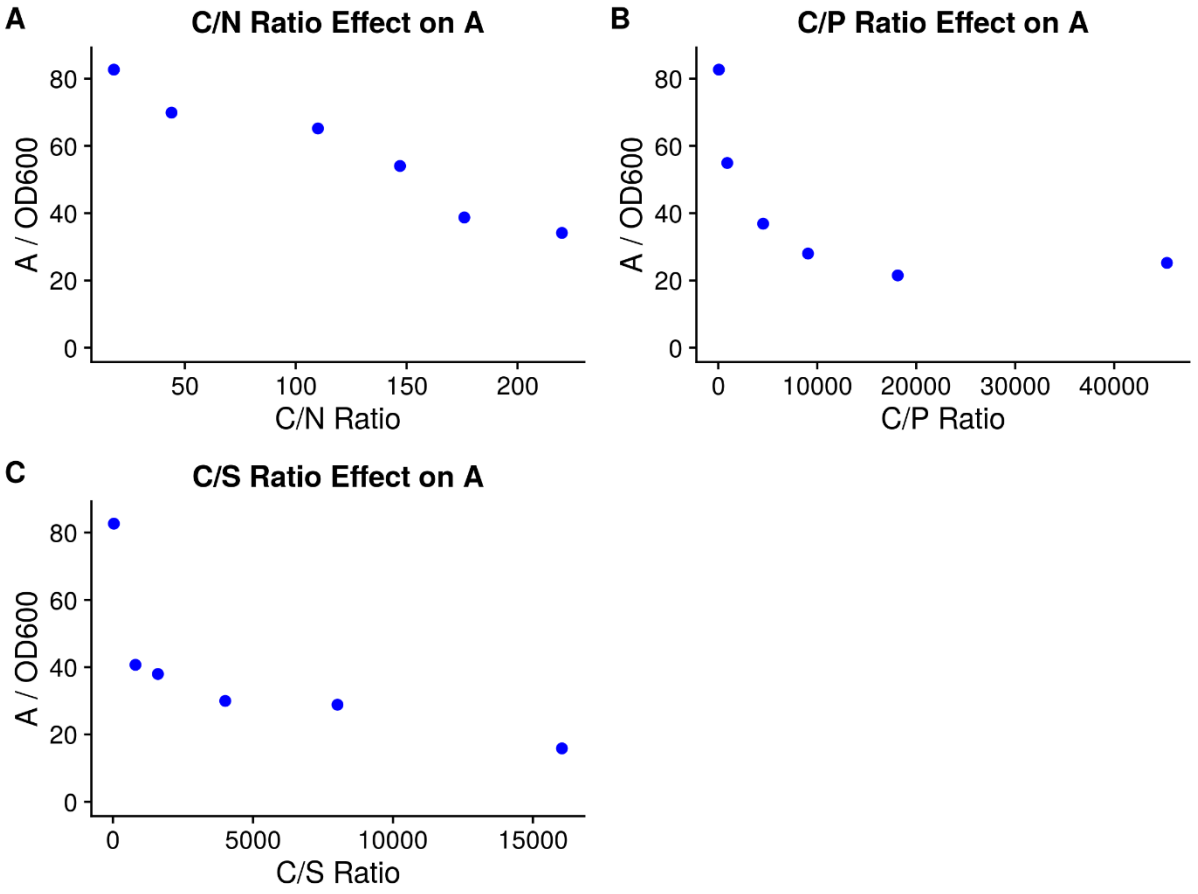

Figure 18: C:N (A), C:P (B) and C:S (C) ratio effect on maximum achieved maximum OD_{600}.

The maximum achieved growth μ was not affected by raising the C:N ratio up to a value of 150 (Figure 18). Beyond this point, a linear decrease down to μ of 1 OD_{600}/minute was observed. For both phosphorus and sulfur limitation, a quick, asymptotic decrease to around 0.5 OD_{600}/minute was visible (Figure 19). Maximum OD_{600} A decreased in a linear way over the entire tested spectrum of C:N ratios. This indicates, that nitrogen was indeed a limiting factor for production of biomass. Similar to the values for growth rate mu, A decreased very rapidly for phosphate and sulfur limitation, but reached a minimum of OD_{600} of around 20, which was obtained even under very strong phosphorus or sulfur stress.

The reason for this could lie in a certain amount of carryover from the preculture despite washing of cells. Further, a minor but consistent decrease in lag phase λ (Figure 19) is most likely attributed to an overall shorter time of cultivation until the maximum OD_{600}=A was reached. Lag phases were consistently between 1.5 and 8 minutes (Supplemental 24).

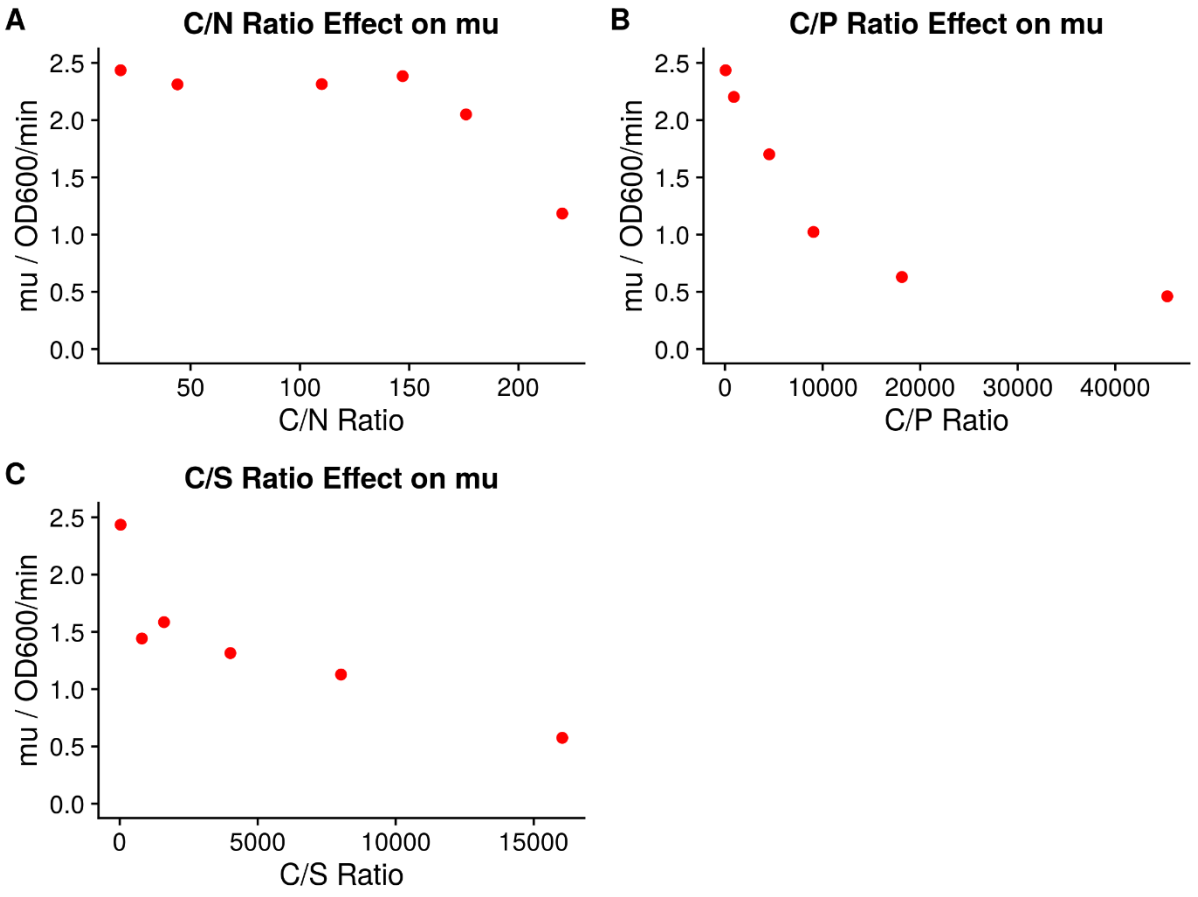

Figure 19: C:N (A), C:P (B) and C:S (C) ratio effect on maximum achieved growth rate μ (mu).

2.4.5.3 Comparison of Nutrient Limitations

C. oleaginosus appears to adapt much more readily to nitrogen limitation than to phosphorus or sulfur limitation. For the latter cases, total biomass concentrations fell below 15 g/l. Total biomass concentrations between 12 and 35 g/l were achieved. The fact that a minimum was reached for very high C:S or C:P ratios hints at a) a readjustment of cell physiology to an environment where these nutrients are not readily available and/or b) recruitment of those nutrients from cells used as inoculum. Lipid yield was also highest for nitrogen limitation and total lipid yield decreased for sulfate as well as phosphate limitation with increasing stress. Presumably iron limitation prevented the observation of clear optima in all limitations. Indeed,

for *C. oleaginosus*, fermentation using combined nitrogen and iron limitation was successfully applied[147].

For Meo[39], sulfate limitation also did not result in accumulation of lipids. In fact, lipid content decreased with increasing sulfate stress in batch (C:S 869 g/g) and fed-batch (C:S 4344 g/g) cultivations. These results, in combination with the data presented in this work, indicate, that it is not possible to use sulfate limitation for the accumulation of lipids. As cells were washed before inoculation, carryover is not impossible, but unlikely. Regarding phosphorus limitation, C:P ratios between 702-35177 g/g were tested in a fed-batch fermentation, resulting in a maximum lipid content of 40% g/g. This is 30% lower than with nitrogen limitation, but sufficient to establish phosphorus limitation as viable alternative to nitrogen limitation in *C. oleaginosus*. Interestingly, for batch processes, C:P ratio had no impact on lipid content. It can be followed that time point of induction of nutrient stress could be a relevant factor.

It can be argued, that the chosen scales of limitation ratios make comparison challenging, however these scales were applied due to data from literature[54], [55], [148] as well as preliminary experiments[39]. In conclusion, presence of organic nitrogen, cultivation mode and possibly other limitations could play important roles. Little is known about how limitations relate to each other. It is possible, that some limitations are additive or even show emergent properties under certain cultivation conditions. This relates to the questions of a) how nutrient presence is detected, b) how nutrient limitation is signaled and c) what the consequences of this limitation on the protein level are. While some progress has been made in clarifying these processes[4], [23], [89], [149], many details remain elusive.

2.4.6 Effect of TORC Inhibition on Lipogenesis and Growth

To explore *C. oleaginosus* cell signaling pathways related to lipid accumulation and to evaluate the possibility of intervention in this network to raise lipid production, the effect of TORC was evaluated. This was done by testing target of rapamycin 1 (TORC1) inhibition by caffeine by and rapamycin.

2.4.6.1 Caffeine Supplementation

Caffeine was added to cultures grown in full medium (YPD) at concentrations between 0 and 100 mM. Cultivation was monitored for 7 days. Cytotoxic effects were observed (Figure 20), however for fluorescence, no significant differences were found (Supplemental 25).

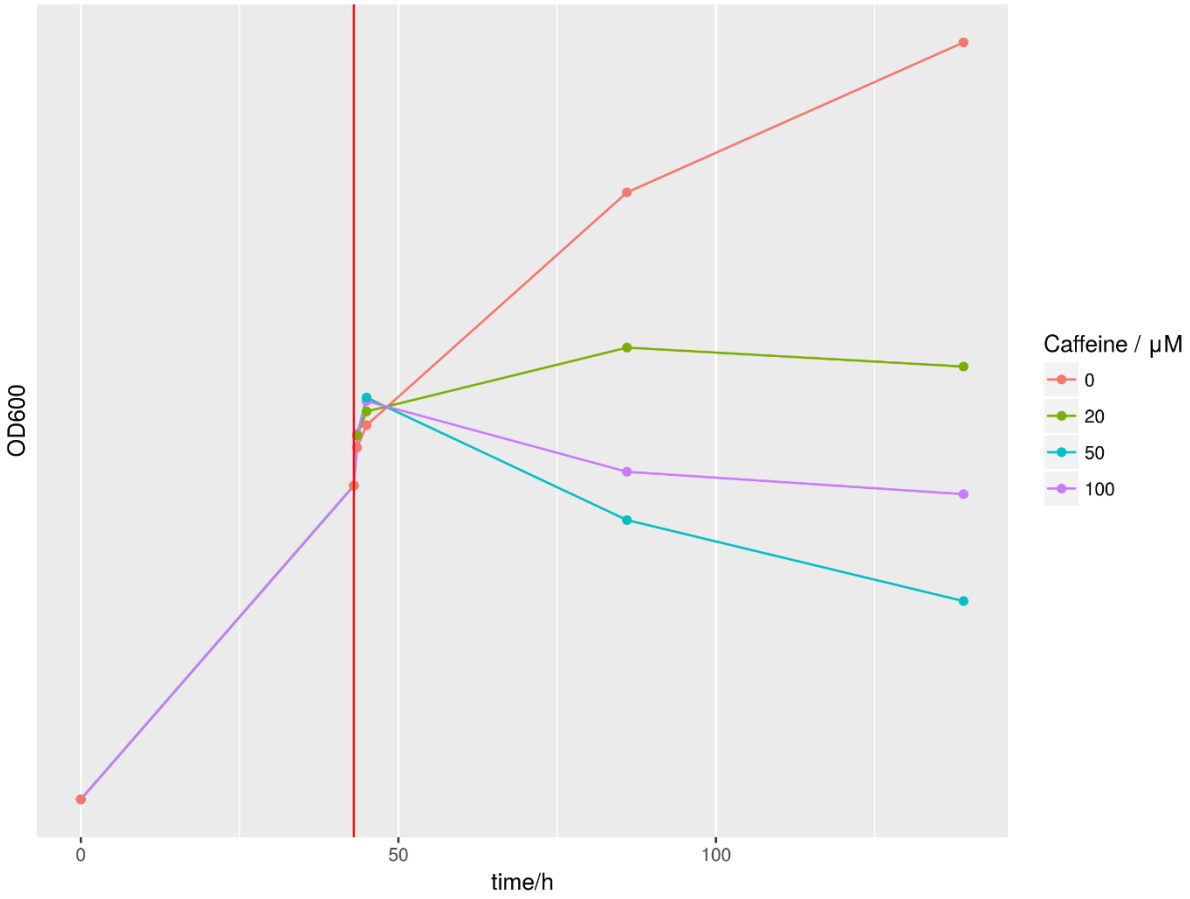

Figure 20: Growth of C. oleaginosus cells grown in YPD with and without caffeine supplementation at different concentrations between 0 and 100 mM measured using OD_{600}.

As the absorption spectrum of caffeine is far from the emission spectrum of Nile red, a quenching effect can be dismissed. It is more likely, that cytotoxic effects of caffeine also interfere with lipid accumulation. Pleiotropic effects of caffeine were described, but are poorly understood. In *S. cerevisiae*, these effects include interference of DNA repair and

recombination pathways, the delay of cell cycle progression and modulation of intracellular calcium homeostasis.

It is apparent, that the compound enters the cells and impacts on cell physiology with at least cytostatic effect[150]. However, it appears not to inhibit TORC1 to a degree sufficient to affect accumulation of lipids. Another possibility is that pleiotropic effects of caffeine drown potential inhibition of TORC1. This suggests a more targeted approach for the inhibition of the TOR complex 1 using rapamycin.

2.4.6.2 Rapamycin Effect on Nile Red Fluorescence

Cultivation of *C. oleaginosus* in full YPD medium does not lead to nutrient limitation and is associated with a low accumulation of intracellular lipids. Supplementation of this medium with rapamycin (20 µM, [151]) after 8 hours cultivation time resulted in significantly higher Nile red fluorescence (corrected for OD) signal indicating an increased lipid production (Figure 21). The increase of 66% FI/OD at 72 hours subsequently decreased to 44% (92 hours) and 40% after 116 hours respectively. During cultivation, no decrease in OD was observed, indicating that the cell growth was not affected by the applied rapamycin concentrations.

It is reported that Nile red is a semi-quantitative lipid stain [152], as its specific fluorescent signal is dependent on the fatty acid profile, the type of lipid (phospho-, triacylglyceride or steran) and the protein content within intracellular lipid bodies.

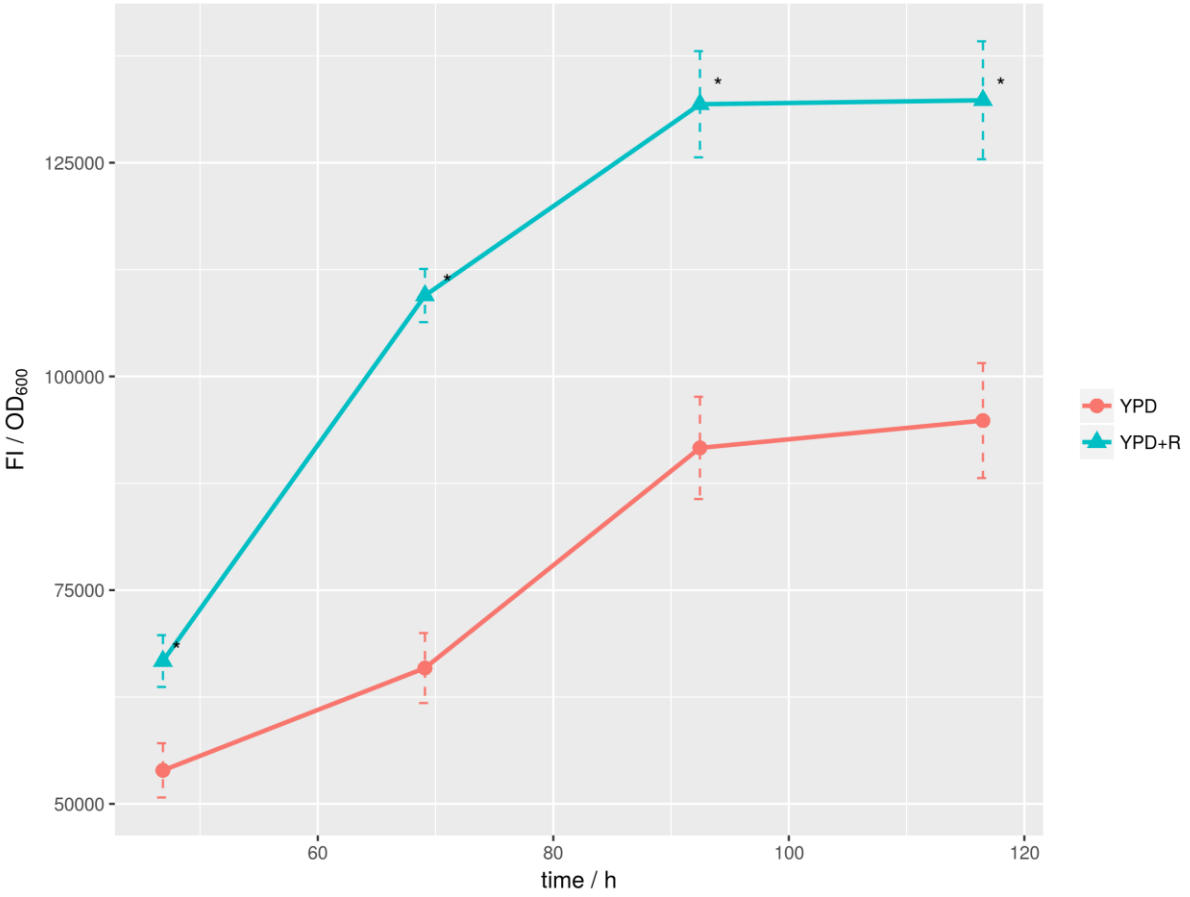

Figure 21: Effect of Rapamycin on Nile red Fluorescence: C. oleaginosus grown in YPD without (YPD) and with 20 µM rapamycin (YPD+R) supplementation. At different time points, Nile red fluorescence (FI) and OD_{600} were measured. The ratio between the latter is plotted on the y axis and is a semi-quantitative indicator of lipid content. Stars show significance at α=0.05 and error bars show standard deviation of n=3.

2.4.6.3 Rapamycin Effect on Lipid Content

To confirm an increase in lipid yield, a gravimetric biomass and lipid determination was conducted using cells grown in cultures containing between 0 and 40 µM rapamycin. The addition of 40 µM rapamycin resulted in a maximum lipid increase of 38% compared to controls without rapamycin. Moreover, at 5 µM rapamycin the total biomass production is significantly increased. These data contrast reports on the effects of rapamycin on algae and bacterial growth, where supplementation of the compound resulted in decreased biomass formation in line with its established cell cycle inhibition effects[153], [154].

Due to the expected logarithmic dependency (Supplemental 26), effects of rapamycin on lipid content (Figure 22) saturate at low concentrations. To confirm the effect of rapamycin on intracellular lipogenesis, a one tailed Welch's t-test between samples was applied in the absence and presence of rapamycin. The null hypothesis of both sample sets being of the same distribution is rejected with p=0.003 and a confidence interval of 1.4-5% g/g increase in the absence and presence of rapamycin.

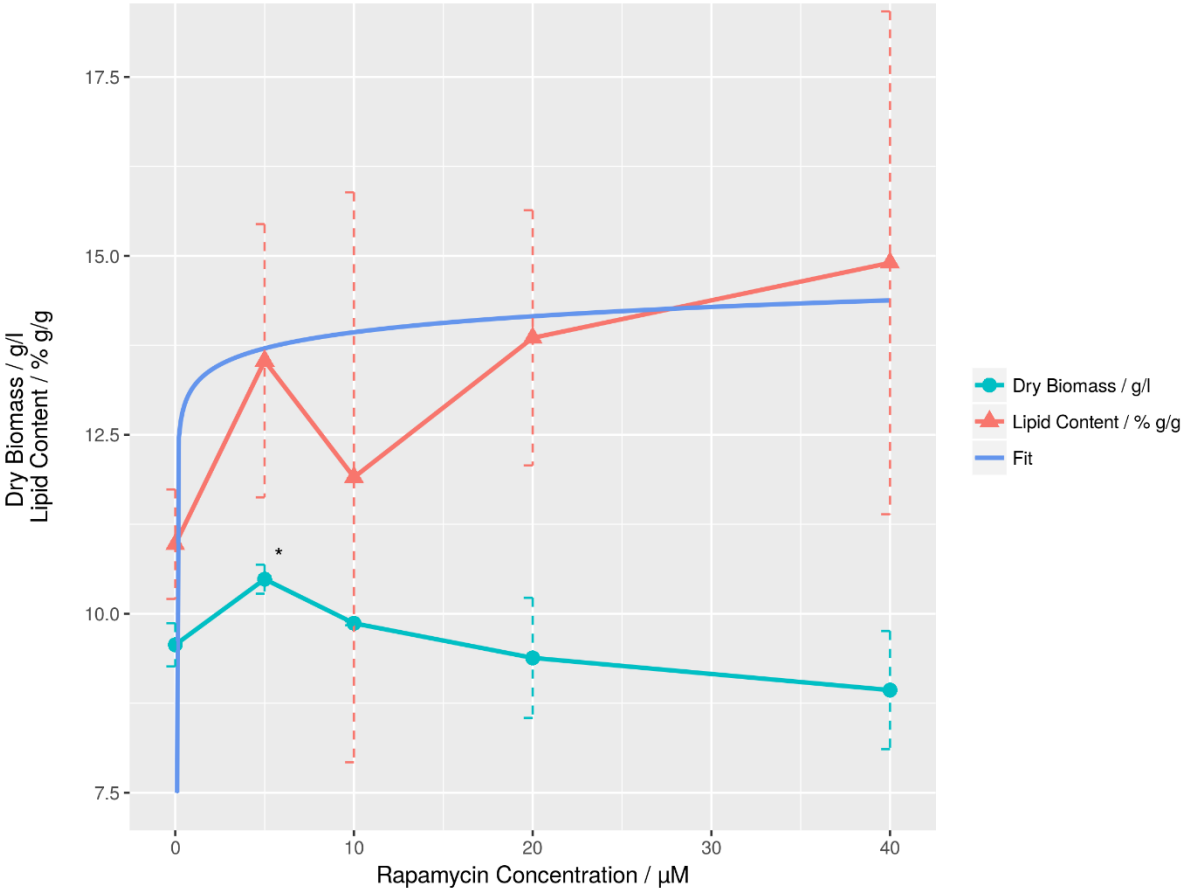

Figure 22: Effect of Rapamycin on Lipid Content and Biomass: Total lipid content (green) and dry biomass (red) of C. oleaginosus after 72 hours of cultivation in YPD are measured with different concentrations of rapamycin supplementation between 0 and 40 µM. Error bars show standard deviation of n=3 and the star shows significance at α=0.05 in comparison to culture without rapamycin supplementation. The blue line shows a robust logarithmic fit of the lipid content in dependence of rapamycin concentration as described in Supplemental 26.

2.4.6.4 Rapamycin Effect on Growth Kinetics

As initial data suggested that at 5 µM rapamycin (at t=8h cultivation time) cell growth was enhanced, a real-time backscatter measurement was used in order to compare cellular growth in the absence and presence of rapamycin (Figure 23). Cell growth was sufficiently described by a fit to a Richards' curve [155], which allowed extraction of μ_{max} (maximum growth rate), λ (lag phase duration) and A (maximum OD_{600}) values (Table 6).

Interestingly, significant differences in the growth parameters of each culture were observed. For the rapamycin treated culture, the maximum growth rate μ_{max} (12% increase) and the maximum optical density (19% increase) were elevated compared to controls.

Table 6: Comparison of growth curve parameters extracted from Richards' fit: Maximum growth rate (μmax), lag phase (λ) and maximum cell density (A) of C. oleaginosus cultivated in YPD with and without rapamycin. All values are given with standard deviations.

	YPD	YPD + 5 μM rapamycin	Change /%
μ_{max} / OD_{600}/hour	$1.2068 \pm 1.779*10^{-3}$	$1.349 \pm 1.362*10^{-3}$	$11.79 \pm 2.6*10^{-3}$
λ / minutes	$12.433 \pm 23.104*10^{-3}$	$12.151 \pm 5.776*10^{-3}$	$-2.27 \pm 3.13*10^{-3}$
A /OD_{600}	$30.754 \pm 7.421*10^{-3}$	$36.578 \pm 6.73*10^{-3}$	$18.93 \pm 0.46*10^{-3}$

This translates to a change in the maximum growth rate from a nominal 1.2 to 1.35 OD_{600}/hour and an increase in the maximum cell density from OD 30.8 (61 g/l) to OD 36.6 (71 g/l) respectively. Hence, in the presence of 5 μM rapamycin the cell density increased by 19% concomitantly with a 25% lipid increase. These cumulative values translate to a 49% improved space time yield compared to controls in the absence of rapamycin.

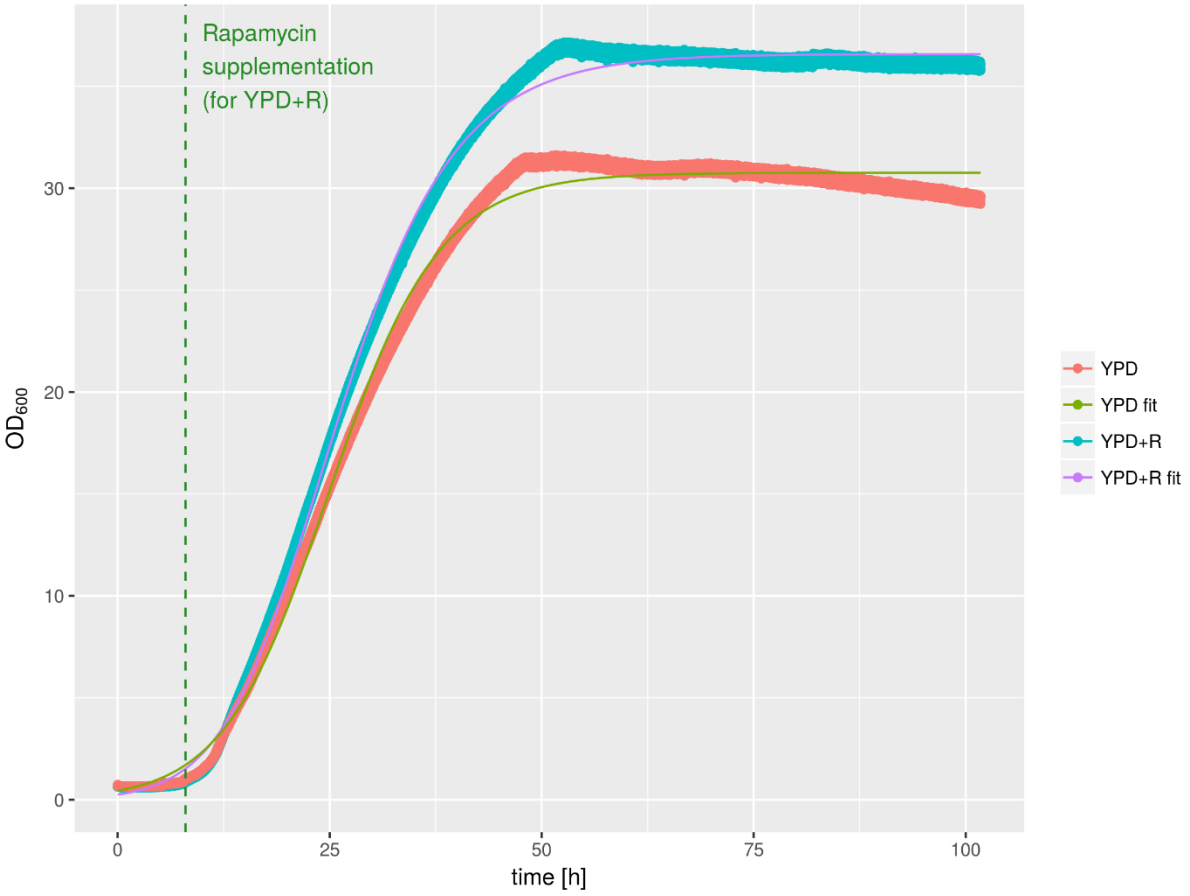

Figure 23: Online-OD Measurement: Growth curves of C. oleaginosus without (YPD) and with 5 μM rapamycin (YPD+R) obtained by measuring backscatter with an online OD system. Thin lines (YPD fit, YPD+R fit) show fit of Richards' growth curves.

The improved growth rate may be attributed to the upregulation of pathways relating to alternative nitrogen sources. A simultaneous assimilation of many different nitrogen sources could be advantageous in a high nutrient environment such as YPD. Furthermore, TORCs are known to affect cell cycle progression. Shortening of the G2 phase could lead to an increased growth rate, while sacrificing replication fidelity and long term offspring survival.

2.4.6.5 Rapamycin Effect on Fatty Acid Spectrum

Supplementation of rapamycin caused a non-concentration dependent shift in fatty acid spectrum (Figure 24). Under these conditions, a major decrease of C18:0 in favor of C18:1 fatty acid was observed. Additionally, a minor decrease of C16:0 and a minor increase in C18:3 was detected. These changes resemble the fatty acid profile obtained by cultivation in nitrogen limiting medium, thereby supporting the notion that rapamycin is at least partially simulating a low nutrient environment to the cells regulatory system. Fatty acid spectra show, that the effect of rapamycin saturates at comparatively low concentrations, confirming the fit in Figure 23.

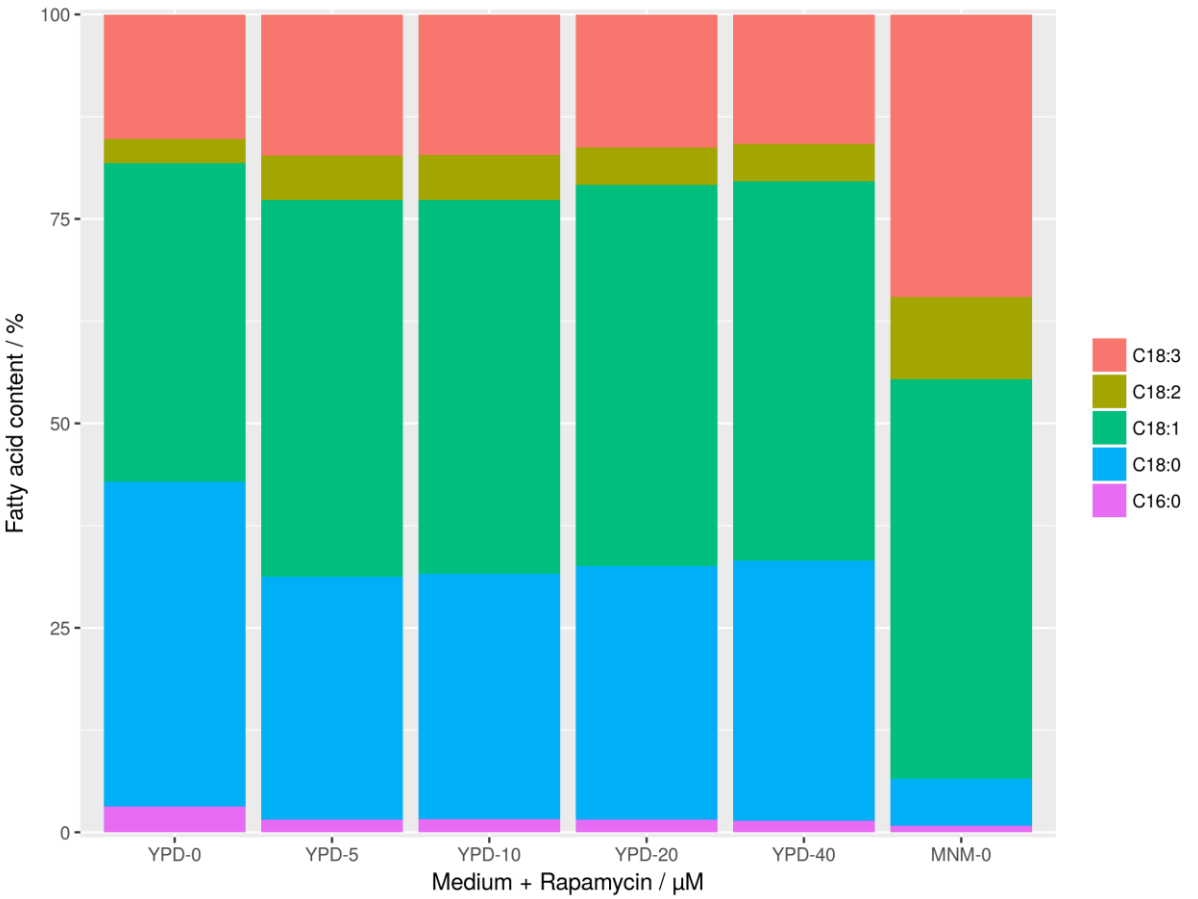

Figure 24: Effect of Rapamycin on Fatty Acid Content: Profile of the main fatty acids of C. oleaginosus after 72 hours cultivation in Minimal N Medium (MNM-0) or YPD with different rapamycin concentrations (YPD-0 – YPD-40).

In *Euglena gracilis,* supplementation of rapamycin led to an increase in lipid amount but almost no change in fatty acid profile was reported [151]. The reason for this appears to lie in the different mechanism of rapamycin response between this algae and previously identified yeasts or animal cells[151]. This observation in this study motivated us to use a bioinformatics approach to investigate the effects of rapamycin on *C. oleaginosus* cell signaling network and lipogenesis.

2.4.7 Assembly of TORC Signaling Network

A homology-based TORC signaling network, including upstream and downstream elements (Figure 25), was assembled. A table of all proposed pathway components can be found in Supplemental 27. The SNF1/AMPK pathway is highly conserved from yeast to mammals, and homologues of its main components could also be detected in *C. oleaginosus*. These homologues termed Elm1, Sak1 and Tos3 are kinases which phosphorylate and activate Snf1 (orthologue to the mammalian AMPK), which in turn is a central regulator required for energy homeostasis. In *S. cerevisiae* Snf1 is mainly responsible for adaption to a glucose limiting environment[156]. Inactivation of Snf1 is caused by dephosphorylation initiated by the Reg1/Glc7 complex[156]. In a low carbon environment, phosphorylated Snf is translocated to the nucleus, where it phosphorylates the transcriptional activator Sip4. Subsequently, Sip4 activates the transcription of glucose-repressed genes[156]. This process is conserved in ascomycetes *S. cerevisiae* and *S. pombe* alike. Interestingly, activated Snf1 also inhibits Acc1p, which is responsible for catalysis of acetyl-CoA to Malonyl-CoA, a main precursor for the production of fatty acids[157]. This indicates a direct link between metabolic signaling under nutrient stress conditions and the regulation of cellular lipid biosynthesis.

Furthermore, Snf1 is reported to inhibit the Tsc1/Tsc2 complex in model yeasts and in mammals. Moreover, the Tsc1/Tsc2 complex further integrates signals from other pathways, including the MAPK/ERK pathway[158], cytokines, hypoxia signals and Wnt signaling respectively. More recently, it has been suggested that in yeast, involvement of other factors, especially in reaction to low nutrient content is feasible [159]. However, a direct inhibition of TORC1 by Vps34, an essential gene which channels amino acid availability to the Tsc1/Tsc2 complex, has been reported in yeasts and mammals [158], [160].

More specifically, TORC1 itself receives inputs from RheB over the Tsc1/2 axis and directly from the EGO complex. In model yeasts this EGO is composed of the kinases Gtr1/2 and Npr2/3 respectively. However, in C*. oleaginosus*, we could not detect homologous of the Npr3 or Ego1-Ego3 complexes, which indicates that the absence of amino acids in the medium are not sensed via the EGO involved signaling. Inhibition of the TORC1 complex by rapamycin occurs via initial formation of an Fkh1 protein-rapamycin complex (mammalian homologue

Fkbp12), which then binds to TORC1. This mechanism is highly conserved throughout the microbial and animal kingdom. Expectantly, C*. oleaginosus* Tor1 contained the characteristic rapamycin binding motif[161]. In nitrogen limited media, the addition of rapamycin has no effect on C*. oleaginosus* biomass formation, growth kinetics and intracellular lipid content. This indicates that TORC1 may already be blocked under nutrient limiting cultivation conditions. Consequently, rapamycin addition had no effect on biomass or lipid formation C*. oleaginosus* (Data not shown).

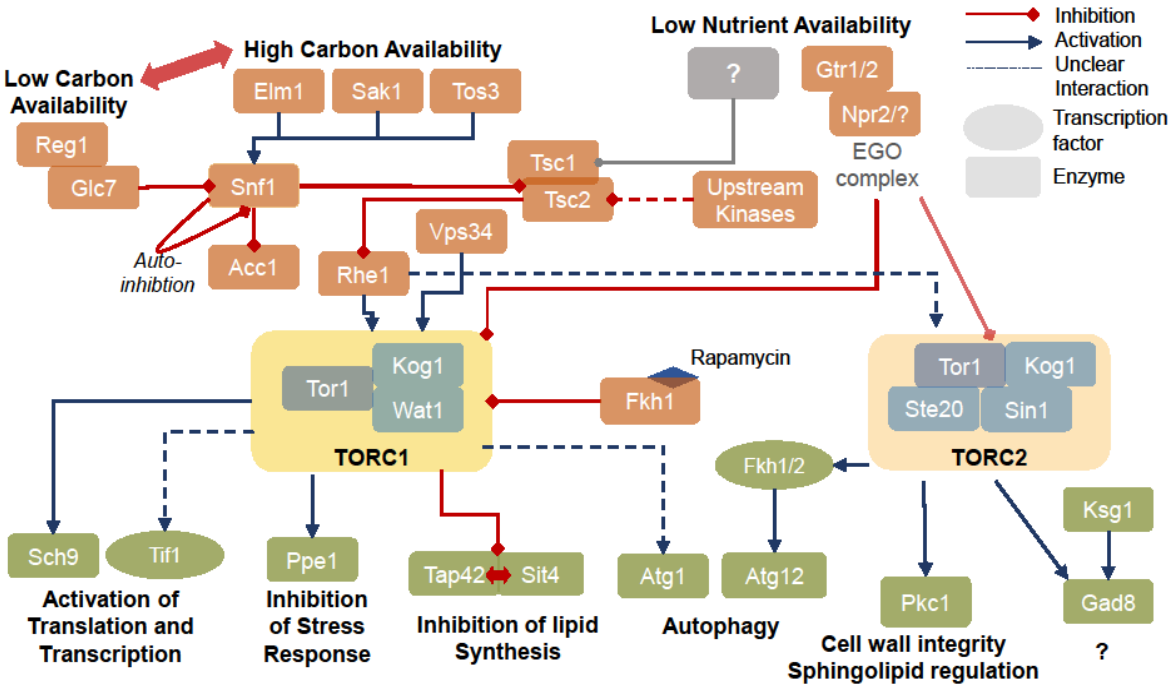

Figure 25: TORC signaling network in C. oleaginosus: Proposed signaling network surrounding TORC in C. oleaginosus inferred by homology and assembled using data obtained from S. pombe and S. cerevisiae.

In consensus with data from model yeasts, we could identify homologues components of the TORC1 complex, namely Tor1 (with strong similarity to Tor2 of *S. pombe*), Kog1 and Wat1 respectively. Wat1 is a scaffold protein facilitating the connection between Tor1 and downstream substrates, like Ppe1 and Sch9[162]. Analogous to model yeasts and mammals the Wat1 protein in C*. oleaginosus* mainly contains 7 WD40 repeats. Specifically, in mice, Wat1 was required for TORC2 but not TORC1 activity. Most interestingly, we could not detect any Tco89 homologue in *C. oleaginosus*, which indicates that a component of the TORC complexes found in model yeast *S. cerevisiae* is absent. Therefore, the TORC1 complex of *C. oleaginosus* more closely resembles the situation reported for *S. pombe* or the oleaginous yeast *R. toruloides*. Indeed, this resemblance is confirmed by the absence of a second Tor gene for TORC2. Furthermore, we could not identify any Avo2 or Bit61 homologues in *C. oleaginosus*, both of which are non-functional TORC2-binding structures [163]. Transcripts for the TORC2 component Sin4 was identified in different splicing isoform, which is consistent

with previous findings in *S. cerevisiae* [160]. Notably, in *S. cerevisiae*, mutation of Sin4 leads to rapamycin resistance[164]. In analogy, the presence of Sin4 isoforms detected in *C. oleaginosus* could render the TOC2 complex resistant to rapamycin.

Downstream of primary TOC effects, significant differences between signals in model yeasts and C*. oleaginosus* affecting autophagy were identified. Particularly, genes essential to the autophagy signaling pathway, namely Atg13, Atg17, Atg31, Atg29 could not found in *C. oleaginosus*. In this respect, the *C. oleaginosus* system may resemble the regulatory system of *Drosophila melanogaster*, in which hyperphosphorylated Atg1 in conjunction with Atg13 are sufficient to inhibit autophagy. In the model yeast S*. cerevisiae* the autophagy signaling is by far more complex and therefore may not apply to C*. oleaginosus* [165]. Further, individual autophagy related homologues (Atg5, Atg6, Atg16) were found, but the actual signaling pathway appears to differ significantly from other yeast systems.

The other main signaling pathways for regulation of lipid biosynthesis, transcriptional and translational initiation appear to be conserved with high similarity. In *S. cerevisiae*, TORC1 inhibition liberates Tap42 and Sit4 from being bound to each other. This in turn activates the downstream transcription factors, Gat1 and Gln3. After Gat1 and Gln3 transport to the nucleus, these transcription factors induce the accumulation of lipids. Our bioinformatics analysis indicates that a similar mechanism is likely for C*. oleaginosus*. The highly conserved Sch9 is homologous to the mammalian S6K, which is responsible for activation of ribosomal protein S6 and therefore directly controls translation. By contrast, no homologue to Gaf1, which in *S. pombe* is central for the response to nitrogen stress[166], was identified. The absence of Gaf1 therefore may modulate the cell cycle in C*. oleaginosus*. Nonetheless, Ppe1 homologue a kinase acting within the *S. pombe* stress response which also affects the cell cycle[167] was identified.

TORC2 activation, especially in yeast, remains elusive. In *S. pombe*, interaction with Rhe1 is confirmed[168]. Furthermore, it was reported in mammals, that activation can be achieved by growth factors (PI3K axis). Furthermore, ribosomal association of the complex suggests its activation by nutrients. Especially the latter is also likely for yeast[169], considering the effect on growth in *S. pombe*[170]. In *C. oleaginosus* however, little can be reported about the effects of downstream TORC2 elements due to the absence of detailed cell biology studies.

Active TORC2 activates Fkh1/2 in *S. cerevisiae* (FOXO genes in mammals), which affects autophagy related genes, life span and stress response[163], [171], [172]. TORC2 as well as the highly conserved Kinase Ksg1 activate Gad8 by phosphorylation[173]. The subsequent cellular effects strongly depend on the organism. For *S. cerevisiae*, this impacts on actin organization and cell wall synthesis, whereas for *C. elegans* mainly lipid metabolism and growth are affected. For the related and well described yeast, *S. pombe*, changes in amino

acid uptake and general changes in stress response are described[163]. Lack Rho/Rac homologues indicate strong differences in the regulation of actin organization from *S. pombe.*

A confirmed element of TORC2 is Pkc activation, as was described for the closely related and pathogenic *Cryptococcus curvatus*. Pkc itself is involved in regulation of sphingolipid biosynthesis, which impacts the structural integrity of the cell wall[174]. Most recently, the GATA transcription factor Gaf1 was reported to be responsible for sexual development in yeast and upregulation of amino acid transporters[166]. It is activated as response to nitrogen stress about 10 to 120 minutes after the onset of nitrogen stress. Therefore, it can be hypothesized that it is part of a first, reversible response to nutrient stress. Persisting lack of nitrogen would then trigger the second, delayed phase which includes elevated mating in *S. pombe*.

Two factors indicate, that the observed effects are not due to rapamycin involvement with TORC2: Rapamycin resistance of TORC2 was structurally substantiated by Avo3 (Ste20), which wraps around the Fkpb-binding domain of Tor1/2[175]. Prolonged exposure of certain mammalian cell types to rapamycin showed inhibited assembly of TORC2[176], however this was not observed in unicellular organisms[163] and therefore appears unlikely for *C. oleaginosus*. Secondly, no obvious differences in cell morphology were observed using microscopy (Supplemental 28) and FACS (Supplemental 29), indicating that for *C. oleaginosus*, rapamycin does not impact on cytoskeleton and actin organization, which are commonly affected by TORC2.

2.4.8 Genetic Modification of *Cutaneotrichosporon oleaginosus*

Overexpression of Dga1/2 and Slc (2.4.8.3) as well as CRISPR/Cas9 based gene editing presented here were executed in part under my guidance as part of the Bachelor's thesis "Genetic Modification of Trichosporon oleaginosus" Kathrin bach 2016. The data were reevaluated and discussed for this chapter.

2.4.8.1 Codon Tables and Codon Adaption Indices

The codon adaption index (CAI) describes the frequency of a specific codon being used in a gene in relation to the most commonly used codon for the relating amino acid. It can take values from 0 (only the least common codons are used) to 1 (only the most common codons are used) and is calculated by determining the weight of each of codon for each amino acid. The distribution is then matched with a reference set containing the frequency of the most frequent codon for each amino acid. Since tRNA distributions vary in organisms, the expression rate of homo- or heterologous proteins can significantly drop, when uncommon codons are used. The CAI can be used as a weak predictor for success of expression[177], although little consistency has been found by correlating the quality of a heterologous expression and CAI. Other parameters, such as GC content, stability, amino acid half-life, solubility and factors that strongly impact on folding such as disordered or fibrous regions have to be considered as well. However, in contrast to heterologous expression on established platforms such as *E. coli*, the impact of these factors on expression in *C. oleaginosus* is unknown. As a rule of thumb, CAIs below 0.5 can be considered unfavorable and values over 0.8 as favorable for expression in *E. coli*[178], but much lower minimum values, such as 0.084 for *E. coli* or 0.041 for *S. cerevisiae* were suggested as well. [179]

For codon optimization and determination of codon adaption indices (CAI), codon tables were generated to describe the codon usage of *C. oleaginosus*. In previous work[51], this was not examined in detail and solely the codon distribution of the glycerinaldehyd-3-phosphat dehydrogenase (GDH) gene was used to optimize the expressed genes. In this work, codon tables from GDH, the entire transcriptome, as well as the top 10 transcribed genes in both MNM-S as well as YPD Medium were considered (Table 7).

Table 7: Genes with 10 highest transcription rates as indicated by the Reads per Kilobase of Transcript per Million reads Mapped (RPKM) under lipid accumulating (MNM) and proliferating conditions (YPD).

Locus Tag	Gene	RPKM MNM	RPKM YPD
Triol1|249059	Aldo/keto reductase family protein	14968.89	572.1
Triol1|289369	Ubiquitin	11784.53	3151.76
Triol1|308253	Delta 9 Fatty acid desaturase	11246.62	7204.26
Triol1|283928	-	10995.83	2875.96

Triol1|284692	Perilipin	8924.71	745.98
Triol1|310356	Endoglucanase	8721.46	0.37
Triol1|276138	Glyceraldehyde 3-phosphate dehydrogenase	7324.36	17315.17
Triol1|288072	ATPase component of ABC transporter	7236.76	504.95
Triol1|292613	-	6761.68	65.87
Triol1|302913	Ammonia permease	6083.98	5.33
Triol1|270049	Mitochondrial ADP/ATP carrier proteins	5256.55	25367.25
Triol1|306950	Cytochrome c	962.97	25272.8
Triol1|286349	-	1941.3	17504.95
Triol1|276138	Glyceraldehyde 3-phosphate dehydrogenase	7324.36	17315.17
Triol1|286945	Cyclophilin type peptidyl-prolyl cis-trans isomerase	944.35	17054.37
Triol1|224393	60S ribosomal protein L37	1828.17	10371.59
Triol1|251192	-	712.04	10310.84
Triol1|226154	Histone H4	2934.98	10112.34
Triol1|248145	Translation elongation factor EF-1 alpha	5728.48	8780.6
Triol1|288478	40S ribosomal protein S12	2352.76	8672.74

In this approach, only the most common codon was deemed relevant for optimization of genes and all non-optimal codons for each respective amino acid were replaced by the most frequently used one. Within the course of the optimization, codon usage of different reference sets were compared: The single GDH gene (GDH), the top 10 transcribed genes under lipid accumulation conditions (MNM-C), the top 10 transcribed genes under proliferation conditions (YPD), both of the latter ones combined (Top19), as well as the whole genome (Total) as shown in Table 8.

Large deviations were found between relative codon usages, as can be found in Supplemental 30. However, the most common codon for each amino acid stays almost always consistent over all data sets (Table 8), strong differences can be seen in comparison to *Y. lipolytica*, another genetically accessible oleaginous yeasts.

Table 8: Most used codons for C. oleaginosus was found in the Top20 expressed genes in full medium and lipid induction medium (Top19) as well as both individually (T10YPD and T10MNM), only the glyceraldehydphosphate dehydrogenase (GDH) and the entire genome (Total). In comparison, codon usage of ascomycete Yarrowia lipolytica is shown.

	Top19	**T10YPD**	**T10MNM**	**GDH**	**Total**	***Y. lipolytica***
Ala	GCC	GCC	GCC	GCC	GCG	GCC
Cys	TGC	TGC	TGC	TGC	TGC	TGT

Asp	GAC	GAC	GAC	GAC	GAC	GAC
Glu	GAG	GAG	GAG	GAG	GAG	CAG
Phe	TTC	TTC	TTC	TTC	TTC	TTC
Gly	GGC	GGC	GGC	GGC	GGC	GGC/GGT
His	CAC	CAC	CAC	CAC	CAC	CAC
Ile	ATC	ATC	ATC	ATC	ATC	CTG
Lys	AAG	AAG	AAG	AAG	AAG	AAG
Leu	AAG	AAG	AAG	AAG	AAG	CTG
Met	ATG	ATG	ATG	ATG	ATG	ATG
Asn	AAC	AAC	AAC	AAC	AAC	AAC
Pro	CCC	CCC	CCC	CCC	CCG	CCC
Arg	CGC	CGC	CGC	CGC	CGC	CGA
Ser	TCG	TCG	TCG	TCG	TCG	TCT/TCC
Thr	ACC	ACC	ACC	ACC	ACC	ACC
Val	GTC	GTC	GTC	GTC	GTC	GTG
Trp	TGG	TGG	TGG	TGG	TGG	TGG
Tyr	TAC	TAC	TAC	TAC	TAC	TAC
End	TAG/TAA	TAG/TAA	TAG	TGA	TGA	TAA

Table 9: Genes expressed in Cutaneotrichosporon oleaginosus with their corresponding CAI before optimization. Stars shows optimization and expression done by Görner[51]*. CAI after optimization is 1 in all cases. Dga1, Dga2 and Slc1 were not codon optimized*

Gene	**Origin**	**CAI before optimization**
Yellow fluorescent Protein (YFP)*	*Aequorea victoria*	0.808
Hygromycin phosphotransferase (HygR)*	*Escherichia coli*	0.440
Delta-9-elongase (IgASE2)*	*Isochrysis galbana*	0.540
Delta-12/Omega-3 desaturase (Fm1)*	*Fusarium moniliforme*	0.671
Linoleic acid isomerase (PAI)*	*Propionibacterium acnes*	0.619
Kanamycin aminophos-photransferase (APH3 II)	*Streptomyces kanamyceticus*	0.279
CRISPR associated protein 9 (CAS9)	*Streptococcus pyogenes* (humanized)	0.435
Acylglycerol-phosphate-acyltransferase (SLC1)	endogenous	0.687
Diacyl-glycerol-acyltransferase (DGA1)	endogenous	0.526
Diacyl-glycerol-acyltransferase (DGA2)	endogenous	0.351

Table 9 shows an overview of all heterologously expressed genes in *C.* oleaginosus. The full sequence of the genes is shown in Supplemental 5.

2.4.8.2 Localization of ATMT Insertion Site

Thermal asymmetric interlaced polymerase chain reaction was used to identify the locus of insertion of the YFP expression cassette of the YFP expression clone previously generated by Görner *et al*[51]. Sequencing of fragment obtained by arbitrary PCR yielded a sequence with high congruence to *C. oleaginosus* genomic DNA at locus scaffold_1: 458750-459800 of the JGI assembly of the respective organism[123].

The respective sequence was identified as a putative carbamate kinase according to homology to a *Leucobacter sp.* gene with a maximum score of 38.1, query cover of 38% and identity value of 34%. Details of the insertion site are shown in Supplemental 31. The result shows that arbitrary PCR can in principal be used to determine loci of insertion sites in ATMT mutants. However, it cannot be excluded that the expression cassettes were integrated multiple times into the genome. In this case, only one of the integration loci might be found by random hexamer amplification. Variation of hexamer primers and PCR conditions are usually employed to alleviate this downside.

2.4.8.3 Overexpression of Dga and Slc

Slc1 and Dga2 were chosen for homologous overexpression due to their essential role in triglyceride synthesis (Section 2.1.2). First, *C. oleaginosus* clones obtained by ATMT were checked for integration of the expression cassettes. Genomic DNA was extracted from different clones and the resistance cassettes were amplified and sequenced (Figure 26). Bands at the expected height (1147 bp) were extracted and sequenced, always yielding the expected sequence of the hygromycin B resistance cassette. The genomic integration of cassettes was confirmed for clones 1, 5, and 6 of pRF_HygDga2. Expected fragment size for pRF_KanSlc was 810 bp and clones 2, 4 and 7 were confirmed by sequencing. However, subsequent subcultivation led to an unexplained loss of growth on G418 selection plates. Thus, the respective clones were not further investigated.

Nile red fluorescence of *C. oleaginosus* Dga2 overexpressing clones did not display significantly higher fluorescence than the wild type (Supplemental 32, all other clones in Supplemental 33). Indeed, clone 1 and 6 showed lower fluorescence than the wild type. This served as a first indicator, that Dga overexpression does not yield higher lipid accumulation in *C. oleaginosus*. The same clones were used for fermentation in YPD.

To exclude the possibility, that nutrient or oxygen limitation was the reason for insufficient Dga2 expression, a fermentation using all three clones and the wild type was conducted.

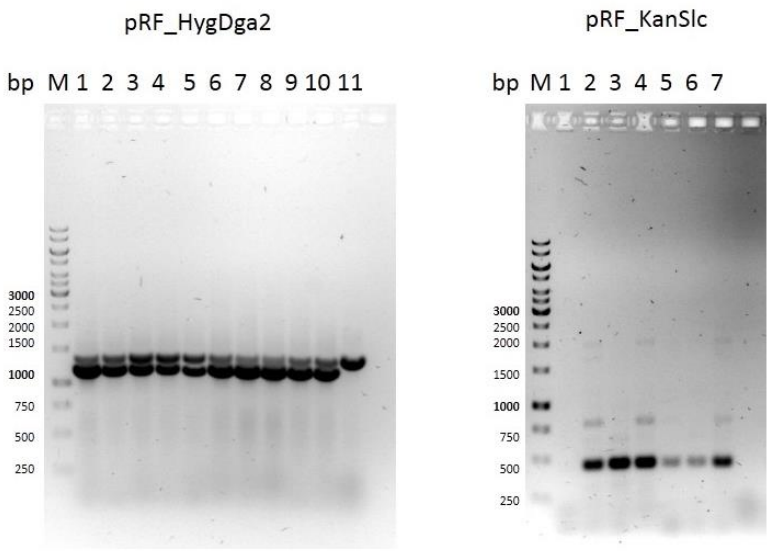

Figure 26: Segments of hygromycin resistance cassette used to confirm the insertion of the expression cassettes into the C. oleaginosus genome. For pRF_HygDga2, the expected size was 1147 bp (lower band), while for pRF_Kan_SLc, the expected size was 810 bp.

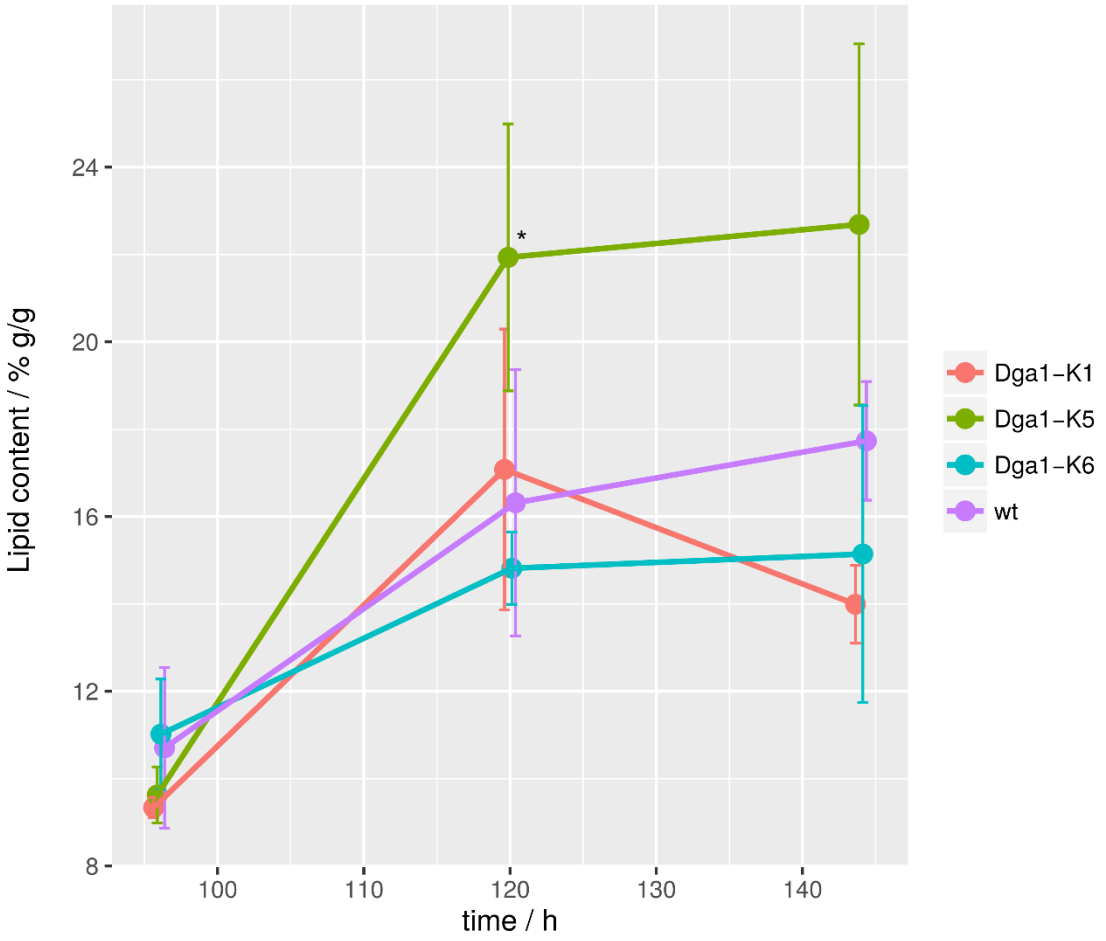

Figure 27: Nile red fluorescence of C. oleaginosus Dga wild type and overexpressing clones 1, 5 and 6 (Dga1-K1, Dga1-K5 and Dga1-K6 respectively) after 96 hours grown in YPD in baffled 50 ml flasks. Star shows significantly high values than the wild type as determined by a two tailed t-test assuming equal variances (α=0.05). Error bars show standard deviations of triplicates.

For fermentation, clone 5 of the overexpression mutants was significantly higher than the wild type. However due to the high deviations and inconsistency between clones and wild type, the result remains inconclusive (Figure 27). Corresponding to work done by Goerner[21], it remains unclear how many expression cassettes were inserted into the genome. This was a source of variation between the different clones. Also, no data about actual expression levels of Dga2 are available, which would require further transcriptomic analyses or characterization on the protein level. Table 9 shows, that the CAI of Dga2 was 0.35, which is not favorable for expression. A higher number of integrations at favorable loci for clone 5 is possible, but speculation based. Deviations in fatty acid spectrum were observed (Supplemental 34, Supplemental 35), but were inconsistent throughout clones. Specifically, possible substrate preference of diacylglycerol acyltransferase for specific fatty acids, which was previously described[180], could therefore not be confirmed.

In summary, it cannot be shown beyond reasonable doubt, that Dga2 expression yields a higher lipid content in *C. oleaginosus*. This is contrasted by data obtained in other organisms. Acylglycerolphosphatidate acyltransferase and diacylglycerol acyltransferase were chosen for their high potential of raising lipid accumulation. In *S. cerevisiae*, overexpression of Dga led to a 171% raise in lipids (lipid content of 15% g/g)[181]. In *Y. lipolytica*, overexpression of the endogenous Dga led to a 206% raise in lipids (lipid content of 72% g/g)[182] or a 246% raise in Nile red fluorescence[183]. Overexpression of Slc1 resulted in an 87% raise in *Y. lipolytica*[183]. Assuming sufficient expression of Dga2, which is somewhat speculative, it can be followed that the last step of lipid synthesis, conversion of diacylglycerol to triacylglycerol, might not a rate limiting step in *C. oleaginosus* as opposed to other yeast.

2.4.8.4 CRISPR Cas9 – In vivo expression

With the current ATMT based methodology, overexpression of heterologous or homologous genes is possible. However, there is currently no possibility for the induction of deletions in *C. oleaginosus*. Multiple approaches using homologous recombination were not successful (Data not shown). The CRISPR-Cas9 system however would make deletions possible and hence was tested. Subsequent to the procedure described in section 2.3.4.6, clones obtained by ATMT were checked for integration of the expression cassette by PCR. Figure 28 shows positive clones containing the resistance cassette and hence Cas9. Fragment identity of clones one and two was confirmed by sequencing.

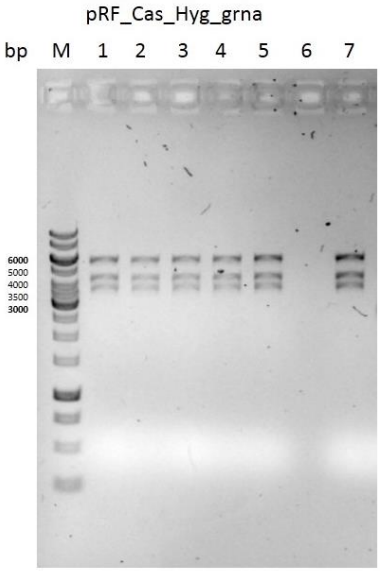

Figure 28: Detection of Cas9 expression cassette in ATMT clones. Positive clones of pRFHyg_Cas9gRNA show a signal at: 1. 5772 bp, 2. 4238 bp, 3. 3546 bp

After cultivation on YPD, Cas9 activity should have generated Ura3 clones with preferred growth on 5-FOA in comparison to the wild type. However, sequencing of a total of 20 clones per gRNA approach (gRNA1 and gRNA2, both targeted at Ura3 of *C. oleaginosus* as described in Supplemental 9) yielded no knockout mutant. This suggests Cas9 inactivity. Lack of Cas9 nuclease activity can be founded in lack of Cas9 expression, insufficient transport to the nucleus as facilitated by the NLS sequence, insufficient gRNA expression, lack of ribozyme cleavage or heavy offsite activity leading to death of cells expressing Cas9 nuclease.

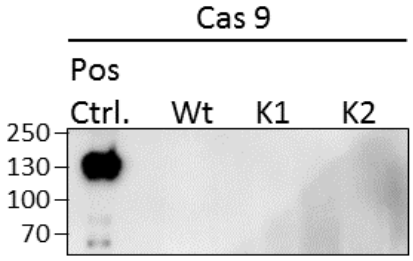

Figure 29: Western blot showing absence of Cas9 expression in two C. oleaginosus clones containing the Cas9 gene cassette (K1, K2) as well as the wildtype as negative control. 10 ng of Cas9 nuclease served as positive control.

As a first step, protein expression was checked by western blotting protein extract of wild type *C. oleaginosus* and clones with integrated Cas9 expression cassettes. The control yielding 10 ng of Cas9 was visible, however the two isolated clones showed no expression (Figure 29). While sufficient to yield hygromycin B resistance, the truncated version of the GDH promoter is likely not suitable for acceptable Cas9 expression for genome editing. This could also be

associated with suboptimal codon usage of humanized Cas9, as all expression cassettes by Görner *et al*.[51] contained codon optimized genes. A codon optimized version of the expression cassette could not be finished in time.

2.5 Conclusion and Outlook

Firstly, the isolation and characterization of new oleaginous yeasts was shown. Yeast substrains were discovered, which exhibited fatty acid profiles of triglycerides and possibly phospholipids significantly different from the described literature values as well as the tested reference strain. The results remain to be confirmed, but varying fatty acid profiles are a promising starting point for discovering and transgenic testing of different fatty acid modifying enzymes in oleaginous yeast.

A fundamental issue in the procedure of isolating new strains lies in the first step of cultivation: Due to the exponential nature of cell proliferation, fast growing strains will always outpace slower strains until the latter are no longer detectable in the culture. There are two main adjustments that can be made to alleviate this problem.

1. One of the main issues is the balance between screening pressure in the form of different media compositions and cultivation conditions, and the amount of strains that can be obtained. In this work, only one cultivation condition with two different media was chosen, representing a strong screening pressure. More media and cultivation conditions could be tested, which would possibly yield useful strains, but also slow growing yeast with possibly specialized requirements in their environmental conditions. These, of course, are undesirable in an industrial environment.
2. Another possibility is the direct single cell isolation using a fluorescent activated cell sorter (FACS). This would possibly allow “in situ” staining with Nile red and isolation according to lipid content. Obviously, the restrictions given in the first point would still apply.

A second important point is the collection of environmental samples. There are a number of facilities with yeast collections, some with many decades of experience in the field of isolation and maintenance of strains, such as: The Centraalbureau voor Schimmelcultures (CBS), the Phaff Yeast Collection, the American Type Culture Collection (ATCC) or the National Collection of Yeast Cultures (NCYC). At this point, obtaining new strains can only be accomplished by combining unusual areas of isolation with new screening methods. However, it is questionable, whether current “top performers” in relation to lipid productivity can be beaten by other natural isolates by significant amounts. As the evolutionary process is aimed at survival and not industrial productivity, further improvement will most likely only be possible through recombinant methods. The technology of single cell oil production is in a similar situation as the technology for amino acid production: Improvements through new strains are unlikely and process-related optimization have been described extensively. Most likely, only cis- or transgenic modifications or even biosystem engineering allow for further improvement.

The sorting experiments yielded the insight, that the average fluorescence per well obtained from measurements in a plate reader is comparable to the distributions obtained from the FACS: A staining method was established and applied in a directed evolution approach. No improved strains could be obtained from this, presumably due to unfit mutation patterns and the “Mullers ratchet” effect.

The supplementation of caffeine yielded toxic effects but no changes in fluorescence and therefore presumably no change in lipid content. By supplementing the pricy compound rapamycin, a sustainable increase in lipids was observed. The fatty acid profile changed towards a pattern characteristic for lipid accumulation. For the first time, lipogenesis was induced in an oleaginous yeast without compromising on growth, resulting in a 1.4-fold increase in total lipid yield. We observed an increase in growth as well as lipid content in the absence of nutrient limitation, using YPD as model substrate with high nutrient content. TORC1 in *Cutaneotrichosporon oleaginosus* can be inhibited by rapamycin, impacting on growth characteristics and lipid accumulation. However, considering a lack of reduction in growth and comparatively minor increases in lipid accumulation, inactivation of TORC1 is not sufficient to induce a cell state resembling nitrogen starvation.

It is possible, that *C. oleaginosus* either relies on TORC2 inhibition, requires additive signals of both complexes or employs another unknown pathway for full activation of nitrogen stress response and associated lipid accumulation. However, TORC2 regulation of lipid synthesis and its strong involvement in the upregulation of amino acid transporters[163], one of the defining features of lipid accumulation in *C. oleaginosus*, make TORC2 involvement in nutrient limitation response in this yeast likely.

Proteomic and transcriptomic approaches are excellent tools for elucidating how rapamycin impacts on *C. oleaginosus* physiology. Comparing these data with previously obtained information about transcriptomic changes[24] in the presence of nitrogen stress will allow for pinpointing more clearly the relevance of TORC1 for lipid accumulation. Employing metabolomic strategies might be a promising approach for a more in-depth study of key intermediates, such as glutamine and glutamate as components of central nitrogen metabolism.

For these reasons, further exploration of *C. oleaginosus*, despite challenges in its genetic accessibility, is worthwhile. Already as wild type, the strain displays high lipid content, fast growth to high biomass concentrations and a favorable fatty acid spectrum, which is modifiable. Further genetic engineering would allow the development of *C. oleaginosus* to a high potential organism for the production of lipids and secondary metabolites

Overexpression of Dga2 or Slc1 did not yield a confirmed increase in lipid- content or productivity. Slc1 clones did not yield stable transformants, possibly associated with the mechanism of G418 resistance using the KanMX cassette used for the respective clones. Dga2 clones were stable and integration into the genome was confirmed. However, increase in Nile red fluorescence or lipid content was not significant for cultivation both in flasks and fermenters. Insufficient overexpression due to low CAI value of Dga2 sequence is possible, however the respective metabolic step also appears to be non-rate-limiting, which contrasts previous results in *S. cerevisiae* or *Y. lipolytica*. Cas9 expression using a homologous truncated GDH promoter did not yield sufficient expression for gene editing, as confirmed by western blot.

3 Flocculation of the Microalgae *Scenedesmus obtusiusculus*

3.1 Introduction

3.1.1 Algae as Biological Feedstock

Microalgae are a potential sustainable feedstock with application in the food, biofuel and cosmetic industry[184]. Algae biomass does not compete with food production and is distinct from terrestrial plant biomass by high areal productivity and space time yields[185]. While biomass production in open and closed bioreactors systems are becoming increasingly efficient, harvest and downstream processing of algae biomass remains a major challenge in industrial process development. At present, harvesting accounts for up to 30% of the total production cost[186]. The challenge of algae biomass harvesting mainly results from small cell size, colloidal stability and low biomass concentrations. As a result, a number of different solutions have been suggested to address this issue[187] including centrifugation[188], [189], filtration[190], flotation[191], [192] and different methodologies of flocculation by employing physical[193], chemical[194], or biological[195] means. Flocculation-sedimentation is regarded as very efficient, however the process conditions strongly depend on the selected algae strain, the specific flocculant, media composition, culture age and cell density. Due to the large number of possible flocculation agents and numerous factors affecting this process step, the application of the Design-of-Experiments (DoE) methodology is a suitable tool for obtaining an accurate description of optimal harvesting conditions[196]**.** As algae harvesting significantly adds to the total production cost of algal biomass[187], the development of effective and robust flocculation processes is key to developing economically viable industrial processes[197]–[199].

3.1.2 Algae Harvest

The entire process of separating biomass from algae itself can be divided into three, often not entirely distinct, steps[200]: thickening, dewatering and drying. In culture, biomass concentration of algal culture is between 0.1 to 1% w/v, which is raised to approximately 5% w/v by thickening. Dewatering is used to further decrease the water content to a dry biomass concentration of 20%. At this point, microalgal biomass exists in the form of a sludge. The employed methods for the first two steps are laid out in section 3.3 and are herein referred to as algae harvest in the strict sense. Some subsequent processing steps, such as lipid extraction, require even further lowering of water content. This treatment, colloquially known as drying, is in most cases highly energy intensive and often lacks economic feasibility when low-value products are generated[201]. Hence, current research also focuses on the possibility

of wet extraction[202]. In summary, no universally applicable, robust and cost efficient process for harvest of different algae strains has been found so far[186].

3.1.2.1 Physical Methods

Centrifugation is a very robust process step, which is in principal applicable to all microalgae. It is very fast in comparison with other methods and highly effective. However, with decreasing size of cells, the required g-forces rise significantly and in turn, so does the demand for energy. Further, cleaning, maintenance and repair of centrifuges are costly and labor-intensive[187]. Hence, this method is only applicable and economically feasible for very high-value products, such as pharmaceuticals or food supplements. Nevertheless, optimization approaches of centrifuge and impeller design are in development and can lead to a significant decrease in energy demand[203].

Filtration is a suitable method for harvest of large microalgae such as *Spirulina sp*., a cyanobacteria. Smaller microalgae such as *S. obtusiusculus* demand smaller pore sizes and in turn higher energy demand[204]. Further, filtration membranes are prone to biofouling and clogging, which raises labor-intensity of this process step[205], [206]. Some disadvantages are partly offset by the high number of available filters for specialized applications.

Air flotation or dissolved air flotation enable harvest by passing air through algae culture medium. This causes algal cells to adhere to the introduced gas bubbles and rise to the surface, where they are typically harvested by a skimmer. This can also be done in combination with chemical supplementation (suspended air flotation).

Gravity based sedimentation is one of the simplest methods at potentially low cost. However, depending on the size of the algae[207] and the density of the medium, settling can take very long, even to the point of biomass degradation. Additionally, the resulting concentrated algal slurry is of low stability as suspension, as the negative surface charge still causes cells to repel each other.

3.1.3 Flocculation of Microalgae

Suspensions in general are stabilized either by steric properties and/or by a surface charge of their suspended particles. For the latter, flocculation is often a promising strategy to break the suspension. Indeed, with increasing strength of surface charge, flocculation efficiency commonly increases[208]. In an optimal case, the respective flocculation agent is cheap, readily available, non-toxic and bio-degradable, requires low dosing and does not interfere with downstream processes. In waste water treatment, flocculation is a well-established method for liquid-solid separation[208] and much of the work done with algae builds on those commercial products.

Flocculation of algae can be induced by overcoming the negative algal surface charge[209]. Different mechanistic approaches are suggested for this: The entire surface charge can be neutralized, especially by changing the pH. A variation of this is the electrostatic patch mechanism, in which only certain areas on the cell surface are neutralized or modified, which leads to agglomeration of cells at patches with complementary patch charges. Flocs can be formed by bridging of multiple cells, which in turn start to “collect” further algae. This mechanism is commonly called sweeping flocculation.

Iron or aluminium salts are very common, cheaply available flocculation agents. However, high loadings are typically required for the induction of flocculation and downstream processing and media recycling are problematic with high concentrations of metal ions[187]. Specifically in *S. obtusiusculus*, aluminium salts have been shown to inhibit phosphate availability in the cell[210].

Synthetic polymers are another class of flocculants with common application in waste water treatment. They are highly stable and capture particles or algae by bridging or sweeping flocculation. The high stability can become a disadvantage as many of the polymers, such as polyacrylamide, are not biodegradable.

Acidic flocculation of microalgae can be induced, as the surface of cells is typically controlled by deprotonation of carboxylic groups. By decreasing pH to approximately 3, those groups, and in turn for the most part the algae surface, become uncharged[209]. In contrast, lowering the surface charge by raising the pH can lead to the attraction of cationic counter ions (specifically Mg^{2+}), which attach to the cell surface. Subsequently other cells attach to this now positively charged surface[211].

Oxidants can also be used to modify the respective functional groups. Ozone, chlorine and potassium permanganate have been used successfully used for flocculation[212], [213]. However, effects are dose- and strain dependent and often also entirely disrupt algae spheroplasts[214].

Biological flocculants are cells, cell wall components or biologically derived products which can be used for flocculation. Commonly, the mechanism of flocculation is the same as for synthetic polymers as bio-derived flocculants are also cationic polymers, but lower dosages are sometimes required[215]. Further, they are non-toxic, highly biodegradable and hence in principal suitable for harvest and media recycling of microalgae.

Examples for this include chitosan, xanthan or tannin. Chitosan has been applied as flocculation agent for over 40 years[216], however the high price has prevented its application in larger scales. Xanthan has been used as flocculant in fresh water for harmful algae

blooms[215]. Very little work has been done to characterize tannin as flocculant, although it is commercially available as de-emulsifier[217].

In addition, tannin was used in wastewater treatment[218] and flocculation of the cyanobacterium *Microcystis aeruginosa*, where it was only effective at pH values under 7 and 9 respectively, depending on method of preparation. Flocculation efficiencies (FE) of over 90% were reached. Polysepar CFL 25 was previously used as flocculant for *Scenedesmus acuminatus* cultivated in fresh water with 70% FE at 70 mg/l[219]. Another tannin-based product, Tanfloc, was used at a concentration of 5 mg/l to harvest *Chlorella vulgaris* at 250 mg/l dry biomass concentration.

This work focuses on microalgae harvest induced by a) alkaline pH shift and b) biological flocculants with a focus on tannins. Both methods are in principle applicable for industrial processes. A common challenge of biological flocculants lies in lack of robustness. This is addressed in this work by employing tannin, which has previously gathered little attention as flocculation agent.

3.1.4 Scenedesmus obtusiusculus

All experiments were conducted using *Scenedesmus obtusiusculus* A189, a green microalgae species between 2 and 10 µm in size which grows in fresh as well as in salt water. The respective strain A189 was isolated by Schultze *et al*.[220], who also optimized media composition for high lipid and carbohydrate content without sacrificing for biomass productivity. This optimized medium was limited in nitrogen and contained artificial sea salt. The high practical and process relevance is given by the high similarity of this medium to brackish sea water, which was demonstrated by the authors.

Nitrogen limitation verifiably affects composition of algae cell wall. Under nitrate starvation, the content of total glucans of *Scenedesmus obtusiusculus* A189 increased from 22% (control) to 34% w/w. The β-glucan content rose from 16.0% (100% N, control) to 23.5% (30% N)[221]. In another strain of the same species, nitrogen limitation also affected the otherwise fast metabolic adaptation to irradiance changes for the worse. Whereas adaption to irradiance was fast in non-limiting conditions, change of metabolic flux towards lipid accumulation was comparatively slow[222].

Growth as colony on plates has been described especially with supply of organic phosphate[223]. During sporulation phase, DNA content of cells transiently increases and a shift in pigment spectrum was reported[224]. In general, lipid droplets, polyphosphate granules and starch grains appear to serve as storage entities and vary in size and composition within the night and day cycle in this species[225]. A characterization of biomass composition was

attempted by Toledo-Cervantes *et al*.[226], which did not yield fully plausible results. Again, the fast growth of the species was nonetheless confirmed.

As previously mentioned, flocculation behavior is determined by surface charge and in turn constituents of the cell wall. Little is known about cell wall composition of *S. obtusiusculus*. Electron microscopy studies were previously published[227] and calcium deficiency has been shown to impact on cell wall assembly[228].

3.1.4.1 Flocculation of S. obtusiusculus

Flocculation of other *S. obtusiusculus* strains in fresh water medium was previously described: Flocculation with chitosan was optimized with response surface methodology (RSM), yielding 92% flocculation efficiency (FE) with 214 mg Chitosan/l culture[197]. In another approach with optimized pH (7.5-8.5), chitosan dosage was lowered to 50 mg/l[229]. Further, full flocculation was achieved using a combination of bacteria and iron salts with successful recycling of the medium[230]. This idea of bioflocculation was further pursued by employing extracellular biopolymers of *Scenedesmus obliquus*[231]. Aluminium salts were especially effective in the absence of phosphate in the medium[232].

It was reported, that in comparison to biological flocculants, induction of autoflocculation by pH shift is the most inexpensive method for flocculation-sedimentation[233]. The resulting medium supernatant is in principle reusable, however this most likely only applies to low numbers of recycling cycles for the medium. The issues of accumulation of salts and evolutionary pressure leading to selection for algae with low surface potential are unsolved by this method. Calcium hydroxide is reported to be the most cost efficient base for induction of flocculation[211]. In another instance, basic pH shift to alkaline conditions was used successfully and yielded the lowest cost in comparison to other flocculation methods[234]. Further, magnesium ions appear to be necessary for induction of autoflocculation, which is consistent with the proposed mechanism of trapping of ions between negatively charged algal surface.

It has been known for some time, that higher concentrations of microalgae require lower loadings of flocculant per dry harvested biomass[235]. Thus, pre-flocculation cell density in the culture as well as surface charge should be as high as possible[235]. In fresh water, *Scenedesmus sp.* was also harvested by using cationic starch. This effect is pH independent[236]. As mentioned above, induction of flocculation by low pH is possible for many algae, including *Scenedesmus sp.*[237]. Flocculation efficiencies of over 90% were achieved and interestingly, algae organic matter in the medium actually aided the harvesting process.

In a more exotic approach, sodium dodecyl sulfate (SDS) and cetyl trimethylammonium bromide (CTAB) were used as flocculant, whereas only with the latter, sufficiently high Fes were achieved. In this instance, flotation instead of sedimentation was used for liquid/solid

separation. Using electroflocculation, 98% FE was achieved by optimizing voltage and electrode material[238]. Chitosan was also used in combination with iron chloride as ballasting compound[239], which yielded better FEs than the polymer alone. Regarding flocculation in salt water, Chitosan was also successfully applied[240]. However, the experiments did not extend to any *Scenedesmus sp*. strain and, if tested, showed pH dependence of the respective flocculant.

3.2 Materials

3.2.1 Instruments

Model	Supplier	Description
VX/VE	Systec	Autoclave
Research Plus	Eppendorf	Pipettes
RCT	IKA	Magnet Stirrer
EKT Hei-Con	Heidolph	pH-Meter
LaminAir HB2448	Heraeus	Sterile Bench
Comfort	Eppendorf	Thermo Mixer
Vortex Genie 2	Scientific Industries	Vortexer
5810R	Eppendorf	Centrifuge
5424R	Eppendorf	Centrifuge
2300 EnSpire	Perkin Elmer	Fluorescence - Plate Reader
Labfors 5 lux	Infors	Fermenter
8453	hp	Photometer
Genesys 103 UV/Vis	Thermo Fisher	Photometer
MX4/4H	dasgip	Gas Mixing Station
S3	BioRad	FACS
M325	oHaus	Infrared scale
JLT4	Velp	Jar Test Apparatus
Axiolab A1	Zeiss	Microscope

3.2.2 Consumables

Consumable	Supplier
Syringe Filter 13 mm w 0.2 µm Nylon	Pall Life
Eppendorf tubes	Eppendorf
Erlenmeyer flasks	VWR
Falcon tubes 15ml, 50ml	VWR
Syringes	Sarstedt
96-well Plates black and transparent	Sarstedt
1 cm Cuvettes	Sarstedt
Bottles	Schott

3.2.3 Chemicals

Chemical	Supplier
Ammonium nitrate	Roth
Ammonium sulfate	VWR
Ammonium iron citrate	Merck
Ammonium molybdate	Merck
Ampicillin	AppliChem
Artificial Sea Water Mix (ASW)	Tropic Meeresaquaristik
Calcium Hydroxide	Alfa Aeser
Citric Acid	Roth
Chitosan	Biolog Heppe
Copper sulfate pentahydrate	Roth
Dipotassium Dihydrogen phosphate	Roth
Ethanol p.a.	Roth
Licocat 29	Sued Zucker
Magnesium sulfate heptahydate	Alfa Aesar
Magnesium hydroxide	VWR
Manganese chloride tetrahydrate	Roth
Manganese sulfate	VWR
Potassium hydroxide	Roth
Potassium phosphate	Roth
Sodium carbonate	Roth
Sodium EDTA	Roth
Sodium nitrate	VWR
Sodium hydroxide	Roth
Starch, cationic	Suedstaerke
Zinc sulphate heptahydrate	Roth

3.2.4 Strains

Organism Name	Strain	Supplier
Algae		
Scenedesmus obtusiusculus A189	A189	EMAU

3.2.5 Software

Software	Application
EnSpire 3.0	Plate reader
8453 UV-Vis	Photometer
R	Statistical Analysis and Plotting

3.3 Methods

3.3.1 Media

Two media were used in the course of this work: Standard BG11 medium for cultivation of freshwater algae[241] and adapted ABV medium, which induces nitrogen stress as described by Schultze *et al*.[220].

Table 10: Composition of BG11 and ABV medium. All values except for trace elements in g/l.

Component	**BG11**	**ABV**
$NaNO_3$	1.5	0.375
K_2HPO_4	0.04	0.4
$MgSO_4 \cdot 7\ H_2O$	0.075	0
$CaCl_2 \cdot 2\ H_20$	0.036	0
Citrate	6.0E-03	0
Na-EDTA	1.0E-03	0
$Citrate \cdot 0.5\ Fe \cdot 5\ NH_4$	$6.0x10^{-3}$	$6x10^{-4}$
Na_2CO_3	0.02	0
Trace Elements	1 ml	0
ASW	0	5

Table 11: Composition of trace element solution used for BG11.

Component	**mg/100 ml**
H_3BO_3	6.1
$MnSO_4$	22.3
$ZnSO_4 \cdot H_2O$	28.7
$CuSO_4 \cdot 5\ H_2O$	0.25
$(NH_4)6\ Mo_7O_{24} \cdot 4\ H_2O$	1.25

Media were generated by creating stock solutions at 1 M. The mix was sterile filtered in previously autoclaved bottles and subsequently trace elements were added.

Chitosan was dissolved in 1% v/v acetic acid with a final concentration of 10 g/l. All Tannins (Polysepar) were dissolved or diluted in ddH_2O. Polycat 29 was diluted to a 10% w/w (3 g/l) working solution. Xanthan was dissolved to a working solution of 10 g/l in ddH_2O.

3.3.2 Algae Cultivation and Growth

Proliferation of microorganism occurs by cell division and is therefore inherently exponential in absence of limitations in terms of e.g. nutrient availability, nutrient assimilation or any other required elements such as reducing agents or, in the case of photosynthetic microbes, electromagnetic radiation in the visible spectrum[242].

Nutrient requirements of microalgae extend to nitrate required for any amino acids and hence protein biosynthesis and phosphate as energy carrier in the form of ATP. Further, metal ions including copper, calcium, iron, magnesium and potassium are required for e.g. electron transduction elements, pigments, and protein cofactors.

Limited by environmental restrictions, exponential growth only occurs under ideal, non-limited conditions. In real cultures, inoculation of media with microorganism is typically followed by a lag phase, during which adaption of cells to the new environment takes place. After a certain amount of time, given unlimited conditions, the maximum growth rate μ is achieved (Figure 30), which is followed by a depletion of resources or decreasing capability for assimilation due to high cell density. For algae, light limitation is at this point commonly limiting growth, as cells increasingly shade each other. Linear growth is then followed by a stationary phase, after which cell death occurs[243].

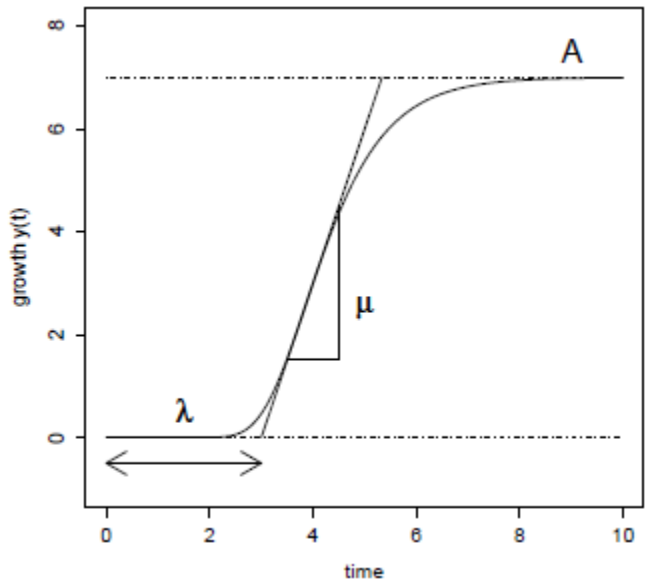

Figure 30: Typical parameters derived from growth curves: length of lag phase λ, growth rate represented by the maximum slope μ and the maximum cell growth A. Image adapted by Kahm et al.[122]*.*

3.3.2.1 Growth Curves and Modeling

Growth curves can be modeled in different ways. A common way is the determination of a timeframe, in which a logarithmic relationship can be observed between time and cell count, OD or biomass at the respective time points. This is commonly done for low numbers of measurement points. However, the method is flawed, as the determination which time points are included in the fit is often made on a subjective basis and linear regression over a subset of data points is not an optimal use of measured data. A better possibility is the fit of a sigmoidal growth curve to the data[244].

There are a number of different formulas applicable for microbiological growth, but the goal is always extraction of key parameters, as shown in Figure 30. Growth curves differ in the number of estimated parameters, most of which resemble a biological function. In detail, maximum achieved cell density A, maximum growth rate μmax and lag phase duration λ are estimated. Formulae of employed growth curves are shown in Supplemental 13.

It was previously shown, that a Gompertz model is suitable for most applications[244]. For higher numbers of data points, modified Gompertz or Richards fits can be used, as the higher number of data points offsets the increased degrees of freedom required for the estimation of the higher number of parameters by the model. In general, 3 parameter models are preferred as they are simpler, more easy to interpret, and more stable due to lower autocorrelation[244].

3.3.2.2 Aerated Flasks

Precultivation was done in 2 l or 5 l Schott bottles aerated with approximately 1 l/min air, which was supplemented with 2% v/v CO_2 (Figure 31). The pH was initially set, but not controlled during cultivation. Flocculation was done after 14 days of cultivation or reaching OD_{680} of 1.6. Media were ABV or BG11 as described in section 3.3.1. Irradiation was continuous using fluorescent tubes at approximately 50 μmol photons $m^{-2}s^{-1}$. Inoculation was done to an OD_{680} of 0.25.

3.3.2.3 Bubble Column Reactor

Construction and maintenance of the bubble column reactor was done by Matthias Glemser. Algae were cultivated in an aerated 30 l bubble column reactor under a constant stream of air at 275 l/min (Figure 31). A Milwaukee MC122 pH sensor was used to stabilize the pH at 8 by controlling CO_2 injections into the air stream. Culture growth and conditions were monitored using $OD_{680}$and microscopy. Temperature was at 28±2°C and cultures were continuously irradiated with fluorescent tubes at approximately 240 μMol photons $m^{-2}s^{-1}$. Cultures were grown for 21 days to a concentration of OD_{680}=1.4-1.6, as given in the results section. Inoculation cell density was OD_{680}=0.25.

3.3.2.4 3 l Fermentation (Infors reactor)

3 l ABV medium were sterile filtered and added to the reactor and cultures were inoculated to an OD_{680} of 0.1-0.2. Regulation of pH to 8 was done by CO_2 injections into the culture, similarly to cultivation in the bubble column. Air stream was set at 1 l/l culture/h and stirrer was at 400 rpm. Irradiation was set at 10%, approximately 74 µMol photons $m^{-2}s^{-1}$ (Figure 31).

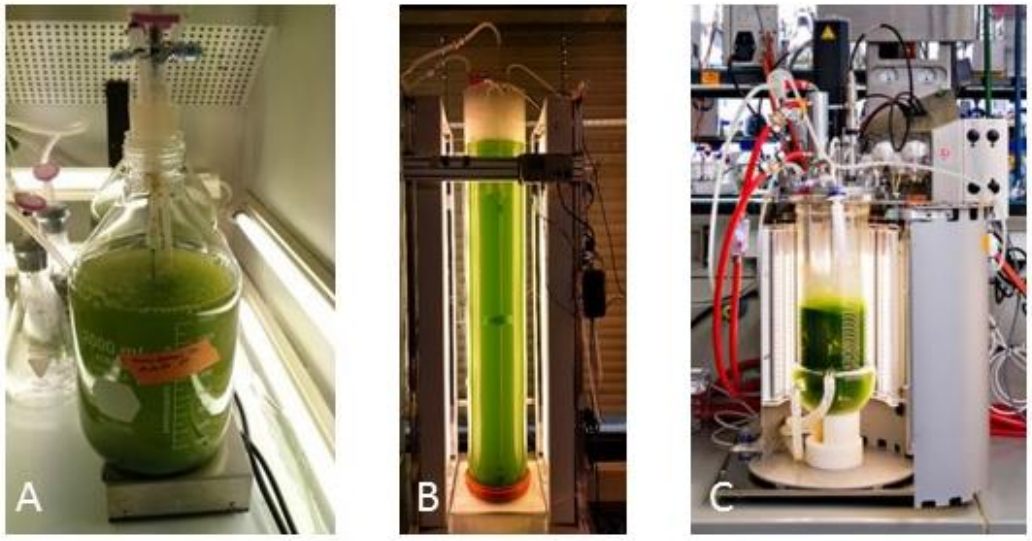

Figure 31: Experimental setup for S. obtusiusculus cultivation in aerated flask (A), bubble column reactor (B) and Infors reactor (C).

3.3.3 Absorbance Measurement (OD)

The main analytical tool for flocculation is measurement of absorbance, often termed optical density or short OD. Absorbance is a unit free estimate of the absorption, reflection and scattering in a sample. Mathematically, it is the decadic logarithm of the ratio of incident to transmitted radiant power through a material. Commonly for DNA measurements, UV light between 200 and 320 nm is used for sample analysis. For microbiological measurements, wavelengths between 580 and 720 nm are used. Wavelengths, time points and photometers were varied for this work. Commonly for flocculation, OD at 680 nm (OD_{680}) was measured.

OD measurement itself was done in a Genesys 103 UV-Vis by Thermo-Fisher using 1 cm cuvettes. The linear range was determined to be between OD_{600} 0 to 0.5. After measurement, dilution factors were then applied to receive the actual OD value. All measurements were done at room temperature, between 24-28°C. Mixing of samples immediately before measurement is key to receive a representative value for uniformly distributed algae.

The method was adapted for use in 96-well plates by using an Enspire 2 plate reader by Perkin Elmer. For this, a 96-well plate was filled with 200 µl of flocculation sample. The plate was

shaken inside the reader for five seconds at 300 rpm (linear) and subsequently OD at 680 nm was measured for every well as triplicate. Results were compared to the measurements obtained by the genesis photometer in section 3.4.1.3.

3.3.4 Biomass Determination

The main assumption of measuring the optical density is, that obtained values correlate with the amount of biomass or the number of cells in the culture. This was addressed by a OD/Biomass correlation as shown in section 3.4.1.2.

For the calibration curve, biomass concentration was determined by centrifuging 50 ml of culture cells at 10'000 rcf for five minutes, washed once with bi-destilled water and dried to constant weight in an Ohause M325 infrared scale. Previously, the number of washes was varied to estimate the effect of salt on dry biomass estimation.

3.3.5 Flocculation Procedure

150 ml algae suspension were poured in a 250 ml beaker, which in turn was placed in a VELP Scientifica JLT4 jar test apparatus. The rotation was set to 300 rpm for 3 minutes using 3.5 cm x 2.5 cm paddle stirrers. Immediately after stirring started, flocculant was added in different concentrations from stock solutions as described in 3.3.1. Settling times were varied, samples were always taken 2 cm below the surface. This was estimated by using markings on the pipette tip. Samples were measured as described in section 3.4.1.3. After measurement of absorbance, flocculation efficiency (FE) was calculated according to $FE=1 - (OD_f - OD_i)$ whereas OD_f is OD of supernatant after flocculation and OD_i is the initial OD of the culture.

For evaluation of the 15 ml and 50 ml formats, falcons were filled with the respective amount of algae culture, pH was set between 10 to 12 to induce autoflocculation and vortexed for 30 seconds. FE was measured in the same way as for the jar test procedure after 1 hour of sedimentation.

3.3.6 Measurement of Compression

Upon completion of all OD measurements, 100 ml of flocculated algae culture was stirred and decanted into a graded settling cone. Volume of algal biomass after flocculation was read after 30 minutes of sedimentation. Compression factor was calculated according to $CF=SV_f/SV_i$ whereas SV_f is the sediment volume of algae biomass after flocculation and SV_i is the initial volume of the culture (=100 ml). Compression factor CF multiplied with flocculation efficiency

FE yielded compression efficiency (CE). CE is a measure for the total amount of flocculated volume found in the respective sedimentation volume.

3.3.7 Zeta Potential Measurement

Instead of measuring the surface potential itself, commonly the zeta potential is estimated. As a rule of thumb, zeta potential beyond 30 mV or under -30 mV are considered stable. Estimation of zeta potential can be done by dynamic light scattering (DLS). If an electric field is applied over an electrolyte, any suspended, charged particles experience an attraction towards the complementary charged electrode. The particles velocity is mainly dependent on the zeta potential of the particle, the viscosity and the dielectric constant of the medium and the strength of the electric field. Measurement of particle velocity can be done using ultra-microscope techniques as well as photometric techniques. For this work, a Malvern Zetasizer employing laser doppler velocimetry was used[245].

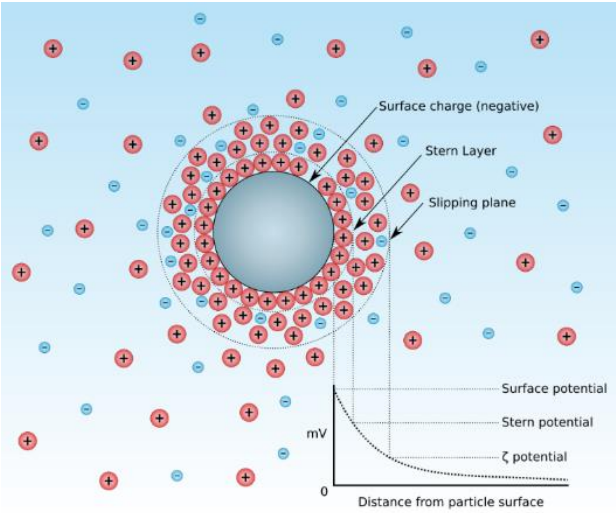

Figure 32: Model of a particle carrying a surface charge, which decreases with increasing distance from the particle. The stern layer defines a layer where ions are strongly bound and the slipping plane characterizes a diffuse outer region, where ions are less firmly associated[246]*. The electric potential at the surface is termed surface charge, the potential at the stern layer stern potential and the potential at the slipping plane zeta potential. Image adapted by wikimedia.org*[247]

Measurement of zeta potential (Figure 32) was done in a Zetasizer ZS using DTS1070 Capillary zeta cells. Algae culture in 1:2 dilutions and flocculants at different pH were placed in cells and measured at 25°C with water as dispersant (dispersant settings: viscosity 0.8872 cP and RI of 1.330). The “material” was set to a refractive index of 1.450 and absorption of 0.001. Measurement types were set to zeta potential or size.

3.3.8 Statistical Analyses

3.3.8.1 Simplex Lattice Design

A mixture design, specifically a simplex lattice design was used to estimate the effect of tannin, chitosan and water on flocculation efficiency (Section 3.3.5). Analysis was conducted as described by Natrella[248]. Following the Scheffé polynomial design[249] the respective regression model omits the intercept and includes all main linear and cross term effects, but no square or other higher order effects. These adjustments are made because this type of mixture model is restricted in that all factors sum up to a constant. Culture for the respective experiment was at OD_{680}=3.6 and at t=113 h. Cultivation was done in an infors fermenter (Section 3.3.2.4). For flocculation procedure, pH was set to 7, flocculant was added and samples were stirred at 300 rpm for 5 minutes. Flocculation efficiency (FE) was measured after 30 minutes.

Table 12: Coded and raw measurement levels of 2^3 mixture simplex lattice design using different mixtures of tannin, chitosan and $_{dd}H_2O$ as well as run- and experiment order.

Run Order	Number	Tannin coded	Chitosan coded	$_{dd}H_2O$ coded	Tannin mg/l	Chitosan mg/ml	$_{dd}H_2O$ ml
9	1	0.33	0	0.66	40	0	20
6	2	0	0	1	0	0	30
7	3	0.66	0.33	0	80	10	0
4	4	0.33	0.66	0	40	20	0
8	5	0.33	0.33	0.33	40	10	10
1	6	0	0.33	0.66	0	10	20
5	7	0	1	0	0	30	0
10	8	1	0	0	120	0	0
3	9	0.66	0	0.33	80	0	10
2	10	0	0.66	0.33	0	20	10

3.3.8.2 Growth Phase Dependency of Flocculation

S. obtusiusculus A189 was cultivated in ABV medium as described in Section 3.3.8.2. Varied factors were time, adjusted pH, flocculation agent and flocculant concentration (Supplemental 36) according to a full factorial 2^3 design with four total replications at each respective time point. Flocculation agents tannin (Polysepar CFL-PT) and chitosan (Heppe A90/400/A1) were tested at 40 and 80 mg/l culture respectively. The pH was set to either pH 8 or 9. At time points t=120, 145, 170, 195 and 220 hours, flocculation procedure as described in section 3.3.5 was conducted. Moreover, at each time point, zeta potential was measured according to section 3.3.7 and bacterial populations were estimated by FACS. Additionally, at time points t=170 and 220 h, replicates of the 2^3 full factorial design of the respective time point with cells in medium without algae organic matter (AOM) were conducted. For this, cells were centrifuged at 14.4 g

for 15 minutes and resuspended in fresh ABV medium. An ANCOVA was used to estimate the effects of the individual independent variables.

3.4 Results and Discussion

Method validation (3.4.1), pH-shift (3.4.2) and general tannin- and chitosan flocculation (3.4.3) presented here were executed under my guidance as part of the Bachelor's thesis "Energie Effiziente Ernte der Alge Scenedesmus obtusiusculus" by Daniel Helmdach (2015). The raw data are reevaluated and discussed for this chapter. Data about tannin/chitosan interaction (3.4.4) and growth phase dependency (3.4.5) were obtained during an internship by Nils Funck (2016). All modeling approaches are original work.

3.4.1 General Validation

3.4.1.1 Format of Flocculation Experiments

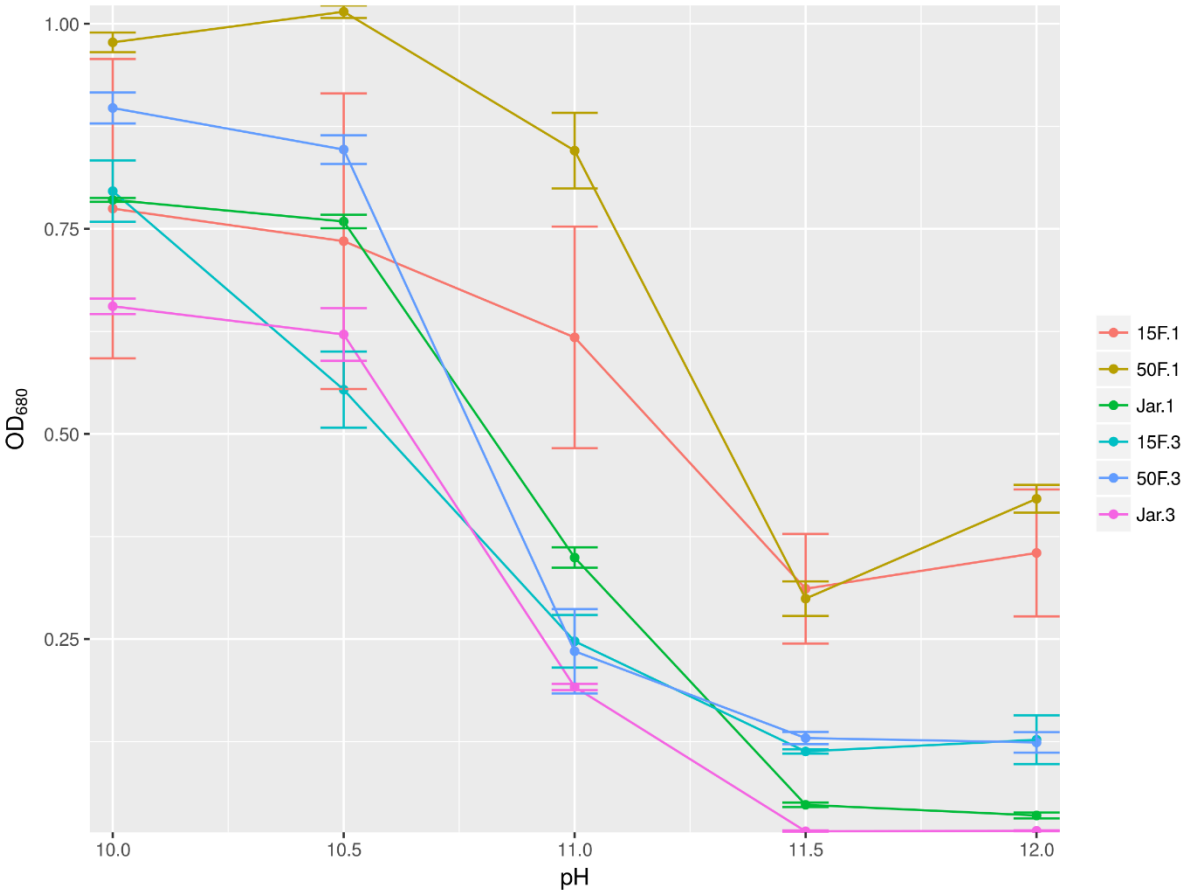

Figure 33: Comparison of different methods of flocculation using 15 ml falcons (15F), 50 ml falcons (50F) and 150 ml Jar test (Jar) at time points 1 and 3 (.1 and .3). Y-axis shows OD_{680} of the supernatant. Error bars show standard deviations of triplicates.

Autoflocculation was induced by supplementation of algal medium with NaOH. After adjusting pH, OD_{680} of the supernatant was measured at different time points. Flocculation using 15 ml falcons showed a relative standard deviation (RSD) of 23% after 1 hour and 10% after three hours. RSD of 50 ml falcon were 4% after 1 hour and 8% after 3 hours and for the jar test 4% after 1 hour and 4% after 3 hours respectively. Hence, estimation of flocculation efficiency using 15 ml falcons was considered too unreliable for application. A comparison of all flocculation methods is shown in Figure 33. RSD of 50 ml falcons were acceptable, however independent of sedimentation time, quantitative harvest was not achieved. In summary, 50 ml falcons might be suitable for high throughput estimation of flocculating activity, however for modeling, only a standard jar test gives sufficiently accurate results. Hence, all subsequent experiments were conducted using the jar test procedure as described in section 3.3.5.

3.4.1.2 OD-Biomass Correlation

First, the effect of salt and soluble organic matter in the medium on the estimation of dry algal biomass was assessed (Table 13). As expected, omitting the washing step leads to overestimation of dry biomass concentration in the medium. However, already a single washing step is sufficient for removal of most non-cellular biomass and subsequent washing does not yield significantly lower biomass concentrations.

Table 13: Evaluation of the effect of salt and soluble organic matter on estimation of dry biomass

$_{dd}H_2O$ Washing Step	Dry Biomass / g/10 ml culture
0	6.2
1	0.8
2	0.76
3	0.78
4	0.79

Correlation of OD_{680} to algal biomass was highly significant (Figure 34) with an R^2 of 0.994. This applies to *S. obtusiusculus* grown in ABV medium and was used as standard to estimate biomass concentration from OD_{680} values obtained by flocculation experiments.

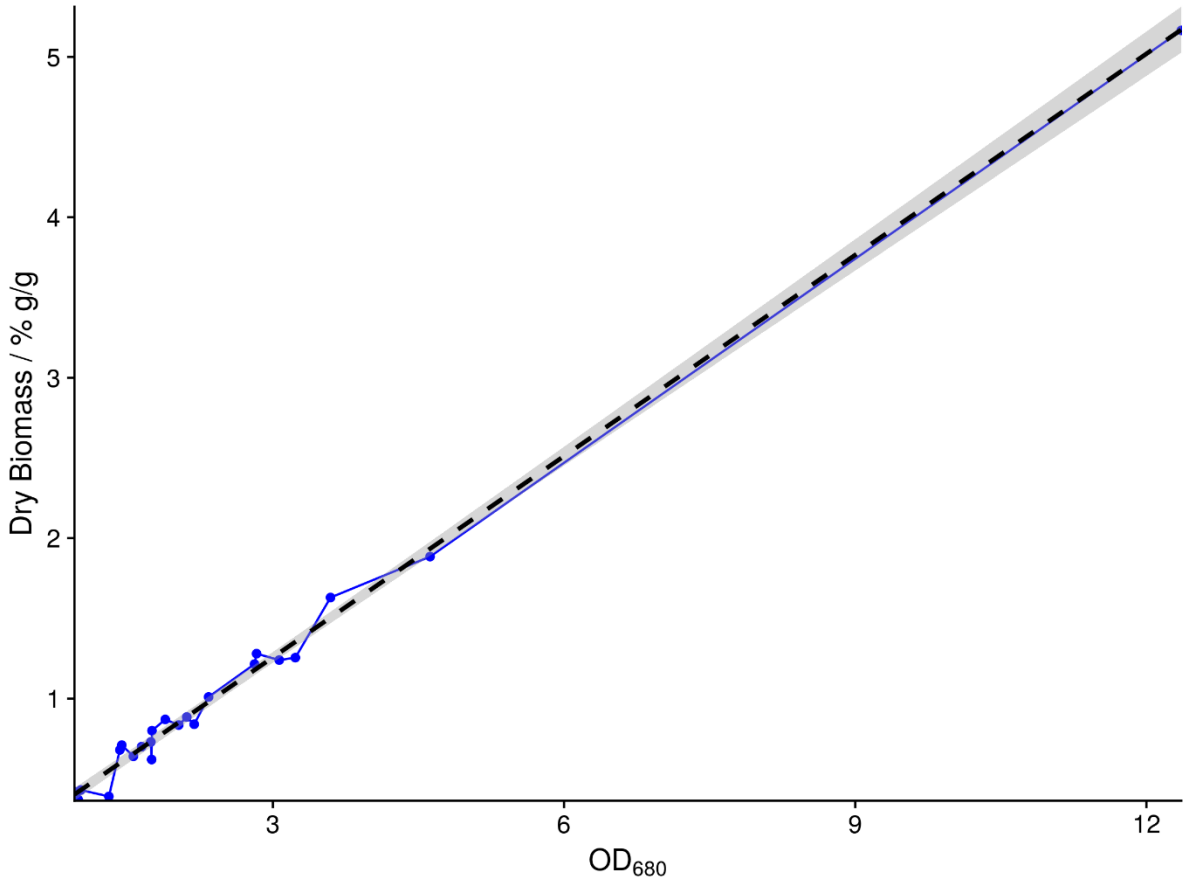

*Figure 34: OD_{680} / Biomass correlation for S. obtusiusculus. Samples were washed once before determination of dry biomass. Regression formula is DBM/g/l=0.0028+0.418*OD_{680} with an R^2 of 0.994.*

3.4.1.3 OD_{680} Measurement in 96-microwell plate

Time did not have an effect on OD_{680} of algal suspension measured inside a 96-well plate (Supplemental 37) and spatial distribution was uniform inside the well (Supplemental 38). Additional shaking between measurements did not yield a more constant OD_{680} value over time (Supplemental 39). More precisely, shaking resulted in decreasing concentrations over time, which was attributed to possible adhering of algae cells to the wall of the 96-well plate. Consequently, all subsequent protocols only included one initial shaking step at 300 rpm (linear). With reliable constant behavior OD measurements of algal cultures in a 96-well format regarding time and space, a linear measurement spectrum in terms of algae concentration was defined.

For this, an algal suspension at 0.72 g/l, corresponding to an OD_{680} of 1.6 in a Genesys cuvette photometer and an OD_{680} of 0.5 for the plate reader was prepared as serial dilution. Measurement of the dilutions showed the much broader linear area of OD_{680} measurements for the plate reader compared to the cuvette based photometer (Figure 35). Furthermore, the higher quality of estimations is reflected in the R^2 values of the fits. For the photometer,

regression could not be extended to the fourth data point at a 1:2 dilution or 0.5 normalized concentration without lowering the respective R^2 to an insufficient value of 0.9 or switching to a higher order regression. The logarithmic pattern of photometer samples was a clear indicator of substrate concentrations exceeding photometric linearity.

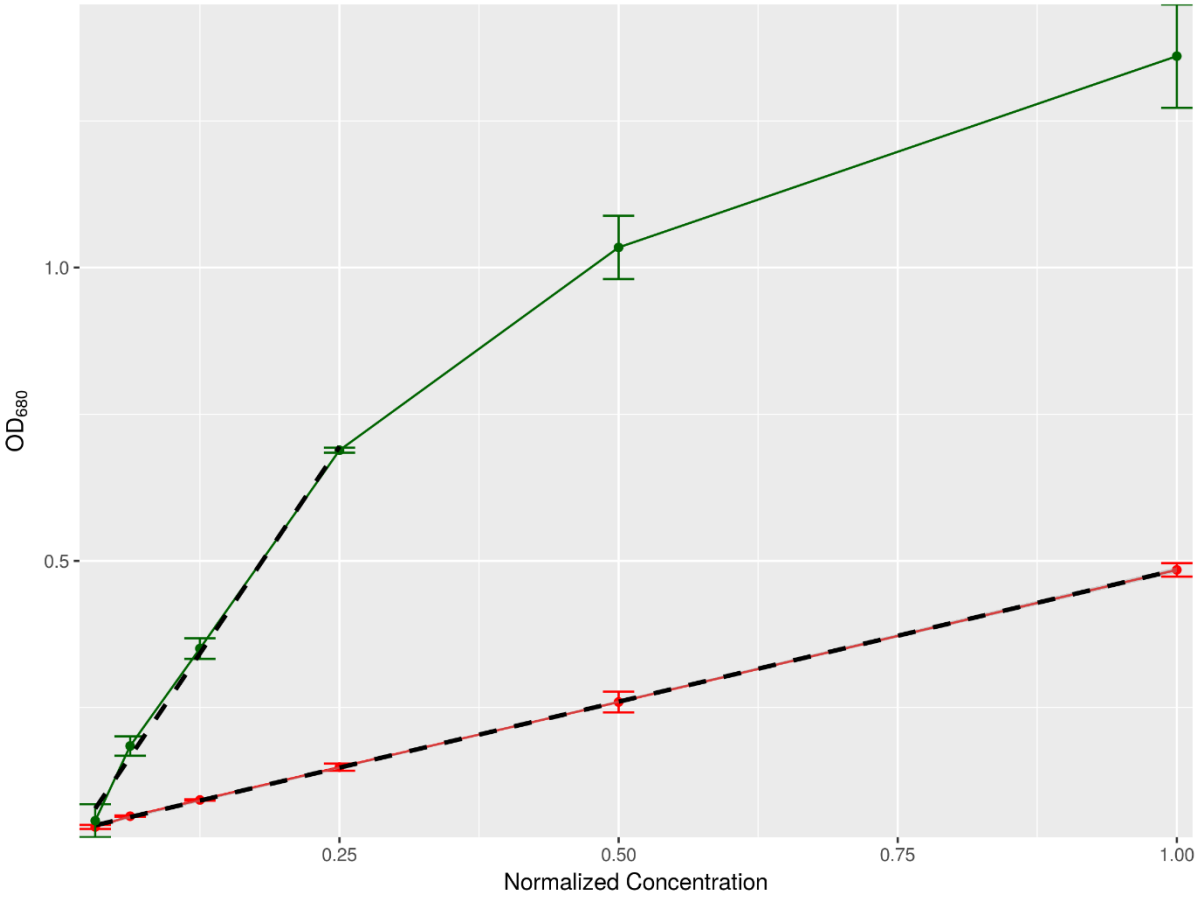

Figure 35: OD_{680} measurement in dependence of algae culture for the plate reader (red, 200 µl sample) and cuvette photometer (green). The dashed line shows the linear regression for each approach. The respective R^2 values were 0.999 for the plate reader and 0.9961 for the cuvette photometer. Error bars show standard deviations of triplicates.

3.4.2 pH Shift

As previously shown to be the cheapest and simplest flocculation method, autoflocculation by alkaline pH shift was considered first[250]. Figure 36 shows flocculation efficiencies of autoflocculation induced by alkaline conditions using different bases. Flocculation efficiency rises with increasing pH in all cases, however magnesium hydroxide precipitates before being able to induce flocculation. In principal, flocculation is induced over a pH of 11 (FE>0.6).

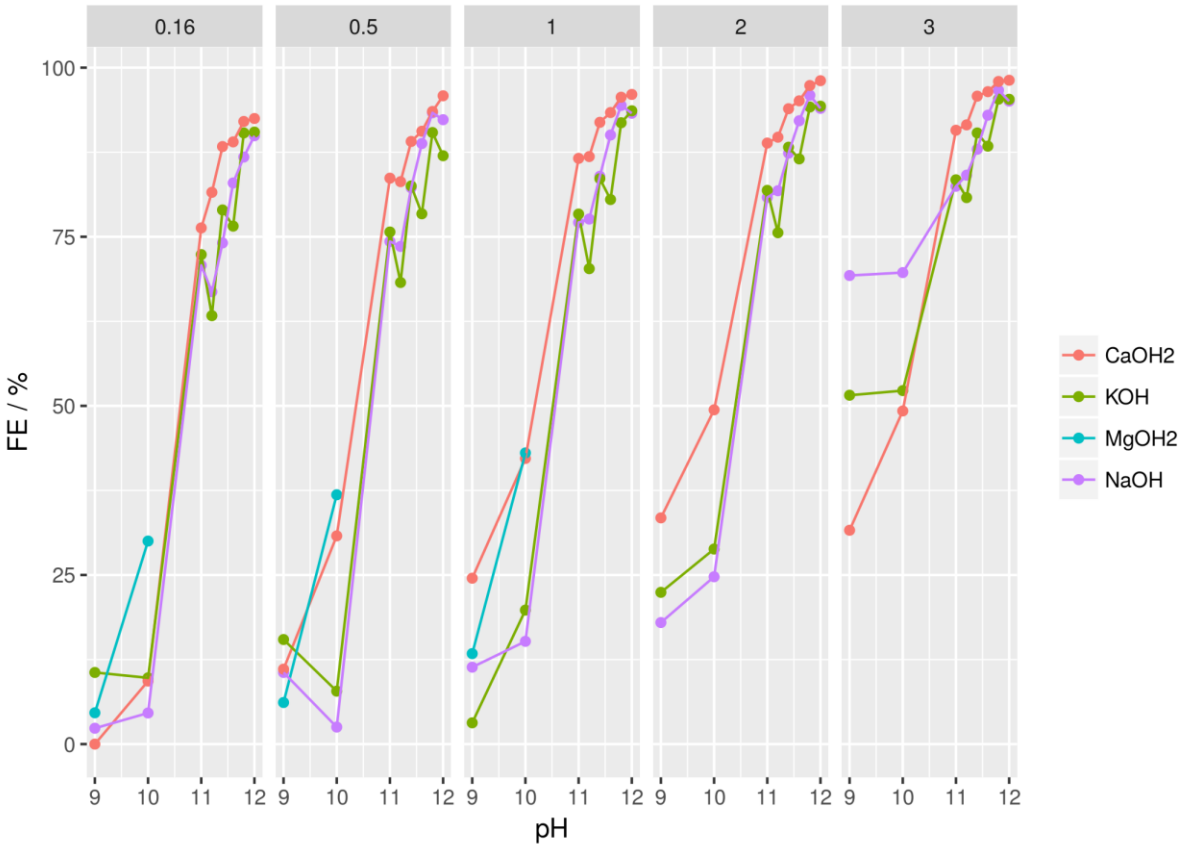

Figure 36: Autoflocculation induced by supplementation of different bases. Number on top of each plot displays sedimentation time in hours.

An increase in sedimentation over time appears to be almost linear within the chosen limits of independent variables, as shown in Figure 36. To substantiate this and for estimation of effects on flocculation behavior, multiple linear regression was applied to the dataset.

Detailed regression results can be found in Supplemental 40. A simple, linear model with the formula FE=pH+t was sufficient to describe flocculation behavior for a subset of the data with pH>11. R^2 values were 0.88 for $Ca(OH)_2$ flocculation, 0.95 for KOH and 0.96 for NaOH supplementation. $Mg(OH)_2$ was not suitable for induction of flocculation and hence could not be included.

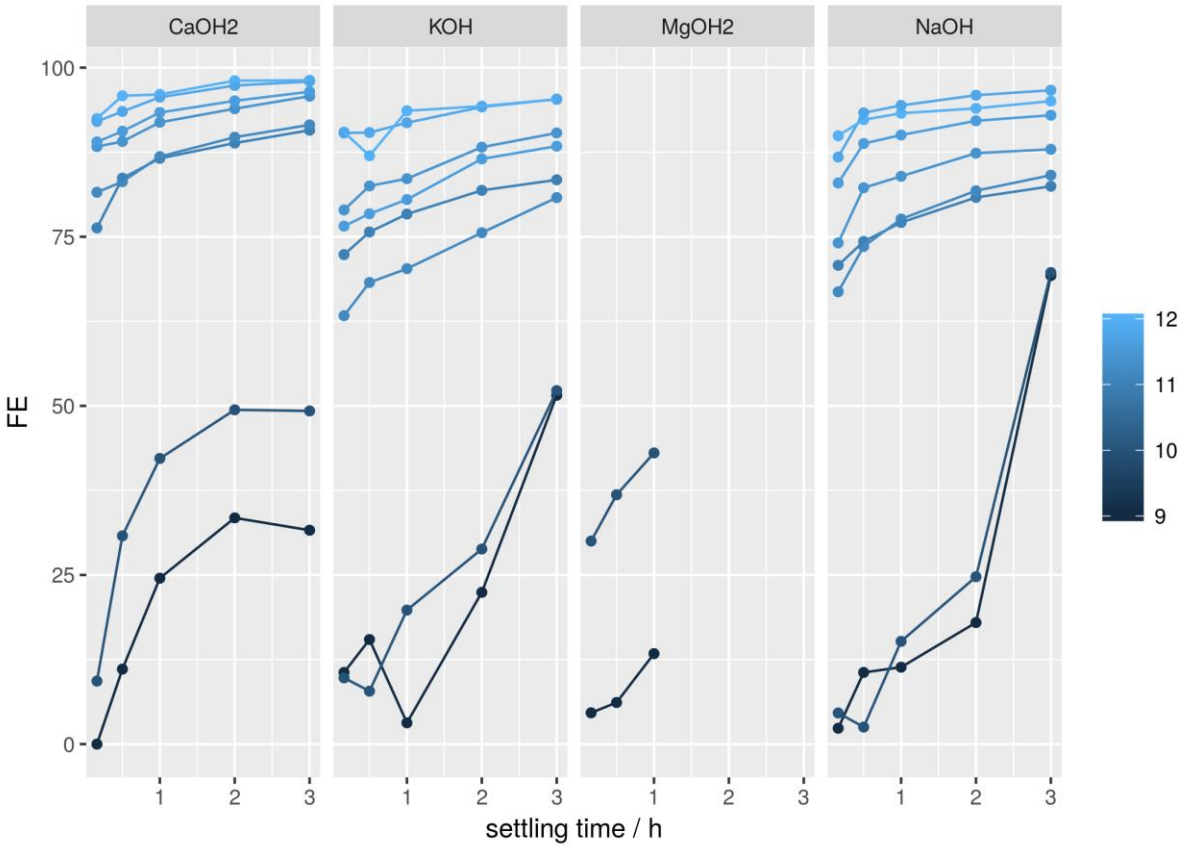

Figure 37: Flocculation efficiencies of autoflocculation induced by supplementation of different bases. Image is analogous to Figure 36. Color is showing pH of the respective sample.

The impact of sedimentation time in FE per hour was not affected by the flocculant, indicating that the mechanism of flocculation was similar independently of the choice of base (Figure 38, A). In contrast, $Ca(OH)_2$ had a significantly higher intercept than the other flocculants (Figure 38, B). This suggests that the respective flocculant leads to higher flocculation efficiencies assuming the same pH. This is especially noticable at lower pH (Figure 36), however with increasing pH, the difference between flocculants disappears, due to the higher effect of pH when using KOH or NaOH (Figure 38, C). Correspondingly at high pH (pH=12), no significant differences (at α=0.05) are observed between the different flocculation agents.

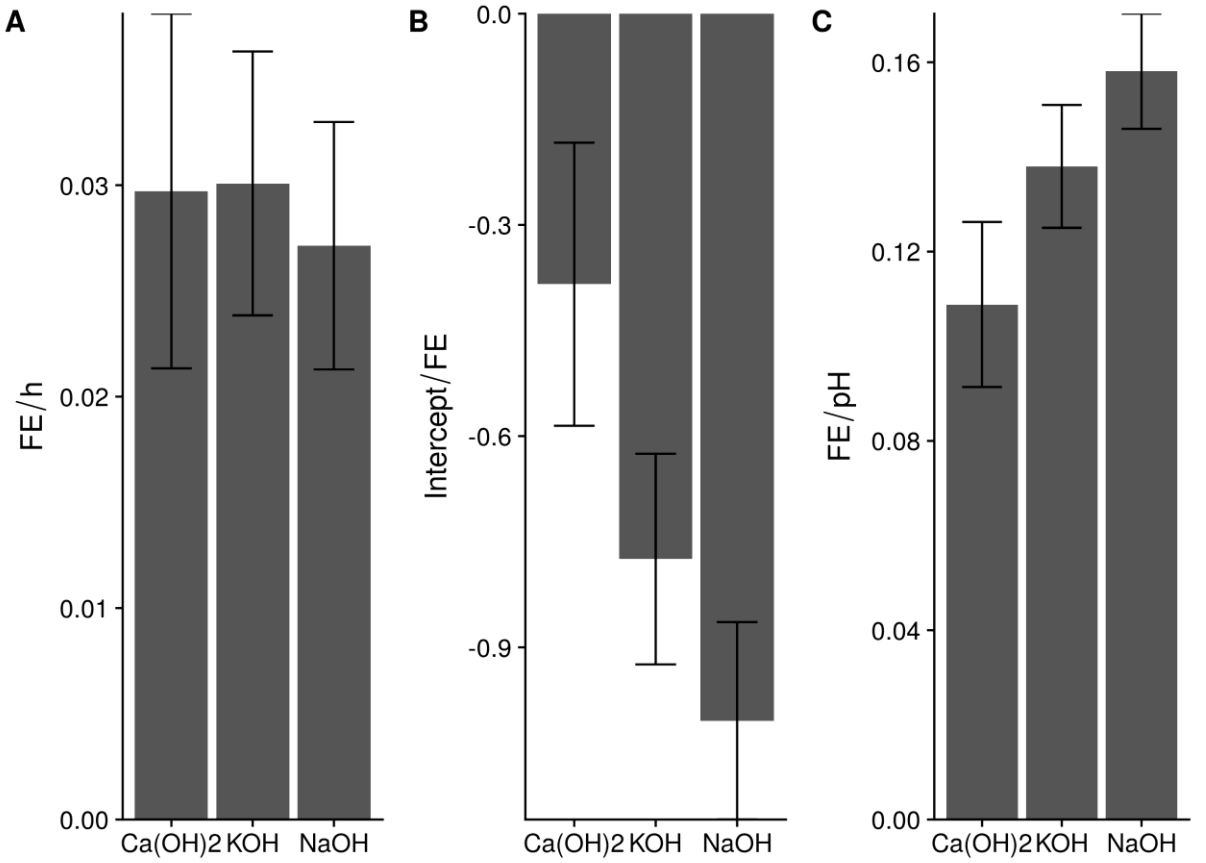

Figure 38: Comparison of regression parameters time (A), intercept (B) and pH (C). Error bars show standard error of the respective parameter with n=3.

The basis for differences in flocculation efficiencies by induction of autoflocculation in dependence of the employed base lies in the properties of its ions. Calcium hydroxide (Ca^{2+} 1.00 Angstrom, pK_B 1.37,2.43) has a lower basicity than sodium (Na+ 1.02 Angstrom, pKB -0.93) or potassium (K+ 1.38 Angstrom, pKB -0.7). Hence, a higher amount of base is required to achieve the respective pH (Table 14). In conclusion, not only the adjusted pH, but also the total number of ions appears to be important to achieve high flocculation efficiencies. Required loading for biomass was done by employing a standard curve as shown in Supplemental 41.

Vandamme also reported flocculation of *Chlorella sp.* in fresh water at pH values of 10.8 for NaOH, KOH and $Ca(OH)_2$ and pH 9.7 for $MgOH_2$. Significantly more base was required to adjust the pH of brackish water culture used in this work (Table 14) emphasizing the buffering effect of the medium. Further, Vandamme showed, that a minimum of 150 µM magnesium ions is required for induction of flocculation. This was not further characterized in this work, although initial magnesium concentration was abundant at approximately 1.35 g/l or 56.25 mM. This explains magnesium hydroxide precipitation at relatively low pH values.

Table 14: Comparison of Ion properties, required base concentration and base loading for pH 10.8 and corresponding cost per kg base in technical quality as well as harvesting cost per ton biomass. Agent costs are in bulk (1.4.2017).

	Ion Properties		[Base]	[Biomass]	Base Load g/g	Cost $/kg	Cost $/t
	Angstrom	pK_B	g/l	g/l	Biomass	Agent	Biomass
NaOH	1.02	-0.93	0.204	1	0.204	0.31	63.24
KOH	1.38	-0.7	0.324	1	0.324	0.65	210.6
$Ca(OH)_2$	1	1.37,2.43	0.385	1	0.385	0.1	38.5

This work confirms results previously obtained by Vandamme[208], in which *Chlorella vulgaris* was harvested by autoflocculation over pH shift to 10.8. He also reported, that calcium hydroxide was the most efficient base for flocculation, with NaOH showing the lowest required loadings. In the respective work, loadings were 9, 12 and 18 mg/g algae biomass for the bases NaOH, KOH and $Ca(OH)_2$. The higher required loadings in comparison to this work (Table 14) are likely due to lower biomass concentration in samples of experiments conducted by Vandamme[208]. Required base concentrations for this previous work (NaOH: 0.23, KOH: 0.32 and Ca(OH)2: 0.3 g/l) were comparable to the salty water medium (ABV) as shown in Table 14. Harvesting by calcium hydroxide required the highest concentration of 0.39 g/l (0.39 g/g biomass at 1 g/l biomass), but due to its low cost ($0.1/kg), cost efficiency is the highest.

As noted by Vandamme[208], the term autoflocculation by pH shift is somewhat misleading, as the reason for separation of algae suspension is conjectured to be binding of magnesium ions to the algae surface, which in turns leads to neutralization of surface charge. It was shown, that this is also feasible for *Scenedesmus obtusiusculus* AB189 in artificial salt water medium resembling baltic brackish water.

3.4.3 Tannin and Chitosan Flocculation

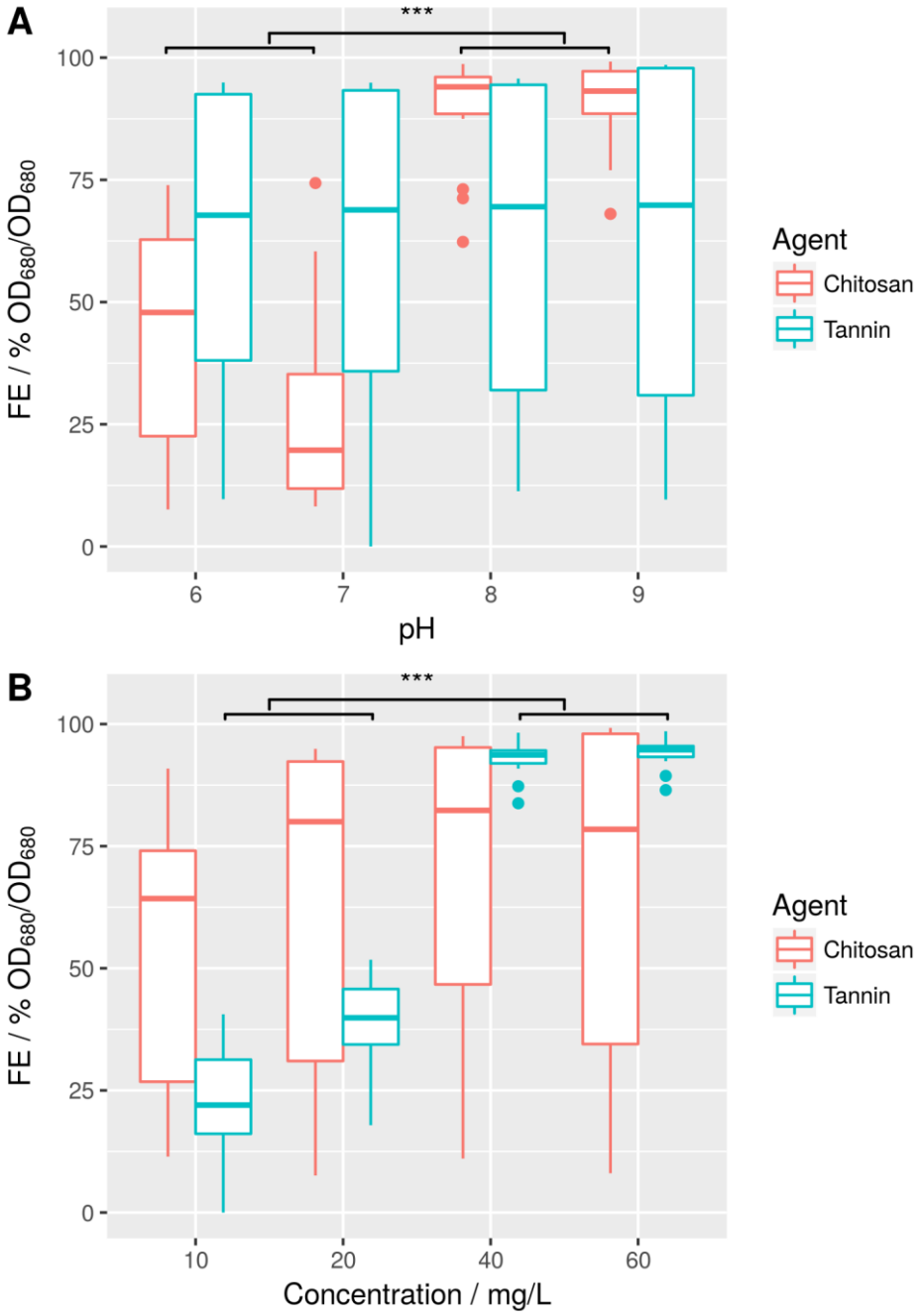

Figure 39 Flocculation efficiencies of chitosan (A, B) and tannin (C) in BG11 (A) and ABV (B,C) medium. Black points show measurement points, blue shows respective flocculation efficiencies with linear interpolation and red dashed lines show contour lines.

Chitosan and Tannin were chosen as flocculants and were tested in fresh water (BG11) and a salty, of natural sources derived medium (ABV). A summary of all raw values can be found in Supplemental 42 and Supplemental 43.

Chitosan showed high flocculation efficiency for all pH values starting at a concentration of 10 mg/l. This confirms previous reports of high flocculation efficiencies achieved with this polymer also with *Scenedesmus sp.* strains[229], [234], [251], [252].

Flocculation efficiency plateaus between 0.96 and 0.98 and does not decrease even at higher doses up to 40 mg/l. In ABV medium however, flocculation is less stable and apparently highly pH dependent. While still active at high pH values over 8, FE strongly decreases at a pH between 6 and 8. In comparison to this, CFL-PT is entirely independent from culture pH even in high salt environment.

Ordinary multiple linear regression could not be applied due to non-normality of the dataset. Flocculation efficiencies are ratio data and therefore inherently censored. This is often not a problem as long as normality of data is still given. However, for the respective data, this does not apply. For data which is strongly bound to the censoring limits, a logistic regression can be applied by assuming binary outcomes (Flocculation/No Flocculation).

In summary, efficiency of chitosan as flocculant was higher than for tannin in salty water medium: FE over 90% was achieved using 20 mg/l chitosan or 40 mg/l tannin. However, cost of the respective tannin ($5 /kg) is significantly lower than for chitosan ($25/kg). This results in an overall reduction in cost from $0.5/kg algae biomass to $0.2/kg algae biomass assuming a cell density of approximately 1 g/l.

3.4.4 Tannin/Chitosan Interaction

Different amounts of tannin and chitosan stock solutions were mixed to be used as flocculant-mix as shown in section 3.3.8.1. Obtained flocculation efficiencies resembles somewhat more a uniform distribution than a normal distribution (Supplemental 42), most likely again caused by censoring, but normality is not rejected by Shapiro-Wilk normality test (W=0.908, p-value=0.27). Again it was shown, that both flocculants are in principal active under the given conditions. However, in this approach, pH was fixed at 8, the optimal pH for growth of the microalgae used in these experiments.

In the chosen experimental setup, flocculation effects appear to result in some degree of synergy between the two flocculants. Firstly, this can be seen in Figure 40. If one flocculant at the chosen concentration would have been better than the other, optima would be observed either at x1=0 or x2=0. If the effect were solely additive, a connection between total flocculant (tannin and chitosan together) would have had a linear dependence to flocculation efficiency, which is not the case.

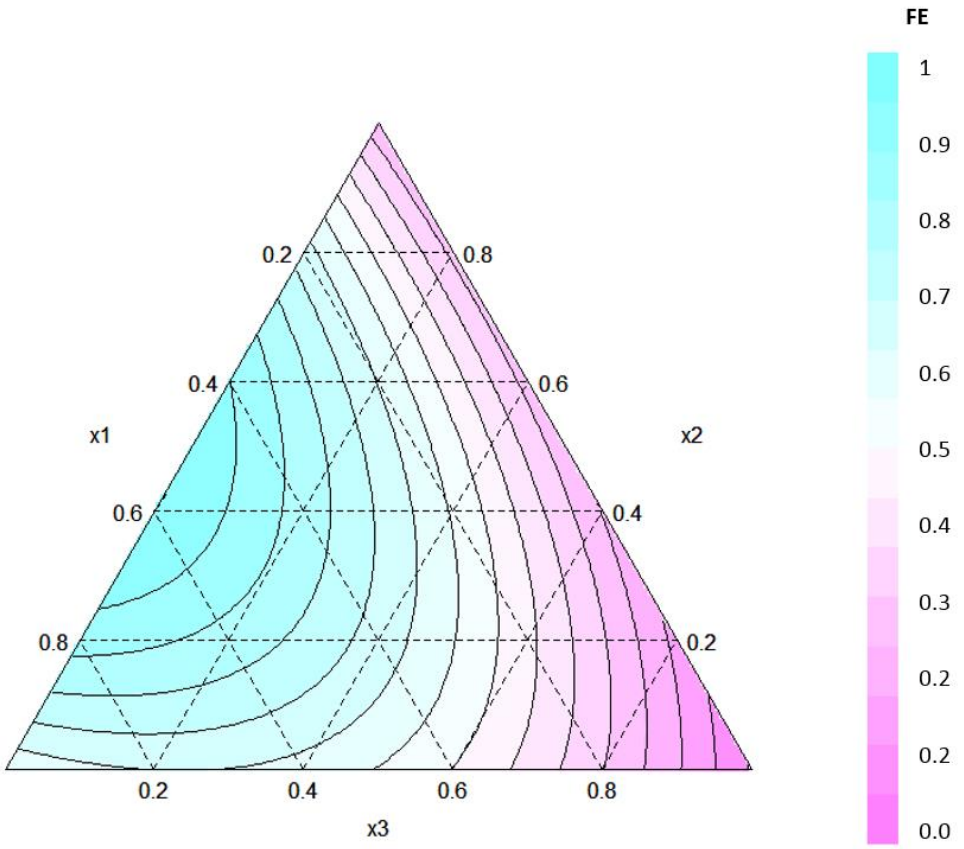

Figure 40: Surface response showing flocculation efficiencies with different ratios of tannin (x1), chitosan (x2) and H_2O (x3). Concentrations are between 0 and 30 mg/l Chitosan and 0 and 120 mg/l tannin. Culture was at OD_{600}=3.6 and at t=113 h Levels are shown in Table 15.

Secondly, the interdependent effect between these two factors can be seen in Supplemental 43. The cofactor for x1:x2 interaction (e.g. between the two flocculants) is the highest of the entire regression. In theory, the mechanism of flocculation should be similar for both flocculation agents: they are both functionalized biopolymers and presumably exert their functionality over bridging and sweeping flocculation. There are however differences in charge density and polymer lengths. DLS allowed for estimation of hydrodynamic particle size as well as zeta potential: Tannin has both a lower zeta potential (-52.7±2.2 mV) and smaller size (z-average: 8016+-3687 nm) than chitosan (-34.8±1.4 mV and 106±55 nm). A detailed summary of all model parameters can be found in Supplemental 43.

It could be speculated that the reason for possible synergistic effects while maintaining the same mechanistic pattern could lie in the diverse and complex structure of algae cell surface. Cell wall polymers are not evenly distributed, which could lead to different preferences of different cell wall surface areas for different flocculants.

Table 15: Run and experiment order, raw flocculant concentration as independent variable levels as well as flocculation efficiency (FE).

Run Order	Number	Tannin mg/l	Chitosan mg/ml	H_2O ml	FE
9	1	40	0	20	0.52
6	2	0	0	30	0.04
7	3	80	10	0	0.97
4	4	40	20	0	0.97
8	5	40	10	10	0.96
1	6	0	10	20	0.18
6	7	0	30	0	0.29
10	8	120	0	0	0.72
3	9	80	0	10	0.59
2	10	0	20	10	0.27

In summary, despite equivalence in mechanistic action of the two flocculants, there appears to be some degree of synergy, most likely founded in the different polymer size and charge. A maximum was observed at 80 mg/ml tannin and 10 mg/ml chitosan at an algae cell density of OD_{600}=3.6. Flocculation optimum was at a tannin to chitosan ratio of 4:1. FE of over 96% was reached at a concentration of 40 mg/l tannin together with 10 mg/l chitosan.

Table 16: Estimated cost to achieve > 95% FE using tannin and chitosan as flocculant.

Cultivation	Agent	Product	[Biomass] mg/l	Load g/g	$/kg Agent	$/t Biomass
Flask	Tannin	PolySepar CFL PT	30	0.03	5	150
Flask	Chitosan	Biolog Heppe A90/400/A1	20	0.02	25	500
Closed Ferm	Mix	Tannin:Chitosan 4:1	50	0.05	10	500

At 1 g/l biomass concentration, this translates to 50 mg/g or a cost of $500 per ton algae biomass (Table 16). Required loadings for flask cultivation were significantly lower, presumably due to higher content of algae organic matter and/or higher bacterial populations. Consequently, harvesting cost for these approaches was relatively low. The obtained data for chitosan fit well with estimated cost by Vandamme[208] ($500/t algae biomass). However, by using tannin or a mix of different flocculation agents, this cost could be reduced significantly. However further experiments are necessary to validate this.

3.4.5 Growth Phase Dependency of Tannin and Chitosan Flocculation

S. obtusiusculus A189 was cultivated in ABV medium in an open bubble column, mimicking open pond cultivation. At five time points, a 2^3 design, varying flocculant, flocculant concentration and pH were conducted.

Growth is slow in comparison to cultivation in the closed infors reactor (Figure 41), owing to suboptimal aeration and illumination. The higher thickness of the bubble column (20 cm in comparison to 10 cm for the closed system) further leads to early shading between cells and lower final dry biomass concentration. The respective dry biomass concentrations can be estimated by applying the standard curve as shown in section 3.3.4.

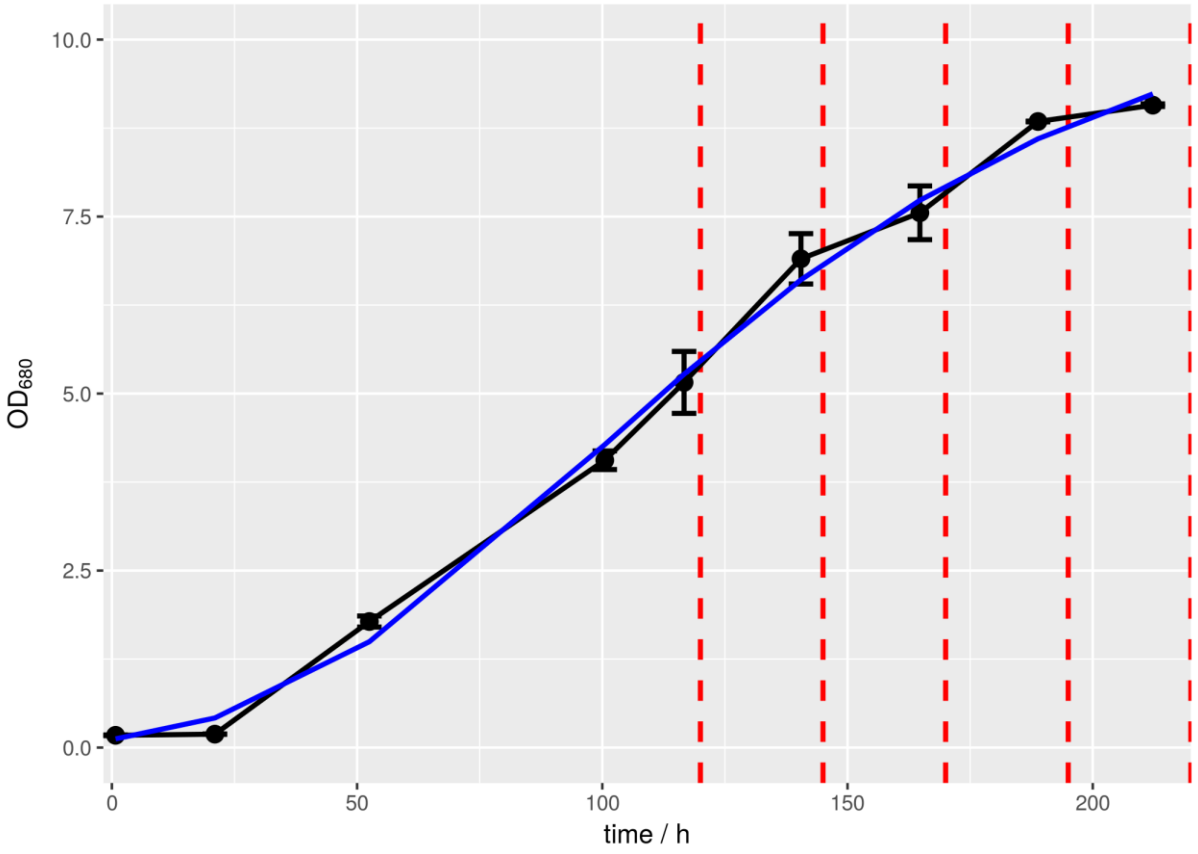

Figure 41: Growth curve of Scenedesmus obtusiusculus *A189 grown in previously published salty medium. Estimated parameters as shown by Gompertz fit (blue) are: mu:0.0628 lambda:32.3981 A.model:10.82623. Dashed red lines show time points of flocculation experiments. Error bars show standard deviations of triplicates.*

Normality of the flocculation efficiencies (FE) and residual OD_{680} of supernatant after flocculation (ROD) was confirmed by Shapiro-Wilk (Supplemental 44), whereas the distribution for FE was heavy tailed and tended towards a uniform distribution (most likely due to censoring of data) and for ROD was skewed to the left, resembling a beta distribution. Data for residual volume did not follow a normal, but resembled binary distribution.

3.4.5.1 Effect of Growth Phase

There appears to be no significant time effect on zeta potential (Figure 42). Repeated Measure ANOVA shows no significant differences between time points. This contrast previous results obtained in the closed infors reactor, where a clear increase in zeta potential over time was observed (Supplemental 46).

Figure 43 shows differences in flocculation efficiency over time are significant according to multiple measure ANOVA (α=0.05). By simple linear regression, time was found to be significant both as linear and quadratic term. However, time effect accounted for approximately 25% of variation found between samples. In summary, an increase of flocculation efficiency over time was found, which however just captures a small amount of variation and effect sizes were small.

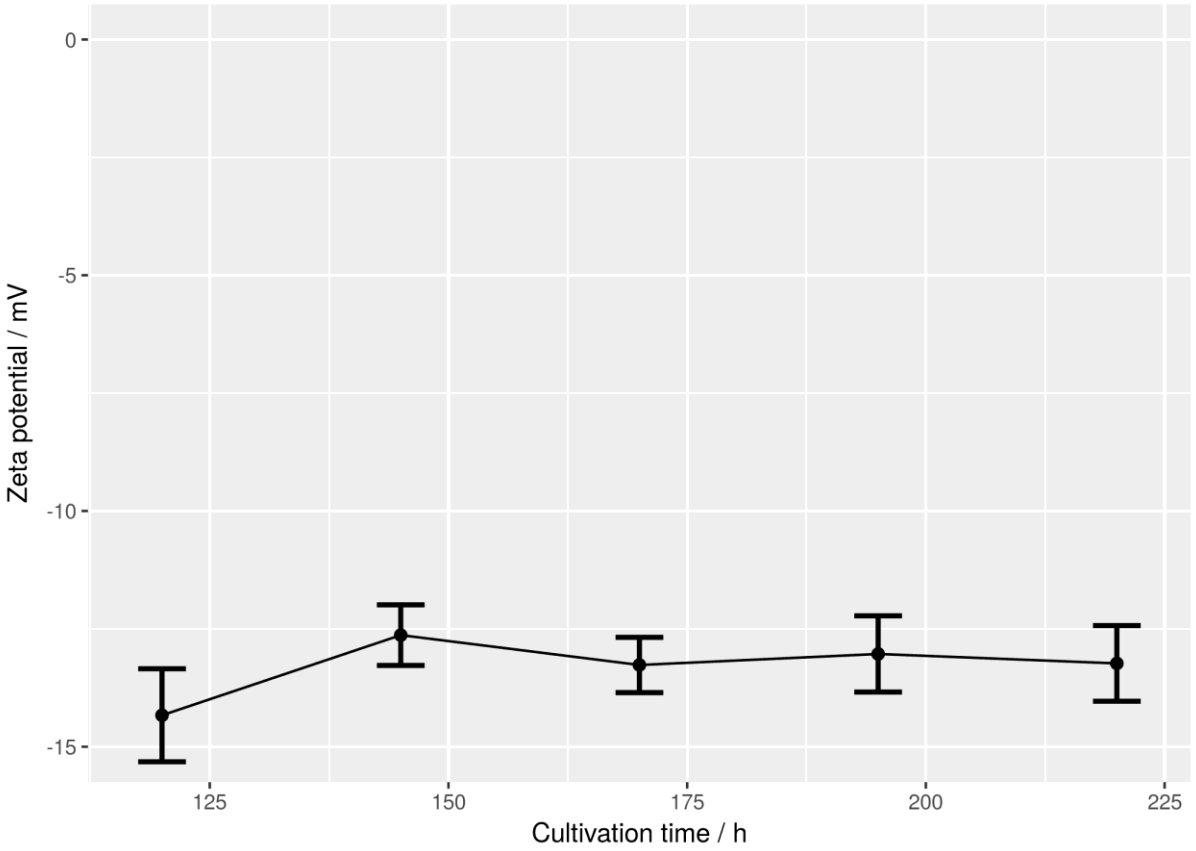

Figure 42: Zeta potential in mV over time of open bubble column reactor cultivation as shown in Figure 41. Error bars show standard deviations of triplicates.

Similarly, differences in residual OD_{680} (ROD) over time were significant according to multiple measure ANOVA (Supplemental 47, p=0.0133). Time as linear factor explains only 27% of variance of residual OD and adding quadratic factors yielded no improvement. Interestingly,

no direct effect of time on residual volume was observed, even if subsetting the data into a high and a low residual volume set (Supplemental 47).

While smaller in size, bacteria and cell fragments made up the majority of the culture at the end of cultivation (Supplemental 48). Only few agglomerated cells were found. Two distinct bacterial populations, neither of which were fluorescent on the FL2 channel (indicating the absence of chlorophyll) could be separated by side scatter. Count and share of both populations as well as the total number of events was observed over time (Supplemental 48). All populations showed exponential growth over time. In addition, the share of bacterial population 1 in relation to the total events is rising exponentially, whereas population 2 stays roughly constant in share. Extrapolating the shown growth kinetics, it can be assumed, that bacterial populations in time overgrow algae.

The impact of bacterial populations on all dependent variables is shown in Supplemental 49: Effect on residual volume cannot be estimated due to binary distribution. Despite an apparent correlation to FE, the effects cannot be untangled from other factors correlating with time. In other words, in the prediction of said dependent variables, time and bacterial populations show collinearity with each other and other factors.

In the same way as effects of bacterial populations, effect of zeta potential on dependent variables could not be estimated. In this case, zeta potential had no clear effect on flocculation efficiency and residual volume, however there was some positive correlation to residual OD. Lack of effect of zeta potential is most likely owed to small variability of this factor: As shown in Supplemental 50, multiple measure ANOVA showed no significant differences.

In relation to calculating the harvesting efficiency (Section 3.3.5), the question arises, whether flocculation efficiency and residual volume relate to each other in a meaningful way.

Even if dividing the dataset into low and high residual volumes (owed to the binary distribution, Supplemental 44), no apparent dependency can be found between the two factors. Taking into account the previous results, this indicates, that the factors affecting flocculation efficiency are different or do so in a different way than factors who exert an effect on the residual volume and therefore the compression factor.

3.4.5.2 Other Effects

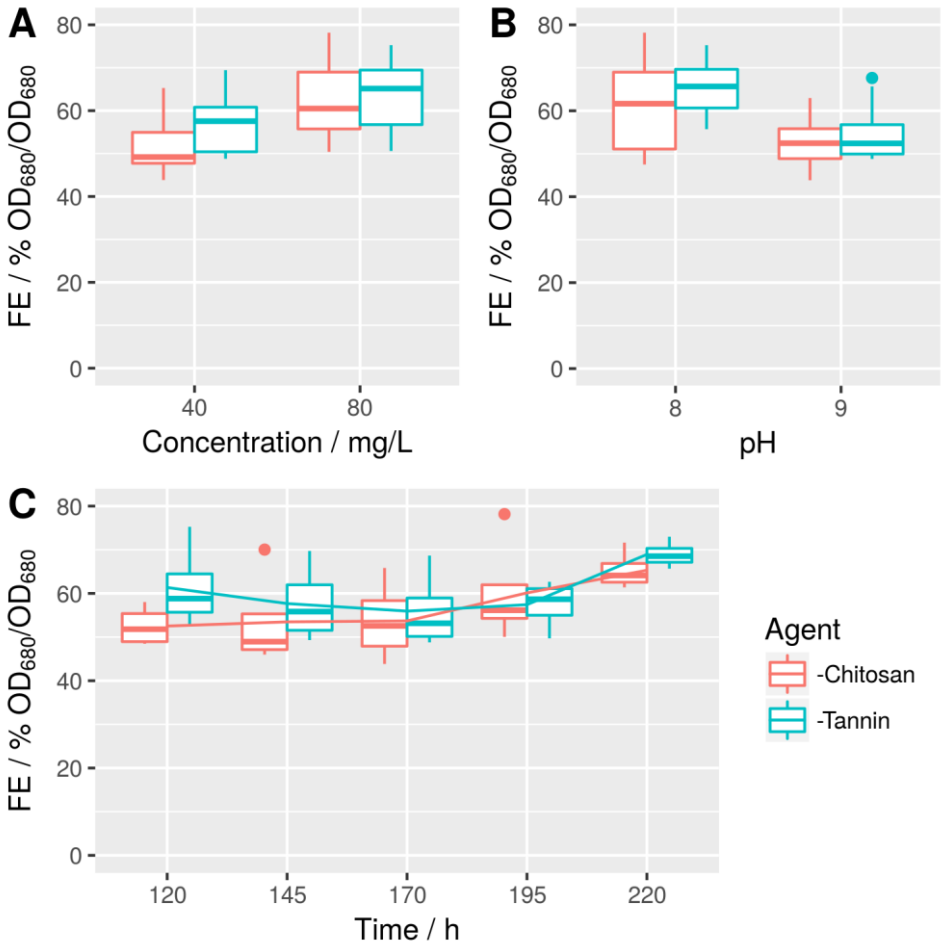

Figure 43: Effect of factors pH, flocculant concentration and flocculation agent on flocculation efficiency (FE). Differences between pH values and flocculant concentrations are significant ($p=5*10^{-4}$ and $p=2.2*10^{-3}$ respectively), whereas differences between flocculation agent are not ($p=0.26$). Testing was done using Welch's-test.

Concentration and pH are significant factors, however the flocculant itself is not (Supplemental 45). This is due to absence of captured interaction effects as opposed to section 3.3.8.1. On average, increase of flocculant dose leads to higher FE, whereas increase of pH from 8 to 9 decreases flocculation efficiency. Supplemental 51 shows the effect of the independent variables on residual volume (RV). In contrast to flocculation efficiency, the compression is almost solely dependent on the type of flocculant. Apart from one value, separation is linear.

3.4.5.3 Time and Other Effects

Three models were generated to predict flocculation efficiency from the four independent variables: The first regression contained all linear and interaction effects as well as a quadratic time effect. The second model was selected according to the Akaike information criterion (AIC), whereas the third model was chosen based on reverse factor elimination based on p-values. Supplemental 53 and Supplemental 54 show corresponding formulas, and R^2 values.

Comparison of cofactors in pareto charts (Supplemental 55) shows the main effects of each model. By comparing the different models (Supplemental 52, Supplemental 53 and Supplemental 54) it is demonstrated, that the main coefficients are stable: The strongest effect is always given by the concentration of flocculant (x2), whereas an increase from 40 to 80 mg/l raises FE by approximately 15%. However, this can be somewhat offset by a negative interaction effect between flocculant concentration (x2) and pH (x1): Flocculation efficiency decreases by 10%, if pH is raised to 9 while the concentration is raised by the respective amount. This indicates, that an increase in pH, (which has a negative linear effect of approximately 4%) cannot be offset by a doubling of flocculant concentration. Tannin yields 7% higher flocculation efficiency compared to chitosan. However, it interacts negatively with concentration. The reason for the negative interaction of factor level tannin with concentration is possibly the censoring of data, yielding a non-linear effect of tannin on flocculation. The same applies to interaction of tannin with time (x3) The interaction with pH is minor in effect size and in fact not significant, so it is not included in the model using reverse factor elimination. Time (x3) has a small positive impact both in a linear and quadratic fashion. As expected, there are no 3-way interactions consistent with all models. High order interactions of significant impact are rarely found. Box-Cox transformation yielded no substantial improvement of regression results.

3.4.5.4 Algae Organic Matter Effects

Boxplots of flocculation efficiency (Figure 44) in dependence of algae organic matter, time, pH, flocculation concentration and flocculation agent show clear increase of FE, when algae organic matter is not present in the medium. Moreover, this increase is much stronger for tannin than it is for chitosan, indicating an interaction.

The models (Supplemental 56, Supplemental 57 and Supplemental 58) are dominated by the positive interaction between factor level tannin and the presence of algae organic matter (AOM). In other words, flocculation efficiency always increases if AOM is removed (+10% FE), however if tannin is used, increase is another 25% FE higher in comparison to using chitosan. pH has a negative effect, which was already previously shown (Section 3.4.3). Interestingly in the present model, effect of pH with concentration is positive. This contradicts the result of the previous model (Section 3.4.3), in which this interaction effect was negative. R^2 values of the models are comparable, consequently the relevant difference might lie in the way the two mentioned factors interact depending on the presence of AOM. However further experiments are required for elucidation of these effects.

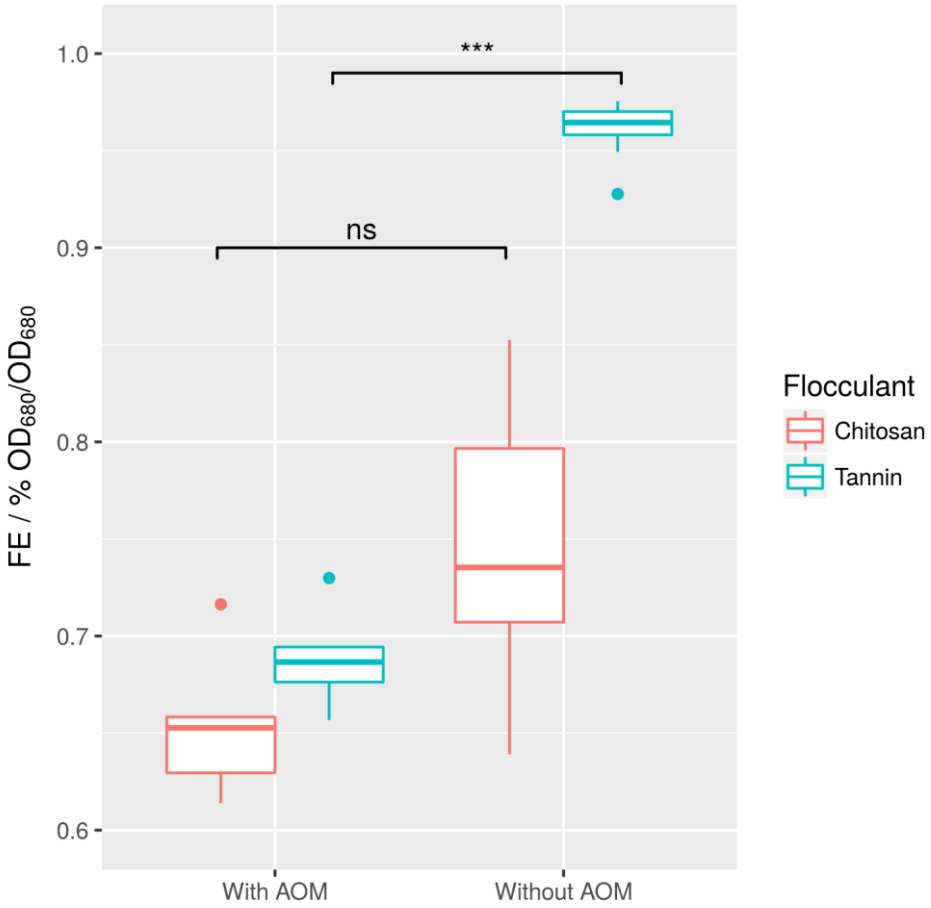

Figure 44: The first row shows the effect of time (170 and 220 hours) and algae organic matter (with AOM:W, without AOM:WO) on flocculation efficiency. The second row shows the effects of pH (pH 8 and 9) and cultivation time (40 and 80 hours) on FE. To display the effect of chitosan as opposed to tannin, the respective flocculation agents are shown separately in different colors.

3.5 Conclusion and Outlook

Measurement of flocculation efficiency in a plate reader was established by

a) showing the absence of sedimentation or adhesion effects in 96-well plates, when samples are not shaken over time and
b) demonstrating linear interval of cell density in comparison to the cuvette photometer.

As flocculation format, the jar test was confirmed as the only method yielding reproducible and reliable results. Flocculation-sedimentation tests in falcons, at best, yield proximate, semi-quantitative values not suitable for accurate modeling. Induction of autoflocculation by pH shift was possible for NaOH, KOH and $Ca(OH)_2$, but not for $Mg(OH)_2$, due to high concentration of salts already present in the artificial brackish water medium. NaOH required the lowest amount of base to set a pH sufficient for flocculation, but $Ca(OH)_2$ yielded slightly higher flocculation efficiencies in a shorter time. Further, it was also the cheapest flocculant and therefore considered the best choice in the current setting. Cost was approximately $40 per ton biomass.

The tannin agent CFL PT by Polysepar, which was characterized as flocculation agent for the first time in this work, is a feasible choice for harvest of microalgae *S. obtusiusculus* cultivated in optimized, salty water medium. Its advantages are its much lower price in comparison to chitosan comparable performance (~ 90% cost reduction). Furthermore, tannin has a strong advantage in the absence of algae organic matter over chitosan A90/400/A1 by Heppe. Dependence of tannin with pH appears to be lower than for chitosan, which means that at very high pH values of algae culture (>9), chitosan still might be the more favorable choice in this respect.

Interestingly, chitosan and tannin, despite presumed same mechanistic effect, appear to exhibit synergistic effects when used together. This is possibly owed to the different and complementary properties of the respective polymers in terms of chain length, particle size and zeta potential.

Measuring kinetics and different cultivation parameters as shown in section 3.3.8.2 showed the complexity of algae response to time. Some of those complex interactions during flocculation procedure could not be untangled. This applies for example to the possible effect of bacterial populations or zeta potential, which could not be evaluated in a model due to high collinearity. As shown in the difference between models for x1/x2/x3/time and AOM effect, small differences in the setup of the experiment can significantly change some effects, while others remain stable.

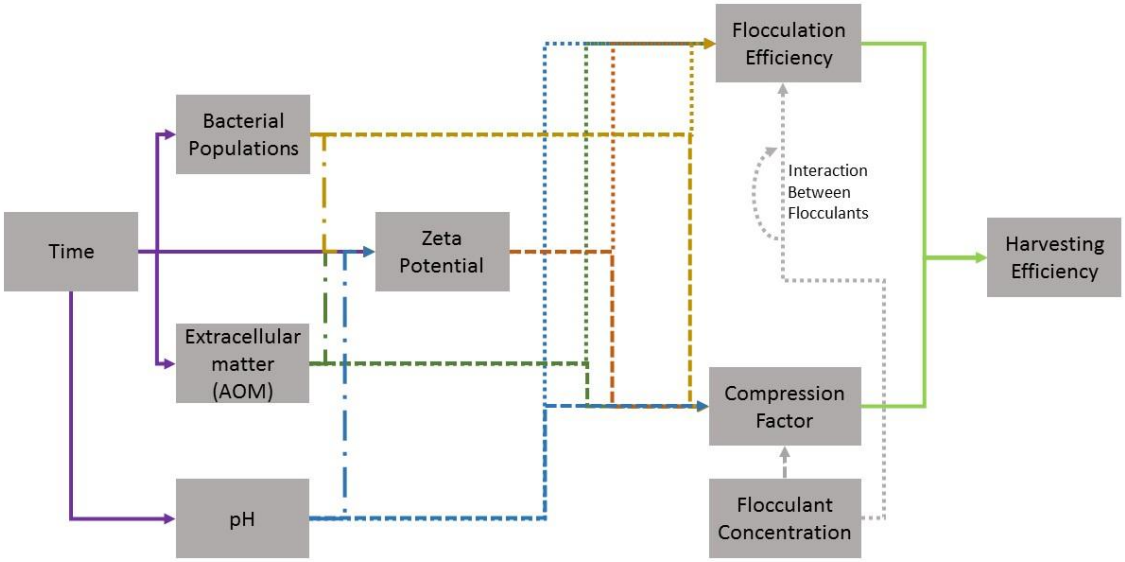

Figure 45: Relevant dependencies for evaluation of flocculation efficiencies. Colors and shapes indicate source and effector: Source of effect: violet-time, yellow – bacterial populations, green – extracellular organic algal matter, blue – pH, grey – flocculant concentration. Green indicates relationship of flocculation efficiency and compression factor to harvesting efficiency, which is given in section 3.3.6. Line type indicates effector: line dash - zeta potential, dotted – flocculation efficiency, dashed – compression factor, dash-dotted – zeta potential, standard line – time.

Bacterial populations are described as playing a key role in flocculation of microalgae[253], however the exact mechanisms and dependencies are largely unknown. It has been shown, that not only flocculation efficiency, but also individual floc size depends on the presence of these bacterial populations. Zeta potential also plays a key role, as outlined in the introduction. Monitoring of Zeta potential is a good indicator for success of flocculation[254], however in a quantitative sense, most interdependencies (Figure 45) between strain (including algal surface structure), medium and cultivation conditions remain elusive.

4 Bibliography

[1] U. von Stockar and J.-S. Liu, “Does microbial life always feed on negative entropy? Thermodynamic analysis of microbial growth,” *Biochim. Biophys. Acta - Bioenerg.*, vol. 1412, no. 3, pp. 191–211, 1999.

[2] R. Renneberg and V. Berkling, *Biotechnologie für Einsteiger*. Springer Spektrum, 2013.

[3] W. M, “Microbial fat: micro-organisms as potential fat producers,” *Prog. Ind. Microbiol.*, vol. 1, pp. 181–245, 1959.

[4] C. Boulton and C. Ratledge, “Correlation of Lipid Accumulation in Yeasts with Possession of ATP : Citrate Lyase,” *J. Gen. Microbiol.*, vol. 127, pp. 169–176, 1981.

[5] H. M. Alvarez and A. Steinbüchel, “Triacylglycerols in prokaryotic microorganisms.,” *Appl. Microbiol. Biotechnol.*, vol. 60, no. 4, pp. 367–76, Dec. 2002.

[6] Q. Li, W. Du, and D. Liu, “Perspectives of microbial oils for biodiesel production.,” *Appl. Microbiol. Biotechnol.*, vol. 80, no. 5, pp. 749–56, Oct. 2008.

[7] J. M. Ageitos, J. A. Vallejo, P. Veiga-Crespo, and T. G. Villa, “Oily yeasts as oleaginous cell factories,” *Appl. Microbiol. Biotechnol.*, vol. 90, no. 4, pp. 1219–27, May 2011.

[8] C. Ratledge, “Microbial Lipids,” in *Biotechnology*, Weinheim, Germany: Wiley-VCH Verlag GmbH, 2008, pp. 133–197.

[9] C. Ratledge and P. S. S. Dawson, *Biotechnology for the Oils and Fats Industry*. The American Oil Chemists Society, 1984.

[10] C. Ratledge, “Fatty acid biosynthesis in microorganisms being used for Single Cell Oil production,” *Biochimie*, vol. 86, no. 11, pp. 807–815, 2004.

[11] Y. Chisti, “Biodiesel from microalgae beats bioethanol.,” *Trends Biotechnol.*, vol. 26, no. 3, pp. 126–31, Mar. 2008.

[12] A. Ykema, E. C. Verbree, H. W. van Verseveld, and H. Smit, “Mathematical modelling of lipid production by oleaginous yeasts in continuous cultures.,” *Antonie Van Leeuwenhoek*, vol. 52, no. 6, pp. 491–506, 1986.

[13] R. Wang, J. Wang, R. Xu, Z. Fang, and A. Liu, “Oil Production by the Oleaginous Yeast Lipomyces starkeyi using Diverse Carbon Sources,” *BioResources*, vol. 9, no. 4, pp. 7027–7040, Oct. 2014.

[14] J. C. Escobar, E. S. Lora, O. J. Venturini, E. E. Yáñez, E. F. Castillo, and O. Almazan, “Biofuels: Environment, technology and food security,” *Renew. Sustain. Energy Rev.*, vol. 13, no. 6–7, pp. 1275–1287, Aug. 2009.

[15] S. Papanikolaou and G. Aggelis, “Lipids of oleaginous yeasts. Part II: Technology and potential applications,” *Eur. J. Lipid Sci. Technol.*, vol. 113, no. 8, pp. 1052–1073, Aug. 2011.

[16] “Home - PubMed - NCBI.” [Online]. Available: https://www.ncbi.nlm.nih.gov/pubmed/. [Accessed: 30-Jan-2017].

[17] C. Huang, X. Chen, L. Xiong, X. Chen, L. Ma, and Y. Chen, “Single cell oil production from low-cost substrates: the possibility and potential of its industrialization.,” *Biotechnol. Adv.*, vol. 31, no. 2, pp. 129–39.

[18] J. M. Rutkowski, J. H. Stern, and P. E. Scherer, “The cell biology of fat expansion.,” *J. Cell Biol.*, vol. 208, no. 5, pp. 501–12, Mar. 2015.

[19] C. D. Meyers, A. Amer, T. Majumdar, and J. Chen, “Pharmacokinetics, pharmacodynamics, safety, and tolerability of pradigastat, a novel diacylglycerol acyltransferase 1 inhibitor in overweight or obese, but otherwise healthy human subjects.,” *J. Clin. Pharmacol.*, vol. 55, no. 9, pp. 1031–41, Sep. 2015.

[20] H. Denison *et al.*, “Proof of mechanism for the DGAT1 inhibitor AZD7687: results from a first-time-in-human single-dose study.,” *Diabetes. Obes. Metab.*, vol. 15, no. 2, pp. 136–43, Feb. 2013.

[21] C. Görner, “Genetic Engineering of the Oleaginous Yeast Trichosporon oleaginosus and the Bacteria Escherichia Coli Aimed at the Production of High Value Lipids and Bioactive Diterpenes,” Technical University Munich, 2016.

[22] S. Papanikolaou and G. Aggelis, “Lipids of oleaginous yeasts. Part I: Biochemistry of single cell oil production,” *Eur. J. Lipid Sci. Technol.*, vol. 113, no. 8, pp. 1031–1051, Aug. 2011.

[23] Z. Zhu *et al.*, “A multi-omic map of the lipid-producing yeast Rhodosporidium toruloides,” *Nat. Commun.*, vol. 3, p. 1112, 2012.

[24] R. Kourist *et al.*, “Genomics and Transcriptomics Analyses of the Oil-Accumulating Basidiomycete Yeast Trichosporon oleaginosus : Insights into Substrate Utilization and Alternative Evolutionary Trajectories of Fungal Mating Systems,” *MBio*, vol. 6, no. 4, pp. e00918-15, Sep. 2015.

[25] S. Wullschleger, R. Loewith, and M. N. Hall, “TOR Signaling in Growth and Metabolism,” *Cell*, vol. 124, no. 3, pp. 471–84, Feb. 2006.

[26] N. J. Moon *et al.*, “Conversion of Cheese Whey and Whey Permeate to Oil and Single-Cell Protein,” *J. Dairy Sci.*, vol. 61, no. 11, pp. 1537–1547, Nov. 1978.

[27] C. Ratledge, “Single cell oils — have they a biotechnological future?,” *Trends Biotechnol.*, vol. 11, no. 7, pp. 278–284, 1993.

[28] R. S. Moreton, “Yeast lipid estimation by enzymatic and nuclear magnetic resonance methods.,” *Appl. Environ. Microbiol.*, vol. 55, no. 11, pp. 3009–11, Nov. 1989.

[29] P. Gujjari, S.-O. S. O. Suh, K. Coumes, and J. J. J. Zhou, “Characterization of oleaginous yeasts revealed two novel species: Trichosporon cacaoliposimilis sp. nov. and Trichosporon oleaginosus sp. nov.,” *Mycologia*, vol. 103, no. 5, 2011.

[30] X.-Z. Liu *et al.*, “Towards an integrated phylogenetic classification of the Tremellomycetes,” *Stud. Mycol.*, vol. 81, pp. 85–147, Jun. 2015.

[31] C. A. Morrow and J. A. Fraser, “Sexual reproduction and dimorphism in the pathogenic basidiomycetes,” *FEMS Yeast Res.*, vol. 9, no. 2, pp. 161–177, 2009.

[32] J. Depree, G. W. Emerson, and P. A. Sullivan, “The cell wall of the oleaginous yeast Trichosporon cutaneum,” *J. Gen. Microbiol.*, vol. 139, no. 9, pp. 2123–2133, Sep. 1993.

[33] A. Ykema, R. H. A. Bakels, I. I. G. S. Verwoert, H. Smit, and H. W. van Verseveld, “Growth yield, maintenance requirements, and lipid formation in the oleaginous yeast Apiotrichum curvatum,” *Biotechnol. Bioeng.*, vol. 34, no. 10, pp. 1268–1276, Dec. 1989.

[34] P. Van Bodegom, “Microbial maintenance: A critical review on its quantification,” *Microb. Ecol.*, vol. 53, no. 4, pp. 513–523, 2007.

[35] B. A. . Glatz, M. D. . Floetenmeyer, and E. G. Hammond, “Fermentation of bananas and other food wastes to produce microbial lipid,” *J. Food Prot.*, vol. 48, no. 7, pp. 574–577, 1985.

[36] Y. Liang, K. Jarosz, A. T. Wardlow, J. Zhang, and Y. Cui, “Lipid Production by

Cryptococcus curvatus on Hydrolysates Derived from Corn Fiber and Sweet Sorghum Bagasse Following Dilute Acid Pretreatment," *Appl. Biochem. Biotechnol.*, vol. 173, no. 8, pp. 2086–2098, Aug. 2014.

[37] J. B. M. Rattray, *Biotechnology and the fats and oils industry — An overview*, vol. 61, no. 11. 1984.

[38] C. T. Evans and C. Ratledge, "A comparison of the oleaginous yeast, Candida curvata, grown on different carbon sources in continuous and batch culture.," *Lipids*, vol. 18, no. 9, pp. 623–9, Sep. 1983.

[39] A. Meo, "Lipidherstellung aus verdünnten Zuckergemischen mit Trichosporon oleaginosus," Technische Universität München, 2016.

[40] E. P. Knoshaug, M. A. Franden, B. U. Stambuk, M. Zhang, and A. Singh, "Utilization and transport of l-arabinose by non-Saccharomyces yeasts," *Cellulose*, vol. 16, no. 4, pp. 729–741, Aug. 2009.

[41] C. D. Smolke, *The metabolic pathway engineering handbook : fundamentals*. CRC Press/Taylor & Francis, 2010.

[42] Y. Zheng, Z. Chi, B. K. Ahring, and S. Chen, "Oleaginous yeast Cryptococcus curvatus for biofuel production: Ammonia's effect," *Biomass and Bioenergy*, vol. 37, pp. 114–121, Feb. 2012.

[43] T. Behrend, E. Gui~ho, J. Tredick, and H. J. Phaff, "DNA base composition and DNA relatedness among species of," *Antonie Van Leeuwenhoek*, vol. 50, pp. 17–32, 1984.

[44] D. R. Iassonova, "Lipid synthesis and encapsulation by Cryptococcus curvatus," Iowa State University, 2009.

[45] P. A. E. P. Meesters, G. N. M. Huijberts, and G. Eggink, "High-cell-density cultivation of the lipid accumulating yeast Cryptococcus curvatus using glycerol as a carbon source," *Appl. Microbiol. Biotechnol.*, vol. 45, no. 5, pp. 575–579, Jun. 1996.

[46] S. Wu, C. Hu, X. Zhao, and Z. K. Zhao, "Production of lipid from N-acetylglucosamine by Cryptococcus curvatus," *Eur. J. Lipid Sci. Technol.*, vol. 112, no. 7, pp. 727–733, Apr. 2010.

[47] C. Ratledge, "Production of fatty acids and lipid by a Candida sp. growing on a fraction of n-alkanes predominating in tridecane," *Biotechnol. Bioeng.*, vol. 10, no. 4, pp. 511–533, 1968.

[48] M. West, G. W. Emerson, and P. A. Sullivan, "Purification and properties of two lactose hydrolases from Trichosporon cutaneum," *J. Gen. Microbiol.*, vol. 136, no. 8, pp. 1483–1490, Aug. 1990.

[49] X. Yang *et al.*, "Simultaneous utilization of glucose and mannose from spent yeast cell mass for lipid production by Lipomyces starkeyi," *Bioresour. Technol.*, vol. 158, pp. 383–387, Apr. 2014.

[50] X. Yu, Y. Zheng, X. Xiong, and S. Chen, "Co-utilization of glucose, xylose and cellobiose by the oleaginous yeast Cryptococcus curvatus," *Biomass and Bioenergy*, vol. 71, pp. 340–349, Dec. 2014.

[51] C. Görner, V. Redai, F. Bracharz, P. Schrepfer, D. Garbe, and T. Brück, "Genetic engineering and production of modified fatty acids by the non-conventional oleaginous yeast Trichosporon oleaginosus ATCC 20509," *Green Chem.*, vol. 18, no. 7, pp. 2037–2046, Mar. 2016.

[52] S. Fakas, S. Papanikolaou, A. Batsos, M. Galiotou-Panayotou, A. Mallouchos, and G. Aggelis, "Evaluating renewable carbon sources as substrates for single cell oil

production by Cunninghamella echinulata and Mortierella isabellina," *Biomass and Bioenergy*, vol. 33, no. 4, pp. 573–580, Apr. 2009.

[53] X. Yu, J. Zeng, Y. Zheng, and S. Chen, "Effect of lignocellulose degradation products on microbial biomass and lipid production by the oleaginous yeast Cryptococcus curvatus," *Process Biochem.*, vol. 49, no. 3, pp. 457–465, Mar. 2014.

[54] S. Wu, X. Zhao, H. Shen, Q. Wang, and Z. K. Zhao, "Microbial lipid production by Rhodosporidium toruloides under sulfate-limited conditions," *Bioresour. Technol.*, vol. 102, no. 2, pp. 1803–1807, 2011.

[55] S. Wu, C. Hu, G. Jin, X. Zhao, and Z. K. Zhao, "Phosphate-limitation mediated lipid production by Rhodosporidium toruloides," *Bioresour. Technol.*, vol. 101, no. 15, pp. 6124–6129, Aug. 2010.

[56] Y. Li, Z. Zhao, and F. Bai, "High-density cultivation of oleaginous yeast Rhodosporidium toruloides Y4 in fed-batch culture," *Enzyme Microb. Technol.*, vol. 41, no. 3, pp. 312–317, 2007.

[57] W.-S. Park, P. A. Murphy, and B. A. Glatz, "Lipid metabolism and cell composition of the oleaginous yeast *Apiotrichum curvatum* grown at different carbon to nitrogen ratios," *Can. J. Microbiol.*, vol. 36, no. 5, pp. 318–326, 1990.

[58] A. Ykema, E. C. Verbree, M. M. Kater, and H. Smit, "Optimization of lipid production in the oleaginous yeast Apiotrichum curvatum in wheypermeate," *Appl. Microbiol. Biotechnol.*, vol. 29, no. 2–3, pp. 211–218, Sep. 1988.

[59] S. Larsson *et al.*, "The generation of fermentation inhibitors during dilute acid hydrolysis of softwood," *Enzyme Microb. Technol.*, vol. 24, no. 3, pp. 151–159, 1999.

[60] Z. Ruan, "Developing Novel Biological Processes to Convert Lignocellulose into lipid based biofuel," Michigan State University, 2014.

[61] X. Yu, Y. Zheng, K. M. Dorgan, and S. Chen, "Oil production by oleaginous yeasts using the hydrolysate from pretreatment of wheat straw with dilute sulfuric acid," *Bioresour. Technol.*, vol. 102, no. 10, pp. 6134–6140, May 2011.

[62] G. Christophe, J. L. Deo, V. Kumar, R. Nouaille, P. Fontanille, and C. Larroche, "Production of oils from acetic acid by the oleaginous yeast Cryptococcus curvatus," *Appl. Biochem. Biotechnol.*, vol. 167, no. 5, pp. 1270–1279, 2012.

[63] Z. Chi, Y. Zheng, J. Ma, and S. Chen, "Oleaginous yeast Cryptococcus curvatus culture with dark fermentation hydrogen production effluent as feedstock for microbial lipid production," *Int. J. Hydrogen Energy*, vol. 36, no. 16, pp. 9542–9550, Aug. 2011.

[64] Y. Cui, J. W. Blackburn, and Y. Liang, "Fermentation optimization for the production of lipid by Cryptococcus curvatus: Use of response surface methodology," *Biomass and Bioenergy*, vol. 47, pp. 410–417, Dec. 2012.

[65] G. H. Fleet, "Composition and Structure of Yeast Cell Walls," Springer New York, 1985, pp. 24–56.

[66] P. A. Sullivan, C. Y. Yin, C. Molloy, M. D. Templeton, and M. G. Shepherd, "An analysis of the metabolism and cell wall composition of Candida albicans during germ-tube formation.," *Can. J. Microbiol.*, vol. 29, no. 11, pp. 1514–25, Nov. 1983.

[67] U. a Ochsner, V. Glumoff, M. Kälin, a Fiechter, and J. Reiser, "Genetic transformation of auxotrophic mutants of the filamentous yeast Trichosporon cutaneum using homologous and heterologous marker genes.," *Yeast*, vol. 7, no. 5, pp. 513–524, 1991.

[68] C. T. Evans and C. Ratledge, "The Physiological Significance of Citric Acid in the Control of Metabolism in Lipid-Accumulating Yeasts," *Biotechnol. Genet. Eng. Rev.*, vol. 3, no.

February 2015, pp. 349–376, 1985.

[69] S. S. Tchakouteu, A. Chatzifragkou, O. Kalantzi, A. a. Koutinas, G. Aggelis, and S. Papanikolaou, “Oleaginous yeast Cryptococcus curvatus exhibits interplay between biosynthesis of intracellular sugars and lipids,” *Eur. J. Lipid Sci. Technol.*, vol. 117, no. 5, p. n/a, May 2015.

[70] P. Meeuwse, “Production of fungal lipids Kinetic modeling and process design,” Wageningen, 2011.

[71] R. S. Moreton, *Single cell oil*. Longman Scientific & Technical, 1988.

[72] N. J. Moon and E. G. Hammond, “Oil production by fermentation of lactose and the effect of temperature on the fatty acid composition1,” *J. Am. Oil Chem. Soc.*, vol. 55, no. 10, pp. 683–688, Oct. 1978.

[73] R. S. Moreton, “Modification of fatty acid composition of lipid accumulating yeasts with cyclopropene fatty acid desaturase inhibitors,” *Appl. Microbiol. Biotechnol.*, vol. 22, no. 1, pp. 41–45, 1985.

[74] I. R. Sitepu *et al.*, “Manipulation of culture conditions alters lipid content and fatty acid profiles of a wide variety of known and new oleaginous yeast species,” *Bioresour. Technol.*, vol. 144, pp. 360–369, Sep. 2013.

[75] C. Ratledge, “Regulation of lipid accumulation in oleaginous micro-organisms.,” *Biochem. Soc. Trans.*, vol. 30, no. Pt 6, pp. 1047–1050, 2002.

[76] B. G. Park, M. Kim, J. Kim, H. Yoo, and B.-G. Kim, “Systems biology for understanding and engineering of heterotrophic oleaginous microorganisms,” *Biotechnol. J.*, vol. 12, no. 1, p. 1600104, Jan. 2017.

[77] C. Ratledge and Z. Cohen, “Microbial and algal oils: Do they have a future for biodiesel or as commodity oils?,” *Lipid Technol.*, vol. 20, no. 7, pp. 155–160, Jul. 2008.

[78] B. D. Brown, “A kinetic study on the oleaginous yeast, Candda curvata D,” Iowa State University, 1984.

[79] Y. Zheng, Z. Chi, and S. Chen, “Biodiesel and Biohydrogen Co-Production with Treatment of High Solid Food Waste Final Report Biodiesel and Biohydrogen Co-Production with Treatment of High Solid Food Waste Ecology Publication Number 09-07-065,” 2009.

[80] E. Z. Vega, B. A., and E. G. Glatz, “Optimization of Banana Juice Fermentation for the Production of Microbial Oil,” *Appl. Environ. Microbiol.*, vol. 54, no. 3, pp. 748–752, 1988.

[81] B. Douglas Brown, K. H. Hsu, E. G. Hammond, and B. A. Glatz, “A relationship between growth and lipid accumulation in Candida curvata D,” *J. Ferment. Bioeng.*, vol. 68, no. 5, pp. 344–352, 1989.

[82] A. Ykema, E. C. Verbree, H. J. J. Nijkamp, and H. Smit, “Isolation and characterization of fatty acid auxotrophs from the oleaginous yeast Apiotrichum curvatum,” *Appl. Microbiol. Biotechnol.*, vol. 32, no. 1, pp. 76–84, 1989.

[83] I. G. S. I. G. S. Verwoert *et al.*, “Modification of the fatty-acid composition in lipids of the oleaginous yeast Apiotrichum curvatum by intraspecific spheroplast fusion,” *Appl. Microbiol. Biotechnol.*, vol. 32, no. 3, pp. 327–333, 1989.

[84] A. Ykema, E. C. Verbree, I. I. G. S. Verwoert, K. H. van der Linden, H. J. J. Nijkamp, and H. Smit, “Lipid production of revertants of Ufa mutants from the oleaginous yeast Apiotrichum curvatum,” *Appl. Microbiol. Biotechnol.*, vol. 33, no. 2, pp. 176–182, May 1990.

[85] A. Ykema, M. M. Kater, and H. Smit, “Lipid production in wheypermeate by an unsaturated fatty acid mutant of the oleaginous yeastApiotrichum curvatum,” *Biotechnol. Lett.*, vol. 11, no. 7, pp. 477–482, Jul. 1989.

[86] M. Hassan, P. J. Blanc, A. Pareilleux, and G. Goma, “Selection of fatty acid auxotrophs from the oleaginous yeast Cryptococcus curvatus and production of cocoa butter equivalents in batch culture,” *Biotechnol. Lett.*, vol. 16, no. 8, pp. 819–824, Aug. 1994.

[87] N. J. Moon and E. G. Hammond, “Process for converting whey permeate to oil-containing yeast,” 4235933, 25-Nov-1980.

[88] Z. Xue *et al.*, “Production of omega-3 eicosapentaenoic acid by metabolic engineering of Yarrowia lipolytica.,” *Nat. Biotechnol.*, vol. 31, no. 8, pp. 734–740, Jul. 2013.

[89] G.-Y. Wang, Y. Zhang, Z.-M. Chi, G.-L. Liu, Z.-P. Wang, and Z.-M. Chi, “Role of pyruvate carboxylase in accumulation of intracellular lipid of the oleaginous yeast Yarrowia lipolytica ACA-DC 50109,” *Appl. Microbiol. Biotechnol.*, vol. 99, no. 4, pp. 1637–1645, Feb. 2015.

[90] R. Ledesma-Amaro and J.-M. Nicaud, “Yarrowia lipolytica as a biotechnological chassis to produce usual and unusual fatty acids,” *Prog. Lipid Res.*, vol. 61, pp. 40–50, Jan. 2016.

[91] J. Blazeck *et al.*, “Harnessing Yarrowia lipolytica lipogenesis to create a platform for lipid and biofuel production,” *Nat. Commun.*, vol. 5, p. 3131, Jan. 2014.

[92] J. Blazeck, A. Hill, M. Jamoussi, A. Pan, J. Miller, and H. S. Alper, “Metabolic engineering of Yarrowia lipolytica for itaconic acid production,” *Metab. Eng.*, vol. 32, pp. 66–73, 2015.

[93] X. Zhao, X. Kong, Y. Hua, B. Feng, and Z. Zhao, “Medium optimization for lipid production through co-fermentation of glucose and xylose by the oleaginous yeastLipomyces starkeyi,” *Eur. J. Lipid Sci. Technol.*, vol. 110, no. 5, pp. 405–412, 2008.

[94] M. L. Kelley, Ž. Strezoska, K. He, A. Vermeulen, and A. van B. Smith, “Versatility of chemically synthesized guide RNAs for CRISPR-Cas9 genome editing,” *J. Biotechnol.*, vol. 233, pp. 74–83, Sep. 2016.

[95] T. Tanaka *et al.*, “A hidden pitfall in the preparation of agar media undermines microorganism cultivability.,” *Appl. Environ. Microbiol.*, vol. 80, no. 24, pp. 7659–66, Dec. 2014.

[96] T. L. Hartman, “The Use of Sudan Black B as a Bacterial Fat Stain,” *Stain Technol.*, Jul. 2009.

[97] C. T. Evans, C. Ratledge, and S. C. Gilbert, “A rapid screening method for lipid-accumulating yeast using a replica-printing technique,” *J. Microbiol. Methods*, vol. 4, no. 3–4, pp. 203–210, 1985.

[98] P. Greenspan, E. P. Mayer, and S. D. Fowler, “Nile red: a selective fluorescent stain for intracellular lipid droplets.,” *J. Cell Biol.*, vol. 100, no. 3, pp. 965–73, Mar. 1985.

[99] P. Greenspan and S. D. Fowler, “Spectrofluorometric studies of the lipid probe, nile red.,” *J. Lipid Res.*, vol. 26, no. 7, pp. 781–789, 1985.

[100] K. E. Cooksey, J. B. Guckert, S. A. Williams, and P. R. Callis, “Fluorometric determination of the neutral lipid content of microalgal cells using Nile Red,” *J. Microbiol. Methods*, vol. 6, no. 6, pp. 333–345, Sep. 1987.

[101] K. Kimura, M. Yamaoka, and Y. Kamisaka, “Rapid estimation of lipids in oleaginous fungi and yeasts using Nile red fluorescence.,” *J. Microbiol. Methods*, vol. 56, no. 3, pp. 331–8, Mar. 2004.

[102] Y. Kamisaka, N. Noda, T. Sakai, and K. Kawasaki, “Lipid bodies and lipid body formation in an oleaginous fungus, Mortierella ramanniana var. angulispora,” *Biochim. Biophys. Acta - Mol. Cell Biol. Lipids*, vol. 1438, no. 2, pp. 185–198, May 1999.

[103] T. A. Cole, A. K. Fok, M. S. Ueno, and R. D. Allen, “Use of nile red as a rapid measure of lipid content in ciliates.,” *Eur. J. Protistol.*, vol. 25, no. 4, pp. 361–8, Jun. 1990.

[104] “A.I.M. Interview: Dr. Keith Cooksey,” *Algae Industry Magazine*, 2011. [Online]. Available: http://www.algaeindustrymagazine.com/aim-interview-dr-keith-cooksey/. [Accessed: 13-May-2016].

[105] I. R. Sitepu *et al.*, “An improved high-throughput Nile red fluorescence assay for estimating intracellular lipids in a variety of yeast species,” *J. Microbiol. Methods*, vol. 91, no. 2, pp. 321–328, 2012.

[106] M. J. Griffiths, R. P. van Hille, and S. T. L. Harrison, “Selection of direct transesterification as the preferred method for assay of fatty acid content of microalgae.,” *Lipids*, vol. 45, no. 11, pp. 1053–60, Nov. 2010.

[107] J. Folch, M. Lees, and S. G. H. Sloane, “A simple method for the isolation and purification of total lipides from animal tissues.,” *J. Biol. Chem.*, vol. 226, no. 1, pp. 497–509, May 1957.

[108] “How do I determine the concentration, yield and purity of a DNA sample?” [Online]. Available: https://www.promega.de/resources/pubhub/enotes/how-do-i-determine-the-concentration-yield-and-purity-of-a-dna-sample. [Accessed: 13-May-2016].

[109] J. Rajendhran and P. Gunasekaran, “Microbial phylogeny and diversity: Small subunit ribosomal RNA sequence analysis and beyond,” *Microbiol. Res.*, vol. 166, no. 2, pp. 99–110, 2011.

[110] “Lehrstuhl für Terrestrische Ökologie - Universität Leipzig,” *François Buscot*, 2016. [Online]. Available: http://www.uni-leipzig.de/~terroek/.

[111] V. Glumoff, O. Käppeli, A. Fiechter, and J. Reiser, “Genetic transformation of the filamentous yeast, Trichosporon cutaneum, using dominant selection markers.,” *Gene*, vol. 84, no. 2, pp. 311–8, Dec. 1989.

[112] N. E. Biolabs, “Gibson Assembly Master Mix,” *Manual*, pp. 1–16, 2012.

[113] A. Wach, A. Brachat, R. Pöhlmann, and P. Philippsen, “New heterologous modules for classical or PCR-based gene disruptions inSaccharomyces cerevisiae,” *Yeast*, vol. 10, no. 13, pp. 1793–1808, Dec. 1994.

[114] Z. Zheng, A. Hayashimoto2, Z. Li, and N. Murai, “Hygromycin Resistance Gene Cassettes for Vector Construction and Selection of Transformed Rice Protoplasts’,” *Plant Physiol*, vol. 97, pp. 832–835, 1991.

[115] Y. Gao and Y. Zhao, “Self-processing of ribozyme-flanked RNAs into guide RNAs in vitro and in vivo for CRISPR-mediated genome editing,” *J. Integr. Plant Biol.*, vol. 56, no. 4, pp. 343–349, 2014.

[116] J. Berman and P. E. Sudbery, “Candida albicans: A molecular revolution built on lessons from budding yeast,” *Nat. Rev. Genet.*, vol. 3, no. 12, pp. 918–932, Dec. 2002.

[117] S. Das, J. C. Noe, S. Paik, and T. Kitten, “An improved arbitrary primed PCR method for rapid characterization of transposon insertion sites,” *J. Microbiol. Methods*, vol. 63, no. 1, pp. 89–94, Oct. 2005.

[118] E. V. Minikel, “Arbitrarily Primed Pcr,” 2014. [Online]. Available: http://www.cureffi.org/media/2014/10/arbitrarily-primed-pcr.png. [Accessed: 17-Feb-2017].

[119] F. Winston, “EMS and UV Mutagenesis in Yeast,” in *Current Protocols in Molecular Biology*, no. SUPPL. 82, F. M. Ausubel, R. Brent, R. E. Kingston, D. D. Moore, J. G. Seidman, J. A. Smith, and K. Struhl, Eds. Hoboken, NJ, USA: John Wiley & Sons, Inc, 2001, pp. 1–5.

[120] “How to use chemical mutagens for mutagenesis. Hirokazu Inoue Background During the 1970s, de Serres and his colleagues (Brockman,” *Mutagenesis*, pp. 1970–1972, 1988.

[121] G. Barth *et al.*, “Physiology and genetics of the dimorphic fungus *Yarrowia lipolytica*,” *FEMS Microbiol. Rev.*, vol. 19, no. 4, pp. 219–237, Apr. 1997.

[122] M. Kahm, G. Hasenbrink, H. Lichtenberg-frate, J. Ludwig, and M. Kschischo, “Grofit: Fitting biological growth curves,” *J. Stat. Softw.*, vol. 33, no. 7, pp. 1–21, 2010.

[123] “JGI MycoCosm Trichosporon oleaginosus Genome.” [Online]. Available: http://genome.jgi.doe.gov/Triol1/Triol1.home.html. [Accessed: 11-May-2016].

[124] B. J. Haas *et al.*, “De novo transcript sequence reconstruction from RNA-seq using the Trinity platform for reference generation and analysis.,” *Nat. Protoc.*, vol. 8, no. 8, pp. 1494–512, Aug. 2013.

[125] “Notepad++.” [Online]. Available: https://notepad-plus-plus.org/. [Accessed: 11-May-2016].

[126] “Correspondence Analysis of Codon Usage.” [Online]. Available: http://codonw.sourceforge.net/. [Accessed: 11-May-2016].

[127] Y. Nakamura, T. Gojobori, and T. Ikemura, “Codon usage tabulated from international DNA sequence databases: status for the year 2000.,” *Nucleic Acids Res.*, vol. 28, no. 1, p. 292, Jan. 2000.

[128] G. Wu, D. E. Culley, and W. Zhang, “Predicted highly expressed genes in the genomes of Streptomyces coelicolor and Streptomyces avermitilis and the implications for their metabolism.,” *Microbiology*, vol. 151, no. Pt 7, pp. 2175–87, Jul. 2005.

[129] P. Puigbò, I. G. Bravo, and S. Garcia-Vallve, “CAIcal: a combined set of tools to assess codon usage adaptation.,” *Biol. Direct*, vol. 3, p. 38, Jan. 2008.

[130] O. Zaragoza and J. M. Gancedo, “Pseudohyphal growth is induced in Saccharomyces cerevisiae by a combination of stress and cAMP signalling.,” *Antonie Van Leeuwenhoek*, vol. 78, no. 2, pp. 187–94, Aug. 2000.

[131] B. Aricha *et al.*, “Differences in membrane fluidity and fatty acid composition between phenotypic variants of Streptococcus pneumoniae.,” *J. Bacteriol.*, vol. 186, no. 14, pp. 4638–44, Jul. 2004.

[132] H. Guillou, D. Zadravec, P. G. P. Martin, and A. Jacobsson, “The key roles of elongases and desaturases in mammalian fatty acid metabolism: Insights from transgenic mice,” *Prog. Lipid Res.*, vol. 49, no. 2, pp. 186–199, 2010.

[133] L. Aymé, S. Baud, B. Dubreucq, F. Joffre, and T. Chardot, “Function and Localization of the Arabidopsis thaliana Diacylglycerol Acyltransferase DGAT2 Expressed in Yeast,” *PLoS One*, vol. 9, no. 3, p. e92237, Mar. 2014.

[134] D. Lamers *et al.*, “Selection of oleaginous yeasts for fatty acid production.,” *BMC Biotechnol.*, vol. 16, no. 1, p. 45, May 2016.

[135] S. Papanikolaou and G. Aggelis, “Yarrowia lipolytica: A model microorganism used for the production of tailor-made lipids,” *Eur. J. Lipid Sci. Technol.*, vol. 112, no. 6, pp. 639–654, Apr. 2010.

[136] H. Takeda, “Classification of Chlorella strains by cell wall sugar composition,” *Phytochemistry*, vol. 27, no. 12, pp. 3823–3826, 1988.

[137] R. Ptacnik, T. Andersen, and T. Tamminen, “Performance of the Redfield Ratio and a Family of Nutrient Limitation Indicators as Thresholds for Phytoplankton N vs. P Limitation,” *Ecosystems*, vol. 13, no. 8, pp. 1201–1214, Dec. 2010.

[138] L. Mezger-Freed, “Effect of Ploidy and Mutagens on Bromodeoxyuridine Resistance in Haploid and Diploid Frog Cells,” *Nat. New Biol.*, vol. 235, no. 60, pp. 245–246, Feb. 1972.

[139] X. Bin Zhang and Y. Ohta, “Binding of Mutagens by Fractions of the Cell Wall Skeleton of Lactic Acid Bacteria on Mutagens,” *J. Dairy Sci.*, vol. 74, no. 5, pp. 1477–1481, May 1991.

[140] J. Haigh, “The accumulation of deleterious genes in a population—Muller’s Ratchet,” *Theor. Popul. Biol.*, vol. 14, no. 2, pp. 251–267, Oct. 1978.

[141] M. F. Montero, M. Aristizábal, and G. García Reina, “Isolation of high-lipid content strains of the marine microalga Tetraselmis suecica for biodiesel production by flow cytometry and single-cell sorting,” *J. Appl. Phycol.*, vol. 23, no. 6, pp. 1053–1057, 2011.

[142] M. Terashima, E. S. Freeman, R. E. Jinkerson, and M. C. Jonikas, “A fluorescence-activated cell sorting-based strategy for rapid isolation of high-lipid Chlamydomonas mutants.,” *Plant J.*, vol. 81, no. 1, pp. 147–59, Jan. 2015.

[143] B. Xie *et al.*, “High-throughput fluorescence-activated cell sorting for lipid hyperaccumulating Chlamydomonas reinhardtii mutants.,” *Plant Biotechnol. J.*, vol. 12, no. 7, pp. 872–82, Sep. 2014.

[144] D. K. Y. Lim, H. Schuhmann, K. Sharma, and P. M. Schenk, “Isolation of High-Lipid Tetraselmis suecica Strains Following Repeated UV-C Mutagenesis, FACS, and High-Throughput Growth Selection,” *BioEnergy Res.*, vol. 8, no. 2, pp. 750–759, Nov. 2014.

[145] L. Liu, A. Pan, C. Spofford, N. Zhou, and H. S. Alper, “An evolutionary metabolic engineering approach for enhancing lipogenesis in Yarrowia lipolytica,” *Metab. Eng.*, vol. 29, pp. 36–45, 2015.

[146] T. Braunwald *et al.*, “Effect of different C/N ratios on carotenoid and lipid production by Rhodotorula glutinis,” *Appl. Microbiol. Biotechnol.*, vol. 97, no. 14, pp. 6581–6588, 2013.

[147] M. Hassan, P. J. Blanc, L.-M. Granger, A. Pareilleux, and G. Goma, “Influence of nitrogen and iron limitations on lipid production by Cryptococcus curvatus grown in batch and fed-batch culture,” *Process Biochem.*, vol. 31, no. 4, pp. 355–361, May 1996.

[148] C. T. Evans and C. Ratledge, “Effect of Nitrogen Source on Lipid Accumulation in Oleaginous Yeasts,” *J. Gen. Microbiol.*, vol. 130, pp. 1693–1704, 1984.

[149] C. Ratledge, “The role of malic enzyme as the provider of NADPH in oleaginous microorganisms: A reappraisal and unsolved problems,” *Biotechnol. Lett.*, vol. 36, no. 8, pp. 1557–1568, 2014.

[150] I. A. Calvo *et al.*, “Genome-wide screen of genes required for caffeine tolerance in fission yeast.,” *PLoS One*, vol. 4, no. 8, p. e6619, Jan. 2009.

[151] S. Mukaida, T. Ogawa, K. Ohishi, Y. Tanizawa, D. Ohta, and M. Arita, “The effect of rapamycin on biodiesel-producing protist Euglena gracilis,” *Biosci. Biotechnol. Biochem.*, vol. 80, no. 6, pp. 1223–1229, Jun. 2016.

[152] J. Rumin *et al.*, “The use of fluorescent Nile red and BODIPY for lipid measurement in microalgae.,” *Biotechnol. Biofuels*, vol. 8, p. 42, 2015.

[153] J. B. Madeira, C. A. Masuda, C. M. Maya-Monteiro, G. S. Matos, M. Montero-Lomelí, and B. L. Bozaquel-Morais, “TORC1 inhibition induces lipid droplet replenishment in yeast.,” *Mol. Cell. Biol.*, vol. 35, no. 4, pp. 737–46, 2015.

[154] N. F. Brown, M. Stefanovic-Racic, I. J. Sipula, and G. Perdomo, “The mammalian target of rapamycin regulates lipid metabolism in primary cultures of rat hepatocytes,” *Metabolism.*, vol. 56, no. 11, pp. 1500–1507, 2007.

[155] F. J. Richards, “A Flexible Growth Function for Empirical Use,” *J. Exp. Bot.*, vol. 10, no. 2, pp. 290–301, 1959.

[156] K. Hedbacker and M. Carlson, “SNF1/AMPK pathways in yeast.,” *Front. Biosci.*, vol. 13, pp. 2408–20, 2008.

[157] M. Zhang, L. Galdieri, and A. Vancura, “The yeast AMPK homolog SNF1 regulates acetyl coenzyme A homeostasis and histone acetylation.,” *Mol. Cell. Biol.*, vol. 33, no. 23, pp. 4701–4717, 2013.

[158] R. Wang and B. Levine, “Autophagy in cellular growth control,” *FEBS Lett.*, vol. 584, no. 7, pp. 1417–1426, 2010.

[159] J. Huang and D. M. Brendan, “The TSC1–TSC2 complex: a molecular switchboard controlling cell growth,” *Biochem. J.*, vol. 290, no. 5497, pp. 1717–1721, 2009.

[160] E. Jacinto, “What controls TOR?,” *IUBMB Life*, vol. 60, no. 8, pp. 483–496, 2008.

[161] J. Choi, J. Chen, S. L. Schreiber, and J. Clardy, “Structure of the FKBP12-rapamycin complex interacting with the binding domain of human FRAP.,” *Science*, vol. 273, no. 5272, pp. 239–42, Jul. 1996.

[162] N. Chantaravisoot and F. Tamanoi, “mTOR Signaling and Human Cancer,” in *Structure, Function and Regulation of TOR complexes from Yeasts to Mammals Part B*, vol. 28, no. 10, Cambridge: Academic Press, 2010, pp. 301–316.

[163] N. Cybulski and M. N. Hall, “TOR complex 2: a signaling pathway of its own,” *Trends Biochem. Sci.*, vol. 34, no. 12, pp. 620–627, 2009.

[164] L. Zhang, N. Liu, X. Ma, and L. Jiang, “The transcriptional control machinery as well as the cell wall integrity and its regulation are involved in the detoxification of the organic solvent dimethyl sulfoxide in *Saccharomyces cerevisiae*,” *FEMS Yeast Res.*, vol. 13, no. 2, pp. 200–218, Mar. 2013.

[165] Y. Chen and D. J. Klionsky, “The regulation of autophagy - unanswered questions.,” *J. Cell Sci.*, vol. 124, no. Pt 2, pp. 161–170, 2011.

[166] D. Laor, A. Cohen, M. Kupiec, and R. Weisman, “TORC1 Regulates Developmental Responses to Nitrogen Stress via Regulation of the GATA Transcription Factor Gaf1,” *MBio*, vol. 6, no. 4, pp. e00959-15, Sep. 2015.

[167] M. Yanagida, N. Ikai, M. Shimanuki, and K. Sajiki, “Nutrient limitations alter cell division control and chromosome segregation through growth-related kinases and phosphatases.,” *Philos. Trans. R. Soc. Lond. B. Biol. Sci.*, vol. 366, no. 1584, pp. 3508–20, Dec. 2011.

[168] T. Matsuo, Y. Otsubo, J. Urano, F. Tamanoi, and M. Yamamoto, “Loss of the TOR Kinase Tor2 Mimics Nitrogen Starvation and Activates the Sexual Development Pathway in Fission Yeast,” *Mol. Cell. Biol.*, vol. 27, no. 8, pp. 3154–3164, 2007.

[169] R. Weisman, A. Cohen, and S. M. Gasser, “TORC2--a new player in genome stability,” *EMBO Mol. Med.*, vol. 6, no. 8, pp. 995–1002, Aug. 2014.

[170] N. Ikai, N. Nakazawa, T. Hayashi, and M. Yanagida, “The reverse, but coordinated, roles

of Tor2 (TORC1) and Tor1 (TORC2) kinases for growth, cell cycle and separase-mediated mitosis in Schizosaccharomyces pombe.," *Open Biol.*, vol. 1, no. 3, p. 110007, 2011.

[171] A. Pic *et al.*, "The forkhead protein Fkh2 is a component of the yeast cell cycle transcription factor SFF," *EMBO J.*, vol. 19, no. 14, pp. 3750–3761, Jul. 2000.

[172] P. C. Hollenhorst, M. E. Bose, M. R. Mielke, U. Müller, and C. A. Fox, "Forkhead genes in transcriptional silencing, cell morphology and the cell cycle: Overlapping and distinct functions for FKH1 and FKH2 in Saccharomyces cerevisiae," *Genetics*, vol. 154, no. 4, pp. 1533–1548, 2000.

[173] W. Du, G. M. Forte, D. Smith, and J. Petersen, "Phosphorylation of the amino-terminus of the AGC kinase Gad8 prevents its interaction with TORC2," *Open Biol.*, vol. 6, no. 3, p. 150189, Mar. 2016.

[174] H. Lee, A. Khanal Lamichhane, H. M. Garraffo, K. J. Kwon-Chung, and Y. C. Chang, "Involvement of PDK1, PKC and TOR signalling pathways in basal fluconazole tolerance in Cryptococcus neoformans.," *Mol. Microbiol.*, vol. 84, no. 1, pp. 130–46, Apr. 2012.

[175] C. Gaubitz *et al.*, "Molecular Basis of the Rapamycin Insensitivity of Target Of Rapamycin Complex 2," *Mol. Cell*, vol. 58, no. 6, pp. 977–988, 2015.

[176] D. D. Sarbassov *et al.*, "Prolonged Rapamycin Treatment Inhibits mTORC2 Assembly and Akt/PKB," *Mol. Cell*, vol. 22, no. 2, pp. 159–168, Apr. 2006.

[177] U. Roymondal, S. Das, and S. Sahoo, "Predicting gene expression level from relative codon usage bias: an application to Escherichia coli genome.," *DNA Res.*, vol. 16, no. 1, pp. 13–30, Feb. 2009.

[178] M. Allert, J. C. Cox, and H. W. Hellinga, "Multifactorial determinants of protein expression in prokaryotic open reading frames.," *J. Mol. Biol.*, vol. 402, no. 5, pp. 905–18, Oct. 2010.

[179] "Structural Genomics Resource." [Online]. Available: http://www.ysbl.york.ac.uk/sgTarget/help_selection.html. [Accessed: 13-May-2016].

[180] B. Chen *et al.*, "Two types of soybean diacylglycerol acyltransferases are differentially involved in triacylglycerol biosynthesis and response to environmental stresses and hormones," *Sci. Rep.*, vol. 6, p. 28541, Jun. 2016.

[181] Y. Kamisaka, N. Tomita, K. Kimura, K. Kainou, and H. Uemura, "DGA1 (diacylglycerol acyltransferase gene) overexpression and leucine biosynthesis significantly increase lipid accumulation in the Δsnf2 disruptant of Saccharomyces cerevisiae," *Biochem. J.*, vol. 408, no. 1, pp. 61–68, 2007.

[182] A. Beopoulos, R. Haddouche, P. Kabran, T. Dulermo, T. Chardot, and J. M. Nicaud, "Identification and characterization of DGA2, an acyltransferase of the DGAT1 acyl-CoA:diacylglycerol acyltransferase family in the oleaginous yeast Yarrowia lipolytica. New insights into the storage lipid metabolism of oleaginous yeasts," *Appl. Microbiol. Biotechnol.*, vol. 93, no. 4, pp. 1523–1537, 2012.

[183] A. M. Silverman, K. Qiao, P. Xu, and G. Stephanopoulos, "Functional overexpression and characterization of lipogenesis-related genes in the oleaginous yeast Yarrowia lipolytica," *Appl. Microbiol. Biotechnol.*, pp. 3781–3798, 2016.

[184] A. M. Sanghvi and Y. M. Lo, "Present and potential industrial applications of macro- and microalgae.," *Recent Pat. Food. Nutr. Agric.*, vol. 2, no. 3, pp. 187–194, 2010.

[185] P. Schlagermann, G. Göttlicher, R. Dillschneider, R. Rosello-Sastre, and C. Posten, "Composition of Algal Oil and Its Potential as Biofuel," *J. Combust.*, vol. 2012, pp. 1–14,

2012.

[186] A. I. Barros, A. L. Gonçalves, M. Simões, and J. C. M. Pires, “Harvesting techniques applied to microalgae: A review,” *Renew. Sustain. Energy Rev.*, vol. 41, pp. 1489–1500, 2015.

[187] E. Molina Grima, E.-H. Belarbi, F. G. Acién Fernández, A. Robles Medina, and Y. Chisti, “Recovery of microalgal biomass and metabolites: process options and economics,” *Biotechnol. Adv.*, vol. 20, no. 7–8, pp. 491–515, 2003.

[188] K.-Y. Show, D.-J. Lee, J.-H. Tay, T.-M. Lee, and J.-S. Chang, “Microalgal drying and cell disruption – Recent advances,” *Bioresour. Technol.*, vol. 184, pp. 258–266, 2015.

[189] A. J. Dassey and C. S. Theegala, “Harvesting economics and strategies using centrifugation for cost effective separation of microalgae cells for biodiesel applications,” *Bioresour. Technol.*, vol. 128, pp. 241–245, Jan. 2013.

[190] N. Rossignol, L. Vandanjon, P. Jaouen, and F. Quéméneur, “Membrane technology for the continuous separation microalgae/culture medium: compared performances of cross-flow microfiltration and ultrafiltration,” *Aquac. Eng.*, vol. 20, no. 3, pp. 191–208, 1999.

[191] J. Masson, E. Liberto, J. C. Beolor, H. Brevard, C. Bicchi, and P. Rubiolo, “Oxygenated heterocyclic compounds to differentiate Citrus spp. essential oils through metabolomic strategies,” *Food Chem.*, vol. 206, pp. 223–233, 2016.

[192] J. Hanotu, H. C. H. Bandulasena, and W. B. Zimmerman, “Microflotation performance for algal separation,” *Biotechnol. Bioeng.*, vol. 109, no. 7, pp. 1663–1673, Jul. 2012.

[193] A. K. Lee, D. M. Lewis, P. J. Ashman, A. K. Lee, D. M. Lewis, and P. J. Ashman, “Harvesting of marine microalgae by electroflocculation: The energetics, plant design, and economics,” *Appl. Energy*, vol. 108, no. C, pp. 45–53, 2013.

[194] S. Şirin, R. Trobajo, C. Ibanez, and J. Salvadó, “Harvesting the microalgae Phaeodactylum tricornutum with polyaluminum chloride, aluminium sulphate, chitosan and alkalinity-induced flocculation,” *J. Appl. Phycol.*, vol. 24, no. 5, pp. 1067–1080, Oct. 2012.

[195] W. Zhou *et al.*, “Filamentous fungi assisted bio-flocculation: A novel alternative technique for harvesting heterotrophic and autotrophic microalgal cells,” *Sep. Purif. Technol.*, vol. 107, pp. 158–165, 2013.

[196] L. Pérez, J. L. Salgueiro, R. Maceiras, Á. Cancela, and Á. Sánchez, “An effective method for harvesting of marine microalgae: pH induced flocculation,” *Biomass and Bioenergy*, vol. 97, pp. 20–26, 2017.

[197] B. Riaño, B. Molinuevo, and M. C. García-González, “Optimization of chitosan flocculation for microalgal-bacterial biomass harvesting via response surface methodology,” *Ecol. Eng.*, vol. 38, no. 1, pp. 110–113, 2012.

[198] Y. Shen, Y. Cui, and W. Yuan, “Flocculation Optimization of Microalga Nannochloropsis oculata,” *Appl. Biochem. Biotechnol.*, vol. 169, no. 7, pp. 2049–2063, Apr. 2013.

[199] D. Surendhiran and M. Vijay, “Exploration on bioflocculation of Nannochloropsis oculata using response surface methodology for biodiesel production.,” *ScientificWorldJournal.*, vol. 2014, p. 202659, 2014.

[200] M. J. Griffiths, R. P. van Hille, and S. T. L. Harrison, “Lipid productivity, settling potential and fatty acid profile of 11 microalgal species grown under nitrogen replete and limited conditions,” *J. Appl. Phycol.*, vol. 24, no. 5, pp. 989–1001, Oct. 2012.

[201] D. L. Sills *et al.*, “Quantitative Uncertainty Analysis of Life Cycle Assessment for Algal

Biofuel Production," *Environ. Sci. Technol.*, vol. 47, no. 2, pp. 687–694, Jan. 2013.

[202] A. Sathish and R. C. Sims, "Biodiesel from mixed culture algae via a wet lipid extraction procedure," *Bioresour. Technol.*, vol. 118, pp. 643–647, Aug. 2012.

[203] R. Plat, "Gravitational and centrifugal oil-water separators with plate pack internals," Delft University Press, 1994.

[204] D. Vandamme, I. Foubert, and K. Muylaert, "Flocculation as a low-cost method for harvesting microalgae for bulk biomass production," *Trends Biotechnol.*, vol. 31, no. 4, pp. 233–239, 2013.

[205] L. Christenson and R. Sims, "Production and harvesting of microalgae for wastewater treatment, biofuels, and bioproducts," *Biotechnol. Adv.*, vol. 29, no. 6, pp. 686–702, 2011.

[206] Huang Haiou, "Microfiltration membrane fouling in water treatment: Impact of chemical attachments," Beijing Normal University, 2006.

[207] I. Larocque, A. Mazumder, M. Proulx, D. R. Lean, and F. R. Pick, "Sedimentation of algae: relationships with biomass and size distribution," *Can. J. Fish. Aquat. Sci.*, vol. 53, no. 5, pp. 1133–1142, May 1996.

[208] D. Vandamme, "Flocculation based harvesting processes for microalgae biomass production," KU Leuven, 2013.

[209] A. Pandey, D. J. D. J. Lee, Y. Chisti, and C. R. Soccol, *Biofuels from Algae*. Newnes, 2013.

[210] M. Greger, J.-E. Tillberg, and M. Johansson, "Aluminium effects on Scenedesmus obtusiusculus with different phosphorus status. II. Growth, photosynthesis and pH," *Physiol. Plant.*, vol. 84, no. 2, pp. 202–208, Feb. 1992.

[211] D. Vandamme, I. Foubert, I. Fraeye, B. Meesschaert, and K. Muylaert, "Flocculation of Chlorella vulgaris induced by high pH: Role of magnesium and calcium and practical implications," *Bioresour. Technol.*, vol. 105, pp. 114–119, 2012.

[212] R. Henderson, S. A. Parsons, and B. Jefferson, "The impact of algal properties and pre-oxidation on solid–liquid separation of algae," *Water Res.*, vol. 42, no. 8–9, pp. 1827–1845, Apr. 2008.

[213] A. Sukenik and G. Shelef, "Algal autoflocculation: verification and proposed mechanism," *Biotechnol. Bioeng.*, vol. 26, no. 2, pp. 142–147, Feb. 1984.

[214] A. Sukenik, B. Teltch, A. W. W. Wachs, G. Shelef, I. Nir, and D. Levanon, "Effect of oxidants on microalgal flocculation," *Water Res.*, vol. 21, no. 5, pp. 533–539, May 1987.

[215] J. Chen and G. Pan, "Harmful algal blooms mitigation using clay/soil/sand modified with xanthan and calcium hydroxide," *J. Appl. Phycol.*, vol. 24, no. 5, pp. 1183–1189, Oct. 2012.

[216] M.-B. Gidas, O. Garnier, and N. K. Gidas, "Performance Of Chitosan As A PrimaryCoagulant For The Wastewater Treatment," *WIT Trans. Ecol. Environ.*, vol. 33, 1970.

[217] Separ-Chemie, "Hocheffektive Chemikalien zur industriellen Abwasserreinigung." [Online]. Available: https://www.separchemie.de/produkte/. [Accessed: 23-Feb-2017].

[218] J. Beltrán-Heredia and J. Sánchez-Martín, "Municipal wastewater treatment by modified tannin flocculant agent," *Desalination*, vol. 249, no. 1, pp. 353–358, 2009.

[219] F. Bleeke, M. Milas, D. Winckelmann, and G. Klöck, "Optimization of freshwater microalgal biomass harvest using polymeric flocculants," *Int. Aquat. Res.*, vol. 7, no. 3,

pp. 235–244, Sep. 2015.

[220] C. Schulze, J. Reinhardt, M. Wurster, J. G. Ortiz-Tena, V. Sieber, and S. Mundt, “A one-stage cultivation process for lipid- and carbohydrate-rich biomass of Scenedesmus obtusiusculus based on artificial and natural water sources,” *Bioresour. Technol.*, vol. 218, pp. 498–504, 2016.

[221] C. Schulze, M. Wetzel, J. Reinhardt, M. Schmidt, L. Felten, and S. Mundt, “Screening of microalgae for primary metabolites including β-glucans and the influence of nitrate starvation and irradiance on β-glucan production,” *J. Appl. Phycol.*, vol. 28, no. 5, pp. 2719–2725, Oct. 2016.

[222] J. Cabello, M. Morales, and S. Revah, “Dynamic photosynthetic response of the microalga Scenedesmus obtusiusculus to light intensity perturbations,” *Chem. Eng. J.*, vol. 252, pp. 104–111, 2014.

[223] T. J. Monahan, “Effects of organic phosphate on the growth and morphology of Scenedesmus obtusiusculus (Chlorophyceae),” *Phycologia*, vol. 16, no. 2, pp. 133–137, Jun. 1977.

[224] G. Das, “Aspects of metabolic development in an illuminated synchronous culture of *Scenedesmus obtusiusculus*,” *Can. J. Bot.*, vol. 51, no. 1, pp. 113–120, Jan. 1973.

[225] I. Sundberg and M. Nilshammar-Holmvall, “The Diurnal Variation in Phosphate Uptake and ATP Level in Relation to Deposition of Starch, Lipid, and Polyphosphate in Synchronized Cells of Scenedesmus,” *Zeitschrift für Pflanzenphysiologie*, vol. 76, no. 3, pp. 270–279, Sep. 1975.

[226] A. Toledo-Cervantes, M. Morales, E. Novelo, and S. Revah, “Carbon dioxide fixation and lipid storage by Scenedesmus obtusiusculus,” *Bioresour. Technol.*, vol. 130, pp. 652–658, 2013.

[227] M. Nilshammar and B. Walles, “Electron microscope studies on cell differentiation in synchronized cultures of the green alga Scenedesmus,” *Protoplasma*, vol. 79, no. 3–4, pp. 317–332, Sep. 1974.

[228] M. Nilshammar, B. Walles, and A. Kylin, “The effect of calcium deficiency on the ultrastructure of the green alga Scenedesmus,” *Zeitschrift für Pflanzenphysiologie*, vol. 66, no. 3, pp. 197–205, Feb. 1972.

[229] B. Nigam and P. Ramanathan, “Application of chitosan as a flocculant for the cultures of the green alga: Scenedesmus acutus.,” *Arch. Hydrobiol.*, vol. 88, no. 3, pp. 378–387, 1980.

[230] D.-G. Kim, “Harvest of Scenedesmus sp. with bioflocculant and reuse of culture medium for subsequent high-density cultures,” *Bioresour. Technol.*, no. 102, pp. 3163–3168, 2011.

[231] S.-L. Guo *et al.*, “Characterization of flocculating agent from the self-flocculating microalga Scenedesmus obliquus AS-6-1 for efficient biomass harvest,” *Bioresour. Technol.*, vol. 145, pp. 285–289, 2013.

[232] M. Greger and M. Johansson, “Aggregation effects due to aluminum adsorption to cell walls of the unicellular green alga Scenedesmus obtusiusculus,” *Phycol. Res.*, vol. 52, pp. 53–58, 2004.

[233] M. Castrillo, L. M. Lucas-Salas, C. Rodríguez-Gil, and D. Martínez, “High pH-induced flocculation–sedimentation and effect of supernatant reuse on growth rate and lipid productivity of Scenedesmus obliquus and Chlorella vulgaris,” *Bioresour. Technol.*, vol. 128, pp. 324–329, Jan. 2013.

[234] L. Chen, C. Wang, W. Wang, and J. Wei, “Optimal conditions of different flocculation methods for harvesting Scenedesmus sp. cultivated in an open-pond system,” *Bioresour. Technol.*, vol. 133, pp. 9–15, 2013.

[235] J. A. Gerde, L. Yao, J. Lio, Z. Wen, and T. Wang, “Microalgae flocculation: Impact of flocculant type, algae species and cell concentration,” *Algal Res.*, vol. 3, pp. 30–35, 2014.

[236] D. Vandamme, I. Foubert, B. Meesschaert, and K. Muylaert, “Flocculation of microalgae using cationic starch,” *J. Appl. Phycol.*, vol. 22, no. 4, pp. 525–530, Aug. 2010.

[237] J. Liu *et al.*, “Freshwater microalgae harvested via flocculation induced by pH decrease,” *Biotechnol. Biofuels*, vol. 6, no. 1, p. 98, 2013.

[238] F. Bleeke, G. Quante, D. Winckelmann, and G. Klöck, “Effect of voltage and electrode material on electroflocculation of Scenedesmus acuminatus,” *Bioresour. Bioprocess.*, vol. 2, no. 1, p. 36, Dec. 2015.

[239] K. V. Gorin *et al.*, “Methods coagulation/flocculation and flocculation with ballast agent for effective harvesting of microalgae,” *Bioresour. Technol.*, vol. 193, pp. 178–184, 2015.

[240] J. Morales, J. de la Noüe, and G. Picard, “Harvesting marine microalgae species by chitosan flocculation,” *Aquac. Eng.*, vol. 4, no. 4, pp. 257–270, Jan. 1985.

[241] R. Y. Stanier, R. Kunisawa, M. Mandel, and G. Cohen-Bazire, “Purification and properties of unicellular blue-green algae (order Chroococcales).,” *Bacteriol. Rev.*, vol. 35, no. 2, pp. 171–205, Jun. 1971.

[242] P. Halldal, “Ultraviolet Action Spectra of Photosynthesis and Photosynthetic Inhibition in a Green and a Red Alga,” *Physiol. Plant.*, vol. 17, no. 2, pp. 414–421, Apr. 1964.

[243] W. R. Hill, M. G. Ryon, and E. M. Schilling, “Light Limitation in a Stream Ecosystem: Responses by Primary Producers and Consumers,” *Ecology*, vol. 76, no. 4, pp. 1297–1309, Jun. 1995.

[244] M. H. Zwietering, I. Jongenburger, F. M. Rombouts, Van ’ A. K., and T. Riet, “Modeling of the Bacterial Growth Curve,” *Appl. Environ. Microbiol.*, pp. 1875–1881, 1990.

[245] Malvern, “Zeta Potential: An Introduction.” .

[246] R. J. Hunter, *Zeta potential in colloid science : principles and applications*. Academic Press, 1981.

[247] “Diagram of zeta potential and slipping plane.svg - Wikimedia Commons,” 2012. [Online]. Available: https://commons.wikimedia.org/wiki/File:Diagram_of_zeta_potential_and_slipping_plane.svg. [Accessed: 23-Feb-2017].

[248] M. Natrella, *NIST/SEMATECH Engineering Statistics Handbook | NIST*. NIST/SEMATECH, 2003.

[249] H. Scheffé, “Experiments with mixtures,” *J. R. Stat. Soc. Ser. B*, vol. 20, no. 2, pp. 344–360, 1958.

[250] M. Castrillo, L. M. M. Lucas-Salas, C. Rodríguez-Gil, and D. Martínez, “High pH-induced flocculation-sedimentation and effect of supernatant reuse on growth rate and lipid productivity of Scenedesmus obliquus and Chlorella vulgaris,” *Bioresour. Technol.*, vol. 128, pp. 324–329, 2013.

[251] R. Divakaran and V. N. Sivasankara Pillai, “Flocculation of algae using chitosan,” *J. Appl. Phycol.*, vol. 14, no. 5, pp. 419–422, 2002.

[252] S. Fierro, M. del Pilar Sánchez-Saavedra, and C. Copalcúa, “Nitrate and phosphate removal by chitosan immobilized Scenedesmus,” *Bioresour. Technol.*, vol. 99, no. 5, pp. 1274–1279, Mar. 2008.

[253] J. Lee, D.-H. Cho, R. Ramanan, B.-H. Kim, H.-M. Oh, and H.-S. Kim, “Microalgae-associated bacteria play a key role in the flocculation of Chlorella vulgaris,” *Bioresour. Technol.*, vol. 131, pp. 195–201, Mar. 2013.

[254] R. K. Henderson, S. A. Parsons, and B. Jefferson, “Successful Removal of Algae through the Control of Zeta Potential,” *Sep. Sci. Technol.*, vol. 43, no. 7, pp. 1653–1666, May 2008.

[255] N. J. Moon, E. G. Hammond, and B. A. Glatz, “Conversion of Cheese Whey and Whey Permeate to Oil and Single-Cell Protein,” *J. Dairy Sci.*, vol. 61, no. 11, pp. 1537–1547, Nov. 1978.

[256] M. Hassan, P. J. Blanc, A. Pareilleux, and G. Goma, “Production of cocoa butter equivalents from prickly-pear juice fermentation by an unsaturated fatty acid auxotroph of Cryptococcus curvatus grown in batch culture,” *Process Biochem.*, vol. 30, no. 7, pp. 629–634, Jan. 1995.

[257] H.-J. Daniel, M. Reuss, and C. Syldatk, “Production of sophorolipids in high concentration from deproteinized whey and rapeseed oil in a two stage fed batch process using Candida bombicola ATCC 22214 and Cryptococcus curvatus ATCC 20509,” *Biotechnol. Lett.*, vol. 20, no. 12, pp. 1153–1156, 1998.

[258] Z. Gong, H. Shen, Q. Wang, X. Yang, H. Xie, and Z. K. Zhao, “Efficient conversion of biomass into lipids by using the simultaneous saccharification and enhanced lipid production process,” *Biotechnol. Biofuels*, vol. 6, no. 1, p. 36, 2013.

[259] A. Meo, X. L. Priebe, and D. Weuster-Botz, “Lipid production with Trichosporon oleaginosus in a membrane bioreactor using microalgae hydrolysate,” *J. Biotechnol.*, vol. 241, pp. 1–10, Jan. 2017.

[260] M. Hassan, P. Blanc, L.-M. Granger, A. Pareilleux, and G. Goma, “Lipid production by an unsaturated fatty acid auxotroph of the oleaginous yeast Apiotrichum curvatum grown in single-stage continuous culture,” *Appl. Microbiol. Biotechnol.*, vol. 40, no. 4, pp. 483–488, Dec. 1993.

5 List of Figures

6 List of Tables

7 List of Supplementary Materials

Supplemental

Supplemental 1: Summary of reported batch and fed-batch fermentations of C. oleaginosus. Cultivation modes include Batch, fed-batch, flask, simultaneous saccharification and fermentation (SSF) as well as a membrane bioreactor approach. If not stated differently, lipid accumulation is induced via nitrogen limitation. Aeration is given in volume air per volume culture per hour if not stated differently. In some cases, aeration was adjusted by setting oxygen concentration in the culture over a threshold value (>10%, >20%). Biomass (CX) and lipid concentration (CL) are given in g/l and lipid content (YLX) is given in g/l/h. LA shows the method of lipid quantification (Fatty acid extraction and GC analysis (f) or total gravimetric lipid analysis (G)). Substrate yield YLS is shown in gram lipid per 100 g sugar.

				C:N	**T**	**O_2**	**pH**	**V**	**C_L**	**Y_{LX}**		**C_X**	**Y_{LS}**	**Y_L**	**C_t**
Year	**Author**	**Mode**	**Substrate**	**g/g**	**°C**	**v/v/h**		**l**	**g/l**	**% g/g**	**LA**	**g/l**	**g/100 g substrate**	**g/l/h**	**h**
1978	Moon[72]	Batch	Whey (Lactose)	nd	30	15	5.8	10	9.3	nd	G	nd	20	0.12917	72
		Batch	Whey Permeate (Lactose)	nd	30	15	5.8	10	15.6	58.209	G	26.8	27	0.21667	72
1978	Moon[255]	Batch	Whey Permeate (Lactose)	nd	30	1	5.2-5.8	14	9.3	20	F	46.5	15	0.12917	72
1983	Evans[38]	Batch	Semi-defined (Glucose)	nd	30	1	5.5	1	33.2	33.2	F	10.2	11.9	0.36889	90
		Batch	Semi-defined (Sucrose)	nd	30	1	5.5	1	37.4	37.4	F	11.2	14.8	0.41556	90
		Batch	Semi-defined (Lactose)	nd	30	1	5.5	1	39.2	39.2	F	12.5	16.5	0.43556	90
		Batch	Semi-defined (Xylose)	nd	30	1	5.5	1	48.6	48.6	F	9.9	17.4	0.54	90
		Batch	Semi-defined (EtOH)	nd	30	1	5.5	1	30.1	30.1	F	8.5	10	0.33444	90
1988	Vega[80]	Fed-batch	Banana Juice	nd	30	1	5.2	0.5	6.18	59	G	10.32	nd	0.08583	72
		Batch	Banana Juice	nd	30	1	5.2	0.5	7.81	73.7	G	10.6	nd	0.10847	72
		Batch	Banana Juice	nd	30	1	5.2	0.5	4.14	28.5	G	14.5	nd	0.0575	72
1988	Ykema[58]	Batch	Whey Permeate (Lactose)	25	30	>10%	4.8	1	4.176	18	G	23.2	nd	0.155	27
		Batch	Whey Permeate (Lactose)	40	30	>10%	4.8	1	8.856	36	G	24.6	nd	0.199	39
		Batch	Whey Permeate (Lactose)	70	30	>10%	4.8	1	11.426	58	G	19.7	nd	0.123	93

		Fed-batch	Whey Permeate (Lactose)	40	30	>10%	4.8	1	29.75	35	G	85	nd	0.372	70
1989	Ykema[58]	Partial Recycling	Whey Permeate (Lactose)	40	30	>10%	4.8	1	30.162	33	G	91.4	nd	0.43089	70
1995	Hassan[256]	Fed-batch	Full Synthetic (Glucose) N-lim	32.4	30	>20%	5.5	1.8	3.825	22.5	F	17	12.75	0.14712	26
		Fed-batch	Full Synthetic (Glucose) Fe-lim	3.5	30	>20%	5.5	1.8	1.62	9	F	18	3	0.06231	26
1996	Meesters[45]	Fed-batch	Semi-defined (Glycerol)	20	30	1.2	5.5	0.5	29.5	25	F	118	11	0.59	50
1998	Daniel[257]	Batch	Whey Permeate (Lactose)	ng	30	ng	5.8	1.5	19.992	58.8	F	34	19.99	0.13788	145
1995	Hassan[256]	Batch	Prickly-Pear Juice	50	30	>20%	5.5	1.8	8.75	46	G	19.02	21	0.25	35
2011	Chi[42]	Fed-batch	Semi Defined (Volatile Fatty Acids)	nd	30	1	7	2	37		G	68.8	nd	0.51	72
2011	Yu[61]	Batch	Wheat straw hydrolysate	nd	28	nd	nd	0.05	5.8	33.5	F	17.2	4.7	0.03452	168
		Batch	Wheat straw hydrolysate, detoxified	nd	28	nd	nd	0.05	4.2	27.1	F	15.6	3.403	0.025	168
2012	Cui[64]	Fed-batch	Semi-defined (Glucose)	30	30.2	0.6	5.5	1	17.4	52.8875	G	32.9	36	0.06042	288
		Fed-batch	Semi-defined (Glucose)	30	30.2	0.6	6	1	21.8	48.9888	G	44.5	26	0.07569	288
2012	Christophe[62]	Fed-batch	Full Synthetic (Glucose) Phase 1	nd	30	0.5	6	4	1.67	16	G	10.46	11	0.06973	24
		Fed-batch	Full Synthetic (Acetate) Phase 2	50	30	0.5	6	4	6.89	51	G	13.5	15	0.1377	50
		Batch	Full Synthetic (Glucose)	nd	30	nd	nd	0.25	3.31	47.3	G	7	15	0.03449	96
		Batch	Full Synthetic (Acetate)	nd	30	nd	nd	0.25	0.83	27.8	G	3	19	0.00869	96
2013	Gong[258]	Flask	Corn Stover Hydrolysate	nd	30	nd	nd	0.05	6	nd	G	nd	nd	0.125	48
		Flask,SSF	Corn Stover	nd	30	nd	nd	0.05	7.2	43.4	G	16.5	nd	0.15	48
2014	Gong[49]	Flask	Corn Stover Hydrolysate	nd	30	nd	nd	0.05	12.07	43.6	G	27.7	15.6	0.14375	72
		Flask,SSF	Corn Stover	nd	30	nd	nd	0.05	14.4	nd	G	nd	15.2	0.18625	72
2014	Liang[36]	Flask	Sorghum Baghasse Hydrolysate	nd	26	nd	nd	0.04	10.8	40	G	27	14	0.075	144

2017	Meo[259]	Fed-batch	Semi-defined (Glucose)	15	30	0.1	6.5	0.01	20.4	56.7	F	35.8	11	0.28333	72
		Fed-batch	Semi-defined (Galactose)	15	30	0.1	6.5	0.01	18.6	61	F	31	13	0.25833	72
		Fed-batch	Semi-defined (Mannose)	15	30	0.1	6.5	0.01	8.9	48	F	18	9	0.12361	72
		Fed-batch	Semi-defined (Sugar Mix)	15	30	0.1	6.5	0.01	21	58	F	35.5	11	0.29167	72
		Fed-batch	Semi-defined (Glucose), P-lim	15	30	0.1	6.5	0.01	11	39.3	F	27.9	5	0.15278	72
		Partial Recycling	Semi-defined (Glucose)	15	30	2	6.5	5	16.2	52	F	31.5	31	0.42632	38
		Partial Recycling	Algae Hydrolysate	5	30	2	6.5	5	30.6	53	F	58	43	0.32553	94

Supplemental 2: Fatty Acid Mutants of C. oleaginosus described in literature.

	Ykema (1989)[83]			Ykema (1990)[84]				Hassan (1994)[260]		Görner (2016)[51]					
Strain	Sphero-plast mutant F22	Sphero-plast mutant F33	wt	wt	Ufa revertant 22.75	Ufa revertant 25.75	Ufa revertant 26.17	wt	Ufa mutant M3	wt	d9 Elongase Mutant	d12 desaturase	LA isom.	elongase desatu-rase Strain 1	elongase desatu-rase Strain 2
Medium	Glucose SD	Glucose SD	Glucose SD	Glucose SD	Glucose SD	Glucose SD	Glucose SD	Glucose SD	Glucose SD	Glucose SD	Glucose SD	Glucose SD	Glucose SD	Glucose SD	Glucose SD
C16:0	18.7	25.9	28.1	23.7	16	29.9	32.1	34	26	13.5	18.1	14.5	17.6	15	14.9
C16:1															
C18:0	21.5	20.9	13.9	16.6	42.8	26.9	38.4	10.2	36.5	1.7	2.7	2.3	3.9	1.6	2.3
C18:1	40.5	36.6	43.7	11.4	26.8	28.7	17.5	42.8	22	35.7	32.3	42.5	35.1	36.3	42.3
C18:2	8.3	7.3	9.6	7.8	6.6	7.4	6.1	7	8	46.2	27.7	19.7	39.5	11.3	2.2
C18:3				1.4	1.2	1.1	1.4	2.3	4.2	28	1.3	21.1	1.3	17	28.5
C20:2										0	16.8	0	0	9.7	0.9
C20:3										0	1	0	0	8.9	9
CLA										0	0	0	2.6	0	0
C24:0	2	3.3	1.1	1.8	1.9	1.8	1.4								

Supplemental 3: Overview of reported continuous fermentations of C. oleaginosus. Cultivation mode is continuous, except for one case of partial recycling. Descriptions apply of Supplemental 2 apply with additions: TR shows residence time in hours and dilution rate RD is given in hours^{-1}.

			C:N	**T**	**O_2**	**pH**	**V**	**C_L**	**Y_{LX}**	**LA**	**C_X**	**Y_{LS}**	**Y_L**	**T_R**	**R_D**
Year	**Author**	**Substrate**	**g/g**	**°C**	**v/v/h**		**l**	**g/l**	**% g/g**		**g/l**	**g/100g substrate**	**g/l/h**	**h**	
1983	Evans[38]	Semi-defined (Glucose)	nd	30	1	5.5	1	3.94	29	F	45	13.1	0.15	25	0.04
		Semi-defined (Sucrose)	nd	30	1	5.5	1	4.54	28	F	53	15.1	0.18	25	0.04
		Semi-defined (Lactose)	nd	30	1	5.5	1	5.6	31	F	60	18.6	0.22	25	0.04
		Semi-defined (Xylose)	nd	30	1	5.5	1	5.5	37	F	51	18.3	0.28	20	0.05
		Semi-defined (EtOH)	nd	30	1	5.5	1	4	35	F	38	13.3	0.2	20	0.05
1989	Ykema[58]	Whey Permeate (Lactose)	20	30	>10%	4.8	1	4.2	20	G	21	nd	0.29	14.3	0.07
		Whey Permeate (Lactose)	40	30	>10%	4.8	1	7.2	36	G	20	nd	0.38	18.9	0.053
1993	Hassan[260]	Semi-defined (Glucose)	38.5	30	>30%	5.5	1	22	45.6	F	48	22	0.33	20.4	0.049
2009	Zheng[79]	Semi-defined (Sucrose)	nd	30	>50%	5.5	0.5	9.2	15	F	61	7.2	0.33	27.6	0.036

Supplemental 4: Validation of automated Nile red screening. The mean relative fluorescence units (RFU) was 384011 with a standard deviation of 14630. resulting in a relative standard deviation of 3.8%. Fluorescence over the plate was normally distributed (Shapiro-Wilk: DF:48; Statistic 0.96894; p-value 0.23026).

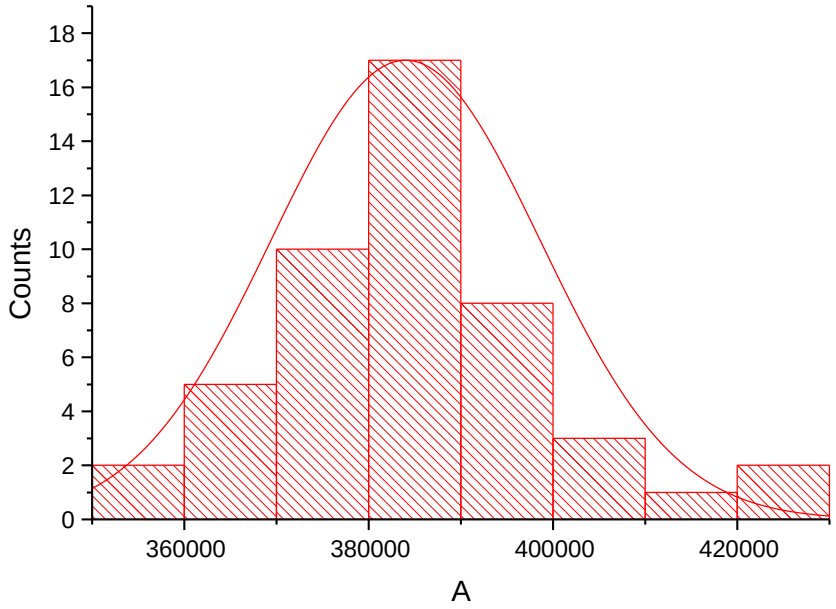

Supplemental 5: Sequences of relevant genes expressed in C. oleaginosus as shown in Table 9.

>Dga2
atggcagcctgttcttttccaagtggctgcggccgctcgccgtcatctacgccgtgtggtttatcgtcgtcgaccgcgcatggcgg
cacaagggcgggcgcaggaaggactgggtccgccgctccgccttctggcgttattttgctggtgagtgaccgcgtggtccccg
ctcacgcagactactaccccatcacgacggtcaaggaggccgacctgcctgcggaccgcaagtacgtgttcgcttatcaccc
gcacggaatcatcagcatgggcgccgcgtgcacgttcgcgaccgaggcaacgggcttctcgtccctcttccccggcgtcacct
gccatctgctaacgcttggtaagtcgcatgataccgtggctcgcgggcgacgtgggcttcggagaatcatcatggccgctgctc
acgccagacgccaacttctggatccccctctaccgcgacatcttgatgggcatgggcctcgcgtccgtcagcaagcgcagctg
ccgctcgattctcaagatggggcgcagcatctgcatcgtcatcggcggcgcctccgagtcactttacgcgtaccccggcacga
acaatctcacgctcaagaagcgcctgggcttcatcaaaatcgcgatccgcgagggcgcaaacctcgtgcccgtgtacggcttt
ggcgagaacgacatctacgagctgctgcccaacgaaaagggcacgatgacgtacaagttccagaagtggttccagggca
cgttcggcttcactgtcccattcttccacggccgcggcgtatttacctacaactacggccttatgcctcaccgccggcccgttactg
tcgtcgtgggagcgccgatccccgtcaagcagatcgaaaagcccacagacgaggaggtgcaggccgtgcacaaccagta
catcgaagcgctgcaggcgctctgggacaagcacaaggacgagtatgccaaggaccgcaagtccgagctcaagcttgtcg
cgtaggcctcggtgctcccatgccgccatctcatgtctcaacaccccatacggcccccacgttcaaccatagatgtatagagat
gtaa

>Hygromycin B Resistance
atgaaaaagcctgaactcaccgcgacgtctgtcgagaagtttctgatcgaaaagttcgacagcgtctccgacctgatgcagct
ctcggagggcgaagaatctcgtgctttcagcttcgatgtaggagggcgtggatatgtcctgcgggtaaatagctgcgccgatgg
tttctacaaagatcgttatgtttatcggcactttgcatcggccgcgctcccgattccggaagtgcttgacattggggaattcagcga
gagcctgacctattgcatctcccgccgtgcacagggtgtcacgttgcaagacctgcctgaaaccgaactgcccgctgttctgca
gccggtcgcggaggccatggatgcgatcgctgcggccgatcttagccagacgagcgggttcggcccattcggaccgcaag
gaatcggtcaatacactacatggcgtgatttcatatgcgcgattgctgatccccatgtgtatcactggcaaactgtgatggacga

caccgtcagtgcgtccgtcgcgcaggctctcgatgagctgatgctttgggccgaggactgccccgaagtccggcacctcgtgc
acgcggatttcggctccaacaatgtcctgacggacaatggccgcataacagcggtcattgactggagcgaggcgatgttcgg
ggattcccaatacgaggtcgccaacatcttcttctggaggccgtggttggcttgtatggagcagcagacgcgctacttcgagcg
gaggcatccggagcttgcaggatcgccgcggctccgggcgtatatgctccgcattggtcttgaccaactctatcagagcttggtt
gacggcaatttcgatgatgcagcttgggcgcagggtcgatgcgacgcaatcgtccgatccggagccgggactgtcgggcgt
acacaaatcgcccgcagaagcgcggccgtctggaccgatggctgtgtagaagtactcgccgatagtggaaaccgacgccc
cagcactcgtccgagggcaaaggaatagagtagatgccgaccgg

>KanMX
atgggtaaggaaaagactcacgtttcgaggccgcgattaaattccaacatggatgctgatttatatgggtataaatgggctcgc
gataatgtcgggcaatcaggtgcgacaatctatcgattgtatgggaagcccgatgcgccagagttgtttctgaaacatggcaa
aggtagcgttgccaatgatgttacagatgagatggtcagactaaactggctgacggaatttatgcctcttccgaccatcaagcat
tttatccgtactcctgatgatgcatggttactcaccactgcgatccccggcaaaacagcattccaggtattagaagaatatcctga
ttcaggtgaaaatattgttgatgcgctggcagtgttcctgcgccggttgcattcgattcctgtttgtaattgtccttttaacagcgatcg
cgtatttcgtctcgctcaggcgcaatcacgaatgaataacggtttggttgatgcgagtgattttgatgacgagcgtaatggctggc
ctgttgaacaagtctggaaagaaatgcataagcttttgccattctcaccggattcagtcgtcactcatggtgatttctcacttgataa
ccttatttttgacgaggggaaattaataggttgtattgatgttggacgagtcggaatcgcagaccgataccaggatcttgccatcc
tatggaactgcctcggtgagttttctccttcattacagaaacggctttttcaaaaatatggtattgataatcctgatatgaataaattg
cagtttcatttgatgctcgatgagtttttctaa

>Dga2
atgcggagtacggagctgcgggatgccctgtggatcctgtggatcgtgagaacagccaacgttcatcaccccgtcagtggag
gcgatcttgttcctcctcctcctcctctttctctttctctttctctctctcttctcttctcatctcttctcatctcctctcaagcgacactctcctcc
tcctctttaacatctctctctctctccctctctctctctccctctccctcactcttccacacctccacacactcgctactcctcctcaactct
gtcactgtgactcacaattccacttccgagctcatcccctccccctccctccttcgtctctcgcaatcgcatcgtgcccaacactt
aaccgtgcactagaacatcccattcactatccccccccctcccctcacatccctcccgccccaacatgtctacttccgcctcctcc
gcgtcctcgagctcgagctcgcctgggacctccccagtcaccacccactctgcactcgacagcgagccaggtactccctcgg
ggctcggcctcaatgtcaagctcgacaccttcggtggccgtatccgcagcgtcgacggccctagcccagcaccctccctcatt
actctccattcgagcctaccagccagcccagaccccacaaccccaagcacagaggaaggcgagctcgagttctcgccaga
ccccgccgaagatgctccccagatgcgtcagcgcaaggtcccctctccaaacatggccatgacaaccctcgcgaacggcg
cagccactcaaaccctcaagaagccccagaagaaattaagccgtcacaagagccccctgctggacgcgctcaagttgccc
ccgctgagcgaaatcagcattcccaggcctgtacagatcaagtgagtgcaggacgcgggcagtagatgccggccccccgg
ggcgcagtgcgatgagtcgcacggactgtgtgtcaggtccgggggaccgggcgggcatacaggcgcgggcagaggcca
agagcggctgggcaattgggcaagaaggcgtcaccatcgcgagttcaactgccgccgcgcttcggacccgacagaccgg
cgcgccctccgtcgccaacaacgtcagctgataccaggtttgcgccccttcacatcc

>YFP
atggtgagcaagggcgaggagctgttcaccggggtggtgcccatcctggtcgagctggacggcgacgtaaacggccacaa
gttcagcgtgtccggcgagggcgagggcgatgccacctacggcaagctgaccctgaagttcatctgcaccaccggcaagct
gcccgtgccctggcccaccctcgtgaccaccttcggctacggcgtgcagtgcttcgcccgctaccccgaccacatgcgccag
cacgacttcttcaagtccgccatgcccgaaggctacgtccaggagcgcaccatcttcttcaaggacgacggcaactacaaga
cccgcgccgaggtgaagttcgagggcgacaccctggtgaaccgcatcgagctgaagggcatcgacttcaaggaggacgg
caacatcctggggcacaagctggagtacaactacaacagccacaacgtctatatcatggccgacaagcagaagaacggc
atcaaggtgaacttcaagatccgccacaacatcgaggacggcagcgtgcagctcgccgaccactaccagcagaacaccc
ccatcggcgacggccccgtgctgctgcccgacaaccactacctgagctaccagtccgccctgagcaaagaccccaacgag
aagcgcgatcacatggtcctgctggagttcgtgaccgccgccgggatcactctcggcatggacgagctgtacaagtaa

Supplemental 6: Cloning strategy for pRF2_HSlc.

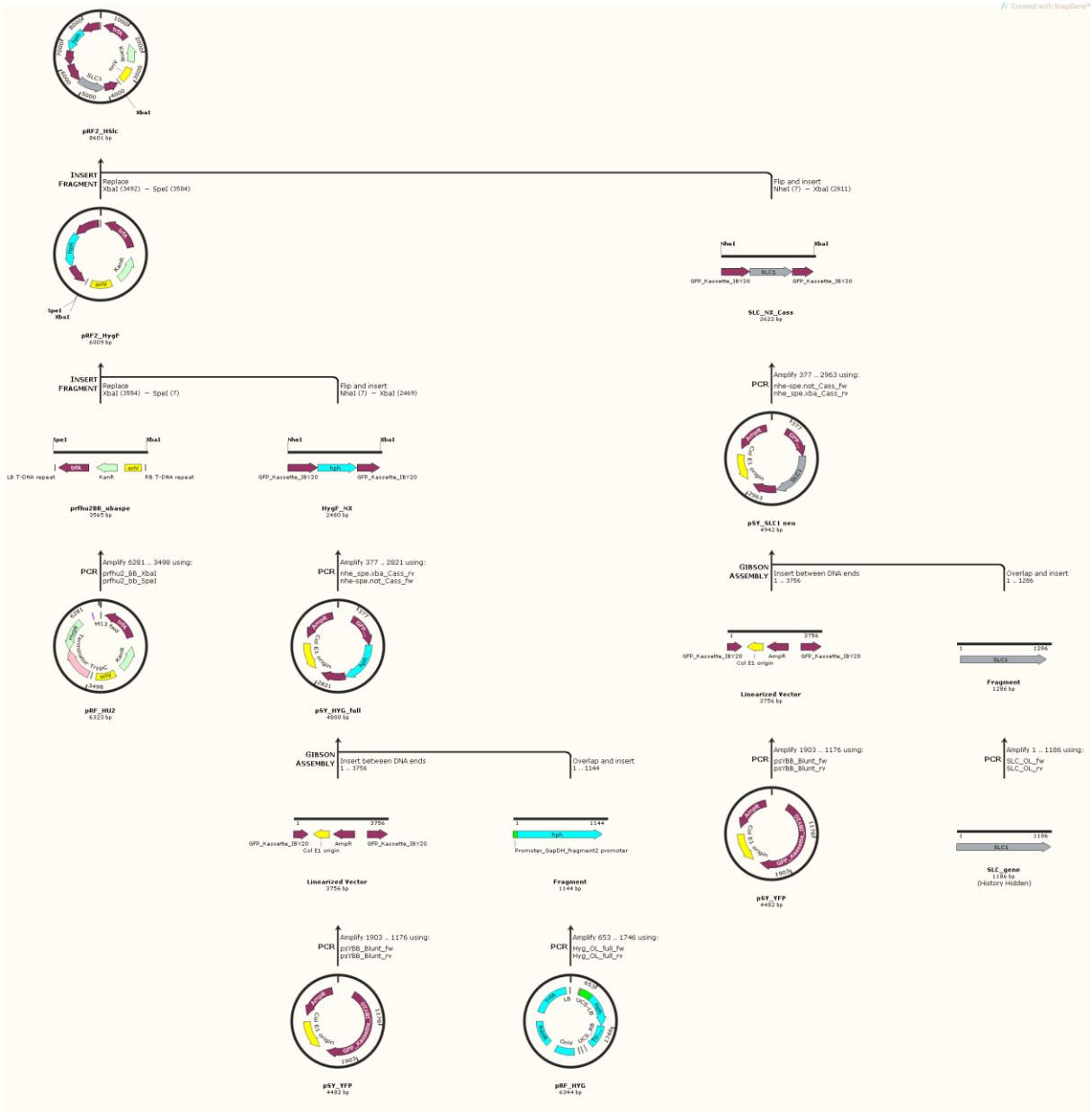

Supplemental 7: Cloning strategy for pRF2_KDga2.

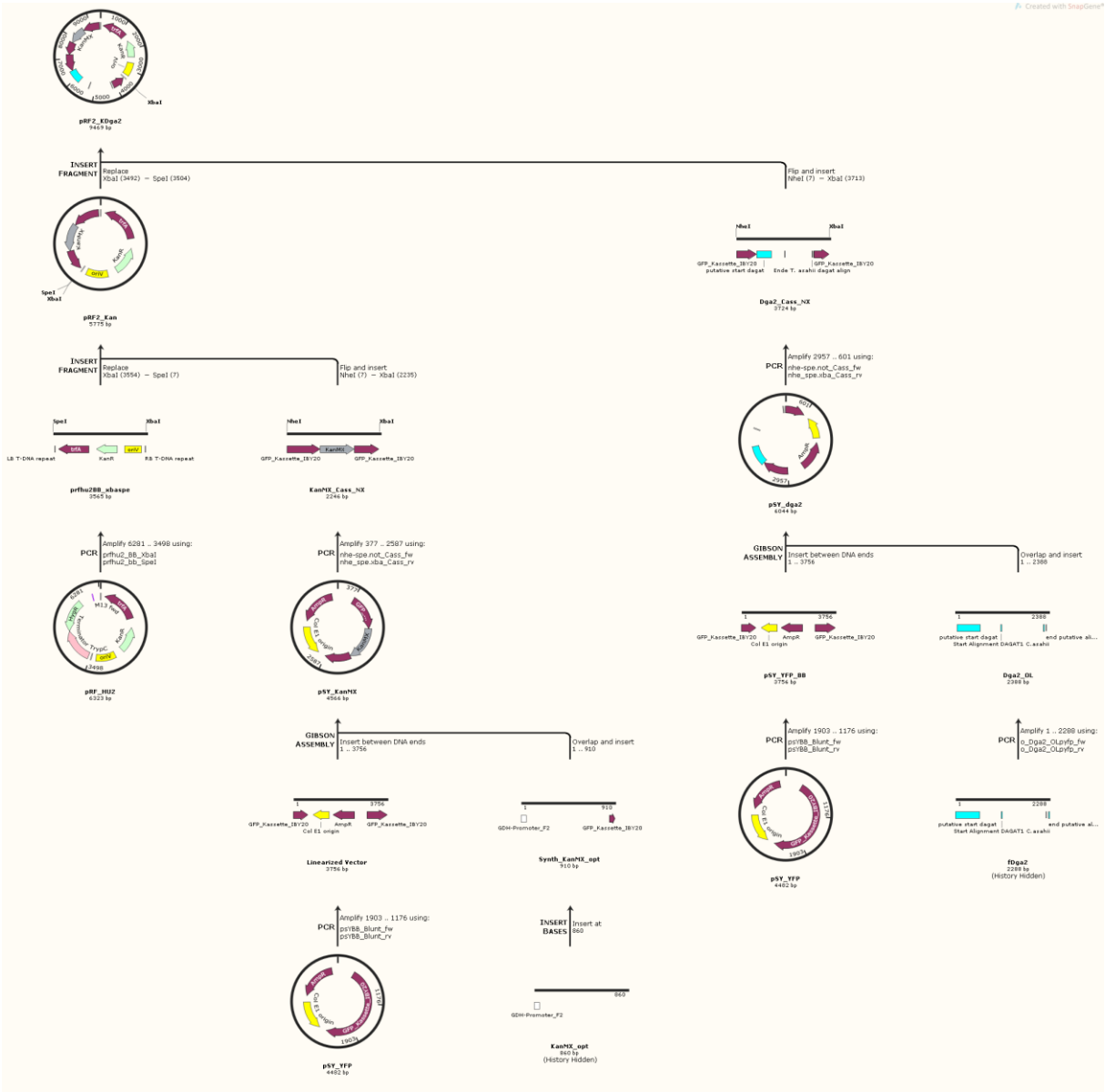

Supplemental 8: Cloning strategy for pRF_Cas_Hyg_gRNA.

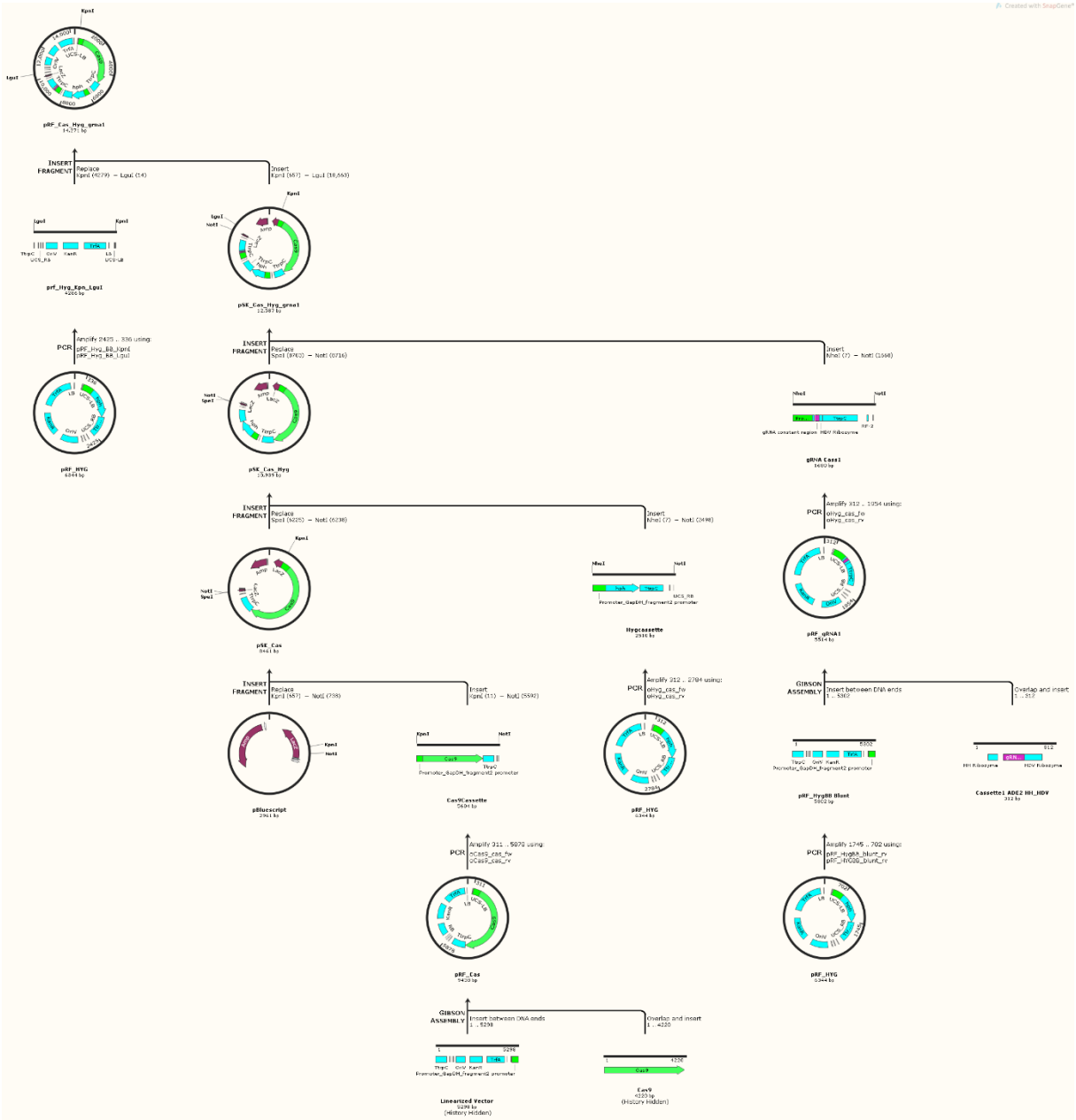

Supplemental 9: DNA sequences of gRNAs used in this work.

Color coding of sequence elements		
Promoter and terminator overlaps	Hammerhead ribozyme (HH)	Hammerhead ribozyme, crRNA binding
HDV Ribozyme (HDV)	crRNA sequence (gRNA variable region)	tracrRNA sequence (gRNA constant region)

Cassette 1: HH_Ade2_HDV

tcctcttctcaaaactattcccctcctcccaaaaatcaacttgatcaacaGCCGACCTGATGAGTCCGTGAGGAC
GAAACGAGTAAGCTCGTCGTCGGCATTCTGGGTGAGTAGGTTTTAGAGCTAGAAATAGC
AAGTTAAAATAAGGCTAGTCCGTTATCAACTTGAAAAAGTGGCACCGAGTCGGTGCTTTT
GGCCGGCATGGTCCCAGCCTCCTCGCTGGCGCCGGCTGGGCAACATGCTTCGGCATG
GCGAATGGGACgatccacttaacgttactgaaatcatcaaacagcttgacgaatctggata

Cassette 2: HH_Ura3_HDV

tcctcttctcaaaactattcccctcctcccaaaaatcaacttgatcaacaGGTCTTCTGATGAGTCCGTGAGGACG
AAACGAGTAAGCTCGTCAAGACCAACCTCTGCGTCTCGTTTTAGAGCTAGAAATAGCAA
GTTAAAATAAGGCTAGTCCGTTATCAACTTGAAAAAGTGGCACCGAGTCGGTGCTTTTG
GCCGGCATGGTCCCAGCCTCCTCGCTGGCGCCGGCTGGGCAACATGCTTCGGCATGG
CGAATGGGACgatccacttaacgttactgaaatcatcaaacagcttgacgaatctggata

Cassette 3: HH_Ura3_HH

tcctcttctcaaaactattcccctcctcccaaaaatcaacttgatcaacaGGTCTTCTGATGAGTCCGTGAGGACG
AAACGAGTAAGCTCGTCAAGACCAACCTCTGCGTCTCGTTTTAGAGCTAGAAATAGCAA
GTTAAAATAAGGCTAGTCCGTTATCAACTTGAAAAAGTGGCACCGAGTCGGTGCTTTTCT
GCTCGAATGAGCAAAGCAGGAGTGCCTGAGTAGTCAAAAGCgatccacttaacgttactgaaatcat
caaacagcttgacgaatctggata

Synthesis was done by Eurofins (Brussels).

Supplemental 10: Media components of full synthetic base medium used for media optimization.

Ratio			Media Component g/l							
C:N	C:P	C:S	Glucose	NH4Cl	MgSO4	(NH4)2SO4	K2SO4	KH2PO4	Na2HPO4	MgCl2
17.603	60.431	31.723f49176	100	0	1.25	12.5	0	7.5	0	1.25
44.008	60.431	31.72461252	100	0	1.25	5	9.89	7.5	0	1.25
110.02	60.431	31.71812531	100	0	1.25	2	13.85	7.5	0	1.25
146.69	60.431	31.71704437	100	0	1.25	1.5	14.51	7.5	0	1.25
176.03	60.431	31.71650393	100	0	1.25	1.25	14.84	7.5	0	1.25
220.04	60.431	31.7159635	100	0	1.25	1	15.17	7.5	0	1.25
7.334	906.46	31.72349176	100	14.17	1.25	12.5	0	0.5	0	1.25
7.334	4532.3	31.72349176	100	14.17	1.25	12.5	0	0.1	0	1.25
7.334	9064.6	31.72349176	100	14.17	1.25	12.5	0	0.05	0	1.25
7.334	18129	31.72349176	100	14.17	1.25	12.5	0	0.025	0	1.25
7.334	45323	31.72349176	100	14.17	1.25	12.5	0	0.01	0	1.25
7.334	60.431	801.7539964	100	24.29	0.5	0	0	7.5	0	1.84
7.334	60.431	1603.507993	100	24.29	0.25	0	0	7.5	0	2.04
7.334	60.431	4008.769982	100	24.29	0.1	0	0	7.5	0	2.16
7.334	60.431	8017.539964	100	24.29	0.05	0	0	7.5	0	2.2
7.334	60.431	16035.07993	100	24.29	0.025	0	0	7.5	0	2.22

Supplemental 11: Table of growth curve parameters obtained for media optimization, part 1.

#	TestId	1:X	used.model	Mu model	Lambda model	A model	Integral model	Stdmu model	Stdlambda model	stdA model	ci90.mu model.lo	ci90.mu model.up	ci90.lambda model.lo	ci90.lambda model.up
1	TestN	18	logistic	2.44	9.03	82.66	1837.14	0.15	1.03	3.77	2.20	2.67	7.33	10.73
2	TestN	44	gompertz	2.31	5.72	69.88	1773.70	0.09	0.54	1.55	2.16	2.46	4.83	6.62
3	TestN	110	gompertz	2.31	5.07	65.19	1760.33	0.09	0.51	1.21	2.16	2.46	4.23	5.91
4	TestN	147	gompertz	2.38	4.29	54.03	1656.71	0.13	0.62	0.96	2.17	2.60	3.28	5.31
5	TestN	176	gompertz.exp	2.05	4.67	38.72	1459.28	0.12	0.94	3.10	1.86	2.24	3.12	6.21
6	TestN	220	gompertz	1.18	1.40	34.13	1027.90	0.05	0.59	0.63	1.10	1.27	0.43	2.37
7	TestP	60	logistic	2.44	9.03	82.66	1837.14	0.15	1.03	3.77	2.20	2.67	7.33	10.73
8	TestP	906	richards	2.20	8.19	54.92	1457.19	0.11	0.68	1.30	2.03	2.38	7.08	9.31
9	TestP	4532	logistic	1.70	7.81	36.86	1076.73	0.24	1.65	1.47	1.31	2.09	5.09	10.53
10	TestP	9065	gompertz.exp	1.02	8.33	28.00	854.55	0.05	0.98	4.64	0.94	1.10	6.71	9.94
11	TestP	18129	logistic	0.63	3.92	21.50	573.47	0.03	0.83	0.55	0.58	0.68	2.56	5.27
12	TestP	45323	gompertz	0.46	2.64	25.22	472.83	0.02	0.75	1.77	0.43	0.49	1.41	3.88
13	TestS	31	logistic	2.44	9.03	82.66	1837.14	0.15	1.03	3.77	2.20	2.67	7.33	10.73
14	TestS	802	logistic	1.44	8.60	40.70	1025.89	0.06	0.65	0.84	1.34	1.55	7.53	9.67
15	TestS	1604	logistic	1.58	10.81	37.97	955.82	0.07	0.53	0.60	1.48	1.69	9.94	11.67
16	TestS	4009	logistic	1.31	7.68	29.97	861.93	0.06	0.60	0.45	1.21	1.42	6.69	8.67
17	TestS	8018	gompertz.exp	1.13	4.70	28.84	836.23	0.07	0.67	1.63	1.01	1.24	3.59	5.80
18	TestS	16035	logistic	0.57	1.39	15.86	509.90	0.04	0.93	0.31	0.52	0.63	-0.14	2.91

Supplemental 12: Table of growth curve parameters obtained for media optimization, part 2.

#	TestId	1:X	ci90.A model.lo	ci90.A model.up	ci95.mu model.lo	ci95.mu model.up	ci95.lambda model.lo	ci95.lambda model.up	ci95.A model.lo	ci95.A model.up	mu.spline	lambda.spline	A.spline	integral.spline
1	TestN	18	76.46	88.87	2.15	2.72	7.00	11.06	75.27	90.05	3.57	16.61	74.36	1842.27
2	TestN	44	67.32	72.43	2.13	2.49	4.66	6.79	66.83	72.92	2.53	6.04	66.56	1779.42
3	TestN	110	63.20	67.17	2.14	2.49	4.07	6.07	62.82	67.56	2.32	5.31	62.10	1767.82
4	TestN	147	52.45	55.61	2.13	2.64	3.09	5.50	52.14	55.91	2.37	4.26	53.04	1665.70
5	TestN	176	33.62	43.82	1.82	2.28	2.82	6.51	32.65	44.79	2.00	3.11	46.84	1461.27
6	TestN	220	33.10	35.17	1.08	1.29	0.25	2.55	32.90	35.36	1.45	2.94	33.70	1027.85
7	TestP	60	76.46	88.87	2.15	2.72	7.00	11.06	75.27	90.05	3.57	16.61	74.36	1842.27
8	TestP	906	52.78	57.07	2.00	2.41	6.86	9.52	52.37	57.48	2.24	7.94	53.87	1461.97
9	TestP	4532	34.44	39.29	1.24	2.17	4.57	11.05	33.98	39.75	1.61	7.07	40.52	1095.21
10	TestP	9065	20.37	35.63	0.93	1.12	6.41	10.25	18.91	37.09	1.16	7.02	32.68	855.23
11	TestP	18129	20.59	22.42	0.57	0.69	2.30	5.53	20.41	22.59	0.64	3.88	20.71	575.07
12	TestP	45323	22.30	28.14	0.43	0.49	1.17	4.11	21.74	28.70	0.76	22.75	19.28	471.33
13	TestS	31	76.46	88.87	2.15	2.72	7.00	11.06	75.27	90.05	3.57	16.61	74.36	1842.27
14	TestS	802	39.32	42.08	1.32	1.57	7.32	9.87	39.05	42.34	1.53	8.64	39.80	1027.16
15	TestS	1604	36.99	38.95	1.46	1.71	9.77	11.84	36.80	39.14	1.86	12.14	38.24	954.85
16	TestS	4009	29.24	30.70	1.19	1.44	6.50	8.86	29.10	30.84	1.29	7.56	29.79	865.29
17	TestS	8018	26.17	31.52	0.99	1.26	3.38	6.01	25.65	32.04	1.31	6.26	30.29	839.89
18	TestS	16035	15.34	16.37	0.50	0.64	-0.43	3.20	15.25	16.47	0.87	4.88	16.37	507.99

Supplemental 13: Growth curves as used in this work and implemented in R package grofit. Image adapted by Kahm et al[122].

Model	Formula	Parameter
Logistic	$y(t) = \frac{A}{1+\exp\left(\frac{4\mu}{A}(\lambda - t)+2\right)}$	A, μ, λ
Gompertz	$y(t) = A \cdot \exp\left[-\exp\left(\frac{\mu \cdot e}{A}(\lambda - t) + 1\right)\right]$	A, μ, λ
modified Gompertz	$y(t) = A \cdot \exp\left[-\exp\left(\frac{\mu \cdot e}{A}(\lambda - t) + 1\right)\right] + A \cdot \exp\left(\alpha(t - t_{shift})\right)$	$A, \mu, \lambda, \alpha, t_{shift}$
Richards	$y(t) = A \cdot \left[1 + \nu \cdot \exp\left(1 + \nu + \frac{\mu}{A} \cdot (1+\nu)^{1+1/\nu} \cdot (\lambda - t)\right)\right]^{(-1/\nu)}$	A, μ, λ, ν

Supplemental 14: Growth of isolates and reference strains in MNM-S at 28°C and 120 rpm at 30 ml volume in baffled flasks.

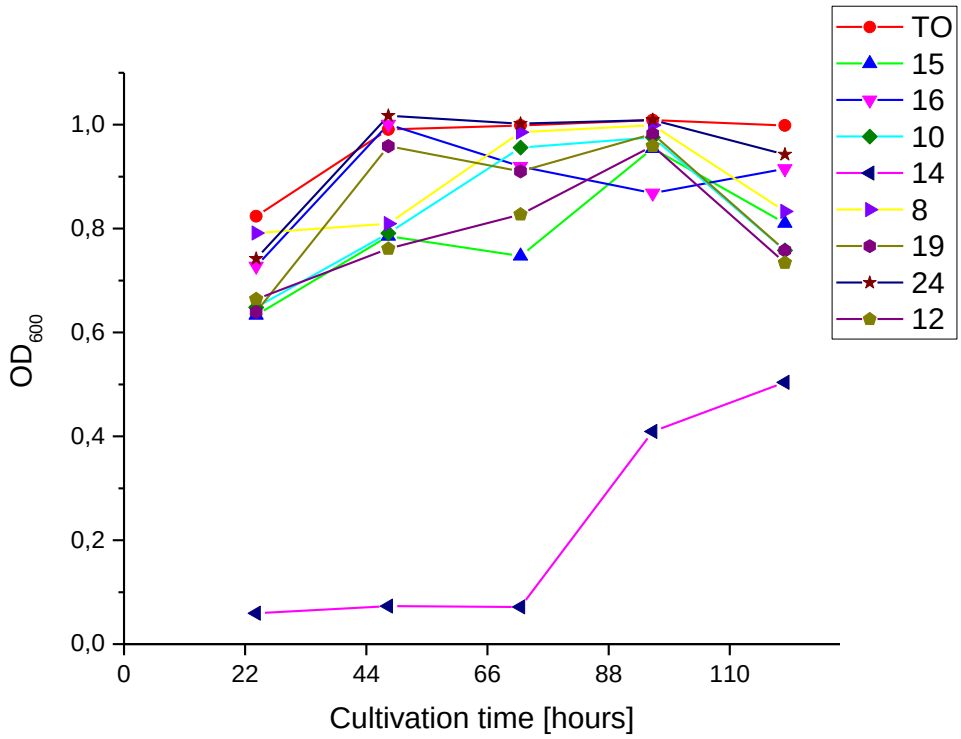

Supplemental 15: Composition of dried algae S. obtusiusculus A189 as determined by the ABV consortium.

Method	Component	Content /% g/g
60°C over night	Water	3.7
Thymol/H_2SO_4	Carbohydrate	33.8
Kjeldahl	Protein	48.7
Hexane extraction	Lipids	8.3
650°C 5h	Ash	1.9
	Pigments, secondary metabolites etc.	3.6
	Total	100.0

Supplemental 16: Result of high-throughput determination of growth: IBY Strains.

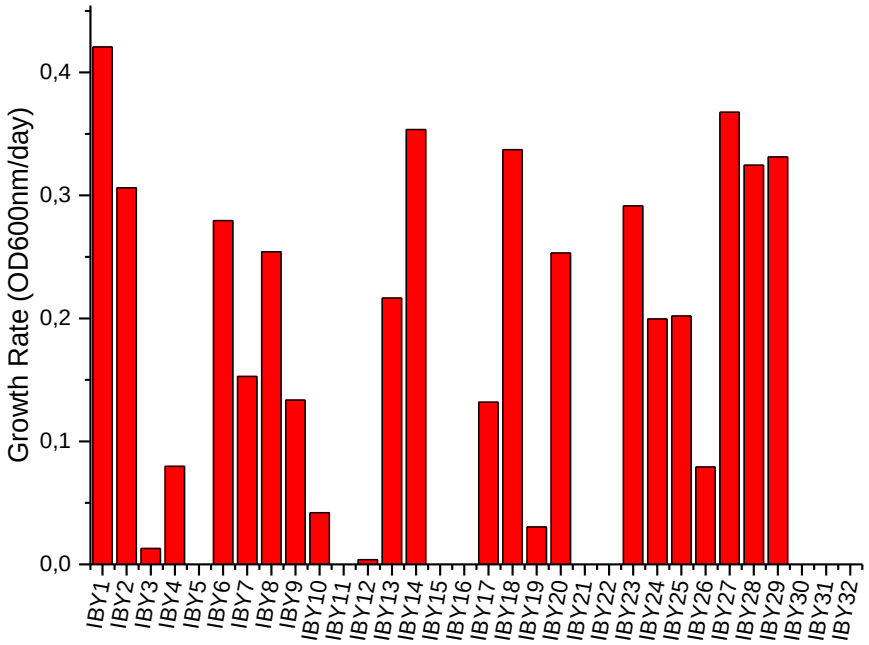

Supplemental 17: Result of high-throughput determination of growth: WO Strains.

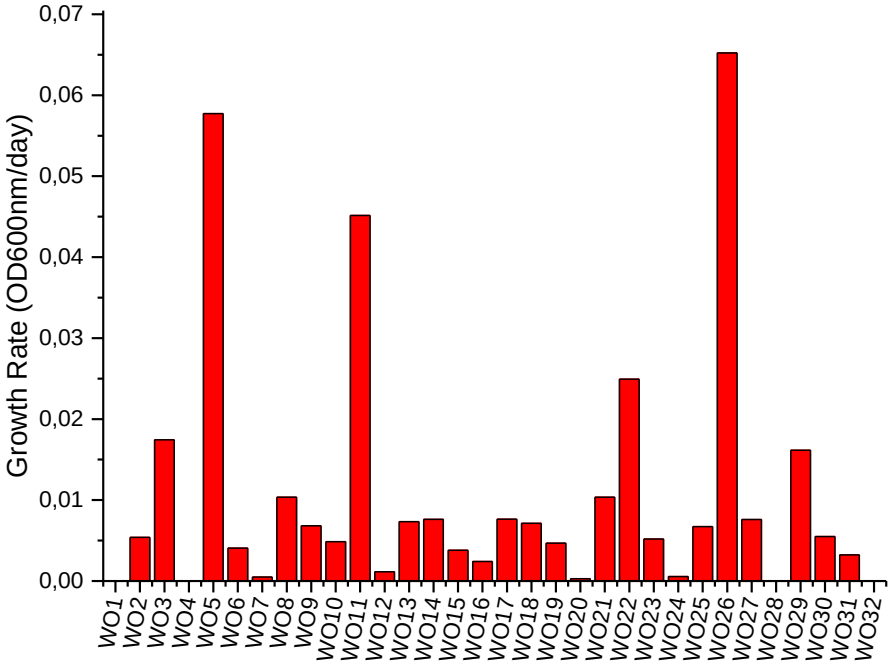

Supplemental 18: Result of high-throughput determination of growth: NZ Strains.

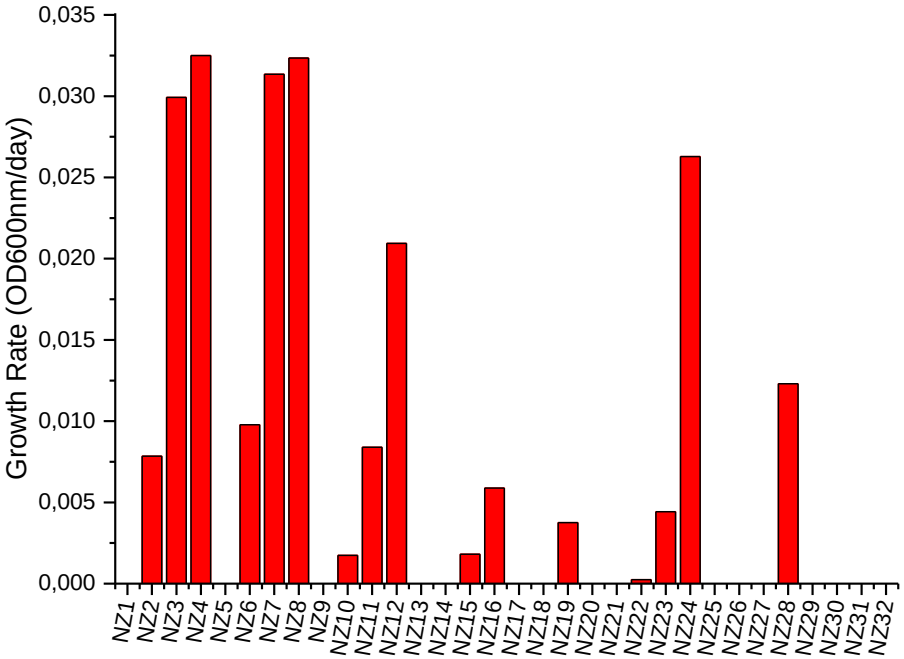

Supplemental 19: Result of high-throughput lipid estimation screen of IBY culture collection.

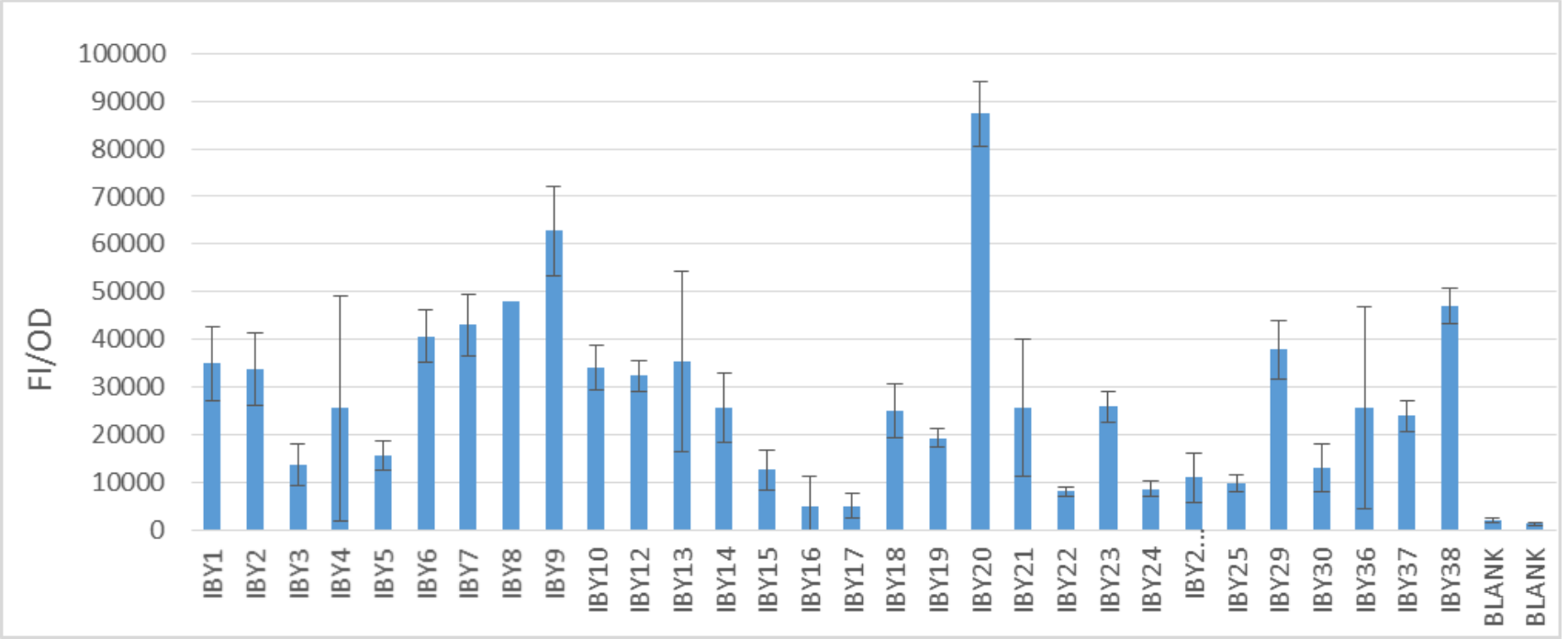

Supplemental 20: FACS protocol for selection of high and low production yeast subpopulations. Aggregates were excluded in panel 1 and 2. In panel 3, the yeast population was selected, excluding possible fragments. Panel 6 was used to observe the kinetics of staining and panel 7 contains the gates for sorting (Sorting Hi and Sorting Low).

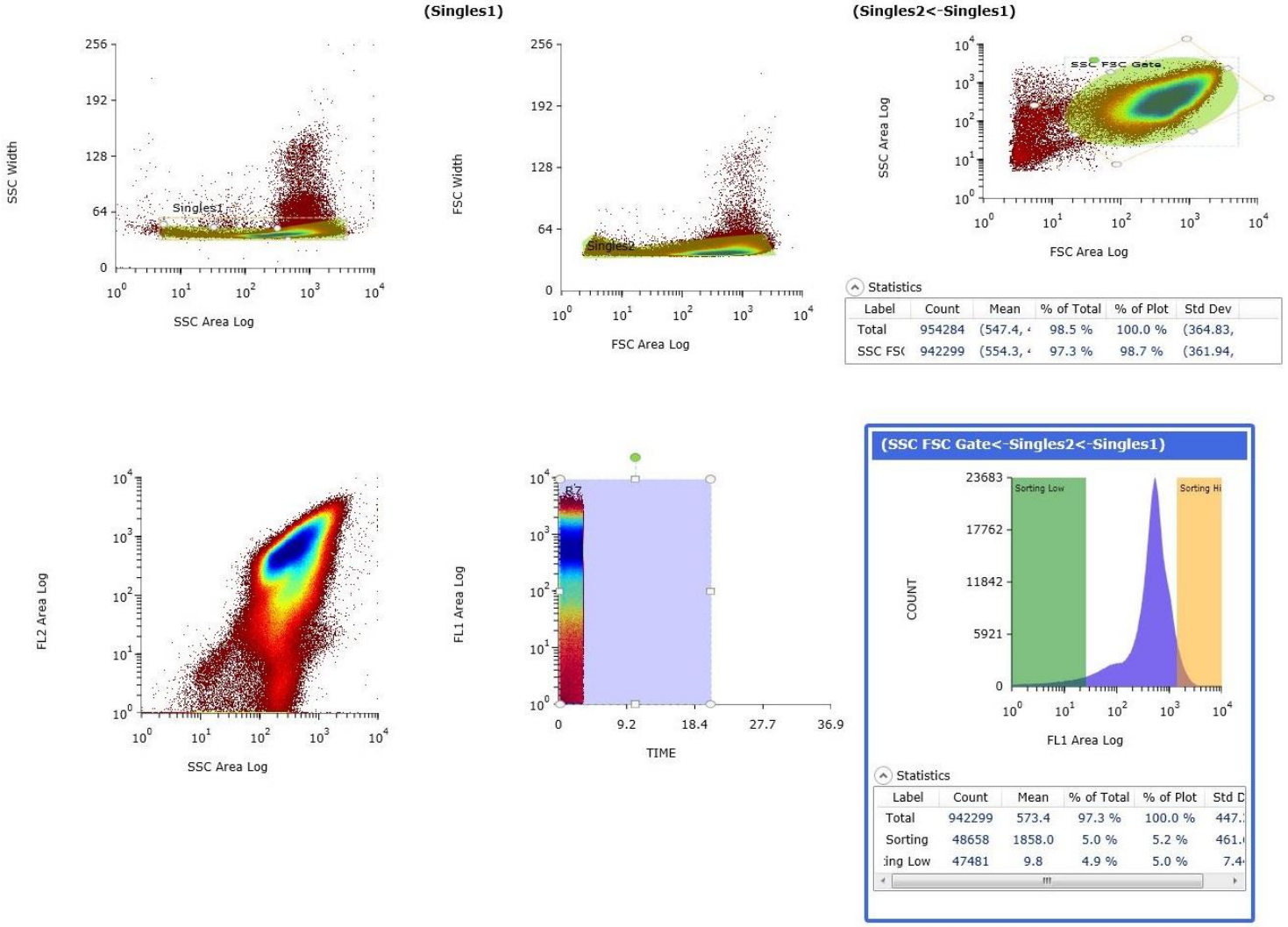

Supplemental 21: Comparison of Nile red fluorescence of cells grown in YPD and MNM-S after staining as described in section 2.3.3.3. For measurement in the plate reader (see upper picture), the factor between low and high lipid C. oleaginosus *is 47725.6/15011.75=3.18, whereas for FACS (lower picture) it is 604.4/189.4=3.19.*

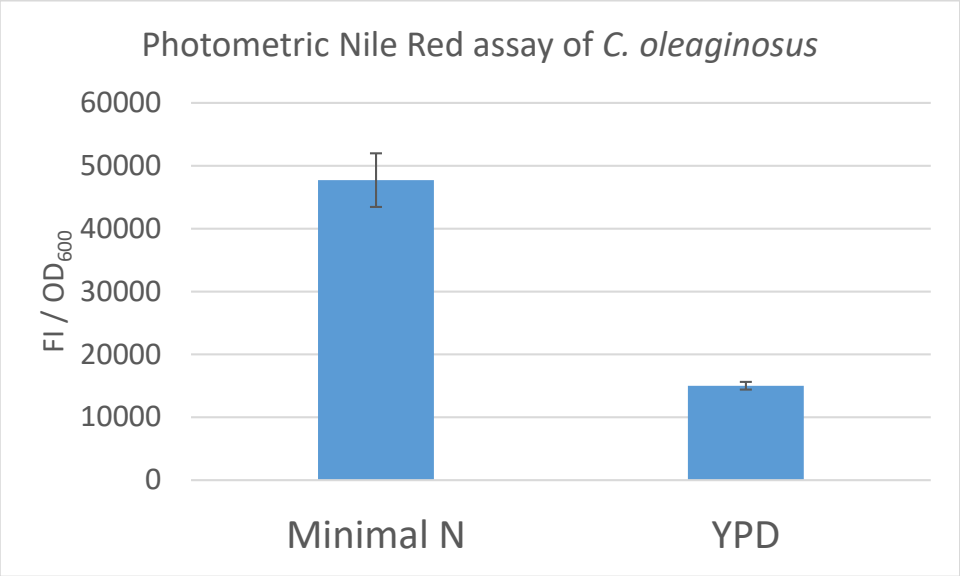

FACS

YPD

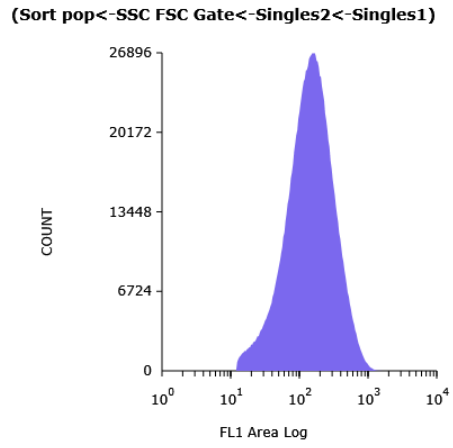

Statistics

Label	Count	Mean	% of Total	% of Plot	Std Dev
Total	1380315	189.4	72.5 %	100.0 %	149.76

Minimal N

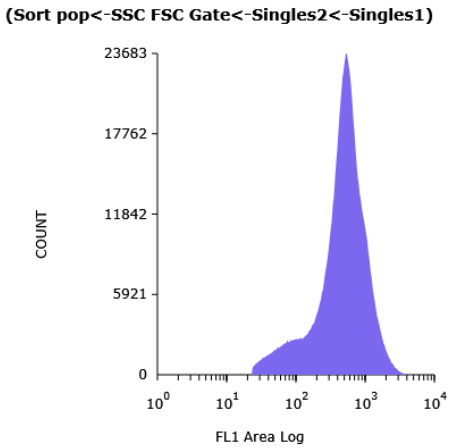

Statistics

Label	Count	Mean	% of Total	% of Plot	Std Dev
Total	892864	604.5	92.2 %	100.0 %	438.87

Supplemental 22: C:P g/g ratio effect on lipid content, biomass and total lipid. Error bars show standard deviations of triplicates.

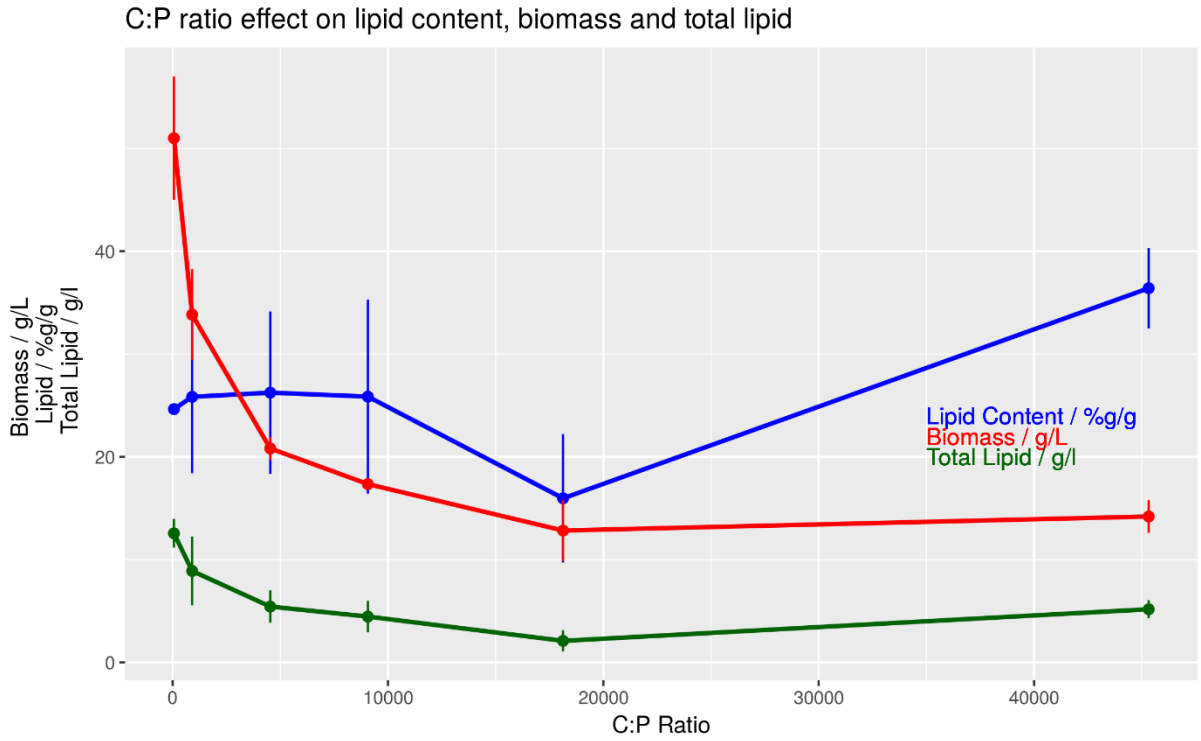

Supplemental 23: C:S g/g ratio effect on lipid content, biomass and total lipid. Error bars show standard deviations of triplicates.

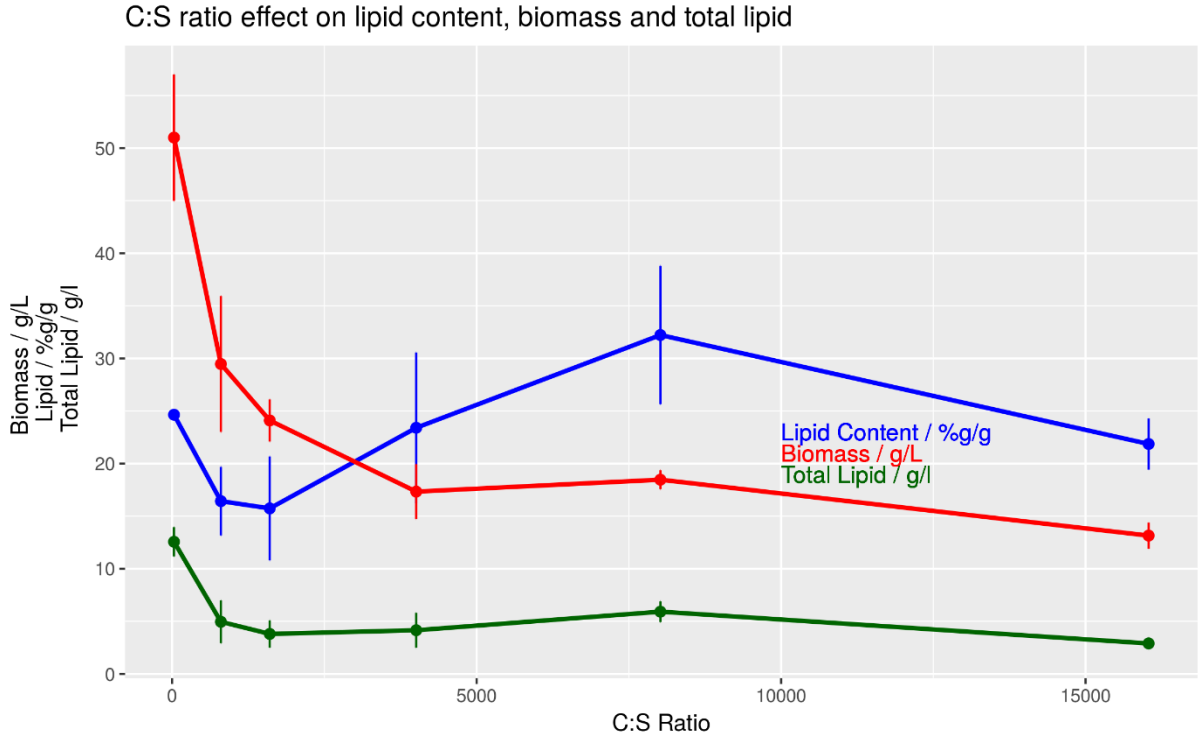

Supplemental 24: Dependency of lag phase λ on C:N, C:P and C:S ratio.

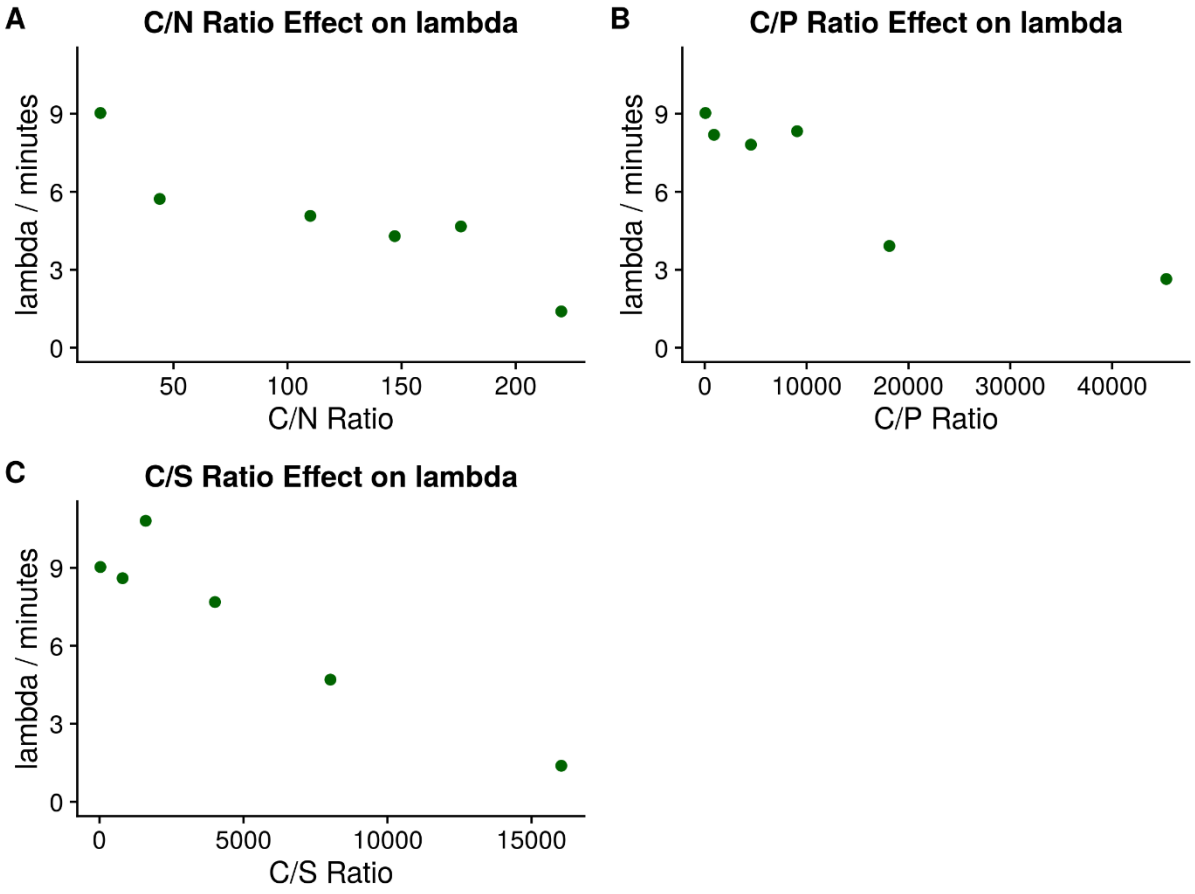

Supplemental 25 Kinetics of Nile red Fluorescence of C. oleaginosus cells grown in YPD with and without caffeine supplementation at different concentrations between 0 and 100 mM. Nile red is corrected for OD_{600} and is used as an estimator for lipid content.

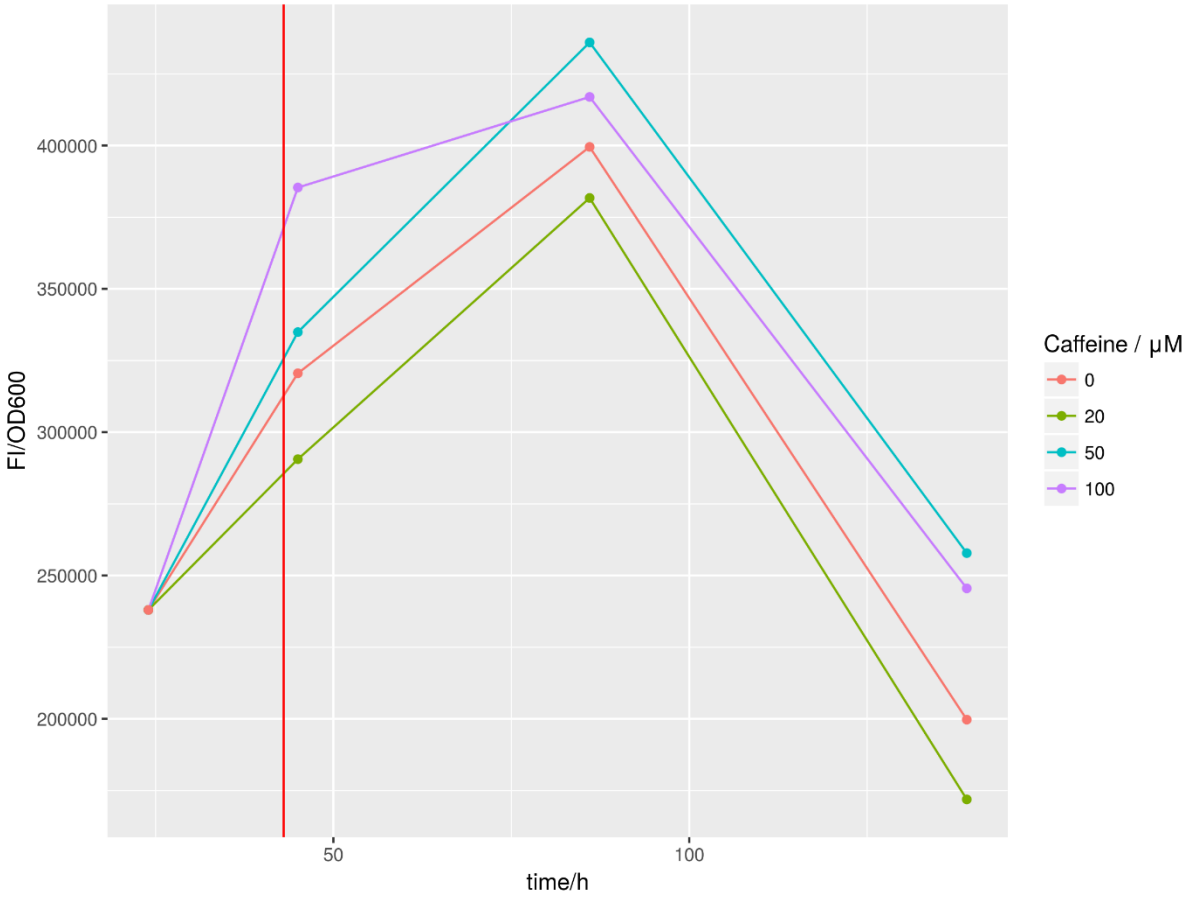

Supplemental 26: Analytical plots of robust regression using M-estimation of yeast lipid content in dependence of rapamycin concentration in full cultivation medium. Data points 9 and 7, both of which outliers causing deviation at [rapamycin]=10 were excluded due to high Cook's distance. The resulting fit was plotted in Figure 22 and was based on the formula shown at the bottom of the supplemental.

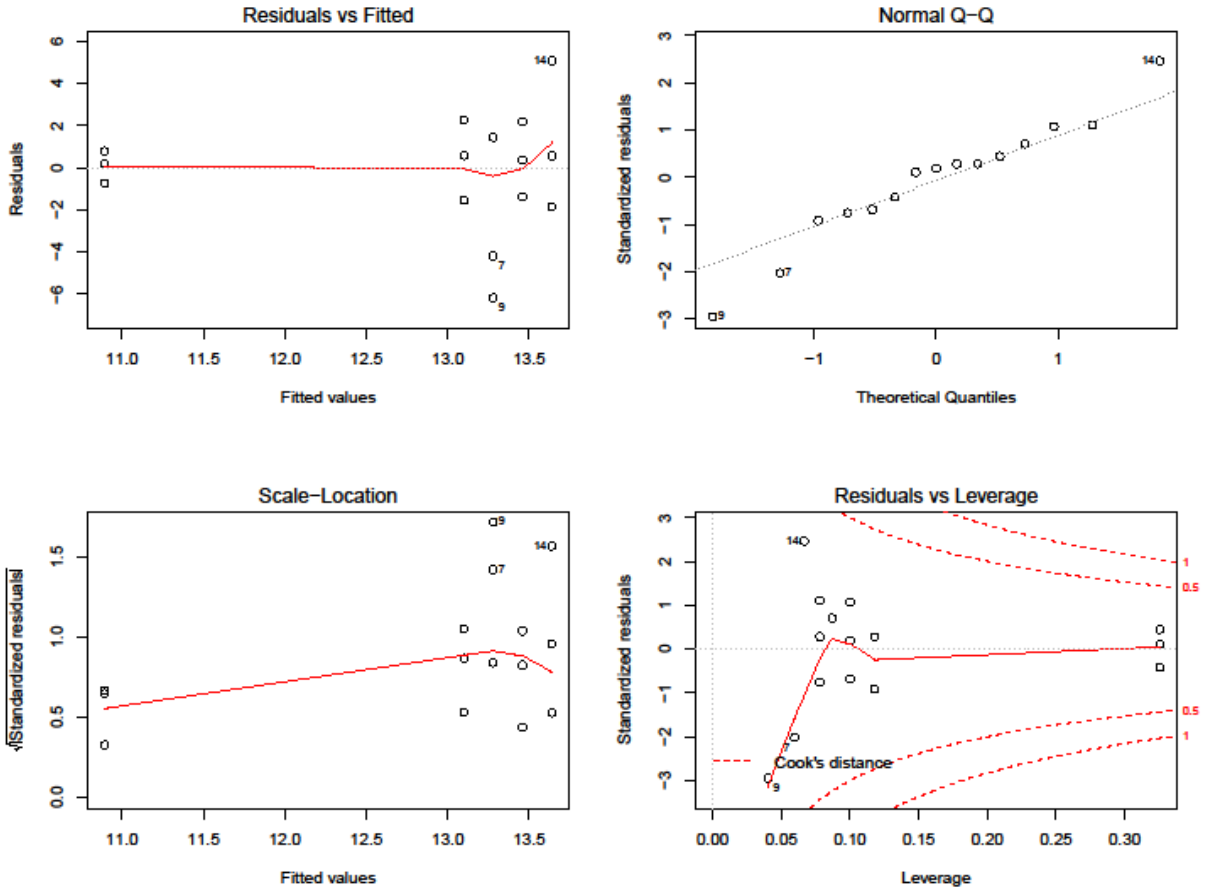

Lipid content=13.1996+0.3197*log([Rapamycin])

Supplemental 27: Table of C. oleaginosus homologues in TORC signaling network.

Abbreviations: Cutaneotrichosporon oleaginosus, TO; Schizosaccharomyces pombe, SP; Nitrogen Catabolite Repression, NCR; Saccharomyces cerevisiae, SC; Dictyostelium discodeum, DD.

Pathway	Gene/Complex	Comment	TO Homologue	ProteinID	Location
		TORC1			
TORC1	*tor1*	Rapamycin binding motif present in TO	Tor2	284088	scaffold_15:21383-29165
TORC1	*kog1*	Scaffold protein facilitating connection between Tor and downstream substrates	Kog1	284831	scaffold_22:52969-57902
TORC1	*wat1*	In mice not essential for TORC1, but for TORC2 activity	Wat1	57020	scaffold_2:285490-286968
TORC1	*tco89*	Deletion results in rapamycin hypersensitivity in SC	not found		
		TORC2			
TORC2	*tor2*	Only one TOR gene in TO	Tor1		see above
TORC2	*wat1*		Wat1		see above
TORC2	*sin1*	Conserved binding to TOR2 N-terminus	Sin1	69103	scaffold_23:36948-39520
TORC2	*avo2*	Non-essential TORC2 component	not found		
TORC2	*ste20*	Conserved in TORC2, no common structural motifs	Ste16	89274	scaffold_3:272899-277627
TORC2	*bit61*	Non-essential TORC2 component	not found		
		SNF (AMPK) Pathway			
SNF-Path	*snf1*	Impacts on TSC1/2	Snf1	283830	scaffold_13:22589-25197
SNF-Path	*LKB1*	Activation of Snf1	not found		
SNF-Path	*tos3*	Activation of Snf1	Tos3	247203	scaffold_38:169274-170546
SNF-Path	*sak1*	Activation of Snf1	Sak1	108990	scaffold_38:167511-171260
SNF-Path	*elm1*	Activation of Snf1	Elm1	292545	scaffold_38:169274-171195
SNF-Path	*sip4*	Central Regulator of carbon repressed genes, activated by phosphorylated Snf1	not found		
SNF-Path	*reg1*	Inhibition of Snf1	Reg1	264283	scaffold_65:2237-5263

SNF-Path	*glc7*		Glc7	250471	scaffold_71:27846-28984
SNF-Path	*arf3*	Activated by Snf1 in low energy environment	not found		

TSC Complex/TORC Upstream

TSC PATH	*FKBP12*	Forms complex with rapamycin and inhibits TORC1	Fkh1	275378	scaffold_36:88698-89351
TSC PATH	*tsc2*	Tuberin homologue	Tsc2	285856	scaffold_33:86602-92917
TSC PATH	*tsc1*	Hamartin homologue	Tsc1	315493	scaffold_117:6411-9393
TSC PATH	*Vps34*	Signals Availability of amino acids, bypassing Tsc/RheB axis	Vps34	268904	scaffold_4:261651-264613
TSC PATH	*RheB*	Connects TSC-Complex to TORC1, possibly TORC2	Rhb1	237912	scaffold_71:7565-8434
TSC PATH	*Erk/Rsk*	Inhibition of Tsc complex (Erk signaling)	Erk/Rsk-like	315969	scaffold_130:19790-24650
TSC PATH	*Rtp801/L*	Activates TSc1/2, conducts signals concerning DNA damage, other stressors	not found		
TSC PATH	*gtr1*	Make up EGO complex localized at vacuolar membrane, confers amino acid availability to TORC. Possibly bypasses Tsc1/2 Rheb axis.	Gtr1	300143	scaffold_8:334087-335551
TSC PATH	*gtr2*		Gtr2	238031	scaffold_4:169222-170531
TSC PATH	*ego1*		not found		
TSC PATH	*ego2*		not found		
TSC PATH	*ego3*		not found		
TSC PATH	*npr2*	Possible TORC1 inhibitors in response to amino acid scarcity	Npr2	257923	scaffold_15:100949-103201
TSC PATH	*npr3*		not found		
TSC PATH	*acc1*	Acetyl-CoA carboxylase, required for initiation of fatty acid synthesis	Acc1	329998	scaffold_61:23648-31248

TORC1 Downstream

Translation	*S6k1*	Ribosomal s6 kinase. Initiation of translation and ribosome biogenesis in eukaryotes	Sch9	307993	scaffold_27:135937-139531
Translation	*S6*	Ribosomal Protein S6, in eukaryotes	S6b	282616	scaffold_5:384088-385762
Translation	*4E-BP1*	Repression of translation, targets eIF4E in eukaryotes	not found		
Translation	*eIF4E*	Initiation of translation, helicase, in eukaryotes	Cdc33-like	280911	scaffold_120:13833-15119
Translation			Cdc33-like	298705	scaffold_1:475432-477187
Metabolism	*gaf1*	Modulates sexual development in SP	not found		

Metabolism	*PP2A*	Transcription factor, PP2A like, involved in cell cycle, stress response in SC	Ppe1	271546	scaffold_13:19582-21194
Lipid	*tap42*		Tap42	240320	scaffold_4:404467-405678
Lipid	*sit4*	Involved in lipid synthesis, possibly autophagy in SC	Sit4	298867	scaffold_2:251612-255231
Lipid	*gat1*	Transcription Activator for NCR genes. Associated with lipid replenishment in SC	Gat1	302500	scaffold_31:151465-152390
Lipid	*gln3*	Transcription activators associated with lipid replenishment. In SC responsible for TORC mediated response to low intracellular glutamine	not found		
Lipid	*rtg1*		not found		
Lipid	*rtg3*		not found		
Transcription initiation	*elf4G*	Transcription factor, Polymerase I, in eukaryotes	Tif1	103441	scaffold_36:30441-32500
Transcription initiation	*maf1*	Polymerase III suppressor	not found		
Autophagy	*atg1*	Autophagy related gene, conserved TORC substrate		231999	scaffold_43:222-3477
Autophagy	*atg13*	Autophagy related gene	not found		
Autophagy	*atg17*	Autophagy related gene	not found		
Autophagy	*atg31*	Autophagy related gene	not found		
Autophagy	*atg29*	Autophagy related gene	not found		

TORC2 Downstream

Autophagy	*akt1/PKB*	Stress response, G1 arrest, sexual development, aa uptake, possible feedback to Tsc1/2	Gad8	288963	scaffold_97:62770-65023
Autophagy	*ksg1*	Involved in cell wall integrity, activates Gad8 in SP, SC	Ksg1	325387	scaffold_4:211245-215591
Autophagy	*FOXO3*	Forkhead box like transcription factor, induces expression of autophagy related genes in SP	Fkh1	300675	scaffold_12:188403-189818
Autophagy	*atg12l*	Activation by Fkh/FoxO3, Induction of autophagy in SP, SC	Atg12	283501	scaffold_10:225120-225896
Autophagy	*ulk2*	Activation by Fkh/FoxO3, Induction of autophagy in SP, SC	not found		
Cell skeleton	*RHO/RAC*	Actin organization in SP	not found		
Cell skeleton	*PKC*	Only one PKC gene in TO, required for cell wall remodeling and sphingolipid regulation in SP	Pkc1	73077	scaffold_24:189607-193675

Autophagy	*PKBA*	Inhibited by Pdk1, affects actin organization, chemotaxi, cell movement in DD	not found		

Other

Autophagy	*atg5*	Autophagy related gene	Atg5	285573	scaffold_30:25886-27199
Autophagy	*atg6*	Autophagy related gene	Atg6	268673	scaffold_3:492871-494478
Autophagy	*atg99*	Autophagy related gene	Atg99	327958	scaffold_26:111275-114356
Autophagy	*atg16*	Autophagy related gene	Atg16	183500	scaffold_77:6693-7765

Supplemental 28: 200 µL C. oleaginosus cells grown for 72 hours in YPD with and without 5 µM rapamycin supplementation were pelleted, washed with ddH_2O and resuspended in the same amount of water. 25 µL DMSO and 25 µL Nile red (50 mg/ml) in DMSO were added and incubated in darkness for 10 minutes. Images were taken on a Zeiss Axio Lab A1 with an Axio Cam ICm1 (Oberkochen, Germany). Fluorescence was measured with a 525/25 filter with an exposure time of 500 ms.

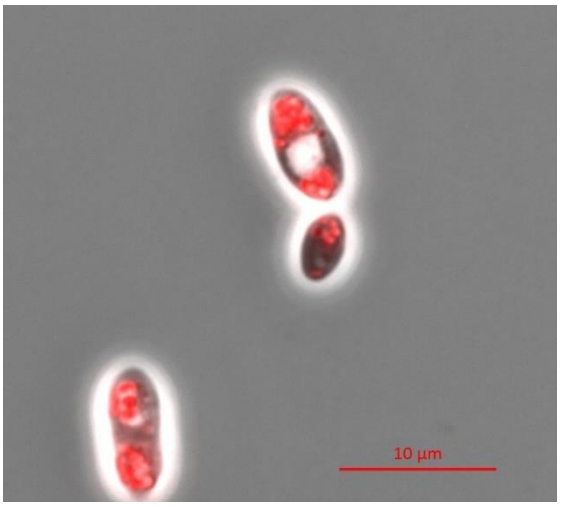

With Rapamycin

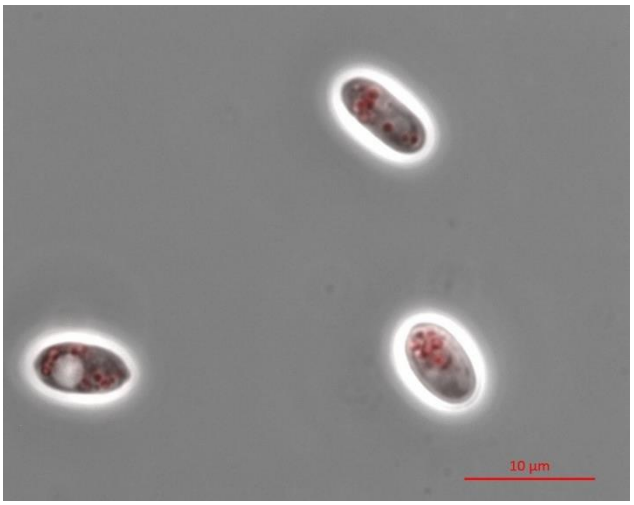

Without Rapamycin

Supplemental 29: FACS of Rapamycin treated cells. 50 µL of cells were diluted and measured in a BioRad S3 Sorter using 488 nm excitation. The measurement was done after 48 hours of cultivation.

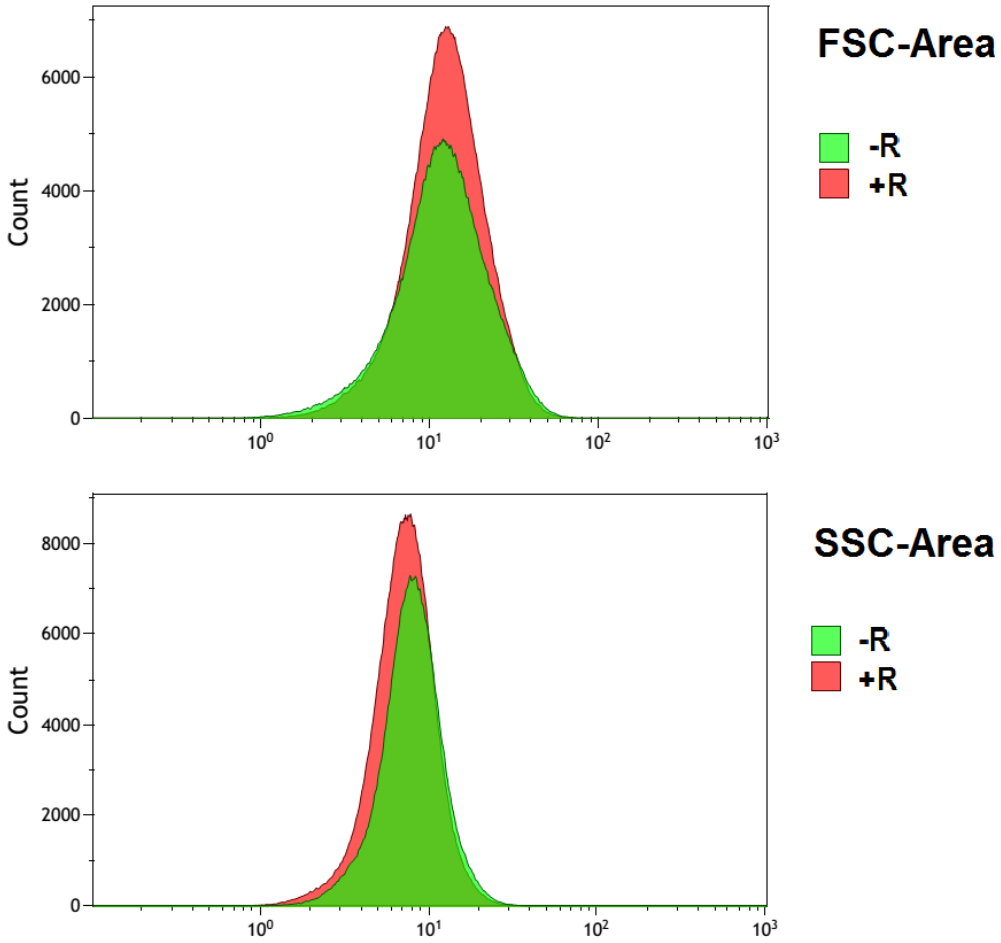

Supplemental 30: Deviations in Codon Usages. Green: YPD, Red: MNM.

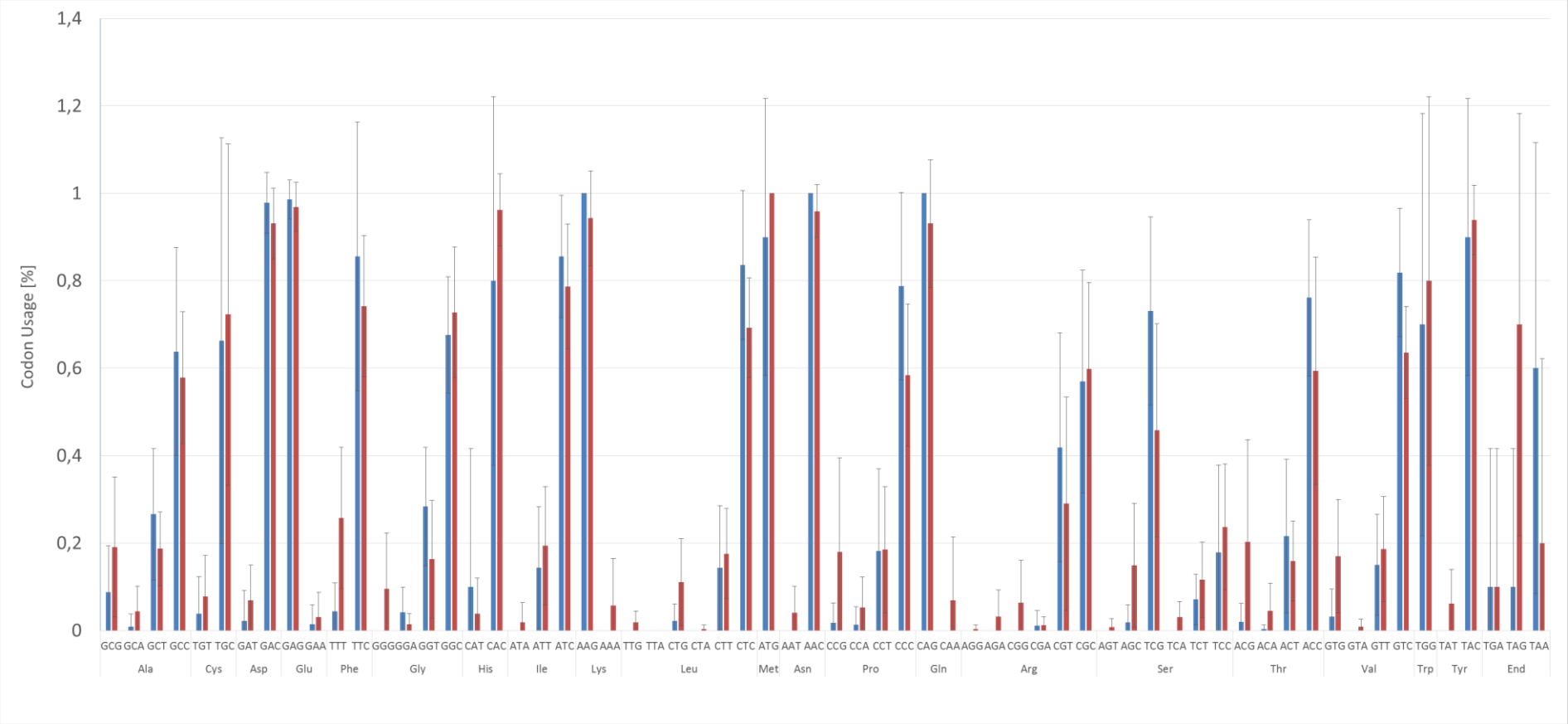

Supplemental 31: Insertion site of YFP expression cassettes in clone described by Goerner et al[51]*. The sequence obtained by the fragment derived from TAIL PCR is*
GCGGGCCCGAGACCCCCTCCCAGGGACGCATCGTGGCCGGCATCACCTCGCTCCACAGGTGCGGTTGTTG
GCGCCTATATCTCCGACATCACCGATGGGGAAGATCGGGCTCGCCACTTCGGGCTCATGAACGCTTGTTTC
GGCATGAAATGGTGGCAGGCCCCGTGGCCGGAGGACAGTTGGGCGCCATCTCCTTGAATGTAAAAA

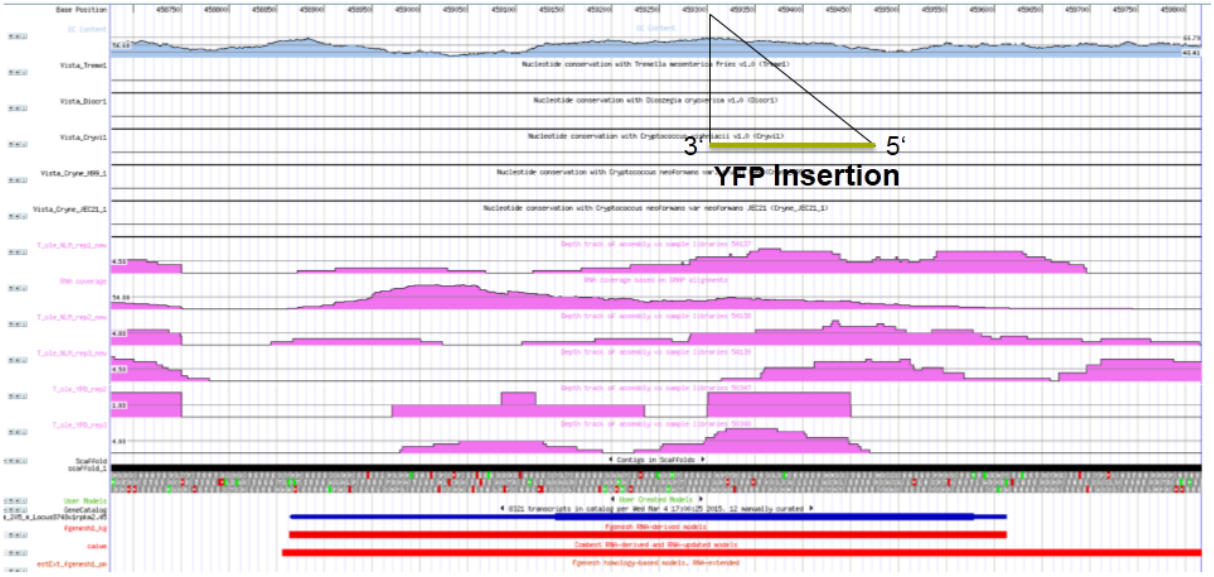

Supplemental 32: Nile red fluorescence of C. oleaginosus wild type and Dga overexpressing clones 1, 5 and 6 after 96 hours grown in YPD in baffled 50 ml flasks. Error bars show standard deviations of triplicates.

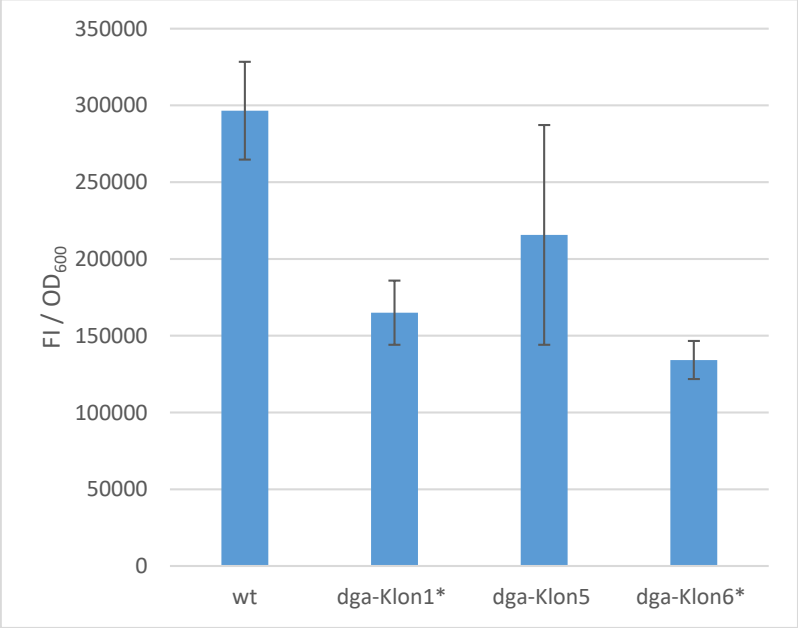

Supplemental 33: Nile red fluorescence of C. oleaginosus wild type and Dga overexpressing clones after 96 hours grown in YPD in baffled 50 ml flasks. Error bars show standard deviations of triplicates.

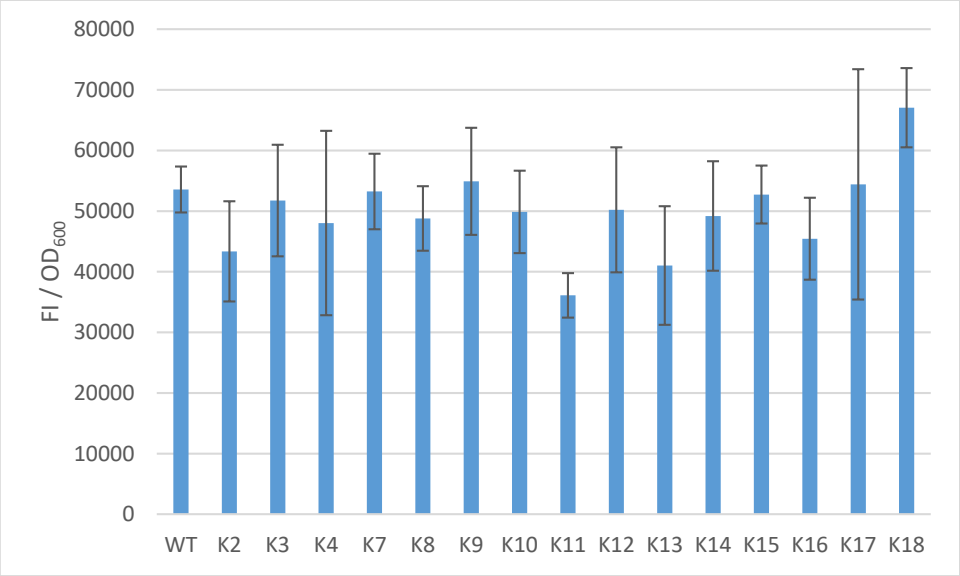

Supplemental 34: Supplemental: Fatty acid spectra of Dga1 mutants (clone 1, 5 and 6) and wild type C. oleaginosus grown in a 1 l infors fermenter in YPD and glucose feed. Fatty acids distributions can be assumed to be from a common distribution, with C16:0=29 ± 3% g/g, C18:0=9 ± 2% g/g, C18:1=43 ± 2% g/g, C18:2=18 ± 5% g/g and C18:0=1 ± 0% g/g.

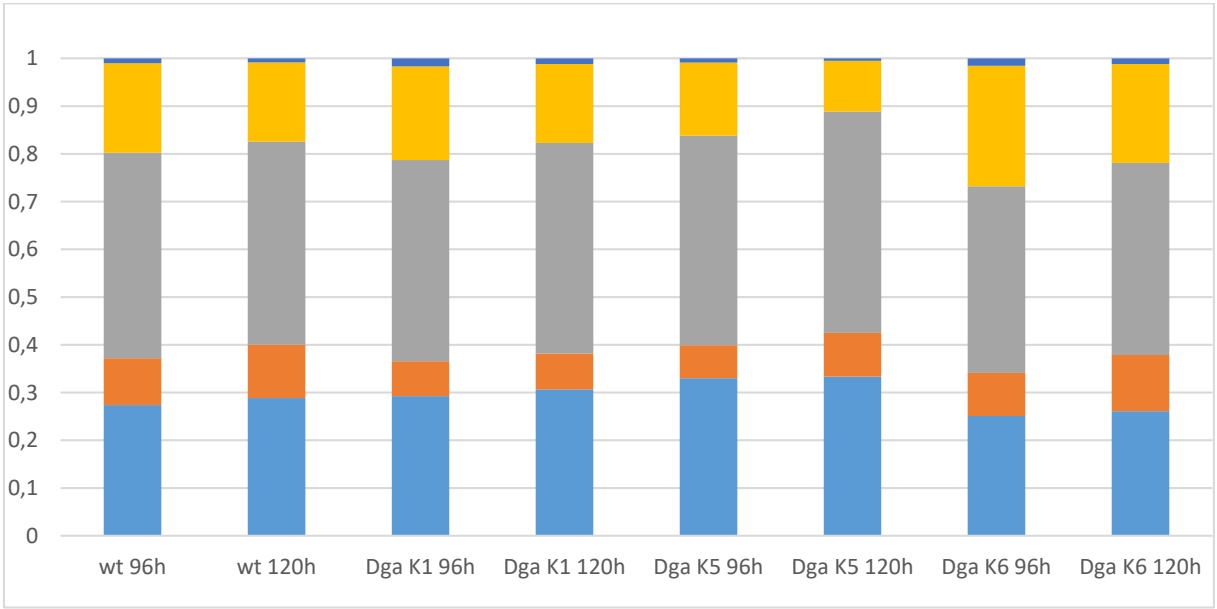

Supplemental 35: Main fatty acids produced by C. oleaginosus wild type (wt) as well as Dga2 overexpressing clones 1 (K1), 5 (K5) and 6 (K6) at different time points during fermentation.

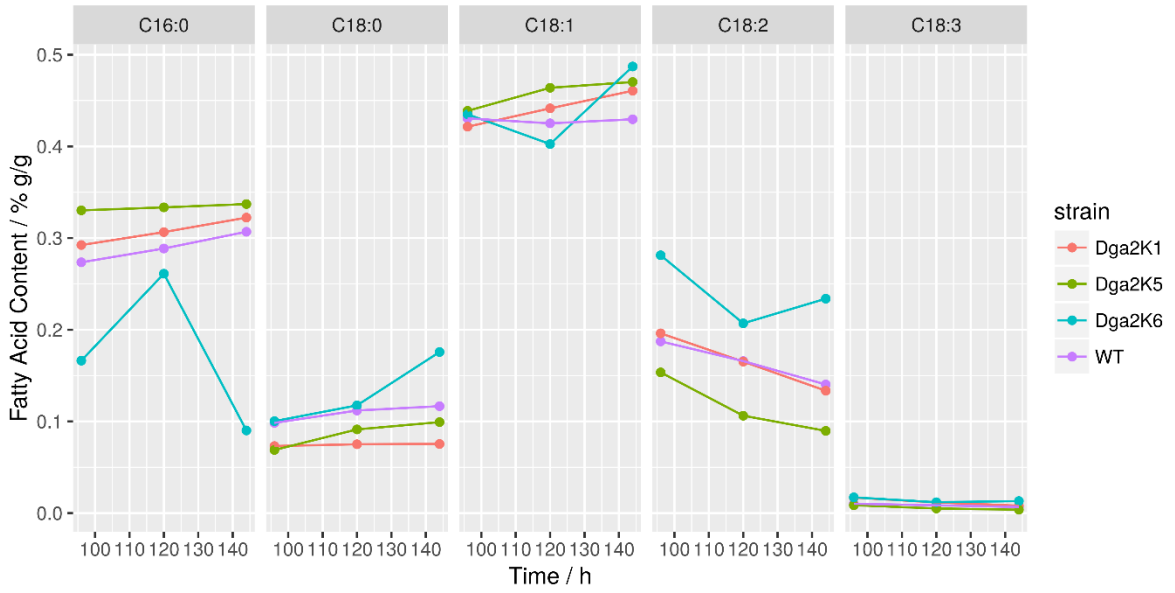

Supplemental 36: List of all tested combinations of independent variables time (x1), pH (x2), flocculant concentration (x3) and flocculation agent (x4) as well as resulting flocculation efficiency (FE) and residual volume (RV) in ml per 100 ml sample.

x1	x2	x3	x4	Time / h	pH	[Agent] / mg/l	Agent	FE	RV / ml
1	0	1	0	120	8	80	Tannin	0.75256971	2
1	0	0	0	120	8	40	Tannin	0.60874427	1.4
1	1	1	0	120	9	80	Tannin	0.56740059	1.9
1	1	0	0	120	9	40	Tannin	0.52521461	0.9
1	0	1	1	120	8	80	Chitosan	0.58024591	100
1	0	0	1	120	8	40	Chitosan	0.49110081	100
1	1	1	1	120	9	80	Chitosan	0.54500903	100
1	1	0	1	120	9	40	Chitosan	0.48471325	100
2	0	1	0	145	8	80	Tannin	0.69720716	3
2	0	0	0	145	8	40	Tannin	0.59384121	1.5
2	1	1	0	145	9	80	Tannin	0.5229217	2.75
2	1	0	0	145	9	40	Tannin	0.49303202	0.8
2	0	1	1	145	8	80	Chitosan	0.70031179	100
2	0	0	1	145	8	40	Chitosan	0.47501298	100
2	1	1	1	145	9	80	Chitosan	0.50405041	100
2	1	0	1	145	9	40	Chitosan	0.45991595	100
3	0	1	0	170	8	80	Tannin	0.68660804	2.6
3	0	0	0	170	8	40	Tannin	0.55712691	1.4
3	1	1	0	170	9	80	Tannin	0.50606639	2
3	1	0	0	170	9	40	Tannin	0.48788442	0.7
3	0	1	1	170	8	80	Chitosan	0.65831853	100
3	0	0	1	170	8	40	Chitosan	0.49270584	100
3	1	1	1	170	9	80	Chitosan	0.55863723	100
3	1	0	1	170	9	40	Chitosan	0.43839231	100
4	0	1	0	195	8	80	Tannin	0.62656059	2.5
4	0	0	0	195	8	40	Tannin	0.60575483	1.7
4	1	1	0	195	9	80	Tannin	0.56765528	2
4	1	0	0	195	9	40	Tannin	0.49704341	0.1
4	0	1	1	195	8	80	Chitosan	0.78161936	1
4	0	0	1	195	8	40	Chitosan	0.56579288	100
4	1	1	1	195	9	80	Chitosan	0.55701295	100
4	1	0	1	195	9	40	Chitosan	0.50034254	100
5	0	1	0	220	8	80	Tannin	0.72987682	2
5	0	0	0	220	8	40	Tannin	0.69433723	1.2
5	1	1	0	220	9	80	Tannin	0.67626942	2
5	1	0	0	220	9	40	Tannin	0.65671147	0.9
5	0	1	1	220	8	80	Chitosan	0.71635389	100
5	0	0	1	220	8	40	Chitosan	0.65268812	100
5	1	1	1	220	9	80	Chitosan	0.62955386	100
5	1	0	1	220	9	40	Chitosan	0.61394476	100

Supplemental 37: Time effect on OD_{680} of algal suspension measured inside a well of a 96-well plate. No significant sedimentation or adhesion effects are observed. Error bars show standard deviations of triplicates.

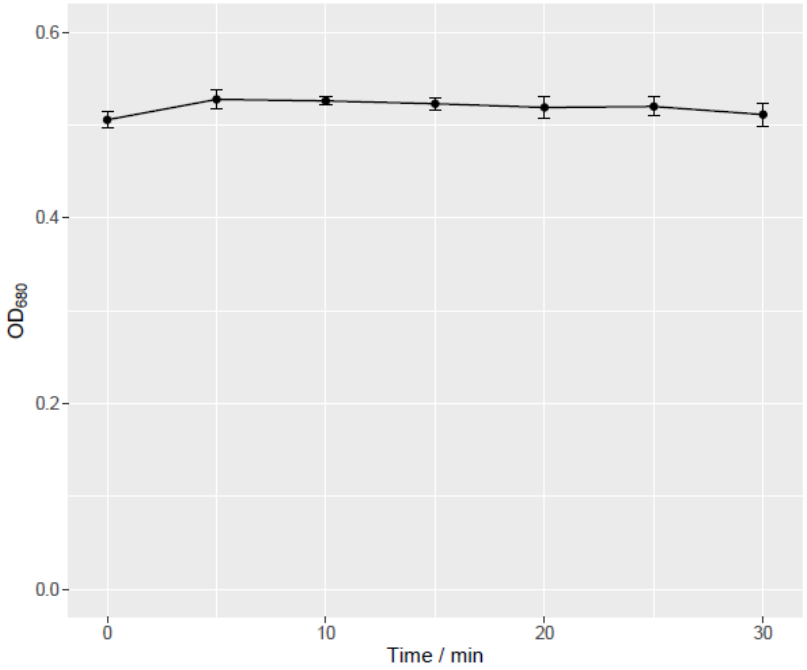

Supplemental 38: Spatial distribution of algal biomass as measured by OD_{680}. Protocol as described in section 3.3.3 was run. Dilutions were: 1:1 (a), 1:10 (b) and 1:20 (c). Measurement was done in a clear 96 well nunc plate. Values show OD_{680}.

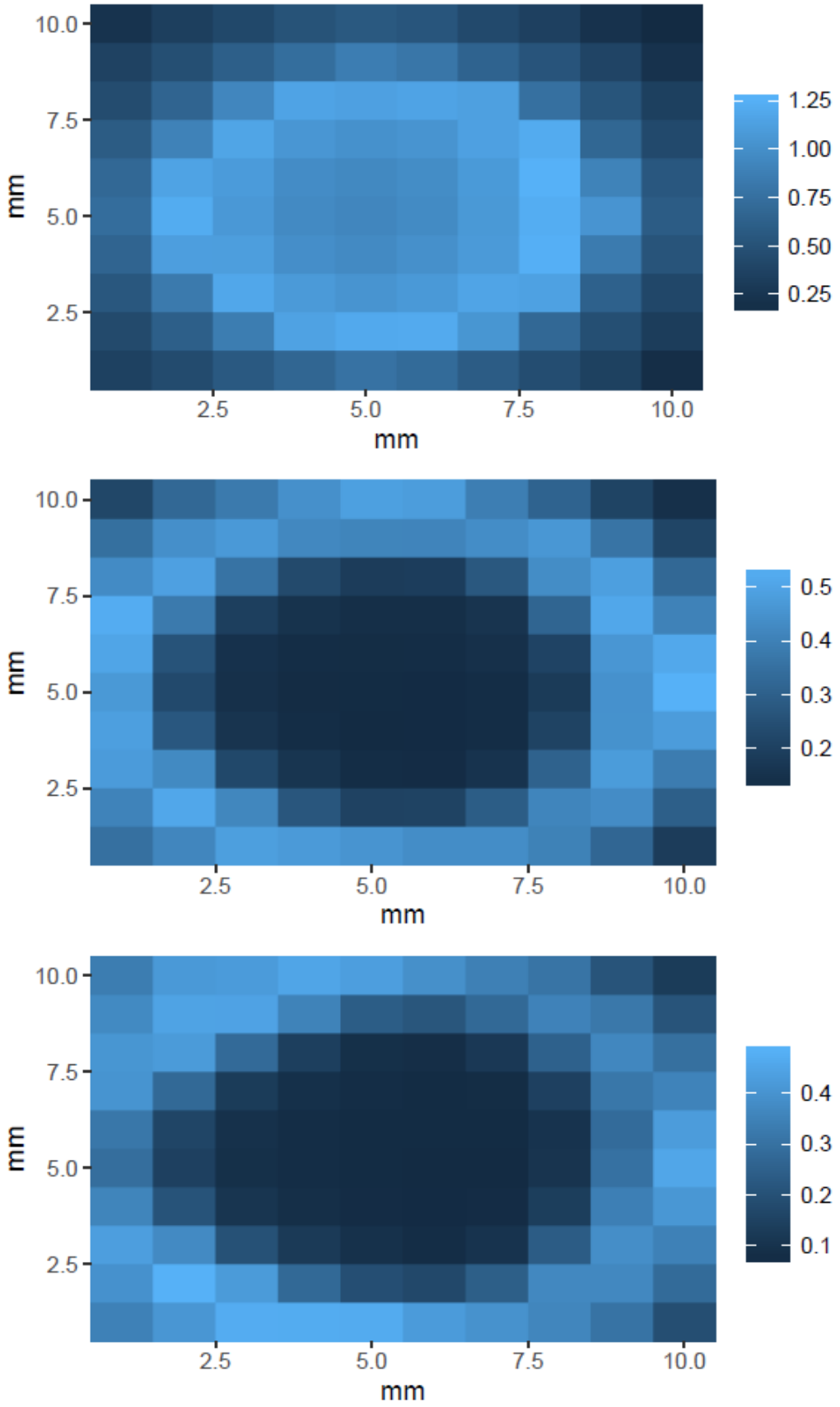

Supplemental 39: Time course of OD_{680} of algal suspension in 96-well plate with included shaking. Algae culture (at OD_{680}=0.52) was placed in a 96-well and OD_{680} was measured every 300 seconds. The plate was shaken at 300 rpm (linear, orbital, double orbital) every 600 minutes. Measurement points taken immediately after shaking (Shake) contrast those taken after sedimentation time (Sedim). Error bars show standard deviations of triplicates.

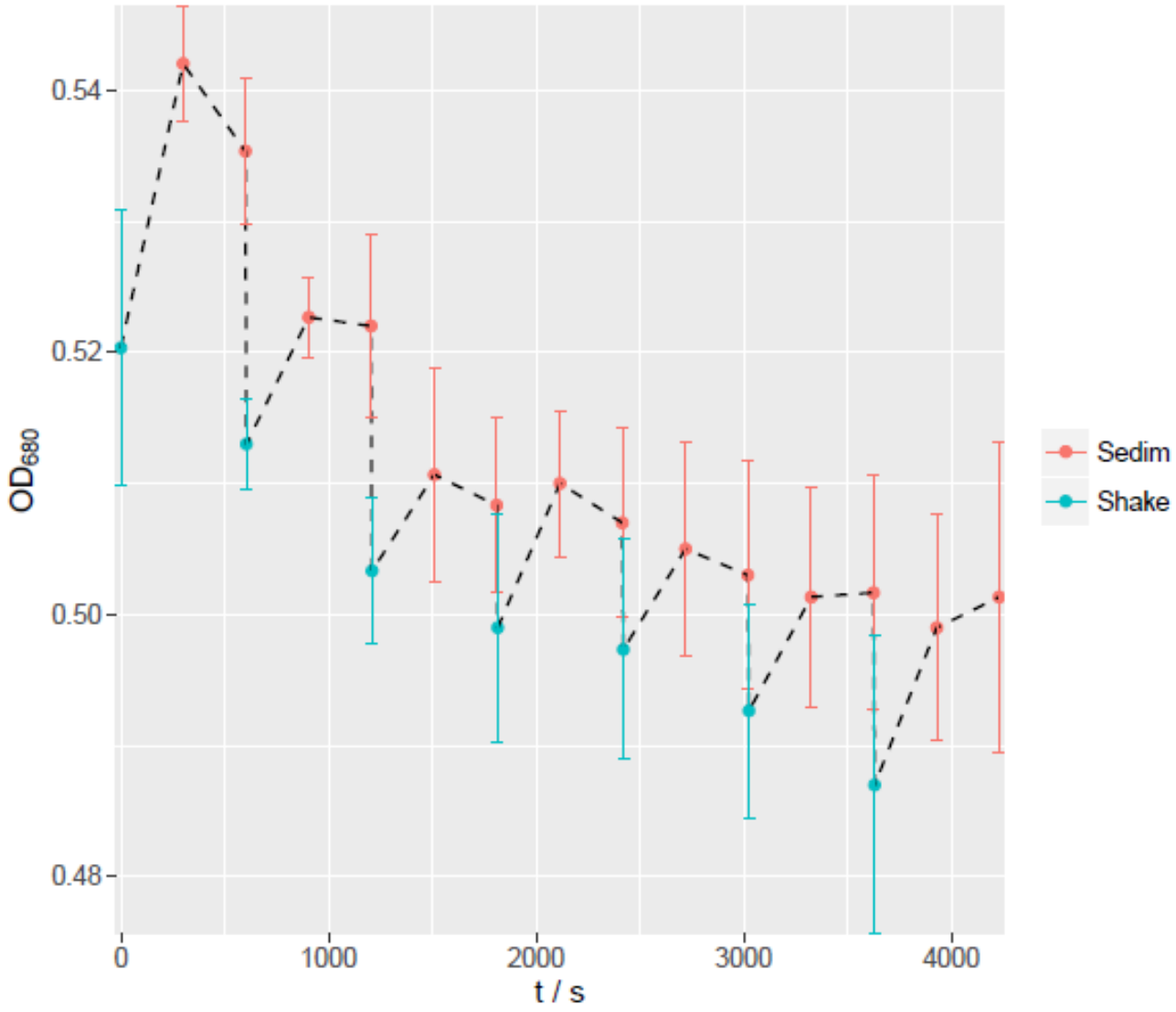

Supplemental 40: Regression parameters of linear regression as shown in section 3.4.2

Coefficients: Estimate Std. Error t value Pr(>|t|) (Intercept) -0.384287 0.201044 -1.911 0.097549 . t 0.029726 0.008387 3.544 0.009414 ** ph 0.108819 0.017439 6.240 0.000428 *** Residual standard error: 0.02757 on 7 degrees of freedom Multiple R-squared: 0.8803, Adjusted R-squared: 0.8462 F-statistic: 25.75 on 2 and 7 DF, p-value: 0.0005926	**Ca(OH)2**
Coefficients: Estimate Std. Error t value Pr(>|t|) (Intercept) -0.774683 0.149559 -5.180 0.00128** t 0.030084 0.006239 4.822 0.00192** ph 0.138003 0.012973 10.638 1.42e-05*** Residual standard error: 0.02051 on 7 degrees of freedom Multiple R-squared: 0.9512, Adjusted R-squared: 0.9372 F-statistic: 68.21 on 2 and 7 DF, p-value: 2.569e-05	**KOH**
Coefficients: Estimate Std. Error t value Pr(>|t|) (Intercept) -1.00432 0.14024 -7.162 0.000183 *** t 0.02714 0.00585 4.639 0.002372 ** ph 0.15810 0.01216 12.997 3.71e-06 *** Residual standard error: 0.01923 on 7 degrees of freedom Multiple R-squared: 0.9645, Adjusted R-squared: 0.9544 F-statistic: 95.23 on 2 and 7 DF, p-value: 8.389e-06	**NaOH** Signif. codes: 0 ‘***’ 0.001 ‘**’ 0.01 ‘*’ 0.05 ‘.’ 0.1 ‘ ’ 1

*Supplemental 41: Change in pH of ABV medium caused by addition of different bases: KOH (red circles), NaOH (blue triangles) and Ca(OH)2 (Green plus signs). Stock solutions of added bases were 1M for NaOH and KOH and 1 g/l for CaOH2. Logarithmic regression yielded the following cofactors with respective R2 values: 6.4+0.69*log(KOH) with R^2=0.96, 5+0.55*log(Ca(OH)2) with R^2=0.86 and 7+0.64*log(NaOH) with R^2=0.96.*

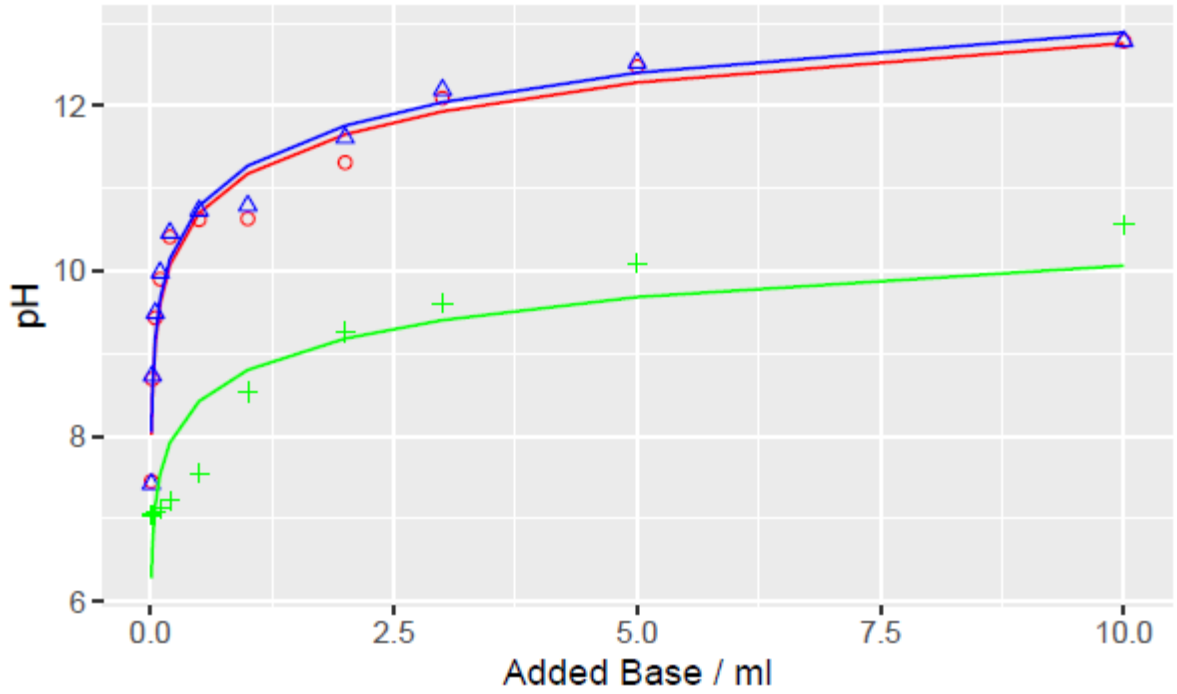

Supplemental 42: Analytic plots of regression of simplex design as described in section 3.3.8.1.

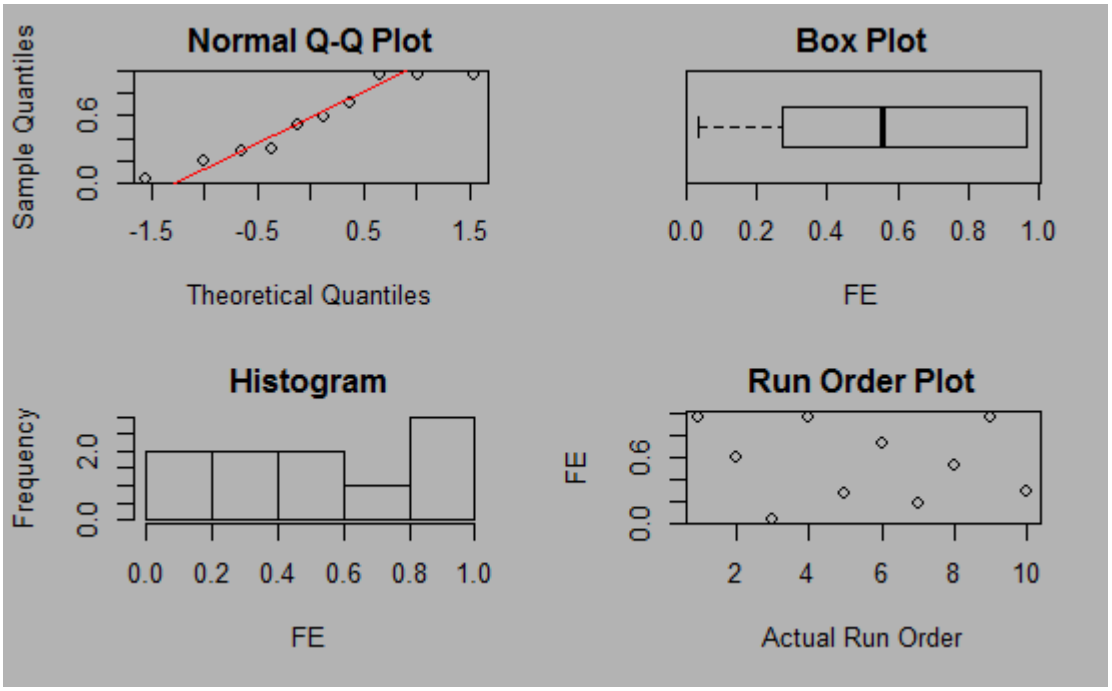

Supplemental 43: Parameters of multiple linear regression of simplex design as described in section 3.3.8.1.

```
lm(formula = FE ~ -1 + x1 + x2 + x3 + x1 * x2 + x1 *
x3 + x2 * x3, data = FlokN3)

Signif. codes:    Estimate Std. Error t value Pr(>|t|)
x1      0.64997    0.12039   5.399   0.0057 **
x2      0.28468    0.12039   2.365   0.0773 .
x3      0.02875    0.12039   0.239   0.8230
x1:x2   2.44685    0.53294   4.591   0.0101 *
x1:x3   1.18384    0.53294   2.221   0.0905 .
x2:x3   0.52895    0.53294   0.993   0.3771

Residual standard error: 0.1279 on 4 degrees of freedom
Multiple R-squared:  0.9842,  Adjusted R-squared:  0.9604
F-statistic: 41.47 on 6 and 4 DF,  p-value: 0.001471```

Signif. codes:  0 '***' 0.001 '**' 0.01 '*' 0.05 '.' 0.1 ' ' 1

Residual standard error: 0.03901 on 31 degrees of freedom
Multiple R-squared:  0.851, Adjusted R-squared:  0.8125
F-statistic: 22.13 on 8 and 31 DF,  p-value: 8.679e-11
```

Supplemental 44: Distributions for flocculation efficiencies (A) residual OD (B) and residual volume (C). Shapiro Wilk was for A W=0.96, p=0.124, for B W=0.98, p=0.3 and for C W=0.64, p=1.3x10-8.

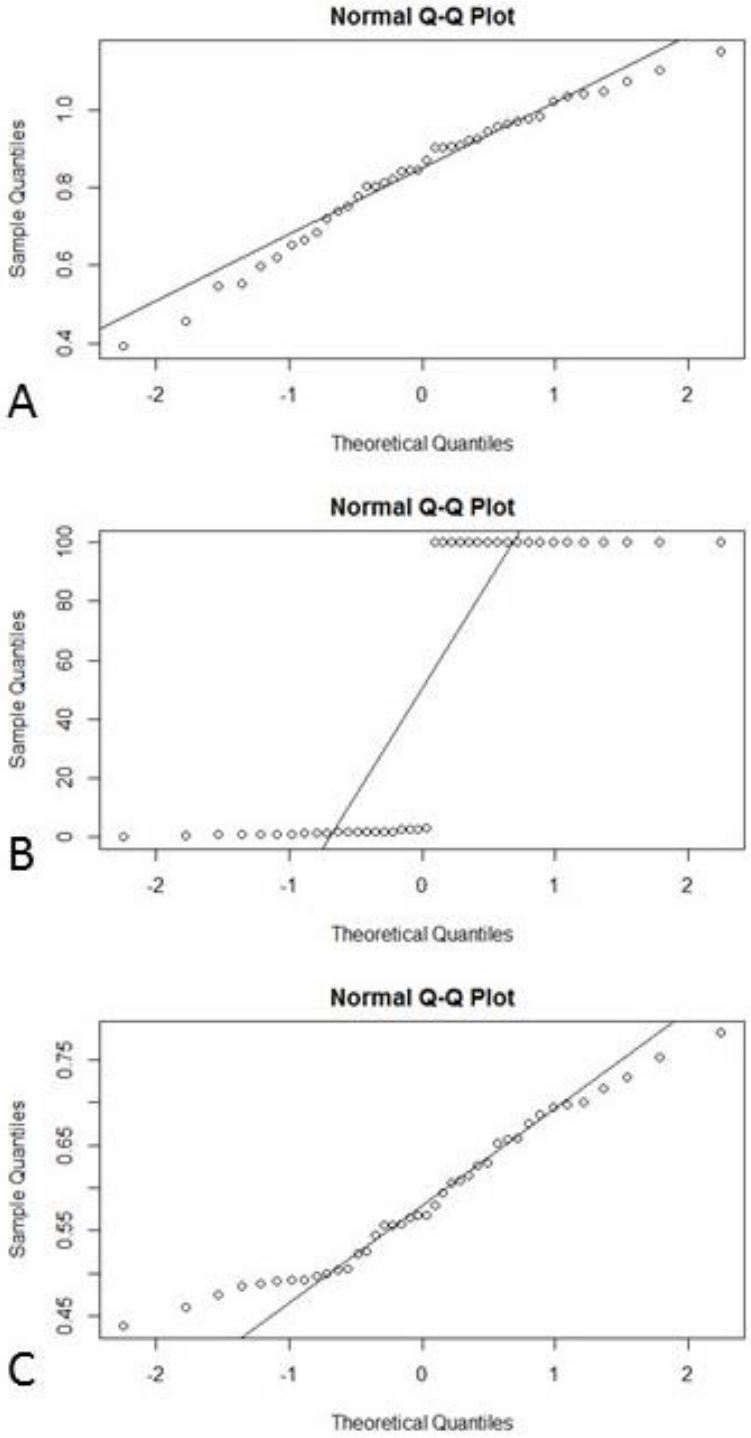

Supplemental 45: Time effect on bacterial populations measured by FACS. Figures on the left column show total numbers of events as count, whereas the right column shows share to the total number of events. Row 1 shows bacterial population 1 as identified in Supplemental 48, Row 2 shows bacterial population 2, row 3 shows total number of events. Blue line shows simple linear regression (second order).

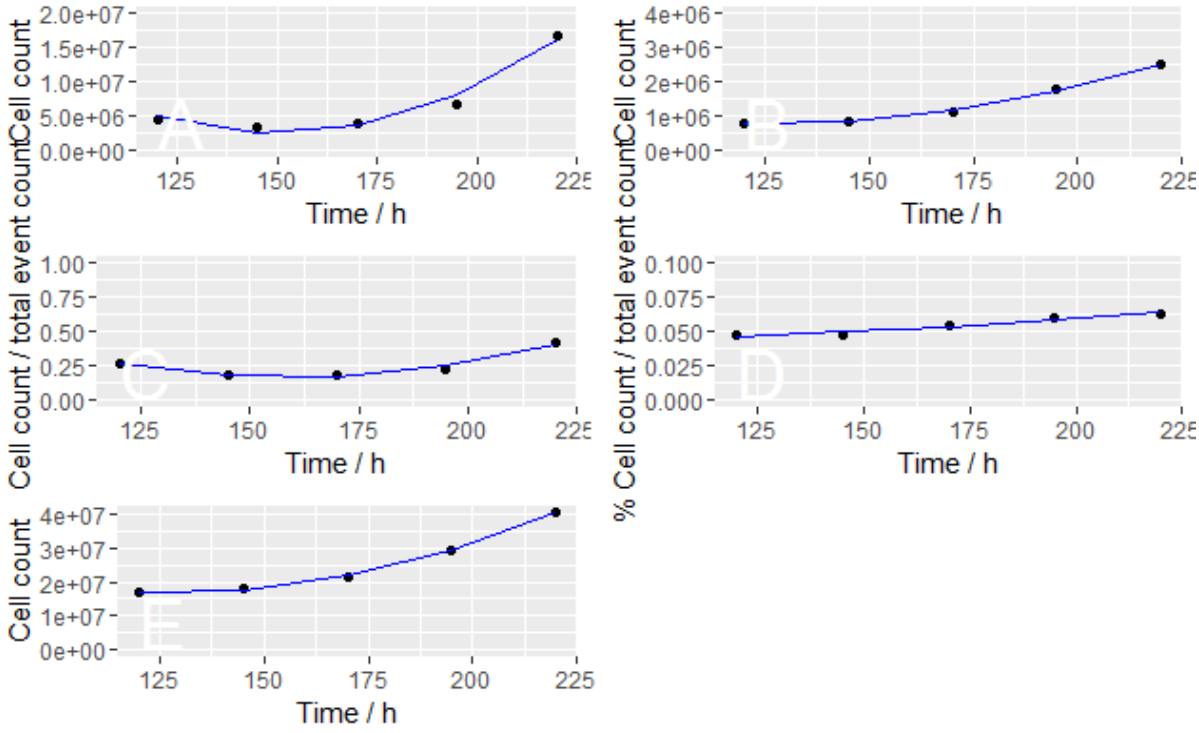

Supplemental 46: Zeta potential of two cultivations (A,B) of S. obtusiusculus in ABV medium in closed infors bioreactor as described in section 3.3.2.4.

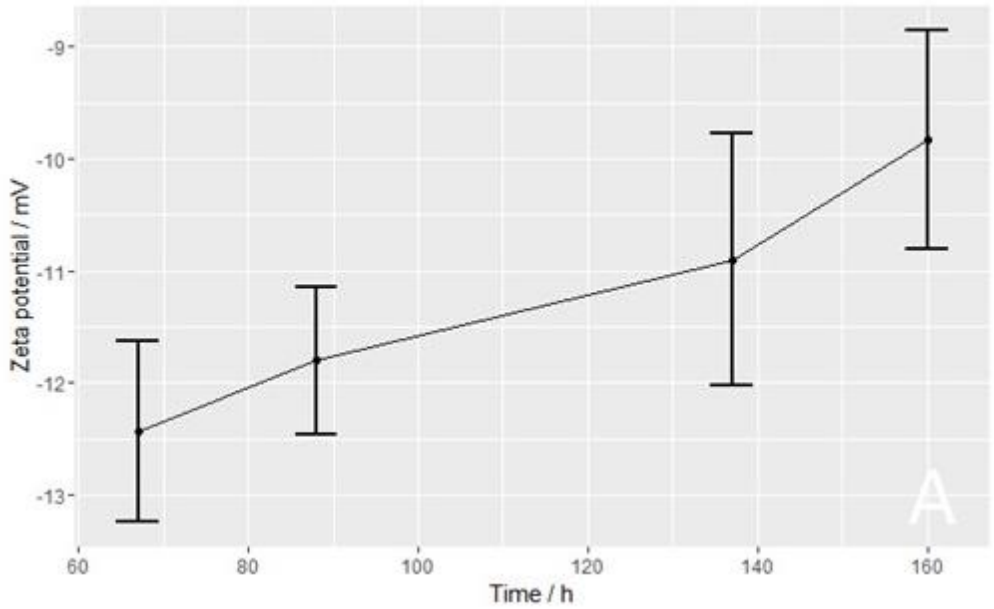

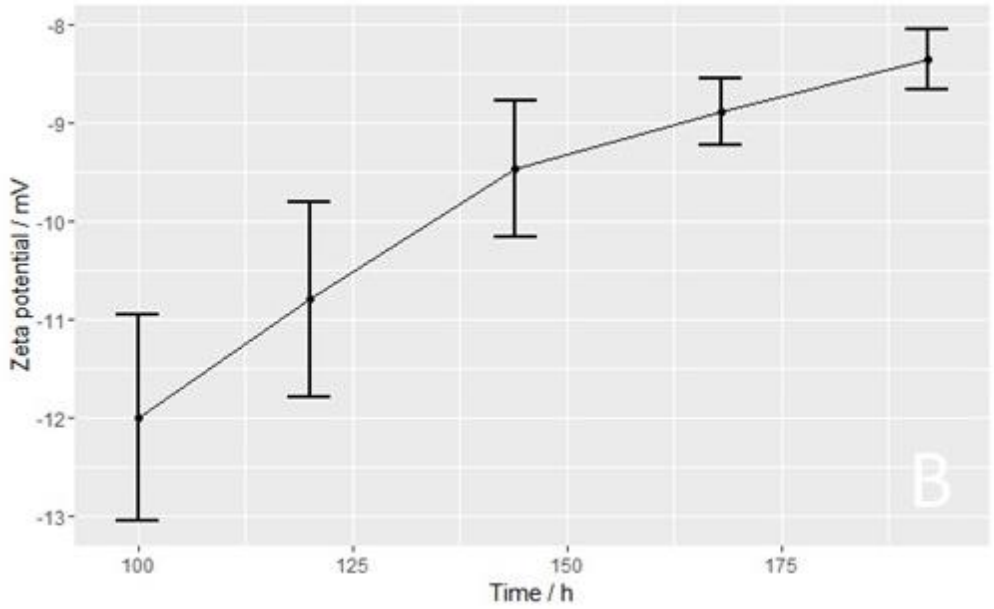

Supplemental 47: Absence of time dependence on residual volume for subsetted dataset. Subsetting was done, since residual volume followed a binary distribution. Subsets were FE<50 (A) and FE>50 (B)

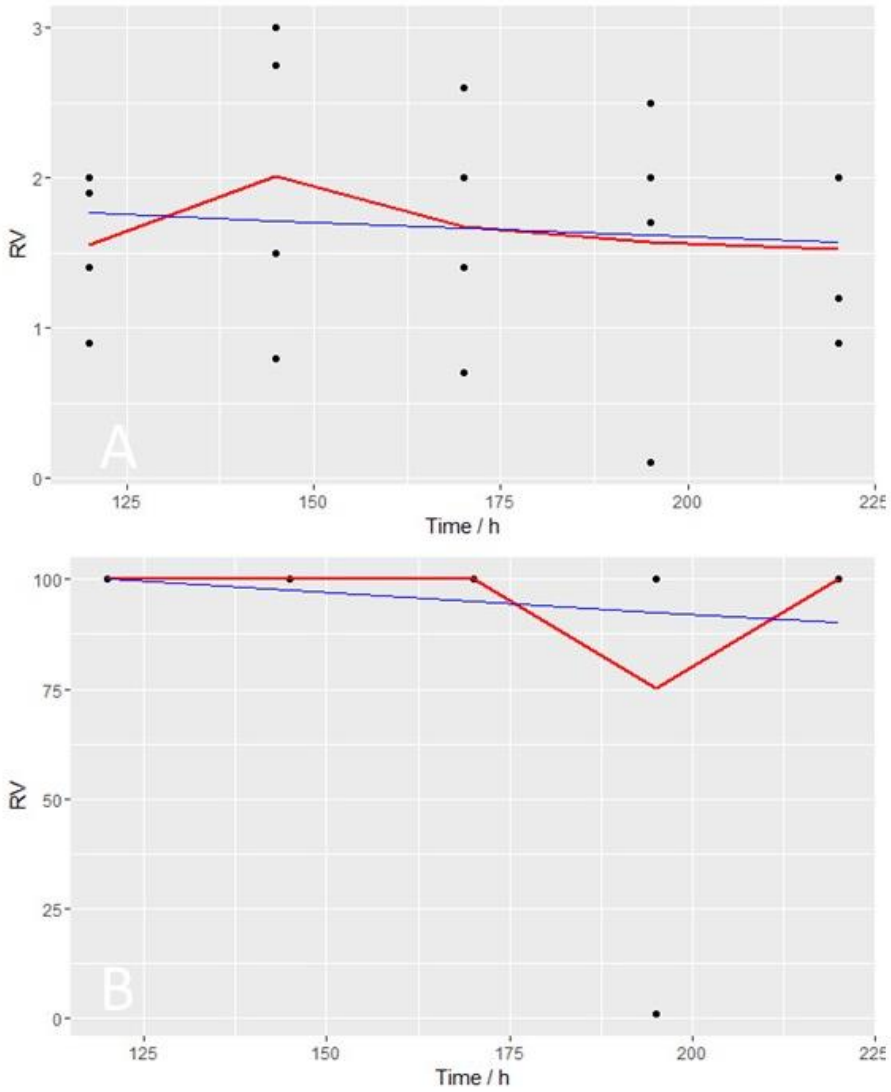

Supplemental 48: Scatterplots and histograms of flow cytometry of S. obtusiusculus cultivated in a bubble column reactor after 7 days.

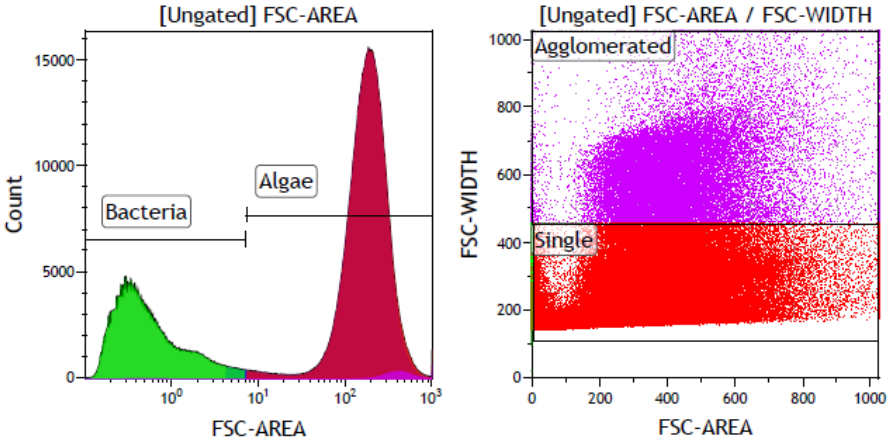

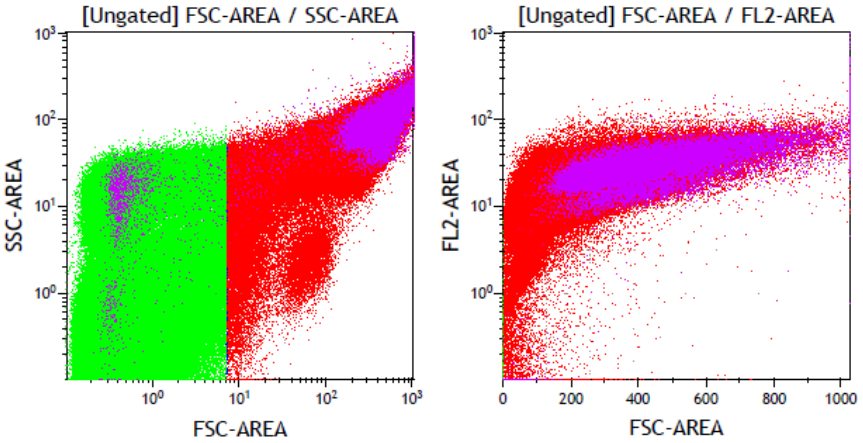

Gate	Number	Logic
All	6.799.373	Ungated
Agglomerated	22.897	Agglomerated
Algae	1.257.802	Algae
Bacteria	5.540.885	Bacteria
Single	1.259.387	Single

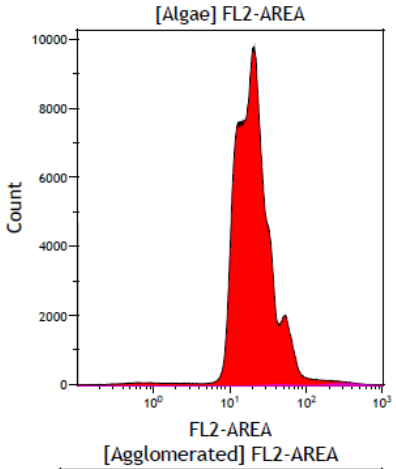

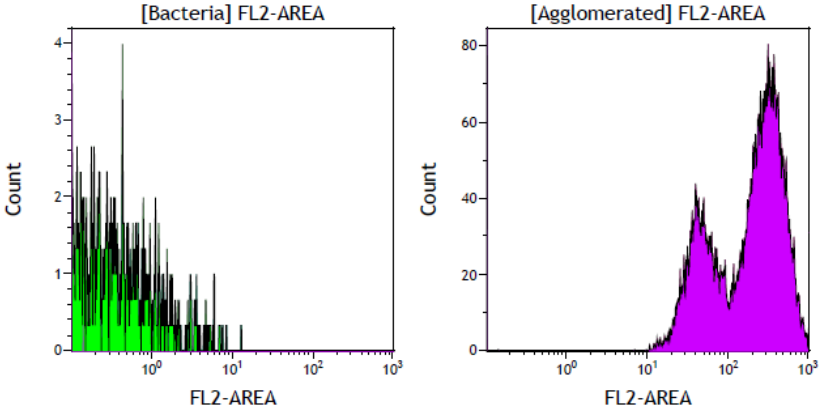

*Supplemental 49: Impact of bacterial populations 1 and 2 on all dependent variables FE, RV and ROD. Regression is shown as blue line. Coefficients are: FE~0.48+0.5*BP1S (R^2=0.23), FE~0.29+5.33*BP1S (R^2=0.14), RV~46+9*BP1S (R^2=0), RV~68+-373*BP1S (R^2=0), OD~0.69+0.58*BP1S (R^2=0.08), OD~0.15+12.63*BP1S (R^2=0.2).*

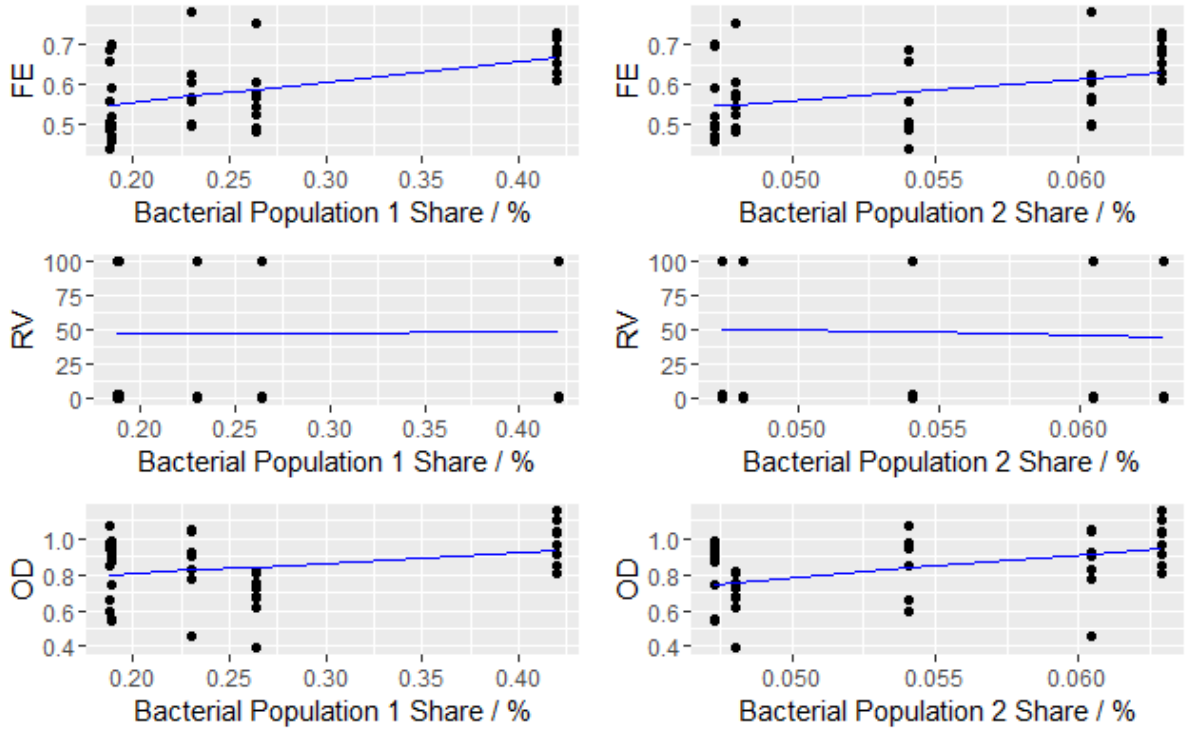

*Supplemental 50: Effect of Zeta potential on all dependent variables FE, RV and ROD. Regression is shown as blue line, coefficients are: FE~0.67+0.007*Zeta (R^2=0), RV~54.31+0.52*Zeta (R^2=0), ROD~2.2+0.12*Zeta (R^2=0.15)*

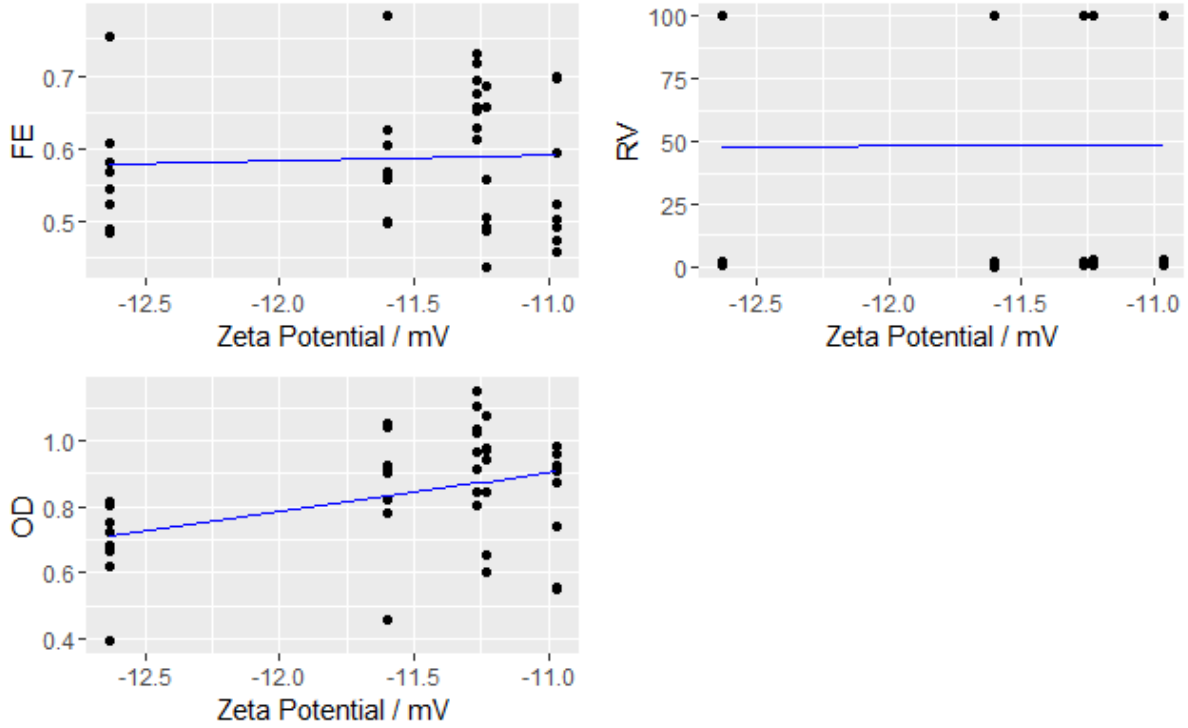

Supplemental 51: Effect of factor flocculation agent on residual volume (RV).

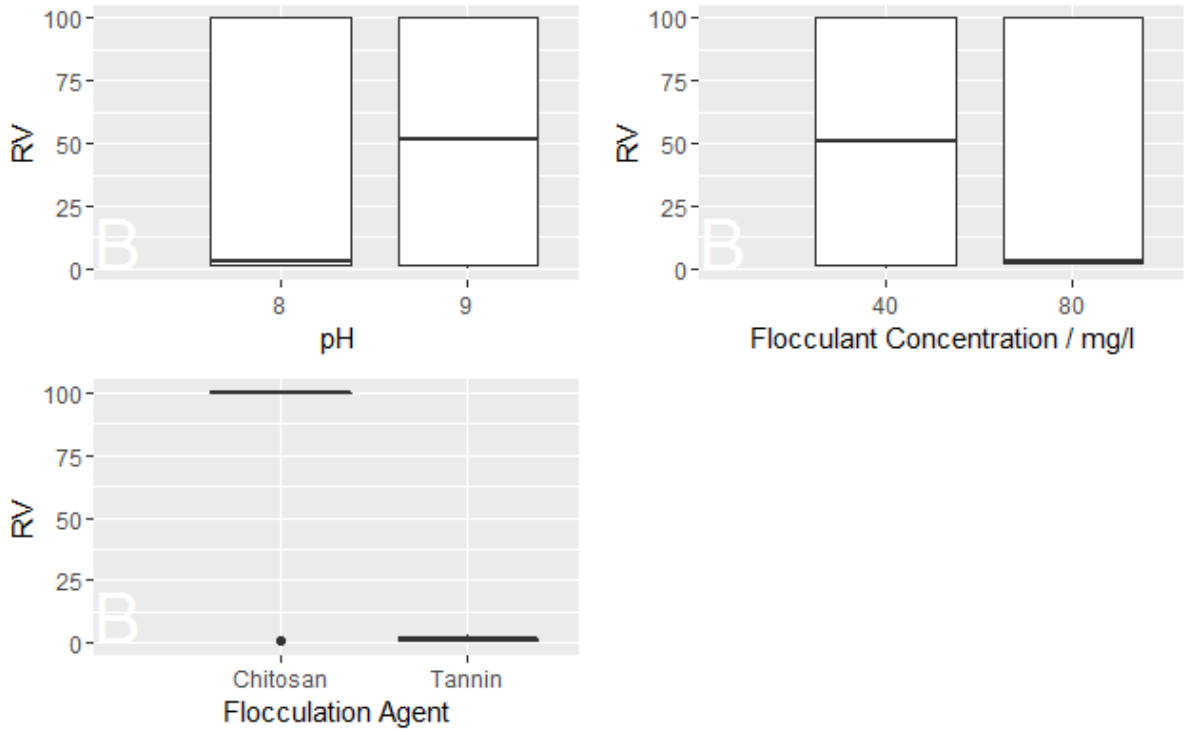

Supplemental 52: Full x1/x2/x3/FM ANCOVA model parameters.

```
lm(formula=FE ~ x1 + x2 + x3 + FM + x1:x2 + x1:x3 + x2:x3 +
    x1:FM + x2:FM + x3:FM + x1:x2:x3 + x1:x2:FM + x1:x3:FM +
    x2:x3:FM + x1:x2:x3:FM + I(x3 * x3), data=FlokN7)

Coefficients:
                   Estimate Std. Error t value Pr(>|t|)
(Intercept)        0.500997   0.018373  27.268  < 2e-16 ***
x1                -0.035998   0.023934  -1.504  0.14618
x2                 0.151910   0.023934   6.347 1.78e-06 ***
x3                 0.041395   0.011967   3.459  0.00213 **
FMTannin           0.076501   0.023934   3.196  0.00401 **
I(x3 * x3)         0.017231   0.003576   4.819 7.32e-05 ***
x1:x2             -0.092519   0.033848  -2.733  0.01185 *
x1:x3             -0.011506   0.016924  -0.680  0.50336
x2:x3             -0.006043   0.016924  -0.357  0.72430
x1:FMTannin       -0.043985   0.033848  -1.299  0.20665
x2:FMTannin       -0.065306   0.033848  -1.929  0.06611 .
x3:FMTannin       -0.023085   0.016924  -1.364  0.18575
x1:x2:x3          -0.001641   0.023934  -0.069  0.94594
x1:x2:FMTannin     0.042001   0.047869   0.877  0.38934
x1:x3:FMTannin     0.019897   0.023934   0.831  0.41434
x2:x3:FMTannin    -0.023870   0.023934  -0.997  0.32899
x1:x2:x3:FMTannin  0.031100   0.033848   0.919  0.36773

Signif. codes:  0 ‘***’ 0.001 ‘**’ 0.01 ‘*’ 0.05 ‘.’ 0.1 ‘ ’ 1

Residual standard error: 0.03784 on 23 degrees of freedom
Multiple R-squared:  0.896, Adjusted R-squared:  0.8236
F-statistic: 12.38 on 16 and 23 DF,  p-value: 9.926e-08
```

Supplemental 53: AIC reduced x1/x2/x3/FM ANCOVA model parameters

```
lm(formula=FE ~ x1 + x2 + x3 + FM + I(x3 * x3) + x1:x2 + x1:x3 +
    x2:x3 + x1:FM + x2:FM + x3:FM + x1:x3:FM, data=FlokN7)

Coefficients:
                Estimate Std. Error t value Pr(>|t|)
(Intercept)     0.506247   0.016893  29.969  < 2e-16 ***
x1             -0.046499   0.020156  -2.307  0.02896 *
x2              0.141410   0.020156   7.016 1.53e-07 ***
x3              0.043886   0.009200   4.770 5.65e-05 ***
FMTannin        0.066001   0.020156   3.274  0.00290 **
I(x3 * x3)      0.017231   0.003477   4.955 3.43e-05 ***
x1:x2          -0.071518   0.023274  -3.073  0.00480 **
x1:x3          -0.012327   0.011637  -1.059  0.29887
x2:x3          -0.011023   0.008229  -1.340  0.19154
x1:FMTannin    -0.022985   0.023274  -0.988  0.33213
x2:FMTannin    -0.044306   0.023274  -1.904  0.06767 .
x3:FMTannin    -0.035021   0.011637  -3.009  0.00562 **
x1:x3:FMTannin  0.035447   0.016457   2.154  0.04034 *

Signif. codes:  0 ‘***’ 0.001 ‘**’ 0.01 ‘*’ 0.05 ‘.’ 0.1 ‘ ’ 1

Residual standard error: 0.0368 on 27 degrees of freedom
Multiple R-squared:  0.8845,    Adjusted R-squared:  0.8332
F-statistic: 17.23 on 12 and 27 DF,  p-value: 1.253e-09
```

Supplemental 54: Reversed factor elimination reduced x1/x2/x3/FM ANCOVA model parameters

```
lm(formula=FE ~ x1 + x2 + x3 + FM + x1:x2 + x2:FM + x3:FM +
    I(x3 * x3), data=FlokN7)

Coefficients:
             Estimate Std. Error t value Pr(>|t|)
(Intercept)  0.511994   0.016812  30.454  < 2e-16 ***
x1          -0.057991   0.017447  -3.324  0.00229 **
x2           0.141410   0.021368   6.618 2.14e-07 ***
x3           0.032210   0.006168   5.222 1.14e-05 ***
FMTannin     0.054508   0.017447   3.124  0.00385 **
I(x3 * x3)   0.017231   0.003686   4.674 5.45e-05 ***
x1:x2       -0.071518   0.024673  -2.899  0.00683 **
x2:FMTannin -0.044306   0.024673  -1.796  0.08230 .
x3:FMTannin -0.017297   0.008723  -1.983  0.05631 .

Signif. codes:  0 ‘***’ 0.001 ‘**’ 0.01 ‘*’ 0.05 ‘.’ 0.1 ‘ ’ 1

Residual standard error: 0.03901 on 31 degrees of freedom
Multiple R-squared:  0.851, Adjusted R-squared:  0.8125
F-statistic: 22.13 on 8 and 31 DF,  p-value: 8.679e-11
```

Supplemental 55: Pareto charts shows effect sizes of x1/x2/x3/FM-models ordered by size of the full model (A), the reduced model according to the AIC (B) and the reduced model according to reverse factor elimination (C).

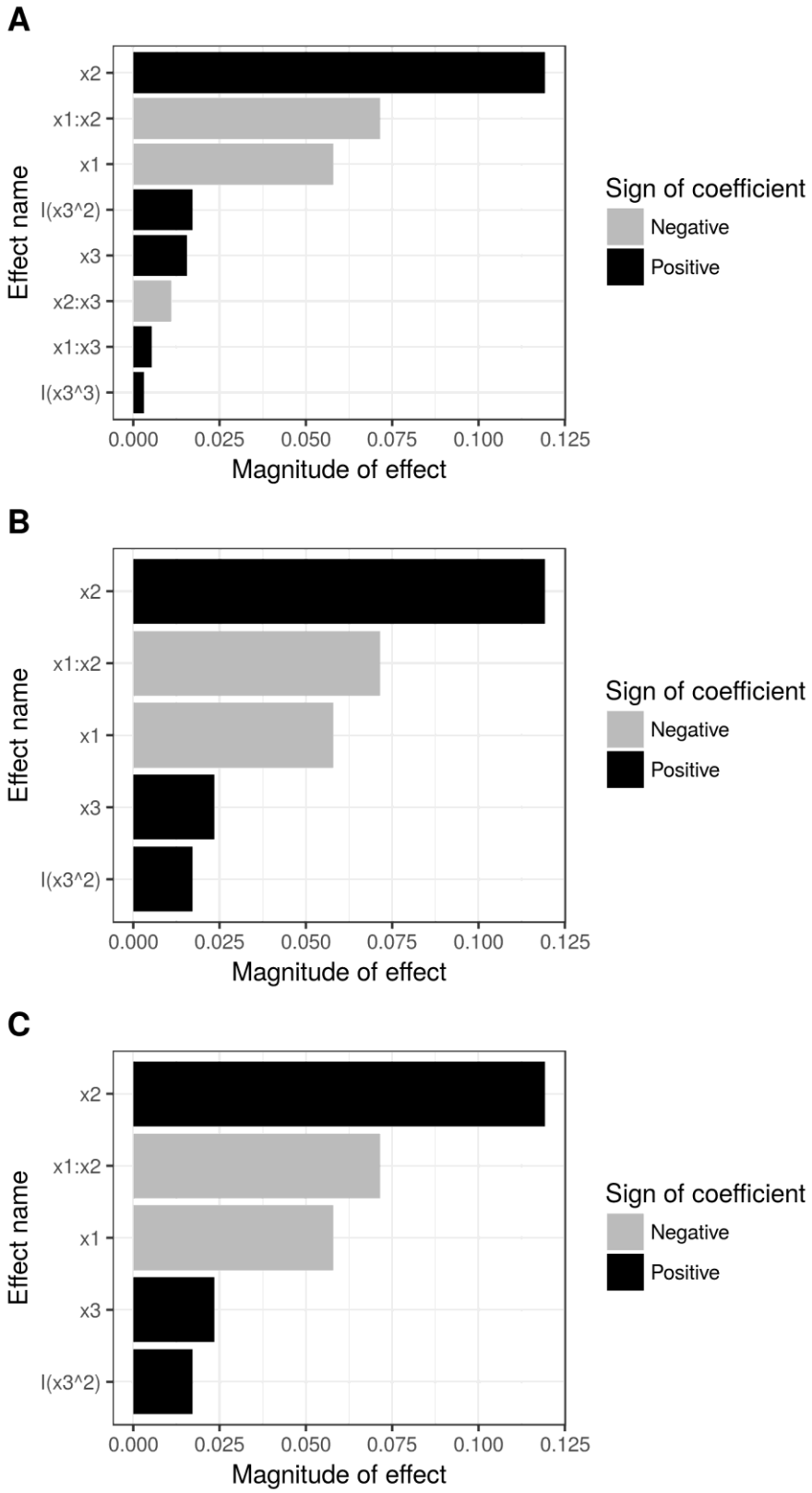

Supplemental 56: Full x1/x2/x3/FM/AOM ANCOVA model parameters.

```
lm(formula=FE ~ x1 * x2 * x3 + I(x3 * x3) + FM * AOM, data=FlokN7aom)
```

```
Coefficients:
               Estimate Std. Error t value Pr(>|t|)
(Intercept)     0.58163    0.04383  13.270 1.12e-11 ***
x1             -0.12623    0.05286  -2.388 0.026423 *
x2              0.01637    0.05286   0.310 0.759911
x3              0.04412    0.02643   1.669 0.109887
I(x3 * x3)           NA         NA      NA       NA
FMTannin        0.02929    0.03738   0.783 0.442098
AOMWO           0.09208    0.03738   2.463 0.022483 *
x1:x2           0.09885    0.07476   1.322 0.200292
x1:x3           0.02626    0.03738   0.702 0.490123
x2:x3          -0.01372    0.03738  -0.367 0.717348
FMTannin:AOMWO  0.24432    0.05286   4.622 0.000147 ***
x1:x2:x3       -0.02694    0.05286  -0.510 0.615633
```

```
Signif. codes:  0 ‘***’ 0.001 ‘**’ 0.01 ‘*’ 0.05 ‘.’ 0.1 ‘ ’ 1
```

```
Residual standard error: 0.07476 on 21 degrees of freedom
Multiple R-squared:  0.8713,    Adjusted R-squared:  0.8101
F-statistic: 14.22 on 10 and 21 DF,  p-value: 3.176e-07
```

Supplemental 57: AIC reduced x1/x2/x3/FM/AOM ANCOVA model parameters.

```
lm(formula=FE ~ x1 + x2 + x3 + FM + AOM + x1:x2 + FM:AOM, data=FlokN7aom)
```

```
Coefficients:
                Estimate Std. Error t value Pr(>|t|)
(Intercept)     0.582097   0.036234  16.065 2.42e-14 ***
x1             -0.099971   0.036234  -2.759  0.01092 *
x2              0.002651   0.036234   0.073  0.94228
x3              0.043659   0.012811   3.408  0.00231 **
FMTannin        0.029286   0.036234   0.808  0.42689
AOMWO           0.092081   0.036234   2.541  0.01792 *
x1:x2           0.071914   0.051243   1.403  0.17331
FMTannin:AOMWO  0.244319   0.051243   4.768 7.49e-05 ***
```

```
Signif. codes:  0 ‘***’ 0.001 ‘**’ 0.01 ‘*’ 0.05 ‘.’ 0.1 ‘ ’ 1
```

```
Residual standard error: 0.07247 on 24 degrees of freedom
Multiple R-squared:  0.8618,    Adjusted R-squared:  0.8215
F-statistic: 21.38 on 7 and 24 DF,  p-value: 7.247e-09
```

Supplemental 58: Reversed factor elimination reduced x1/x2/x3/FM/AOM ANCOVA model parameters.

```
lm(formula=FE ~ x1 + x3 + AOM + FM:AOM + x1:x2, data=FlokN7aom)
```

```
Coefficients:
               Estimate Std. Error t value Pr(>|t|)
(Intercept)     0.58342    0.03075  18.974 2.33e-16 ***
x1             -0.10130    0.03075  -3.294  0.00295 **
x3              0.04366    0.01255   3.478  0.00187 **
AOMWO           0.09208    0.03551   2.593  0.01566 *
AOMW:FMTannin   0.02929    0.03551   0.825  0.41728
AOMWO:FMTannin  0.27360    0.03551   7.706 4.62e-08 ***
x1:x2           0.07456    0.03551   2.100  0.04598 *
```

```
Signif. codes:  0 ‘***’ 0.001 ‘**’ 0.01 ‘*’ 0.05 ‘.’ 0.1 ‘ ’ 1
```

```
Residual standard error: 0.07101 on 25 degrees of freedom
Multiple R-squared:  0.8618,    Adjusted R-squared:  0.8286
F-statistic: 25.98 on 6 and 25 DF,  p-value: 1.344e-09
```